CELL AND DEVELOPMENTAL BIOLOGY

MORPHOLOGICAL AND MOLECULAR CHARACTERIZATION OF SOMATOSENSORY NEUROGENESIS

CODY J. SMITH

Dissertation under the direction of Professor David M. Miller III, Ph.D.

Organisms across phylogeny have neuronal circuits that control everyday activities. The somatosensory network, for example, is specifically utilized to sense the external environment and is important to properly inform the animal on its surroundings. The information encoded in this sensory circuit allows an animal to distinguish painful strikes from gentle brushes. Thus, it is clear that the proper development of this circuit and the neurons in the network are essential for animal survival.

My work describes the development of somatosensory neurons in *C. elegans* and establishes *C. elegans* as a model for studying the generation of pain-sensing cells known as nociceptive neurons that typically have large non-overlapping dendritic arrays that innervate the skin. The *C. elegans* nociceptive neuron, PVD, is generated through a dynamic error-correction mechanism. This work describes the transcriptional profile of the PVD neuron and identifies multiple transcription factors that are required for the mature dendritic array.

I further identify a transcription factor cascade that is required to generate the proper balance of somatosensory neuronal types *in C. elegans*. We show that MEC-3, AHR-1, and ZAG-1 define a transcriptional code that generates specific somatosensory neurons to ensure the animal can distinguish different environmental stimuli. Together these proteins define the modality and dendritic architecture of somatosensory neurons.

Lastly, I show that the non-overlapping array of PVD is generated through a mechanism known as self-avoidance. I demonstrate that self-avoidance requires a contact-induced retraction event that requires UNC-6/Netrin signaling and actin polymerization. Interestingly, the UNC-6/Netrin pathway is also utilized earlier in development to generate the PVD asymmetric dendritic array. The two functions of UNC-6/Netrin, however, are temporally and modularly different. Together my work provides foundation for studying nociceptive neuron development.

Approved: Date: July 11, 2012

MORPHOLOGICAL AND MOLECULAR CHARACTERIZATION OF SOMATOSENSORY NEUROGENESIS

By

Cody Jean Smith

Dissertation

Submitted to the Faculty of the

Graduate School of Vanderbilt University

in partial fulfillment of the requirements for

the degree of

DOCTOR OF PHILOSOPHY

in

Cell and Developmental Biology

August 2012

Nashville, Tennessee

Approved:

David M. Miller III, Ph.D.

Christopher V. E. Wright, *D. Phil*

Matthew J. Tyska, Ph.D.

Donna J. Webb, Ph.D.

Joshua T. Gamse, Ph.D.

To my Family,
Friends and Teachers

ACKNOWLEDGEMENTS

My years in graduate school have been filled with people who have not only helped me grow as a scientist but also as a person. Vanderbilt is truly a special community and I cannot imagine doing my graduate work in a better institution. I must start by thanking my mentor, David Miller. David often recounts to others the time I told him I felt like a “kid in a candy shop” to demonstrate my passion for science, but he harnessed that passion and guided me. I thank him for the independence he provided early on, knowing that I worked best when I could come up with my own ideas. I appreciate David’s patience with me, in the design of presentations, manuscript preparation and every day in the lab. His attention to detail in these aspects of science will certainly be mirrored in my work as my career progresses. Lastly, I would like to thank David for his tireless teaching both in the laboratory setting and the classroom. I hope to one day possess his composure and depth of knowledge when in the front of a classroom.

I would also like to thank members of my thesis committee, Christopher Wright, Matthew Tyska, Donna Webb, and Joshua Gamse. I have enjoyed every minute of our interactions and appreciate your willingness to support me in my scientific goals.

I must give special thanks to Christopher Wright for our many discussions about the attributes of a good scientist and teaching me that there is a substantial difference between doing research and being a scientist. You have displayed a

tremendous amount of faith in my scientific abilities and I hope to someday reach that potential. I would also like to thank all members of the Cell and Developmental Biology Department and the Program in Developmental Biology. I have learned more from DB journal club than I have ever learned in a classroom!

To Steven Mauro, my undergraduate mentor who originally recognized my passion and taught me how to do research efficiently. You molded my scientific foundation that will continue to support my career in the future.

To members of David's lab throughout the years that have been involved in this thesis. Thank you Mallory Hacker for being my scientific sibling. We entered David's lab together, qualified one day apart and have remained great friends throughout; you are a remarkable scientist and I am honored to have had the chance to work with you. Thank you Clay Spencer, Tim O'Brien and Rachel Skelton for being my soundboards and great friends; your help has been immeasurable. Thank you Sarah Petersen, Tyne Miller, Judsen Schneider, Kathie Watkins and Joseph Watson for your wisdom throughout. Lastly, thank you Andrew Hardaway; your help throughout this thesis has been great and I hope we continue to be both good friends and colleagues.

Most importantly I must thank my family for their continued support; they have encouraged my questions since I was a kid despite how annoying they once were. To my parents, Darrell and Linda, who are the models for unconditional love. You have guided me through all the stages of my life and have always been there when I needed you during my studies. I hope to one day

have the attributes you continually display to me. To my siblings, Keith, Becky, Brian, Trevor, and Amber who have always supported me throughout and know the way to motivate me. I hope I have made you proud. Lastly, to Ashley, who has showered me with an unlimited amount of support, has unselfishly adapted so I can achieve my dreams and has continued to push me to become the scientist she thinks I can be.

TABLE OF CONTENTS

LIST OF TABLES

LIST OF FIGURES

CHAPTER I

INTRODUCTION

Neurons display polarized structure with dendrites and axons

The nervous system allows animals to respond to a myriad of environmental stimuli and directs simple everyday activities such as breathing and walking. Glia and neurons are the two basic cell-types that populate the nervous system. Neurons are the fundamental feature of neuronal circuits. Neurons send and receive sensory information from the environment to motivate different motor movements of the animal. In the brain, neurons have multiple functions including mediating learning and memory. Glial cells provide support for neurons and play an important role in regulating neuronal development and function. Both glia and neurons are required for the proper function of the nervous system and defects in either cell type can result in disease. My work has primarily focused on the development of neurons and thus will be the focus of this introduction.

Neurons are capable of both sending and receiving signals. Each of these activities depends on the demarcation of discrete neuronal domains (Figure 1.1) [1]. This polarity is a fundamental characteristic of neurons across phylogeny [1]. The axon functions as the presynaptic apparatus or the area of the neuron that is used to send neuronal signals. Neurons usually display a single axonal branch that must navigate through the extracellular space to connect with their

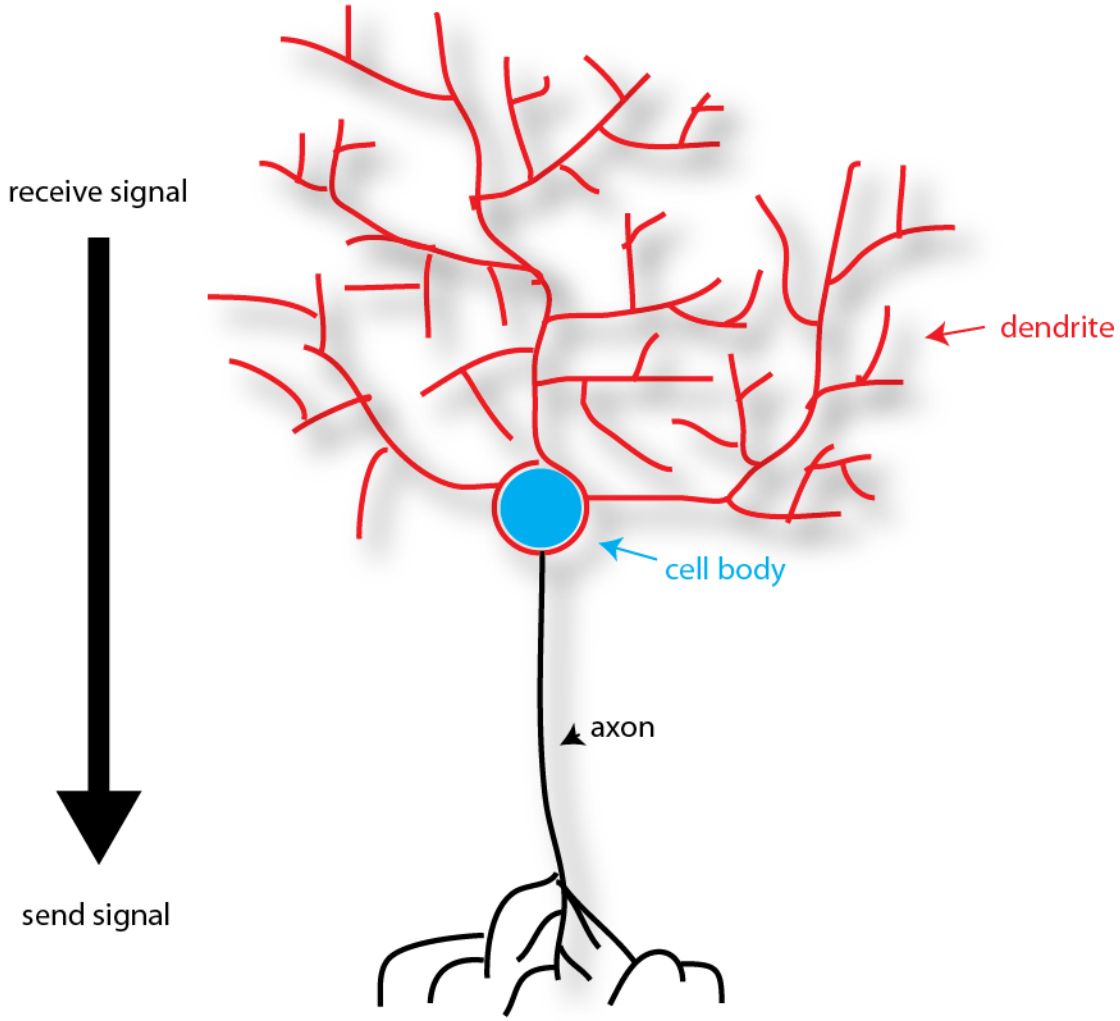

Figure 1.1 Neurons have two distinct domains. A typical neuron has a dendritic domain (red) that receives information. Dendrites can either be stimulated by the external environment (sensory neurons) or by other neurons (central nervous system). The cell body (blue) contains the cell nucleus where genetic material is maintained. The axon (black) represents the part of the cell that sends signals. Most neurons do not have multiple axons but have a single axon that can branch at the area distal from the cell in order to connect with other neurons (central nervous system) or muscle (neuromuscular junction).

postsynaptic partners [2]. In contrast, the neuronal compartment that receives neuronal signals or the postsynaptic dendrite may be morphologically complex with multiple dendritic branches emanating from the cell (Figure 1.1)[1]. Outgrowing branches must navigate in the extracellular space to form synapses with axons of other neurons or in the case of sensory neurons, to fill a given receptive field to maximize detecting environmental stimuli [3]. Because axons normally adopt a simple morphology the mechanisms that govern process outgrowth and guidance are much better known for axons than for dendrites [4]. The proper development of both of these neuronal domains, nonetheless, is essential for the function of neuronal circuits [4].

An extensive body of literature describes mechanisms governing the establishment of neuronal polarity (see review [1, 3, 5]). My thesis focuses on the stages in dendritic development that occur after the neuron is initially polarized. My review will therefore feature literature that describes the mechanisms of dendritic and axonal morphogenesis that are initiated after polarized neuronal domains are established. Neuronal polarity is clearly an important aspect of dendritic morphogenesis and readers can learn more about the earlier events in neuronal morphogenesis by consulting these excellent reviews [1, 5].

The diverse nature of dendritic trees

Neurons are defined by their morphological and functional characteristics. Each neuronal sub-type can display a unique morphology which suggests that

thousands of distinct types of dendritic arbors are likely found in the vertebrate nervous system (Figure 1.2) [6]. The diversity of dendritic arbors can be seen in Ramon y Cajal's early tracings of neurons and neuronal circuits [7] (Ramon y Cajal, 1899-1904) (Figure 1.2). This diversity is particularly well characterized in the mammalian retina where subtypes of neurons are easily visible and can be readily classified on the basis of their distinctive dendritic arbors [8]. For example, retinal ganglion cells display large dendritic arbors that are easily distinguishable from amacrine cells (Figure 1.2) [8]. This diversity can also be seen in the mammalian brain. For example, Purkinje neurons show highly elaborate branching patterns that are different than cerebellar granule neurons [6]. Because of the diverse nature of dendritic arbors in the vertebrate nervous system, invertebrate model organisms with simpler, better-defined nervous systems are now widely used to identify the molecular underpinning of dendritic arbor diversity [3, 5, 6].

Drosophila and nematode sensory neurons adopt distinctive dendritic arrays

Neurons in the *Drosophila* peripheral nervous system display dendritic trees of varying complexity [9, 10]. Each abdominal segment contains 44 sensory neurons. These are classified according to morphology, which range from sensory neurons with unbranched unipolar neurons to dendritic arbors rivaling the size and complexity of vertebrate nervous system [6]. Class I dendritic arborization (da) neurons display simple unbranched arbors (Figure

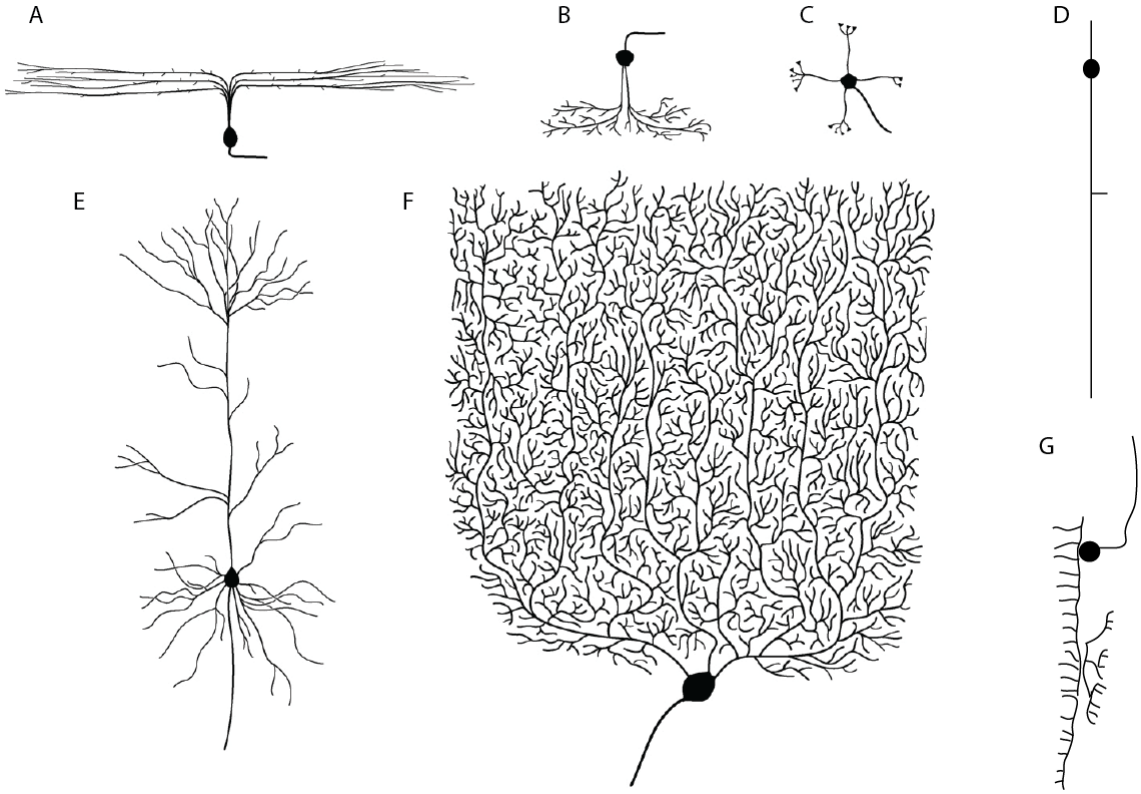

Figure 1.2. Dendritic diversity in the nervous system. Tracings of neurons throughout animalia that show the diversity of dendritic arrays in the nervous system. A. A retinal ganglion cell in vertebrates. B. amacrine cell in vertebrates. C. A cerebellum granule neuron in the mammalian brain. D. *C. elegans* light touch neuron. E. Purkinje Cell in the mammalian brain. F. Cortical pyramidal neuron of vertebrates. G. A *C. elegans* nociceptive neuron. Images A-C, E,F are adapted from Gao et. al. 2007.

1.3). In contrast, Class IV neurons display large non-overlapping arrays that cover a wide receptive area (Figure 1.3) [9, 10]. Neurons with different morphological features are also observed in the *C. elegans* nervous system. Although a majority of these neurons show a relatively simple bipolar, unbranched morphology, recent studies revealed two types of sensory neurons, PVD and FLP, display large dendritic arrays that mirror dendritic trees observed in the *Drosophila* and the mammalian peripheral nervous system [11, 12] (Figure 1.2). As a result of this conservation, recent studies using *C. elegans* and *Drosophila* as a model for generating diverse dendritic arbors have begun to reveal molecular pathways that specify different arbor types.

Transcription Factors Involved in Dendritic Morphogenesis

Studies of transcription factor mutants have emphasized the key role of intrinsic genetic programs in the specification of dendritic morphology. The transcriptional programs that govern sensory neuron morphogenesis in the *Drosophila* PNS neurons are the best understood [3]. In a genome-wide RNAi screen of transcription factors, over 70 proteins were shown to influence dendritic morphogenesis in *Drosophila* sensory neurons [13]. This screen demonstrates the importance of transcription factors to diversify dendritic arrays.

Multiple transcription factors have been described to limit dendritic branching. Hamlet, a zinc-finger transcription factor, is expressed in both precursors and in post-mitotic sensory neurons. The loss of Hamlet causes class I dendritic arbors to adopt a more highly branched dendritic arbor resembling that

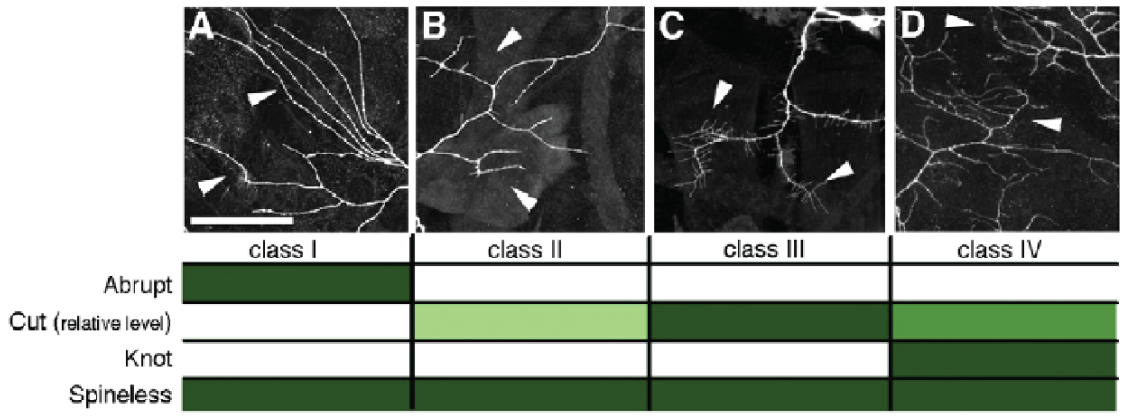

Figure 1.3 A genetic code defines *Drosophila* sensory neurons. Figure was published in Corty et. al. 2009. Class 1 (A), II (B), III (C) and IV (D) neurons display varying levels of dendritic complexity. Class I neurons are the least elaborate whereas class IV neurons display large complex arrays. Below are transcription factors that are expressed in each class type that controls a specific dendritic morphology. Expression in a given class type is represented by the green bars. The levels of Cut protein, at low concentration in class II and higher concentrations in Class IV differentially control dendritic complexity. Spineless is expressed in all md neurons but has different roles depending on the complexity of the neuron.

of class II neurons [14] (Figure 1.3). Abrupt also limits dendritic arbor complexity and is selectively expressed in class I neurons [15]. Abrupt is sufficient to reduce dendritic branching when expressed in class IV neurons(Figure 1.3). Abrupt and Hamlet represent transcription factors that limit dendritic outgrowth and when absent can switch unbranched arbors into highly branched trees.

Knot is also expressed exclusively in Class IV neurons where it functions to induce dendritic branching (Figure 1.3). Interestingly, ectopic expression of Knot is sufficient to induce branching in normally unbranched sensory neurons [16-18]. Knot is thought to promote branching by regulating Spastin, a microtubule severing protein that can induce higher order branches [18]. Together, Hamlet, Abrupt and Knot are examples of transcription factors that diversify dendritic arbor morphology by being exclusively expressed in one type of neuron.

Other transcription factors that regulate dendritic morphology in *Drosophila* are expressed in multiple types of sensory neurons. For example, Cut is expressed in most dendritic arborization (da) neurons in *Drosophila* but at different concentrations (Figure 1.3) [19, 20]. The level of Cut expression is correlated with the complexity of the dendritic arbor. For instance, class II neurons express low levels of Cut and display simple dendritic trees. Class IV neurons, however, express a high level of Cut and adopt elaborate dendritic arrays. These observations led to the hypothesis that Cut regulates threshold-dependent pathways that promote dendritic branching [20, 21]. Interestingly, the Cut homolog in vertebrates, Cux, also controls dendritic complexity [22]. These

results support the hypothesis that Cut could be an ancient transcriptional program that controls dendritic morphology.

Spineless was also identified in *Drosophila* to regulate dendritic branching [23] (Figure 1.3). Spineless is a member of the basic loop helix transcription factor family that closely resembles the mammalian aryl hydrocarbon dioxin receptor AHR. Spineless is expressed in multiple types of sensory neurons that display varying dendritic arrays. Spineless has different effects on branching depending on the arbor complexity of affected neurons. In unbranched neurons such as class I neurons, *spineless* mutants display class I neurons that resemble more branched dendritic arbors. Interestingly, class IV neurons in *spineless* mutants display dendritic arbors with reduced branching [23]. How Spineless has differential effects on dendritic arbors is not known but it likely interacts with other transcription factors. For example, Class IV neurons express high levels of Cut, Spineless and Knot [4]. In contrast, class I neurons express low levels of Cut, Spineless and Abrupt. In these contexts, Knot could affect a different set of Spineless targets in class IV neurons than in class I neurons (Figure 1.3). These transcription factors might also have task-specific roles in dendritic morphogenesis. Cut, for example, may induce actin-containing filopodia-like branches whereas Knot may regulate microtubule-dependent dendritic branches [4]. Studies that define the interaction of transcription factors in sensory neurons will be an interesting direction for the future.

Transcription factors are thought to regulate dendritic morphology by controlling specific targets. For example, Cut has been shown to drive

expression of Turtle, a transmembrane protein that regulates dendritic morphology [24]. Interestingly, Cut can also regulates levels of abrupt. Knot, as mentioned above, regulates Spastin to promote dendritic branching [18]. Knot also controls Pickpocket, an ion channel that is essential for Class IV neuron function [16-18, 25]. Thus, these transcription factors have dual roles: 1. Diversify dendritic morphology and 2. Define different sensory modalities. Identification of targets of these transcription factors would certainly strengthen this hypothesis. It is worth noting that despite the extensive identification of transcription factors that influence dendritic morphology the targets of these proteins are largely unknown and thus remain an outstanding question in neuronal development.

Mammalian Transcription Factors in Dendritic Development

Transcription factors that are expressed in multiple cell types and effect dendritic morphogenesis have also been described in mammalian development. For example, NeuroD and CREST are widely expressed in the nervous system and are thought to promote dendritic branching [26, 27]. How NeuroD and CREST promote dendritic branching is not understood but they may drive general dendrite branching factors in all cell types since reduced levels have similar effects in multiple neuronal types.

EXTRACELLULAR CUES THAT REGULATE NEURONAL BRANCH MORPHOLOGY

Axon guidance molecules

Ramon y Cajal predicted that neurotropic factors must exist to pattern the nervous system and guide axons to their targets (Cajal, 1899-1904). Scientists over the years have sought to identify these potential neurotropic factors. To date, four main signaling pathways have been identified to function in axon guidance (Figure 1.4) [2]. These signaling pathways represent an ancient mechanism that can be seen across phylogeny. Two main mechanisms exist for axon guidance, either signaling molecules function at a distance from their source (e.g. long-range guidance) or they function as a contact-dependent component (e.g. short-range signaling) (Figure 1.4) [2].

Slit, Netrin and Semaphorin represent proteins that have the potential to participate in long-range guidance mechanism (Figure 1.4). Slit was first identified to direct axon guidance of the *Drosophila* nerve cord [28-30]. In this setting, Slit functions as a repulsive cue to limit commissural axons from crossing back over the nerve cord. Slits also function in longitudinal axon guidance to prevent growth cone attraction to other axon guidance molecules [31, 32]. The role of Slit as a repulsive axon guidance cue is conserved from nematodes to mammals [33, 34]. Slit signaling is mediated through the transmembrane receptor, Robo, which is also conserved across phylogeny (Figure 1.4) [28, 32, 35]. In flies and mammals there are multiple isoforms of Robo that are

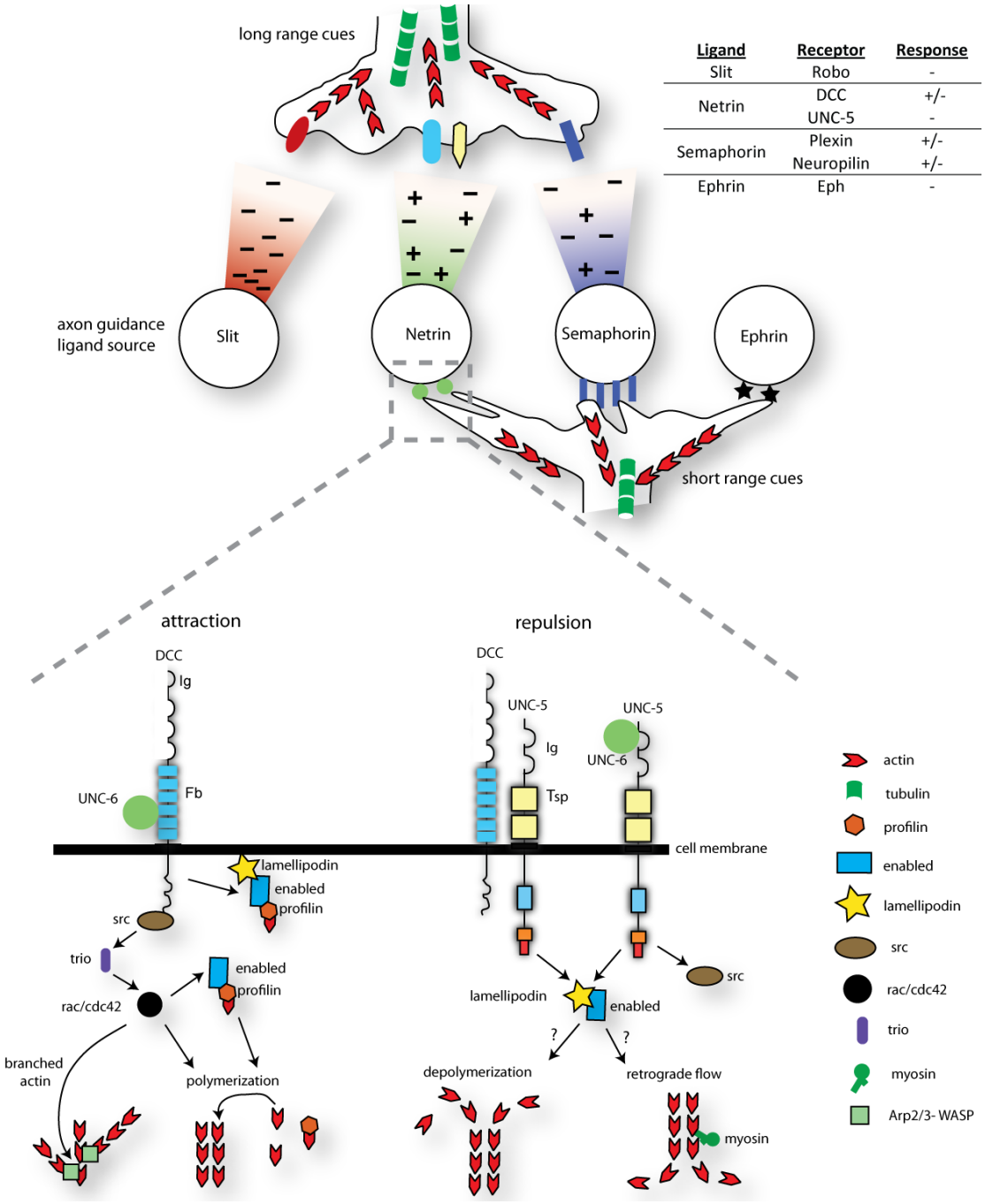

Figure 1.4 Axon guidance molecules steer growth cones. Long range-cues, Slit (red), Netrin (green) and Semaphorin (purple), steer axons by rearranging the actin (red) or microtubule (green) cytoskeleton. Slit functions as a repulsive long-range cue whereas Netrin and semaphorin function in repulsion and attraction. Netrin (green) and Semaphorin (purple) can also function at short-range. Ephrin (black star) is a short-range repulsive molecule. Table summarizes axon guidance molecules. Bottom depicts molecular signaling complexes within inset. Attraction utilizes DCC to polymerize actin. Ena aids in actin polymerization and can be localized to the membrane by lamellipodin. Ena also interacts with trio, rac and profilin. Rac can also activate WASP and Arp2/3 to generate branched actin. Repulsion utilizes UNC-5 or UNC-5/UNC-40 heterodimeric receptors and requires src, lamellipodin and ena. The mechanism of UNC-5 repulsion, however, is poorly understood. Growth cone retraction is hypothesized to be mediated by depolymerization or retrograde flow.

expressed at different times in development to control commissural axons. Interestingly, a specific isoform of Robo can inhibit other Robo molecules to properly pattern axons [35]. The Robo receptor has also been shown to repress other axon guidance receptors including the Netrin receptor, DCC which prevents the commissural axons from re-entering the midline where Netrin is secreted [36].

Netrin and semaphorins are known to function at a distance from their source but also have the ability to act as short-range guidance molecules. The semaphorin protein class includes both secretable and transmembrane forms (Figure 1.4) [37]. Semaphorins were first identified in the grasshopper as determinants of sensory axon guidance [38]. In these roles, Semaphorins function as repulsive molecules [39]. In the mammalian nervous system Semaphorins also function as a repulsive guidance cues to steer motor and sensory axon outgrowth (Figure 1.4) [40]. The Semaphorin receptors are Plexins and Neuropilins (Figure 1.4) [41]. Interestingly, Semaphorins also have the capability of functioning as an attractant (Figure 1.4) [2]. This dual attractive and repulsive potential is also seen in Netrins.

Netrin was first identified in *C. elegans* and then rediscovered in vertebrates to function as either an attractive or a repulsive cue (Figure 1.4) [42-45]. The *C. elegans* Netrin homolog, UNC-6, is expressed on the ventral side where it can function as a repulsive cue to direct outgrowth of motor neuron commissures to the dorsal nerve cord. Ventrally derived UNC-6 may also function as an attractive signal for axonal processes that grow toward the ventral

side [42, 43]. These dual roles are also observed in *Drosophila* where Netrin can either attract axons to the ventral nerve cord where it is expressed or function as a repulsive molecule to guide axons away from the midline region (Figure 1.4) [46, 47]. Ventral midline expression of Netrins in the axial nerve cord is conserved in vertebrates where Netrin can also mediate both attraction and repulsion [44, 45](Figure 1.4). Attractive and repulsive responses to Netrin are mediated by different receptors. In attraction, the DCC receptor (Frazzled-*Drosophila*, UNC-40-*C. elegans*) activates downstream components that rearrange the actin cytoskeleton (Figure 1.4) [48-50]. In contrast, repulsion utilizes the UNC-5 receptor or the DCC/UNC-5 heterodimer [51-54]. The understanding of UNC-5 downstream signaling, however, is much less known than the downstream signaling of DCC (Figure 1.4).

Netrin can also function as a short-range molecule, but unlike Semaphorins, the canonical Netrin molecule does not possess a transmembrane form (Figure 1.4) [54-56]. In some cases, it is not clear how Netrin is maintained at the surface of a cell in order to function as a short-range contact-dependent molecule. For example, in *Drosophila* axon guidance, Netrin appears to signal through UNC-5 to mediate repulsion. Netrin however, does not need to be secreted in this case since repulsion involves contact with Netrin expressing cells. This model was confirmed by an experiment in which the repulsive guidance function for Netrin could be provided by a cell-surface-tethered chimeric Netrin protein fixed to a transmembrane-spanning domain [54, 55]. A similar strategy was used to show that Netrin can function as a short-range attractive

molecule through UNC-40 to guide dendrites and in synaptogenesis in *C. elegans [57, 58]*. In both of these scenarios, the Netrin molecule functions as a short-range cue on the cell in which it is expressed. *In vivo* mechanisms that limit Netrin to this location are not understood but could involve interactions with a local receptor that limits Netrin diffusion. For example, a recent study showed that a secreted form of Netrin could be captured at a distant location from its source to serve a short-range guidance cue [59]. In this case, Netrin is captured on a distant cell by its receptor Frazzled/DCC. Frazzled/DCC, however, does not appear to function as a signaling molecule but rather as a "catcher's mitt" to localize Netrin. Axons then use this localized Netrin as a guidance cue. Interestingly, the signaling receptor that responds to the distal Netrin cue is not known in this case [59]. These studies represent examples of the diverse roles that Netrin may adopt to pattern axon guidance and connectivity in the nervous system.

Lastly, Ephrins and their receptors Eph, guide axons exclusively as short-range molecules [60] (Figure 1.4). Ephrins function in vertebrates to guide retinal ganglion cells [2, 61]. Peripheral and central nervous system axons also utilize Ephrin during outgrowth. As with Netrin and Semaphorin, Ephrins also have the ability to function as either attractive or repulsive cues [2]. Interestingly, the Ephrin signaling pathway appears to be more complex than originally hypothesized. The Ephrin ligand can also function as a receptor in a mechanism known as "reverse" signaling [62]. Ephrins also function in dendritic morphogenesis and synaptogenesis suggesting that axon guidance molecules

may adopt diverse roles in neuronal development beyond the experimentally discovered functions [2, 63]. This hypothesis is an emerging concept in neuronal development.

Extrinsic factors that control dendritic development

Dendrites must navigate similar extracellular space as axons and thus are likely to utilize common sets of signaling molecules (Figure 1.4). Because of the complex nature of dendritic arrays it has been difficult to identify the impact of these molecules in dendritic development. However, recent evidence suggests that axon guidance molecules also function in dendritic development (Figure 1.4) [3, 4, 6].

Semaphorin was first shown to have a role in dendritic development in the mammalian brain where it patterns apical dendrites of cortical pyramidal neurons [64]. A role of Semaphorin in dendritic development was also observed in *Drosophila* where Semaphorin controls initial targeting of dendrites [65]. Interestingly, Semaphorin appears to function as a receptor in the pathway that controls dendritic morphogenesis. This suggests that the signaling pathway in dendritic development may be distinct from what is utilized to guide axons. Nonetheless, the discovery of this evident function for Semaphorin in dendritic development supports the hypothesis that axon guidance molecules can be used to pattern dendrites.

Slit and Netrin have also been shown to function in dendritic development. In *Drosophila*, Slit functions as a repulsive cue for dendrites. Netrin functions in a

similar way to repel dendrites from the nerve cord source [66]. In both cases, these axon guidance signals appear to function as long-range cues for dendritic outgrowth. The long-range role of Netrin in dendritic guidance is also conserved in vertebrates. In Zebrafish, dendrites are attracted toward a Netrin source through DCC [67]. Lastly, in *C. elegans*, UNC-6/Netrin functions as a short-range cue to guide dendritic outgrowth [57]. It is worth noting that the list of known roles of Netrin signaling in dendritic morphogenesis is very limited in comparison to the extensive knowledge of Netrin signaling pathways in axon guidance. As mentioned above, this disparity can be attributed to the challenge of studying outgrowth of complex dendritic arbors as opposed to guidance of single unbranched axons. Advanced imaging techniques should facilitate the study of dendritic morphogenesis. This problem can also be addressed by studying neurons with dendritic arbors that are readily accessible to imaging studies. In the future it will be important to fill in the gap of knowledge about the role of guidance molecules in dendritic morphogenesis.

Downstream Signaling of Extracellular Ligands

There is an extensive body of literature that discusses the downstream effectors that are activated by axon guidance molecules; however I will only discuss those that are relevant to my studies. An overarching theme of these components is their ability to control the cytoskeleton in the growth cone (Figure 1.4) [68]. For example, in attraction Netrin activates downstream components that are thought to polymerize actin at the tip of the growing axon [68-70](Figure

1.4). UNC-34/Ena functions downstream of Netrin and interacts with actin capping proteins to enhance actin filament growth (Figure 1.4)[69-71]. UNC-34/Ena interacts with Trio, which has a specific domain that controls Rac activity in the cell [72](Figure 1.4). Rac, Rho and CDC42 are all small GTPase molecules that are tightly controlled during axon guidance to indirectly regulate the cytoskeleton[73, 74]. UNC-34/Ena also directly interacts with MIG-10/Lamellipodin (Lpd) and its localization in some contexts is dependent on MIG-10/Lpd [75, 76]. Interestingly, MIG-10/Lpd contains domains that allow it to interact with the membrane and thus has been proposed to localize actin-polymerizing components at sites of receptor activation [75-78]. Disruption of MIG-10 causes defects in lamellipodia advancement of growth cones[77]. MIG-10/Lpd and UNC-34/Ena are also thought to have independent functions because animals harboring mutations in each gene do not directly phenocopy each other [75, 77]. Fak and Src, cytosolic kinases, are thought to phosphorylate the receptors and potential downstream components. It has been proposed that FAK and SRC may promote key interactions between receptors and downstream proteins [79](Figure 1.4). Fak also interacts with N-WASP which can rearrange the branched cytoskeletal network in the growth cone [80](Figure 1.4). Thus, receptors control two populations of actin filaments in the growth cone during attraction: 1. Unbranched actin filaments via molecules such as UNC-34/Ena and 2. Branched actin networks comprised of Arp2/3 and N-WASP-like proteins (Figure 1.4).

Src also functions downstream of the repulsive Netrin receptor UNC-5 (Figure 1.4)[81]. UNC-34/Ena and MIG-10/Lpd are also required for axonal repulsion[75]. However, the mechanism of how actin-polymerizing components UNC-34/Ena and MIG-10/Lpd promote repulsion is not understood because repulsion was thought to be driven by actin depolymerization [82](Figure 1.4). Retrograde flow is also utilized to mediate axonal repulsion [83](Figure 1.4). Myosin proteins such as non-muscle myosin II have been shown to function in retrograde flow to induce axonal repulsion (Figure 1.4)[84, 85]. It is worth noting that despite the extensive body of literature that describes axonal attraction very little is known about the downstream components of repulsion and many outstanding questions remain. Moreover, though many proteins have been identified to be required for axon guidance, their direct link to the receptors and the cytoskeleton is not clear. A comprehensive understanding of how a receptor activates a downstream signaling pathway that directly interacts with the cytoskeleton will be important for the future.

Calcium (Ca^{++}) signaling has also been implicated in Netrin signaling[79]. Increased cytosolic Ca^{++} is correlated with Netrin-mediated attraction whereas decreased Ca^{++} is visualized in repulsion [86]. Cytosolic Ca^{++} increase is thought to activate downstream components such as Calcium/Calmodulin Kinase II, CamKII, which through an unknown mechanism controls the cytoskeleton [87]. However, since CamKII can regulate tubulin it has been proposed that Netrin signaling through CaMKII could control the growth cone via tubulin [88].

Neuronal Activity Regulates Dendritic Morphogenesis

Neuronal activity can also influence dendritic array morphology [89-92]. In mammals, neuronal activity may refine the overall architecture of the dendritic tree and shape specialized protrusions from the dendrites known as dendritic spines [4]. For example, activity is sufficient to induce dendritic spine formation in the vertebrate brain [93]. The affect of neuronal activity on dendritic morphogenesis is thought to depend on calcium influx that accompanies neuronal depolarization [93]. In *Drosophila*, neuronal activity also functions to shape dendritic arrays. This hypothesis is underscored by the analysis that mutants in *Drosophila* that increase neuronal excitability of motor neurons causes increased arbor size [89, 90]. The affect of neuronal activity on somatosensory neurons in the skin is not clear and will not be a significant focus of my thesis.

DENDRITIC SPACING

As discussed above, dendritic arbors can be shaped by diffusible cues that are derived from distant sources. Recent evidence suggests that local cues can also influence dendritic overlap. In the best-studied examples, these short-range cues are utilized to limit dendritic growth. The ability for sister dendrites from the same cell to avoid overlap is known as self-avoidance (Figure 1.5). In a related mechanism known as tiling, neurons that exercise similar sensory functions also avoid overlap. These dual mechanisms of self-avoidance and

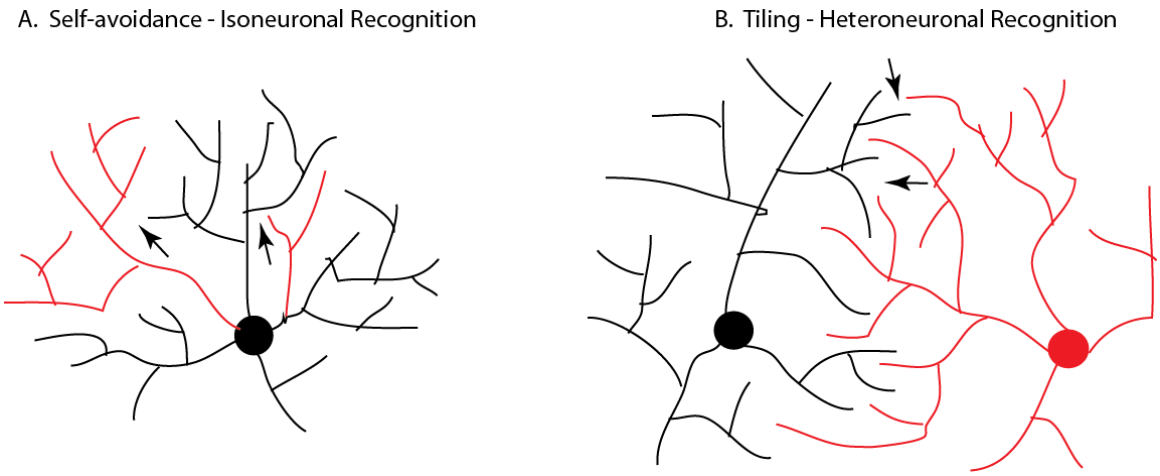

Figure 1.5. Dendrites non-redundantly cover the receptive area. A. Self-avoidance is defined as a phenomenon that ensures that sister dendrites (branches from the same cell) do not overlap. A neuron has multiple dendritic branches that extend from the cell soma (black circle) but do not overlap. For example, red dendrites do not overlap black dendrites. Arrows demarcate neurons that display self-avoidance (isoneuronal recognition) B. Tiling refers to a phenomenon in which dendrites from two neurons do not overlap. Tiling is typically observed for neurons that share common sensory modalities. As visualized, the red dendrites from the red neuron do not overlap with the black dendrites. Arrows denote points of avoidance between the two different neurons.

tiling are widely observed and thought to ensure that sensory neurons occupy unique receptive fields (Figure 1.5) [4].

Self-avoidance prevents dendrite overlap

Self-avoidance is a universally observed phenomenon but most of what we know about this process has been learned from studies in *Drosophila* sensory neurons [9, 21, 94-97]. It is important to note, however, that many other types of neurons display self-avoidance behavior. For example, early drawings of Ramon y Cajal illustrate complex dendritic trees from the vertebrate brain that display limited branch overlap (Figure 1.5) [7, 98]. Although the functional significance of dendritic avoidance has not been directly demonstrated, the observation of this phenomenon across phylogeny suggests it is important for proper function of the nervous system.

Down Syndrome Cell Adhesion Molecule (Dscam) was the first molecule shown to exercise a role in self-avoidance [99, 100]. Dscam is a membrane-bound Immunoglobin domain containing cell-adhesion molecule that exhibits homophilic binding activity [101]. In *Drosophila*, the genomic region of Dscam1 can express over 38,000 unique spliceforms through differential splicing [102]. Experiments that limit the number of potential spliceforms result in self-avoidance defects thereby suggesting that the diversity of Dscam spliceforms in the *Drosophila* nervous system is essential for dendrite organization [103]. Because the Dscam genomic region in *Drosophila* codes many various spliceforms of the protein it was thought that the Dscam protein could provide a simple model for

self-avoidance [99, 100, 103]. With potentially thousands of available Dscam isoforms for use, each neuron could distinguish itself from other neighboring cells with a unique combination of Dscam markers. Although this mechanism may be sufficient to explain self-avoidance in *Drosophila*, mammalian Dscam does not have multiple isoforms and thus could not provide a general solution for vertebrate self-avoidance [104]. In addition, Dscam mutants in mice do not seem to have self-avoidance errors like those observed in fly [104]. It is also worth noting that the Dscam protein is not present in some invertebrates that display self-avoidance. This therefore suggests that additional molecules must be utilized to achieve self-avoidance.

Another cell-surface Ig-domain-containing protein, Turtle has also been shown to mediate self-avoidance in flies [105]. Turtle functions independently of Dscam and therefore represents an independent signaling pathway for self-avoidance. Although the intracellular domain of Turtle is required for self-avoidance, cytoplasmic components for mediating a downstream signaling pathway that prevents sister dendrite overgrowth have not been identified [105]. Because of its role in the fly, the vertebrate homolog of Turtle is a good candidate for a vertebrate self-avoidance molecule. Interestingly, Turtle does not have multiple spliceforms like the Dscam molecule. How Turtle might mark the identity of sister dendrites to distinguish it from neighboring cells is an intriguing question.

Flamingo, a transmembrane protein with a cadherin domain, is also required to repress dendritic crossing in *Drosophila* sensory neurons. Flamingo functions in the planar cell polarity pathway (PCP). Components of the PCP

pathway (e.g.. Van Gogh, Furry, Tricorned) show genetic interactions with Flamingo in self-avoidance and are thus hypothesized to function with Flamingo in self-avoidance. In addition, the cytoplasmic domain of Flamingo interacts with Espinas, which is also essential for self-avoidance. However, the mechanism whereby these components regulate the rearrangement of the cytoskeleton to drive self-avoidance are not known [106].

It is worth noting that the crossing of dendrites in *Drosophila* was thought to occur in a two-dimensional space. However, recent evidence suggests that developing dendrites are not restricted to a two-dimensional plane but rather grow in three dimensions [107, 108]. Dendrites can be enclosed in membranes of the epidermis or can be located in a plane between the extracellular matrix and the epidermis. In this arrangement, not all dendrites that overlap actually contact each other. In fact, the Dscam mutant animal display overlapping branches that do not physically contact each other because they are enclosed in different epidermal plans suggesting Dscam may function in other aspects of dendritic development to ensure that dendrites grow in a restricted two-dimensional plane [108]. Interestingly, Integrins function in sensory neurons to prevent overlap by minimizing the occurrence of epidermal enclosures [107, 108]. Laminins derived from the epidermis are also thought to mediate attachment of dendrites to the extracellular matrix [107]. These studies underscore the importance of surrounding tissues to dendritic morphogenesis. In the future it will be important to understand the role of the epidermis in sensory neuron morphogenesis.

Turtle, Integrins and Flamingo do not have multiple spliceforms and thus are unlikely to be sufficient to drive self-avoidance in all neurons. As noted above, the multiple distinct isoforms produced from the Dscam locus could be sufficient for a neuron specific code in the nervous system but would not explain self-avoidance in the vertebrate brain, where there is a limited set of alternatively spliced Dscam proteins. Protocadherins that are expressed in multiple forms in the mammalian nervous system have been proposed to fulfill this role but this idea remains to be substantiated experimentally [109].

The mechanisms whereby these transmembrane receptors (i.e. Dscam, Turtle, Flamingo) rearrange the dendritic branch to prevent overlap are also poorly understood. The cytoplasmic domains of both Dscam and Turtle are required for self-avoidance suggesting they activate some downstream effectors [99, 105]. However, the downstream components in these pathways have remained a mystery. Recently, the cytoplasmic proteins, Tricorned and Furry have been identified to function in self-avoidance; however they may function more to ensure dendritic attachment to the epidermis [107, 110, 111]. It will be important to identify cytosolic proteins that function with self-avoidance receptors in order to understand the mechanisms of self-avoidance.

Tiling prevents overlapping cells

Both tiling and self-avoidance are utilized to limit dendritic branch overlap [4]. Dscam and Turtle are dispensable for tiling [99, 105]. The seven-transmembrane-pass Cadherin protein Flamingo, however, has been shown to

restrict growth of dendritic arrays in both tiling and self-avoidance [9, 10, 112, 113]. In late stages Flamingo functions to prevent heteroneuronal dendritic overlap [10, 113, 114]. Tropomyosin, a protein that genetically interacts with flamingo, also shows overlap phenotypes [115]. The role of Flamingo may be conserved in mammals as overlap can be seen in cultured rat neurons when the seven-transmembrane-pass protein Cadherins, Celsr2 and Celsr3, are reduced. Celsr2 binds homophilically to induce Ca^{++} influx [116]. However, the downstream signaling that is activated by the Ca^{++} transient has not been identified.

In *Drosophila,* Tricornered and Furry are also required for tiling [110, 111]. This role is conserved in nematodes as mutations in *sax-1/trc* or *sax-2/fry* also cause overlapping neuronal branches in *C. elegans* [117]. Interestingly in *Drosophila*, Hippo, a Ste20 family kinase protein that functions in tissue growth size has been shown to function in tiling. Mutants of Hippo genetically interact with Tricornered suggesting that Tricornered may function downstream of Hippo signaling to prevent overlap [111]. The dual role of these cytosolic proteins in tiling and self-avoidance may indicate that downstream signaling could be similar in heterodendritic and homodendritic repulsion and that the difference between recognizing self from non-self may require specific receptors.

HOW THE ANIMAL SENSES ITS ENVIRONMENT

C. elegans mechanosensitive circuit

In *C. elegans*, light touch evokes a behavioral response; contact with the tip of an eyelash evokes rapid movement away from the stimulus [118-120]. This observation led to the hypothesis that *C. elegans* must possess a mechanosensitive network that controls motor movement. This light touch behavior is mediated by six mechanosensitive touch neurons (Figure 1.2, 1.6)[118, 120]. Four of these sensory neurons are generated embryonically (PLMR, PLML, ALMR, ALML) and two develop later during larval development (AVM and PVM) [119]. All six light touch neurons display simple unbranched neuronal morphologies [121]. Light touch mechanosensation requires a specific DEG/ENac channel that is thought to be activated when the animal is touched [118, 122].

It was also observed that *C. elegans* responds differently to light touch with an eyelash vs. harsh touch with a metal prod. Two pairs of sensory neurons, FLP and PVD, mediate this harsh touch response in *C. elegans* (Figure 1.6, 1.7) [123, 124]. The FLP neurons are located in the head and produce dendritic branches that envelop the animal on the left and right side (Figure 1.2, 1.7) [125]. PVD displays dendrites that cover the animal from the tail to the posterior border of the head [11, 125-127]. Both PVD and FLP are polymodal. For example, PVD responds to harsh touch, cold temperature and hyperosmolarity (see Chapter 2). FLP responds to harsh touch and robust

increases in temperature [124]. Thus, although they have similar dendritic patterns the harsh touch neurons have different polymodal characteristics.

Because the *C. elegans* nervous system has been reconstructed by electron microscopy it has been possible to identify the synaptic partners of these mechanosenstive neurons (Figure 1.6) [121]. This has provided researchers with invaluable information to understand the entire touch circuit from the stimulation of the sensory neuron to the eventual control of muscle cells by excitatory or inhibitory neurons and thus allows researcher to determine the consequence of disrupting a particular portion of mechanosensation to animal behavior (Figure 1.6). For example, PVD synapses with two interneurons, AVA that mediates forward movement and PVC, which mediates backward movement. Stimulation of PVD normally forces the animal to move forward; however when PVC is ablated the nematodes behavioral response changes to backward movement [128].

Drosophila touch-sensing neurons

As discussed above each abdominal segment of *Drosophila* includes 44 sensory neurons with varying levels of dendritic complexity and function. Flies respond to touch through specialized sensory bristles that cover the cuticle [129, 130]. Each sensory bristle contains a ciliated sensory neuron (type I neuron) that responds to displacement of the bristle. These type I sensory neurons resemble ciliated neurons that are present in the *C. elegans* head and the vertebrate ear [129]. Type I neurons are also thought to function as proprioceptors [131].

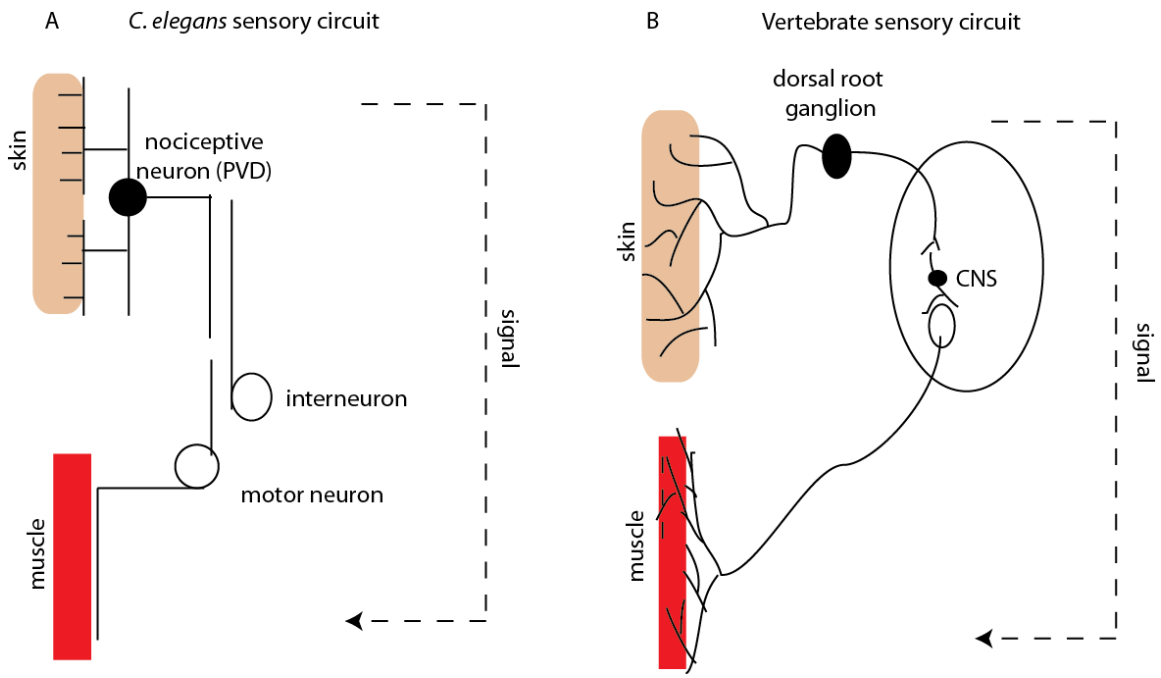

Figure 1.6 Sensory circuits are similar across phylogeny. A, The *C. elegans* sensory circuit. Nociceptive neurons sense stimulus on the skin. Information travels from the nociceptive neuron through the interneuron to the motor neuron. The motor neuron then activates the body muscle which drive movement. B, A similar circuit is observed in vertebrates. Dorsal root ganglion neurons sense stimulus in the skin and send information into the nerve cord in the central nervous system. Interneurons send information to the brain or directly to motor neuron in the spinal cord which stimulates the muscle at the neuromuscular junction. In each case, the neuronal signal travels from the skin to the muscle through a series of neurons.

Drosophila also have unciliated sensory neurons (type II neurons) that display naked dendritic arrays (i.e. unmyelinated). These respond to a myriad of sensory stimuli (Figure 1.3, 1.7) [9, 10, 132]. *Drosophila* sensory neurons innervate the area just below the cuticle [9, 10]. For example class IV neurons, which display complex dendritic trees reminiscent of the *C. elegans* PVD and FLP neuron, function as polymodal nociceptors that respond to noxious heat and harsh mechanical force [133-135]. This function requires Pickpocket, a Deg/ENac channel [133]. The specific sensory modality of other *Drosophila* sensory neurons is not well understood. It seems likely that future studies will reveal the modalities that correspond to the different dendritic patterns.

Vertebrate sensory cells

Vertebrate animals, such as zebrafish respond to mechanical stimulus as early as 21 hours post fertilization [136, 137]. Rohon Beard neurons are utilized early in development of zebrafish and *Xenopus* to respond to external stimulus [138]. These neurons display morphological characteristics that resemble *Drosophila* and *C. elegans* sensory dendritic arrays (Figure 1.7) [96, 139, 140]. Rohon Beard neurons have also been described in humans [141, 142]. Interestingly, Rohon Beard cells undergo programmed cell death during development and are replaced by cells of the mature somatosensory network [143, 144].

The cell bodies of somatosensory neurons in mature vertebrates are located in the dorsal root ganglion [145]. The cell bodies display bipolar

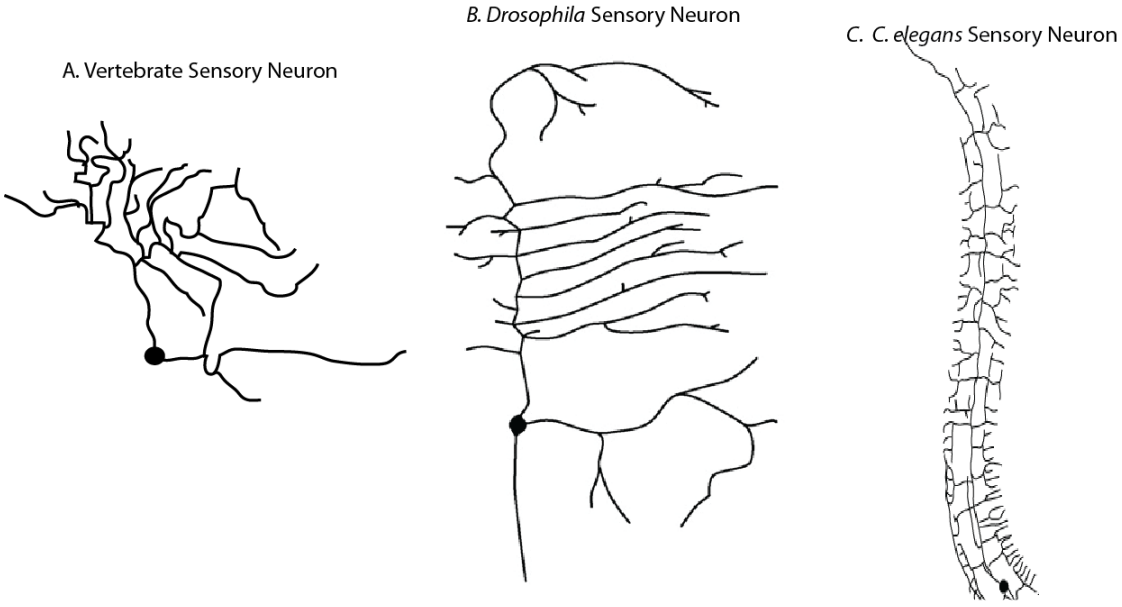

Figure 1.7. Sensory neurons across phylogeny adopt similar morphologies. A. Tracings of a vertebrate trigeminal sensory neuron (adapted from Sagasti et. al. 2005) showing a large dendritic array with limited overlap. B. Tracing of *Drosophila* sensory neuron type III md neuron (Gao et. al. 2007) also has no overlap. C. The *C. elegans* sensory neuron PVD has a large array that non-redundantly covers the receptive area.

morphology with one axon that targets the periphery to innervate the skin and another axon that travels toward the spinal cord and connects with the central nervous system (Figure 1.6). The axon that innervates the skin receives signals from the environment and sends an electrical signal through the cell body to the axon that connects with the central nervous system (Figure 1.6)[146]. Thus, the peripheral sensory neuron process in the skin functions similar to a dendrite in that it receives signal.

The vertebrate somatosensory system possesses a remarkable ability to distinguish multiple different environmental stimuli. Lanceolate endings, Meissner's corpuscles, pacinian corpuscles and Merkel cell-neurite complexes are all specialized sensory organs that detect specific modalities. For example Lanceolate endings sense hair movement whereas Meisnner's corpuscles react to vibration to classify textural information [131]. Each of these sensory organs are closely associated with a specific nerve fibre, (*e.g.* sensory afferent) that sends sensory information to the central nervous system.

Afferent fibers are classified in three groups by the speed of their action potential propagation, which is determined by myelin thickness. A β afferents have the thickest myelin sheath and have low mechanical thresholds. These A β neurons likely represent light touch neurons. A δ neurons are thinly myelinated and function as nociceptors. Lastly, C-fibers are unmyelinated nociceptors. Both A δ and C fibers respond to high mechanical thresholds. The nociceptive fibers display large dendritic arrays that have free endings (*e.g.* unmyelinated endings) in the skin [147](Figure 1.6). The morphology of these single dendritic

arrays is difficult to visualize because of the lack of techniques to label single vertebrate cells. However, recent studies using a mosaic technique to mark single zebrafish somatosensory neurons shows that these free ending fibers have many attributes similar to those seen in less complex organisms [96, 139]. In zebrafish, these neurons occupy distinct spatial domains and thus do not overlap. Both heteroneuronal and isoneuronal repulsion can be observed in developing neurons (Figure 1.5) [96]. The conservation of these phenomena across phylogeny is significant and provides strong rationale for using simple organisms like *C. elegans* and *Drosophila* for studies of somatosensory dendritic development.

Thus sensory circuits across phylogeny share key conserved attributes:

1. Specialized neurons for specific modalities
2. Neurons with complex dendritic arrays that innervate the skin.
3. Somatosensory neurons that control animal behavior

Though sensory circuits share common attributes, the development and maturation of these circuits is largely unknown. My thesis addresses these conserved concepts in *C. elegans*. The *C. elegans* nociceptor, PVD, displays many characteristics typical of sensory neurons in vertebrates. Chapter 2 defines the morphological characteristics of PVD that are shared with sensory neurons across phylogeny and also describes the first detailed characterization of the development of its complex dendritic array that innervates the skin.

Chapter 2 provides a foundation for future work utilizing PVD to study dendritic development. Chapter 3 discusses a novel transcriptional program that is utilized to generate diversity in the somatosensory circuit so the animal can respond with the appropriate behavior to environmental stimuli. Lastly, Chapters 4-6 address the extrinsic signaling factors that pattern the PVD dendritic array. These Chapters discuss the surprising finding that a diffusible molecule controls a contact-dependent event and addresses how an axon guidance molecule can function in different aspects of dendritic development by initiating distinctive downstream pathways. Together, my work identifies a combination of intrinsic transcriptional codes as well as extrinsic signaling pathways that are utilized to generate a specific nociceptive neuron.

CHAPTER II

TIME-LAPSE IMAGING AND CELL-SPECIFIC EXPRESSION PROFILING IDENTIFY DYNAMIC PROCESSES AND MOLECULAR DETERMINANTS OF A MULTI-DENDRITIC NOCICEPTER IN *C. ELEGANS*

INTRODUCTION

Somatosensory neurons detect external stimuli such as touch and temperature. The nociceptor class of somatosensory neurons responds to noxious stimuli to trigger the sensation of pain and to evoke aversive behavior. Nociceptors typically display a complex, highly branched arbor of dendritic processes directly beneath the skin. As discussed in the Introduction, this feature of nociceptor architecture has been widely observed in both vertebrate and invertebrate organisms and thus is likely to reflect fundamental, conserved mechanisms of development and function [134, 148, 149].

Different classes of sensory neurons are distinguished by the size and branching complexity of their dendritic arbors. Recent studies have shown that these differences in dendritic architecture are subject to transcriptional control [13, 14, 16, 18, 20]. The general importance of transcriptional control in dendritic morphogenesis is underscored by a recent study in which a genome-wide RNAi screen identified > 75 transcription factors with roles in somatosensory neuron architecture [13]. It is noteworthy that homologs of many of these transcription

factors are expressed in vertebrate neurons [6, 150]. Moreover, studies of mammalian neurons in culture have shown that different classes of neurons maintain their distinctive morphologies *in vitro* suggesting in some cases dendritic morphology is driven strictly by cell intrinsic determinants and not dependent on extrinsic signaling components[151, 152]. Together these findings are indicative of evolutionarily conserved genetic programs that drive intrinsic pathways of neuronal differentiation [153].

Studies in the nematode *C. elegans* have identified specific nociceptive neurons that mediate avoidance responses to mechanical force, temperature or noxious molecules[122, 154, 155]. Although this repertoire of sensory modalities parallels that of vertebrate nociceptors, *C. elegans* nociceptive neurons typically adopt a much simpler architecture with little or no dendritic branching [121]. A striking exception to this difference was described in recent reports showing that the *C. elegans* PVD neuron displays a large and highly branched dendritic arbor directly beneath the hypodermal “skin” that envelops the worm [11, 125-127]. The occurrence of this elaborate subdermal array of PVD dendritic branches is also consistent with an earlier finding that PVD mediates an avoidance response to the application of harsh mechanical force to the external surface of the animal [123]. Here we use live imaging studies with a bright PVD-expressed GFP reporter gene to provide a comprehensive description of PVD anatomy. We suggest a simple classification scheme for PVD dendritic branches and use time-lapse imaging to describe their emergent morphology and the developmental timing of each branching decision. We find that subsets of PVD branches

fasciculate with an underlying network of peripheral nerve cords, which are likely sources of local guidance cues. Time-lapse imaging also revealed that PVD dendritic morphology is sculpted by striking examples of self-avoidance. To identify genes with potential roles in PVD differentiation or function, we utilized a cell specific microarray profiling strategy to catalog PVD genes [156, 157]. This approach revealed > 2,000 highly expressed genes encoding a wide array of proteins of different molecular classes. To illustrate the utility of this data set, we used RNAi knockdown or genetic mutants of 86 transcription factors from this list and identified eleven genes that control PVD dendritic architecture. Thus, this report firmly establishes the PVD neuron as a useful model for nociceptor development and provides a detailed anatomical and molecular foundation for future studies of nociceptor morphogenesis and function that exploit the simplicity and genetic utility of *C. elegans* biology.

METHODS

Nematode Strains and Genetics

The wild-type *C. elegans* Bristol strain N2 was used for all experiments and cultured as previously described [158]. Also used in this study were mutants: CZ2485 *ahr-1 (ju145),* FX00321 *ceh-38 (tm321),* FX00237 *ceh-48 (tm237),* MT2246 *egl-43 (n1079),* MT2247 *egl-44 (n1080),* MT2243 *egl-46 (n1076),* GR1373 *eri-1 (mg366),* VC349 *lim-9 (gk210),* CB1338 *mec-3 (e1338),* CB845 *unc-30 (e191),* CB1416 *unc-86 (e1416),* RB774 *zfp-1 (ok554),* VH4 *zag-1*

(rh315); rhIs4. The following transgenic strains were used: NC1733 (*otIs173, F25B3.3::*dsred; *wdIs52, F49H12.4::*gfp + *unc-119*), NC1686 *(wdIs51, F49H12.4::GFP* + *unc119), NC1687* (*wdIs52, F49H12.4*::gfp + unc119), NC1841 (*wdIs52, F49H12.4::*gfp; *rwIs1*, *pmec-7::*RFP), NC1908 (*wdEx240, myo-3::dsRed; wdIs52, F49H12.4::gfp*)

GFP reporter strains for transcripts enriched in the PVD/OLL data set were obtained from the British Columbia *C. elegans* Gene Expression Consortium and are listed in Table 2.2. Some of the nematode strains were provided by the *Caenorhabditis Genetics* Center, which is funded by the NIH National Center for Research Resources (NCRR). All studies in this work used *C. elegans* hermaphrodites.

Confocal Microscopy

Nematodes were immobilized with 15 mM levamisole on a 2% agarose pad in M9 buffer. Images were obtained in a Leica TCS SP5 confocal microscope. Z-stacks were collected with either 40X (1 um/step) or 63X (0.75 um/step) objectives; single plane projections were generated with Leica Application Suite Advanced Fluorescence software.

Time-Lapse Imaging

Nematodes were immobilized with a 15 mM levamisole/0.05% tricaine mix on a 2% agarose pad, all of which was diluted with M9 buffer. Slides were sealed with 1:1 vasoline/paraplast tissue embedding medium [159]. For each

time point, the 40X or 63X objective was used to collect a Z-stack (0.75 um/step) spanning the focal depth of the PVD neuron and its dendritic branches. Dendritic branch outgrowth at each time point was evaluated from a Z-projection. Larval stages were identified from morphological features: L2 (postdeirid) [119]; L3, L4, and young adult (vulval development) [160]. In some cases, gut autofluorescence was removed through subtraction of background autofluorescence. The 488 nm laser was used to excite the sample. Signal was collected both in the GFP range (500 nm-552 nm) and from 568 nm-667 nm. Leica Application Suite Advanced Fluorescence software was used to subtract out the gut autofluorescence (collected from 568 nm-667 nm) from the GFP channel.

At least three independent movies verified each example of dynamic dendritic growth described in this report.

PVD expression profiling

The 1.6 kb *ser-2*prom3B promoter fragment was amplified from genomic DNA using the primers: *ser-2*prom3-sal-1 (5'-CGAAACGCTGTCGACTTCAACTGTAGGCG-3') and *ser-2*prom3-p2b (5'-GGTACCGTTGTGATGTCACAAAAATATGCC-3') adding a KpnI site to the 3' end [11]. The resultant PCR product was cloned into pCR2.1-TOPO to generate the plasmid pWCS5 (Invitrogen). pWCS5 and the 3X::FLAG::PAB-1 plasmid pSV15 were digested with BamHI and KpnI and ligated to generate the *ser-2*prom3B::3XFLAG::PAB-1 mRNA-tagging construct pWCS8 [161]. The transgenic line, NC221, was obtained by co-bombardment of pWCS8 with the co-

selectable marker *unc-119*(+) minigene plasmid (MM051) [162]. PVD and OLL expression of 3X FLAG was confirmed by immunostaining. PVD transcripts were obtained from synchronized L3-L4 larvae by the mRNA tagging strategy [157]. A reference RNA sample was obtained from total L3-L4 larval cells. Samples were prepared in triplicate and RNA (25ng) amplified by the WT-Pico method [163], labeled and hybridized to the Affymetrix Gene Chip array. Data sets were normalized by RMA and transcripts showing relative PVD enrichment ($\geq$ 1.5 X) vs the reference sample were identified by SAM analysis (False Discovery Rate, FDR < 1%) as described [164]. Expressed Genes (EGs) were estimated as previously described [157].

RNAi screen for PVD morphological defects

eri-1 (mg366); wdIs52 animals were used for RNAi transcription factor screening. Bacterial clones from an RNAi library [165] were grown overnight at 37C. 200 ul of overnight culture was seeded to beta-lactose NGM-lite plates [166]. The plates were incubated at room temperature for 3 days for induction of dsRNA expression. L4 larval stage hermaphrodites were picked to the RNAi plates and grown at 21C until the F1 progeny were at the L4 larval stage. F1 progeny at the L4 larval stage were mounted on slides as above and viewed in a Zeiss Axiovert 200M microscope. $\geq$20 hermaphrodites were screened for each RNAi clone. A clone that disrupted PVD morphology in > 1 animal in each of three independent screenings was considered a positive hit. RNAi clones with effects on PVD morphology were confirmed by DNA sequencing. Mutants for

specific transcription factors were crossed into the PVD::GFP strain *NC1687* and examined as adults for PVD defects (Table 2.2). Mutant alleles of *dpl-1* (sterile), a*ft-2*, and *thoc-2* (sterile/lethal) were not examined.

Distance measurements.

Measurements were taken from a collapsed z-stack. ImageJ was used to draw a line and pixel distance of this line was measured. In each case, a 15 um scale was used to convert pixel distance to um. The distance between two adjacent 2^{O} branches was taken at the base of the branch where it connected with the 1^{O} branch. Similarly, 4^{O} branch distance was determined at the base at the point of intersection with the 3^{O} branch.

Hypergeometric calculation for data files published in Smith and Watson et. al 2010.

The hypergeometric test was used to test for overrepresentation of nociceptor genes in the PVD enriched gene data set (http://elegans.uky.edu/MA/progs/overlap_stats.html).

RESULTS

PVD displays a net-like array of dendritic branches that envelops the animal

C. elegans contains two PVD neurons (PVDL and PVDR), one on each side of the adult animal. Both PVD neurons are generated post-embryonically during the L2 larval stage from an ectodermal precursor cell (V5). The PVD cell body is located in a posterior-lateral sensory organ (postdeirid) that also includes other V5-derived cells [119]. Reconstruction of the *C. elegans* nervous system from electron micrographs (EM) of serial sections suggested a relatively simple PVD architecture comprised of elongated, unbranched lateral processes projecting from anterior and posterior sides of each PVD soma and a single axon that grows downward to enter the ventral nerve cord [121]. However, images of PVD obtained in the light microscope after immunostaining for a PVD-expressed membrane receptor [126, 127, 167] or with a PVD-specific GFP reporter revealed a much more elaborate morphology with many additional dendritic branches[168]. Here we have used a bright PVD::GFP marker (*F49H12.4::*GFP)[163] (Figure 2.1) to reveal that PVD architecture is defined by a complex but well-ordered array of non-overlapping sister dendrites and that the creation of this structure involves a stereotypical series of branching decisions. The single PVD axon projects downward from the PVD cell body to join the ventral nerve cord. Dendritic branching, however, is much more elaborate. A 1^{O} dendritic branch extends from the PVD cell soma along the anterior/posterior

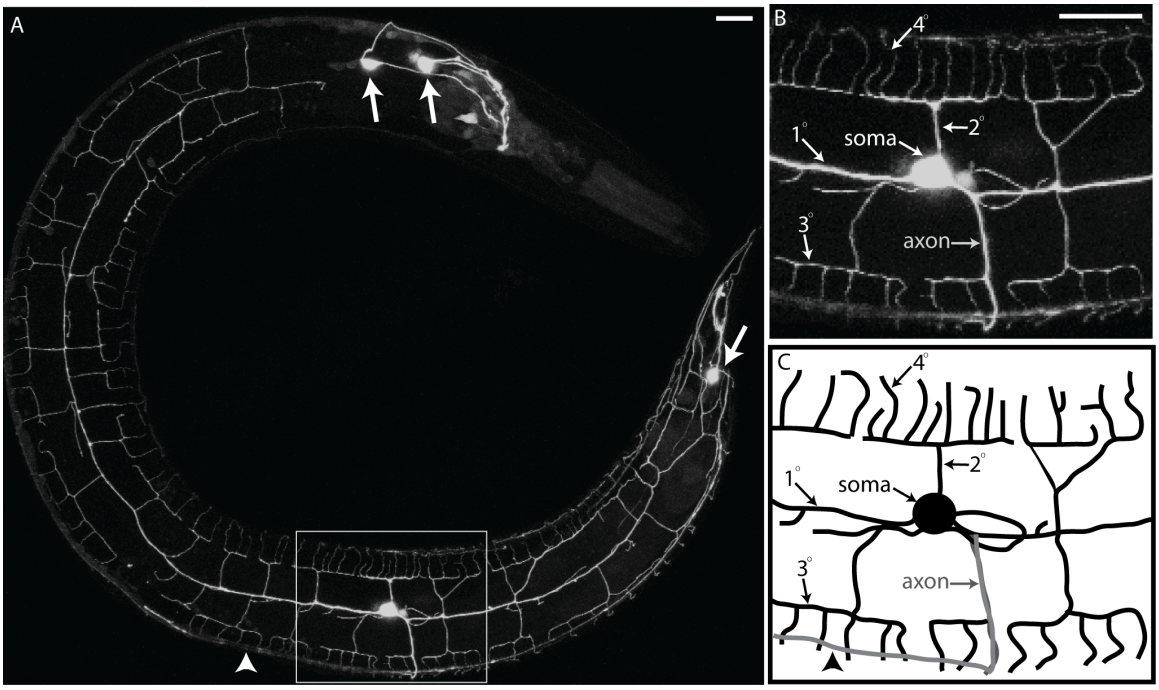

Figure 2.1. PVD displays an elaborate dendritic arbor that envelops the animal in a net-like array. (A). Confocal image of an adult worm (anterior to left, ventral to bottom) showing the PVD::GFP marker (arrows denotes other neurons in head and tail that express GFP). Insets show more highly magnified image (B) and schematic tracing (C) of region surrounding PVD soma. Note dendritic branches (1^O, 2^O, 3^O, and 4^O) and single ventrally projecting axon (arrowhead denotes location of ventral nerve cord). Scale bar is 15 um.

(A/P) axis at the location of the lateral nerve fascicle (Figure 2.1B,C). Orthogonal arrays of 2^{O}, 3^{O}, and 4^{O} dendritic branches envelop the animal along the dorsal/ventral (D/V) and anterior/posterior (A/P) axes to produce a network of sensory processes. A single 2^{O} branch can be seen as the "stem" for a "menorah-like" collection of 3^{O} ("base") and 4^{O} ("candles") branches (Figure 2.1B,C). A mature PVD (adult stage, see below) exhibits ~38 menorah-like structures (Table 2.1). This web-like dendritic architecture is stereotypic of a wild-type PVD neuron.

FLP sensory neurons in the head adopt a dendritic morphology similar to PVD

We first characterized the posterior and anterior reach of the PVD dendritic array. PVD processes extend posteriorly into the tail. In the head region, however, PVD terminates near the base of the pharynx (Figure 2.1A). We have established that this location corresponds to the posterior reach of two bilaterally symmetric sensory neurons, FLP (L + R)[121]. Interestingly, FLP neurons show a dendritic architecture that is strikingly similar to that of PVD with prominent menorah-like structures located along the sub-lateral nerve cords (Figure 2.2B). By examining animals co-expressing dsRed (FLP) and GFP (PVD) markers, we established that FLP and PVD dendritic branches rarely overlap (Figure 2.2C, inset). This "tiling" effect is characteristic of functionally related sensory neurons in other species and ensures efficient coverage of the receptive field [169]. The similar dendritic branching patterns and distinct receptive fields

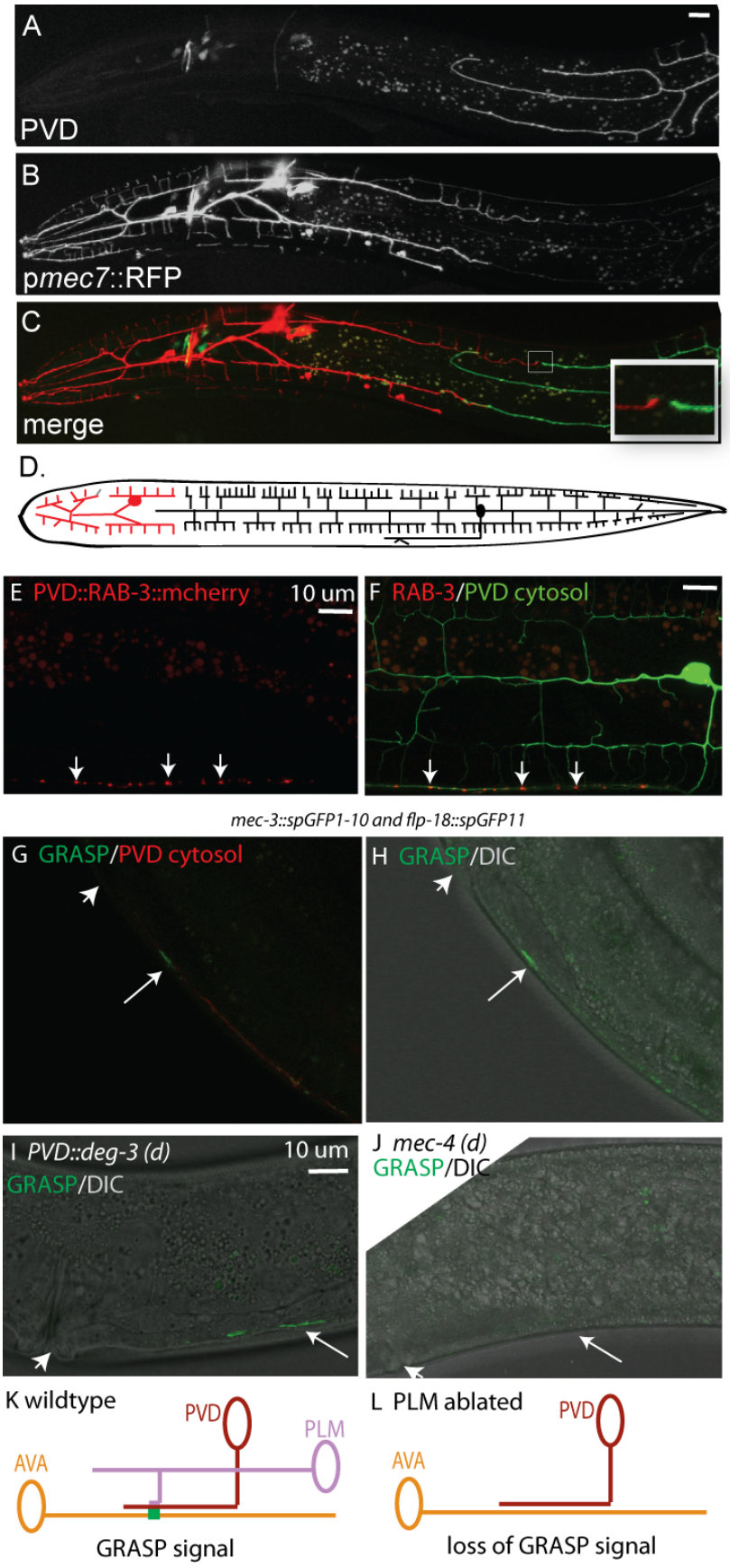
A
PVD
B
pmec7::RFP
C
merge
D.
E PVD::RAB-3::mcherry
10 um
F RAB-3/PVD cytosol
mec-3::spGFP1-10 and flp-18::spGFP11
G GRASP/PVD cytosol
H GRASP/DIC
I PVD::deg-3 (d)
GRASP/DIC
10 um
J mec-4 (d)
GRASP/DIC
K wildtype
PVD
PLM
AVA
GRASP signal
L PLM ablated
PVD
AVA
loss of GRASP signal

Figure 2.2. PVD dendrites tile with FLP dendritic branches in the anterior and the PVD axon has specific synaptic connectivity. Lateral view of adult from left side (anterior to left, ventral to bottom). PVD::GFP (A) with FLP neuron marker, p*mec-7*::RFP, (B) and merged image (C) demonstrate that PVD dendritic branches (green) do not overlap with FLP (red) in the anterior (inset). Schematic showing that PVD and FLP envelop the animal with similar dendritic branching patterns (D). Scale bar is 15 um in A-C. Lateral view of adult from left side, PVD::RAB-3::mcherry (F) and merged with PVD::GFP (F) show PVD synapses only in axonal region in ventral nerve cord. Arrows indicate RAB-3 puncta in the PVD axon. (G-J) GRASP *mec-3::spGFP1-10* and *flp-18::spGFP11* constructs show reconstitution of GFP (green signal) across *mec-3* expressing cells and AVA in wildtype (G,H), animals that do not have PVD (I) and animals that lack touch neurons (J). Note that GRASP signal is not present when touch neurons are ablated (J). Arrowheads indicate vulva. Arrows indicate GRASP signal. (K,L) Summary of GRASP data showing *mec-3* and *flp-18* construct mark specific synapse between AVA and PLM.

for each neuron (Figure 2.2D), are consistent with evidence that FLP and PVD function as nociceptive neurons [124, 125, 170].

PVD branches innervate the area between the muscle and hypodermis

Somatosensory neurons across phylogeny innervate the area between the muscle and the skin of the animal [140]. To determine if PVD also is located in this area we used confocal microscopy to visualize the location of PVD branches compared to the muscle cells. Using PVD::GFP to mark PVD dendrites and *myo-3*::Dsred to mark muscle cells we confirmed that PVD dendrites are located between the hypodermis and the muscle (Figure 2.4). These results were later confirmed by our collaborator with electron microscopy [125]. Thus, similar to their mammalian counterparts, PVD nociceptive dendrites innervate the area just below the skin of the animal.

The synaptic connectivity of PVD and other sensory neurons

The EM reconstruction of the *C. elegans* nervous system showed that the PVD axon projected into the ventral nerve cord and forms synaptic connections with AVA and PVC. To confirm these observations we first determined where synapses were present in PVD. To characterize the location of PVD synapses we visualized the localization of the synaptic protein, RAB-3. Consistent with the EM analysis, RAB-3 synapses were only present in the PVD axon in the ventral nerve cord and were not visualized in the dendritic branches (Figure 2.2E,F). To determine the synaptic connectivity of PVD we first visualized the synaptic

Table 2.1 PVD 2^{o} branches fasciculate with motor neuron commissures. A higher fraction of PVDR 2^{o} branches fasciulate with motor neuron commissures than PVDL 2^{o} branches. The average numbers of dorsal vs ventral menorahs are statistically different. A students t-test was used to detect statistically significant differences. Motor neuron commissures were visualized with the panneural reporter (*F25B3.3::*dsred) and scored for fasciculation with PVD (marked with PVD::GFP) in the ventral nerve cord between the retrovesicular ganglion (RVG) at the anterior end and the preanal ganglion (PAG) at the posterior end. n=20 animals

	PVDL	PVDR	PVD avg.
Dorsal 2^{o} branches	19.2 ± 3.0	23.1 ± 1.9	21.8 + 3.2
Ventral 2^{o} branches	15.8 ± 2.9	19.5 ± 2.7	17.1 + 2.9
Total 2^{o} branches	35.0 ± 4.7	42.6 ± 2.6	38.9 + 5.4
motor neuron commissures (White et al, 1986)	7	27	
Dorsal 2^{o} branches that fasciculate with commissures:	15%	45%	24%
Ventral 2^{o} branches that fasciculate with commissures:	12%	41%	21%
Average number of D/V 2^{o} branches that fasciculate with commissures	12%	42%	23%

P < 0.005 PVDL vs PVDR 2^{o} branches
P < 0.001 dorsal vs. ventral 2^{o} branches
P < 0.001 PVDL vs PVDR 2^{o} branch fasciculation

connection of PVD and AVA with GPF Reconstitution Across Synaptic Partners (GRASP). To do this, we expressed *spGFP1-10* with the PVD promoter *F49H12.4* and *spGFP11* in AVA with the *flp-18* promoter. Unfortunately, we did not visualize specific puncta in the PVD axonal region in this strain (data not shown). Next, Clay Spencer generated a line that expressed *spGFP1-10* in PVD, PVC and FLP with the *des-2* promoter and *spGFP11* in AVA with the *flp-18* promoter. The combination of these two constructs generated specific GFP intensity along the entire ventral nerve cord. Intensity increased around the PVD axonal region suggesting PVD connected with AVA (data not shown). Lastly we generated a line that expressed *spGFP1-10* with the *mec-3* promoter to label mechanosensitive neuron synpases (PVD, FLP, PLML/R, ALML/R, PVM, AVM) and *spGFP11* in AVA with *flp-18*. This line displayed specific GFP intensity in a small region of the PVD axonal domain just posterior to the vulva (Figure 2.2G,H,K). However, this region also corresponded with the synaptic region of PLML/R and AVA. To rule out that the GFP intensity was specific to the PVD/AVA synapse we selectively ablated PVD using a transgene that drove expression of a dominant ion channel specifically in PVD and still visualized GFP intensity (Figure 2.2I). We confirmed that the GFP intensity was specific to the PLML/R-AVA synapse by specifically ablating sensory neurons with a *mec-4* dominant mutant; GFP intensity was lost in the *mec-4* dominant background (Figure 2.2J,L). These experiments, however, should be analyzed with caution since non-specific GFP intensity was visualized throughout the entire cell in which it was being expressed. Non-specific GFP intensity appears to be a

caveat of these experiments since others have also observed non-specific fluorescent signals in other spGFP strains (see Rachel Skelton dissertation)

PVD dendrites fasciculate with pre-existing neuronal tracks

The predictable architecture of PVD processes is suggestive of distinct landmarks that determine the location of dendritic branches. To test this idea, we used a panneural reporter to mark neurons (CAN, ALA) in the lateral nerve cord. Dual color imaging of the DsRed panneural and PVD::GFP markers confirmed that PVD 1^0 branches are closely apposed to the lateral nerve cord as previously observed by EM reconstruction (Figure 2.3D,H,L) [121].

The panneural reporter also revealed that some PVD 2^O branches fasciculate with motor neuron commissures (Figure 2.3A-L)[12]. Motor neuron commissures extend around the circumference from the ventral to dorsal sides. These commissural processes are located directly beneath the hypodermis and course over the top of body muscle quadrants on dorsal and ventral sides (Figure 2.3E-H)[121]. Confocal imaging indicates that PVD 2^O branches are also located in this subdermal region and that a significant fraction of PVD 2^O branches fasciculate with motor neuron commissures (Figure 2.3A-C, 2.3E-G, 2.3I-K) (Table 2.1). The left and right sides contain unequal numbers of motor neuron commissures with 7 on the left and 27 on the right [121]. This asymmetry is also reflected in the fraction of PVD secondary branches that fasciculate with motor neuron commissures which is greater on the right (43%) than on the left (14%) (Table 2.1). This result shows that the frequency of 2^O branch fasciculation is

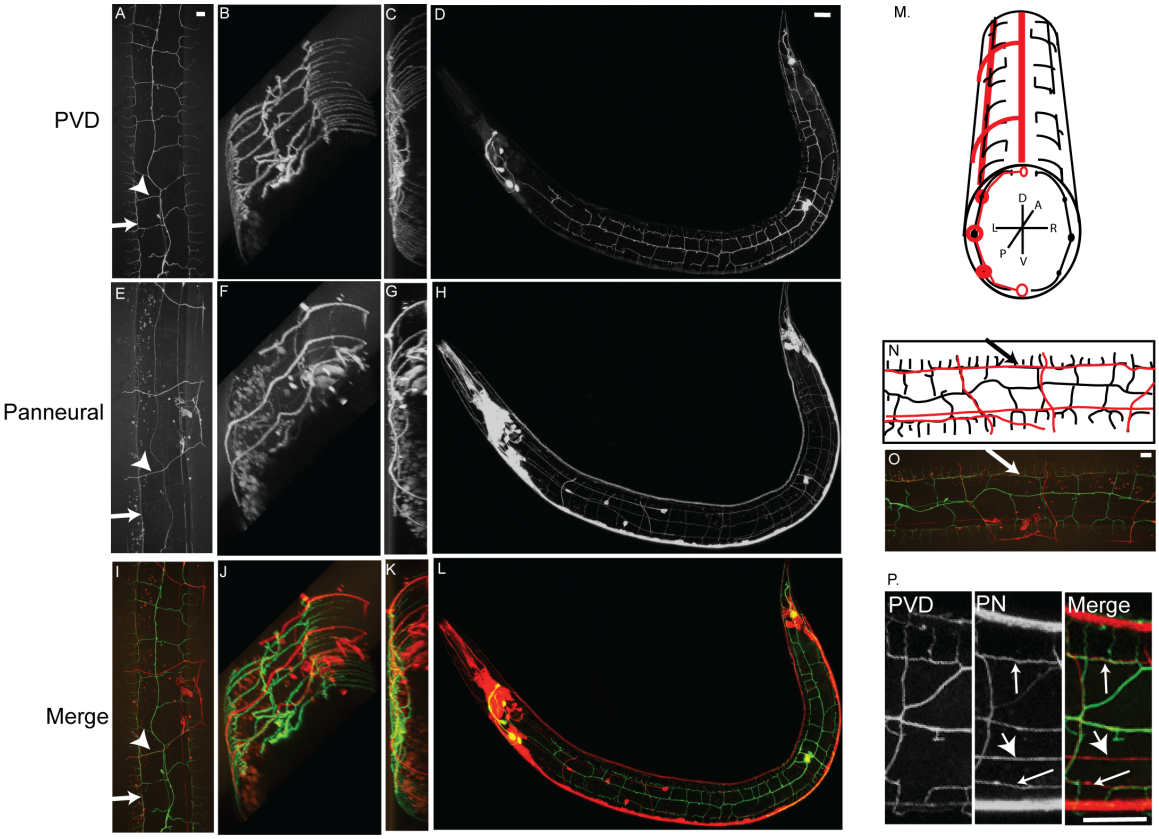

Figure 2.3. PVD branches fasciculate with motor neuron commissures and sub-lateral nerve cords Confocal images of PVD::GFP marker (A-D,P), panneural::dsRed (E-H,P) and merged reporters (I-L,O,P) show PVD dendritic branches, motor neuron commissures (arrow head) and sub-lateral nerve cords (arrow). PVD secondary branches lie in the same plane as motor neuron commissures as shown in rotated Z-stack from PVDR [(B,F,J)(rotated 55^{O} on the X-axis and 45^{O} on the y-axis)]. Rotated Z-stack of left side (ventral up) shows circumferential 4^{O} branches [(C,G,K (rotated 80^{O} on X-axis and 90^{O} on Y-axis)]. PVD 3^{O} branches fasciculate with dorsal and ventral sublateral nerve cords (D,H,L,O)(anterior left, ventral down). Schematic transverse section (M) shows PVD (L+R) (black) and fasciculation of some 2^{O} branches (left) but not others (right) with motor neuron commissures (red). Lateral view of PVDR (N,O) showing 3^{O} branches fasciculated with sub-lateral nerve chords (arrow). PVDR fasciculates with processes in the sub-lateral nerve cords (P, arrow) but does not contact the touch neuron, PVMR (P, arrowhead). Scale bars are 10um (A-C,E-G,I-K,O) or 15 um (D,H,L,P). See supplemental movie 2.1.

correlated with the number of available motor neuron commissures on each side. In both cases, however, the majority of PVD secondary branches do not fasciculate with motor neuron commissures which suggests that 2^{O} branch outgrowth may depend on separate mechanisms that either rely on the existing motor neuron commissure or extend independently. The occurrence of more PVD secondary branches on the right side vs the left is consistent with a model in which fasciculation with motor neuron commissures stabilizes 2^{O} branches (Table 2.1). This aspect of the PVD dendritic array will be discussed more thoroughly below. We also note the both PVDL and PVDR show a greater number of dorsally projecting 2^{O} branches than ventral 2^{O} branches (Table 2.1). In chapter VI, I describe a signaling pathway that is required for dendritic asymmetry of PVD.

PVD 3^{O} branches are consistently positioned adjacent to sublateral nerve cords on both dorsal and ventral sides and fasciculation is extensive along the A/P axis in these locations (Figure 2.3D, 2.3H, 2.3L, 2.3M-O). The dorsal and ventral sub-lateral nerve cords are composed of processes contributed by a small number (2-5) of neurons. These co-linear nerve cords are discontinuous with specific processes exiting and new ones joining the sublaterals in the vulval region [121]. In the posterior, PVD 3^{O} branches on the dorsal side fasciculate with posterior-dorsal sub-lateral neurons, presumably ALN and SDQ (Figure 2.3P dorsal arrow). 3^{O} branches on the ventral side fasciculate with the posterior-ventral sub-lateral nerve cord, likely comprised of PLN (Figure 2.3P ventral arrow), but do not fasciculate with the more dorsally located sub-lateral neuronal

process of the touch neuron PLM (Figure 2.3P arrowhead). PVD 3^{O} branches anterior to the vulva also fasciculate with specific sub-lateral processes. In this anterior region, 3^{O} branches on the ventral side fasciculate with ventral sub-lateral nerve cord neurons, likely SIAV, SIBV, SMBC, SMDV, and PLN (Figure 2.3L). On the dorsal side, 3^{O} branches fasciculate with the anterior-dorsal sub-lateral neuronal processes of SDQ, SIAD, SIBD, SMBD and SMDD. PVD 3^{O} branches located on the dorsal side do not fasciculate with the dorsal sub-lateral process of the touch neuron ALM, which is located more ventrally than the dorsal sub-lateral nerve cord (Figure 2.3D, 2.3H, 2.3L, 2.4). In summary, PVD 3^{O} branches fasciculate with either the dorsal or ventral sublateral nerve cords but different individual neurons contribute to each of these process bundles in anterior vs posterior regions. Fasciculation of PVD 3^{O} branches with the discontinuous sublateral nerve cords could be indicative of a local signal from surrounding tissues that guides independent outgrowth of both sublateral nerve processes and PVD 3^{O} branches in this location. For example, the PVD 3^{O} branches and sublateral nerve cords are positioned along the medial edges of the body muscle quadrants which are thus potential sources of a morphogenic cue. In an alternative model, PVD 3^{O} branches could respond directly to fasciculation signals provided by both anterior and posterior sub-lateral processes.

PVD 4^{O} branches are also located directly beneath the hypodermis but fasciculation with motor neuron commissures is rarely observed (Figure 2.3A-L). PVD 4^{O} processes originate from 3^{O} branches located at medial edge of the

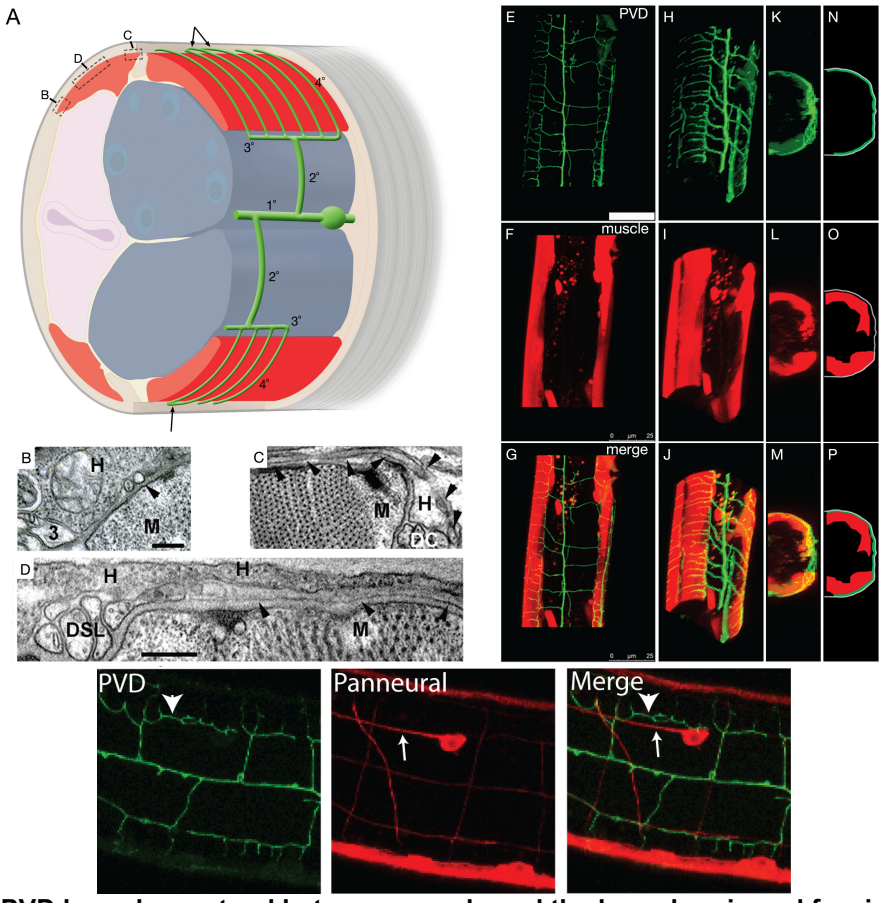

Figure 2.4 PVD branches extend between muscle and the hypodermis and fasciculate with the sublateral nerve cord. A) Cartoon (oblique lateral view) shows the relative positions of the lateral PVD cell body (green sphere), the 1° process, 2° processes, 3° processes at the lateral margin of dorsal or ventral muscle quadrants (red), and many fine branches (4° processes, PVD cell body and branches are in green) passing between the body-wall muscle (red) and the outer hypodermis (pale brown, most hypodermis has been cut away to view beneath it). The tiling of consecutive fine branches while crossing the muscle quadrant is shown, and occasional fusions of their terminal ends with neighboring fine branches indicated by arrowheads. Gonad, blue; Intestine, pale pink; Cuticle, grey. The cartoon is a schematic, showing PVD's fine processes rather longer for clarity. Boxes indicate position of TEM images B, C, and D relative to muscle. (B) Transverse TEM image shows a presumptive 3° PVD branch (3), embedded in the lateral hypodermis (H) at the lateral edge of a dorsal body-wall muscle (M), and a much smaller presumptive 4° branch (arrowhead) seen in 28 cross-section before moving beneath the muscle (animal N501C from the Hall archive). Scale bar indicates 200 nm for panels B, C. (C) Transverse TEM image of a PVD quaternary branch (arrowheads) running laterally across the muscle, and then emerging medially, adjacent to the dorsal nerve cord (DC) (animal N2U, MRC archive). Note the much larger diameter of the dorsal cord axons, sublateral nerve axons, and tertiary PVD process compared to PVD fine branches (D) Transverse TEM image of a PVD 4° branch (arrowheads) running laterally across the muscle quadrant near the dorsal sublateral nerve (DSL) (animal N501A from the Hall archive). Scale bar, 200 nm. (E-P). 3-D reconstructions and projections of PVD in green (F49H12.4:GFP in E H, K, N), muscles in red (*myo-3*:dsRed2 in F, I, L, O and merged images (G, J, M, P). Rotated confocal images (H-M) and schematic tracings (N-P) show PVD branches (green) extending over the body-wall muscle quadrants (red) and beneath the outer hypodermal layer (grey). Scale bar indicates 25 um (E-G). Below PVD branches (green) do not fasciculate with ALM neuronal process (arrow) but do fasciculate with more dorsal sublateral nerves (arrowhead).

longitudinal bands of underlying body muscle cells to produce a series of finger-like projections that extend across the width of each body muscle quadrant (Figure 2.4). Although the significance of the close association of PVD dendritic branches with body muscle cells is unclear, recent studies showing that PVD could function as a proprioceptor suggest the intriguing possibility that this arrangement could provide a feedback mechanism of stretch-induced PVD activity that controls body posture [125].

PVD dendritic morphology emerges from a series of orthogonal branching decisions

We used the PVD::GFP marker to visualize PVD dendritic branching during development in order to provide a detailed description of each step in PVD morphogenesis. The PVD::GFP reporter is initially detected in the mid-L2 larva immediately after the PVD cell soma appears in the postdeirid [119]. By the end of the L2 stage, the single PVD axon has projected to the ventral nerve cord (Figure. 2.5A,B). During this period, the 1^{O} dendritic branches emerge from the PVD cell body to join the lateral nerve cord, one extending toward the anterior and the other growing posteriorly (Figure 2.5A,B). The lateral and sub-lateral nerve cords with which adult PVD dendritic branches fasciculate are already in place before PVD dendritic outgrowth is initiated (Figure 2.5 C-F). Beginning in the late L2 larva and continuing into the early L3, the 2^{O} branches emerge at periodic intervals from both the dorsal and ventral sides of the 1^{O} processes. In each case, 2^{O} branches are perpendicular to the established 1^{O} dendritic branch.

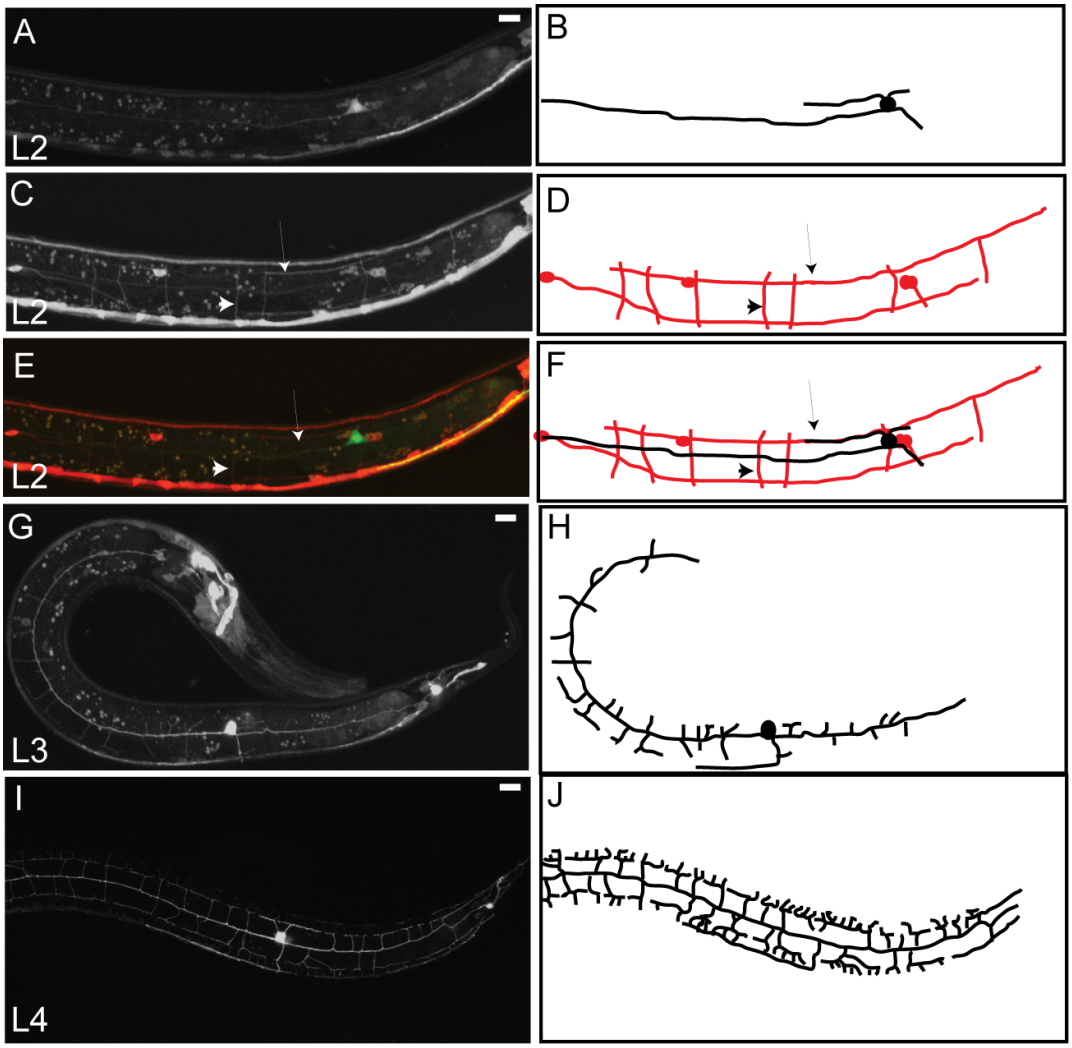

Figure 2.5. PVD dendritic architecture is defined by orthogonal branches. Confocal images (left) and schematic tracings (right) of PVD in L2 larval stage (A,B), panneural (C,D) and merged panels (E,F) demonstrate that both motor neuron commissures (arrowheads) and sub-lateral nerve cords (arrow) are established before the majority of PVD dendritic branches emerge. PVD 1^{O} branches arise in the L2 stage (B,D) followed by sequential orthogonal branching of 2^{O} and 3^{O} branches in L3 larval stage (G,M). A mature PVD neuron with 4^{O} branches is largely completed by late L4 larval stage (I,J). Scale bar is 15 um.

3^O branches ("base of the menorah-like structure") appear in the early L3 and extend along the sub-lateral nerve cords (Figure 2.5G,H). 3^O branch outgrowth continues into the early L4 stage when 4^O dendrites begin to emerge. The mature PVD dendritic arbor is established by the end of the L4 larval stage when it ultimately envelops the animal in a non-overlapping web of sensory processes (Figure 2.5I,J).

Time-lapse imaging of PVD dendritic outgrowth reveals dynamic branching events.

As described above, we deduced the order and timing of PVD dendritic branching by observing several different animals at successive stages during larval development. Our results are suggestive of an orderly progression of dendrite outgrowth along alternating orthogonal axes. Time-lapse imaging of single animals confirmed the successive outgrowth of dendritic branches but also revealed important details of how these branches are generated.

In the first instance, we noted highly dynamic outgrowth of 2^O branches throughout the anterior/posterior length of the PVD 1^O process. In L2 animals, 2^O dendrites grow ventrally or dorsally toward sub-lateral nerve cords. Time-lapse imaging revealed that potential 2^O branches are frequently initiated and then retracted. At periodic intervals, a subset of these projections appears to stabilize and reach the sub-lateral nerve cord whereas other nascent 2^O branches in flanking regions are consistently withdrawn (Figure 2.6 A, C, D [12]). This pattern

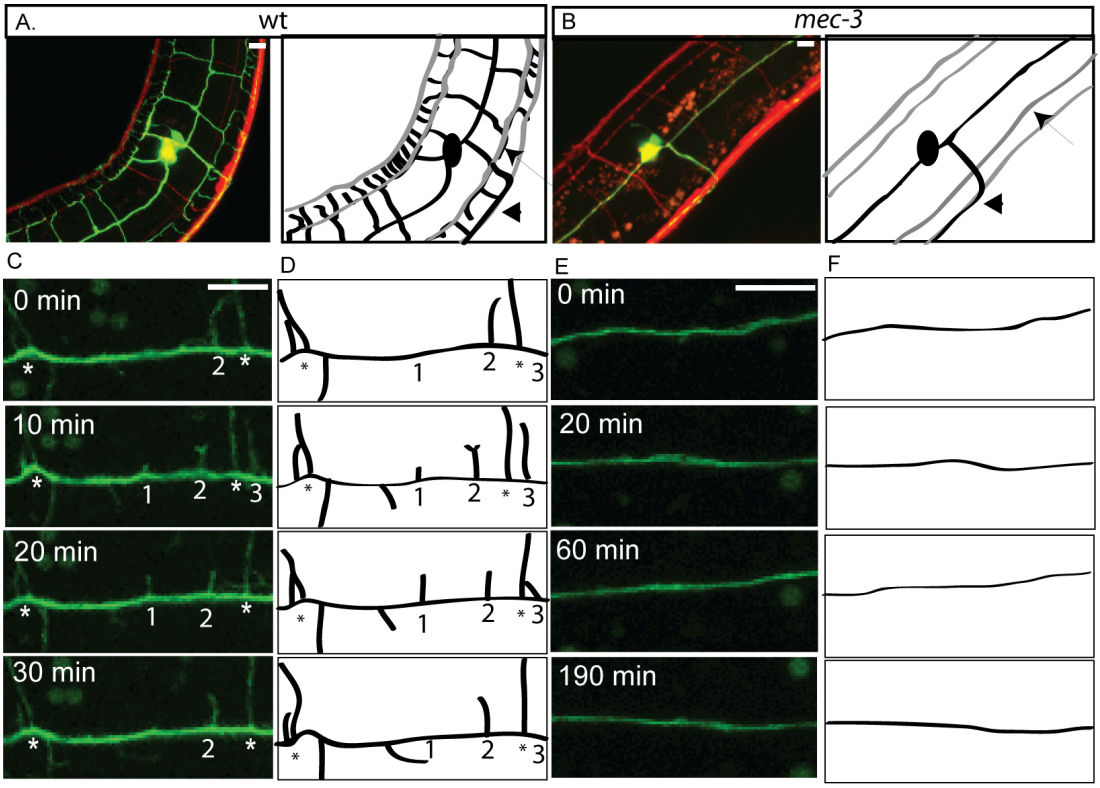

Figure 2.6. Dynamic initiation of PVD secondary branches is disrupted in *mec-3* mutants. Confocal images and schematic tracings of PVD::GFP (green/black) and panneural::dsRed (red/gray) (anterior left, ventral down) show that sub-lateral nerve cords (arrow) and PVD axon (arrowhead) are not altered in *mec-3* mutants (B) in comparison to WT (A). Images (C) and schematics (D) from time-lapse confocal microscopy of *wt* L2 larval stage demonstrate dynamic PVD 2^{O} branches (1-3) that initiate and retract in vicinity of established 2^{O} branches (*) over 30 min period. Images (E) and schematics (F) of *mec-3* mutants do not show PVD 2^{O} branch initiation during 190 min of observation. Scale bar is 5 um.

of dynamic growth is replicated at successive stages with processes alternately extending and retracting until the final adult pattern is produced (Figure 2.7).

As 2^{O} dendrites approach the sub-lateral nerve cord, they initiate 3^{O} branch morphogenesis by turning 90^{O} to project along the A/P axis. In each case, the initial 3^{O} process growing in either the anterior or posterior direction is joined by a new process that sprouts at the point of turning (Figure. 2.8, arrow) to extend in the opposite direction along the A/P axis. The net result is that each 3^{O} branch is composed of an anterior and posterior arm both emanating from a single 2^{O} dendrite.

The development of 4^{O} branches proceeds via a similar mechanism with the tip of an outgrowing 3^{O} dendrite eventually making an orthogonal turn (see below) to project along the D/V axis (Figure 2.8, arrowhead). Additional 4^{O} branches emerge at intervals along the length of each 3^{O} branch (Figure 2.9, arrow). PVD 4^{O} branches demonstrate dynamic growth, with branches initiating and retracting throughout the L4 larval stage (Figure 2.9). This pattern of rapid branch initiation and withdrawal is strikingly similar to that seen for 2^{O} branch outgrowth during the L2 larval stage (Figure 2.9, asterisk). 4^{O} branches terminate as they approach either the dorsal or ventral nerve cords to complete the architecture of the menorah-like structures rooted in the PVD 1^{O} dendritic process (Figure. 2.1).

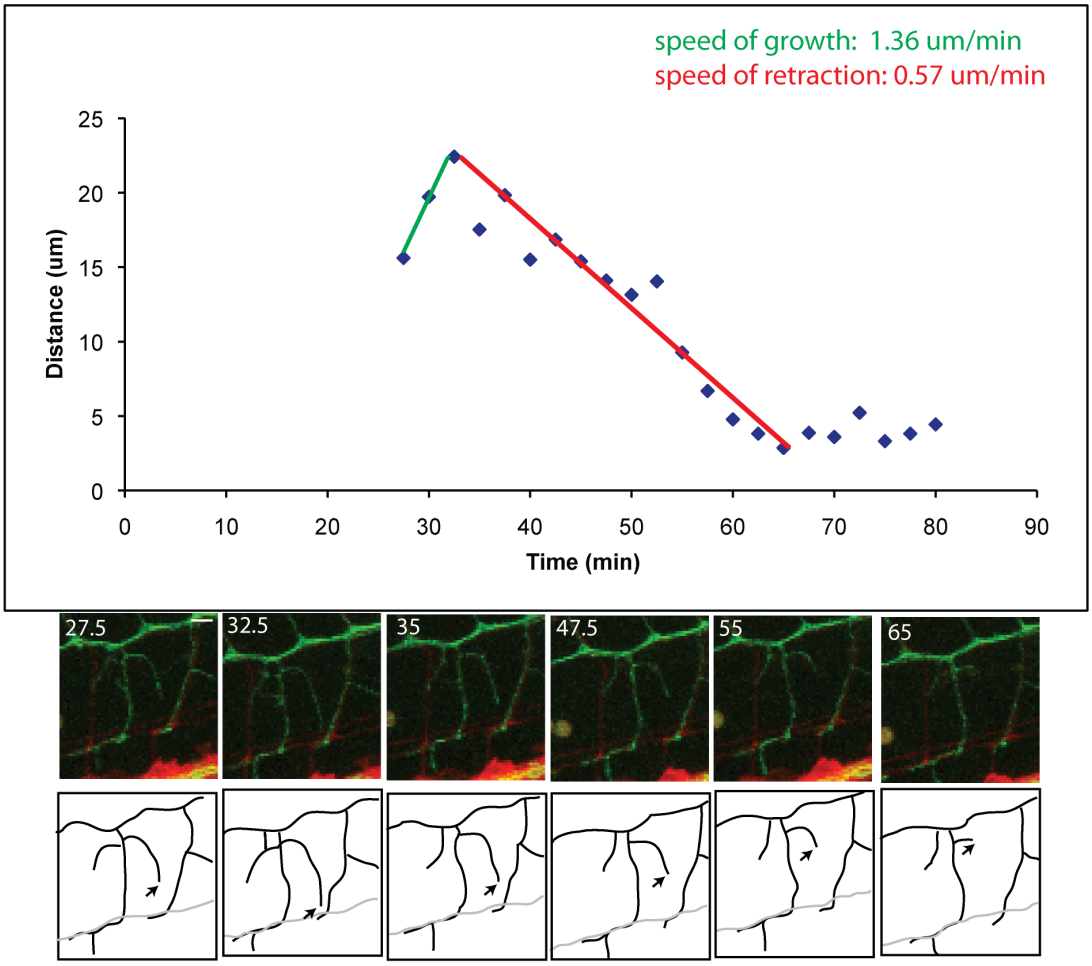

Figure 2.7. Example of PVD branch outgrowth and retraction. A. Time-lapse series (27.5 - 65 sec) of PVD branch (green, top panel; black, bottom panel) extension and retraction. Arrow indicates the tip of the growing branch. Pan-neural marker (red, top panel; grey, bottom panel). Branch length was measured at 2.5 min intervals to estimate speed of growth (~1.4 um/min) (slope of green line) vs. speed of retraction (~0.6 um/min) (slope of red line) (line represents a best fit).

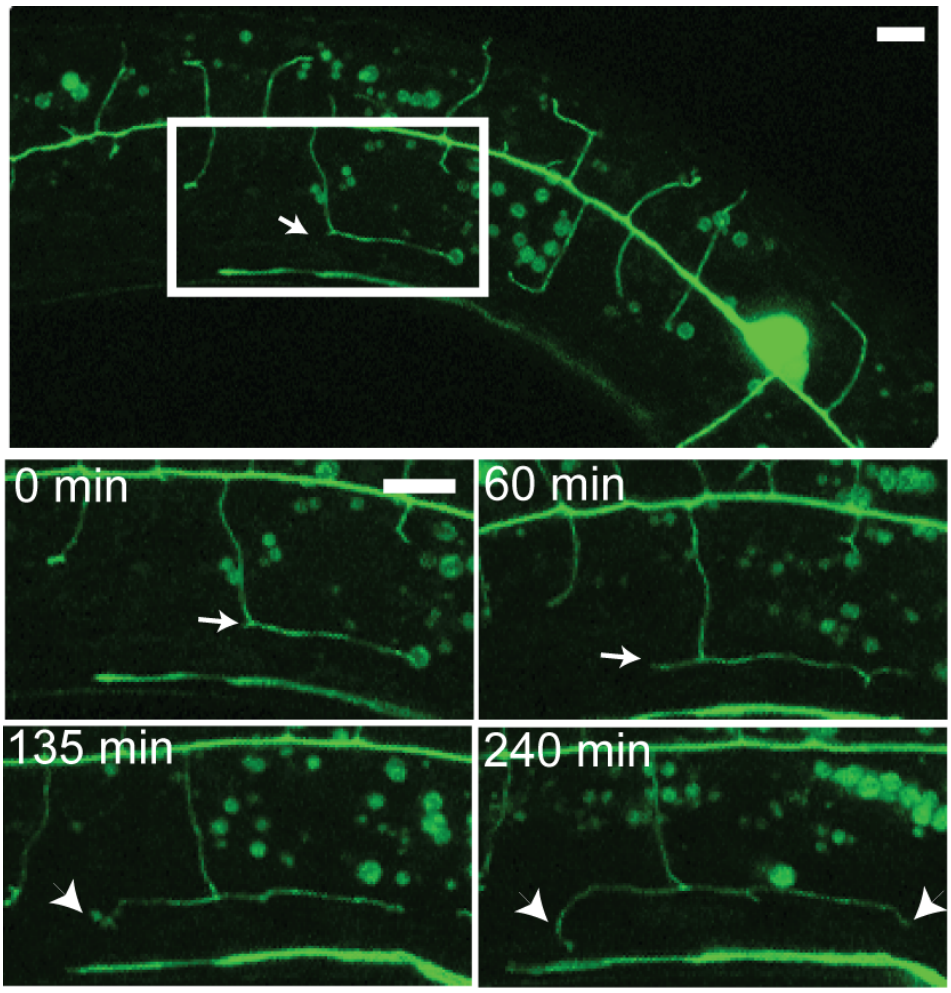

Figure 2.8. PVD dendritic branches turn 90^{o} to establish orthogonal pattern. Time-lapse confocal images of L3 larva depict PVDL dendritic outgrowth (anterior left, ventral down). (Top panel) PVD 2^{O} branch makes a 90^{o} turn (arrow) to fasciculate with sub-lateral nerve cord where it becomes a tertiary branch (inset, 0 min). A 3^{O} branch with opposite polarity emerges from the point of turning (arrow) and grows toward the posterior (60 min). 4^{O} branches are established by a similar mechanism (240 min) in which 4^{O} branches at each end of the menorah-like structure (arrowheads) are generated by 90^{O} turns. Additional, interstitial 4^{O} branches emerge from the outer edge of the 3^{O} branch. Scale bar is 5 um.

Motor neuron commissures stabilize 2^O dendrites during outgrowth

We established that PVD 2^O dendrites fasciculate with motor neuron commissures that traverse the animal from the ventral to dorsal side. We hypothesized that growth of 2^O dendrites could therefore utilize two different, commissure-dependent and commissure-independent, modes of branch outgrowth. To ask if 2^O dendritic outgrowth was dependent on commissures we used an *unc-30* mutant to reduce the number of GABAergic commissures. All but one GABA commissure are located on the right side of the animal. Thus, this approach uses a genetic strategy to answer the question: If commissures aid in PVD dendritic growth, what is the consequence of their removal? In wild-type animals, there are significantly more 2^O dendrites on the right side compared to the left side (Figure 2.10). In *unc-30* mutants, there is a reduction of 2^O dendrites only on the right side in which the GABA commissures have been eliminated (Figure 2.10). Thus in *unc-30* mutants, the number of 2^O dendrites on the left side is equal to that of the right side. These data are consistent with the hypothesis that a portion of 2^O dendrites utilize motor neuron commissures to stabilize.

To further characterize this commissure dependent growth we visualized PVD 2^O dendrite growth in a transgenic background in which we could simultaneously observe motor neuron commissures (panneural::RFP vs PVD::GFP). These movies revealed that 2^O dendrites that initiate along commissures stabilize at a much higher rate than 2^O dendrites that initiate away from commissures (Figure 2.10). This result is consistent with the model that

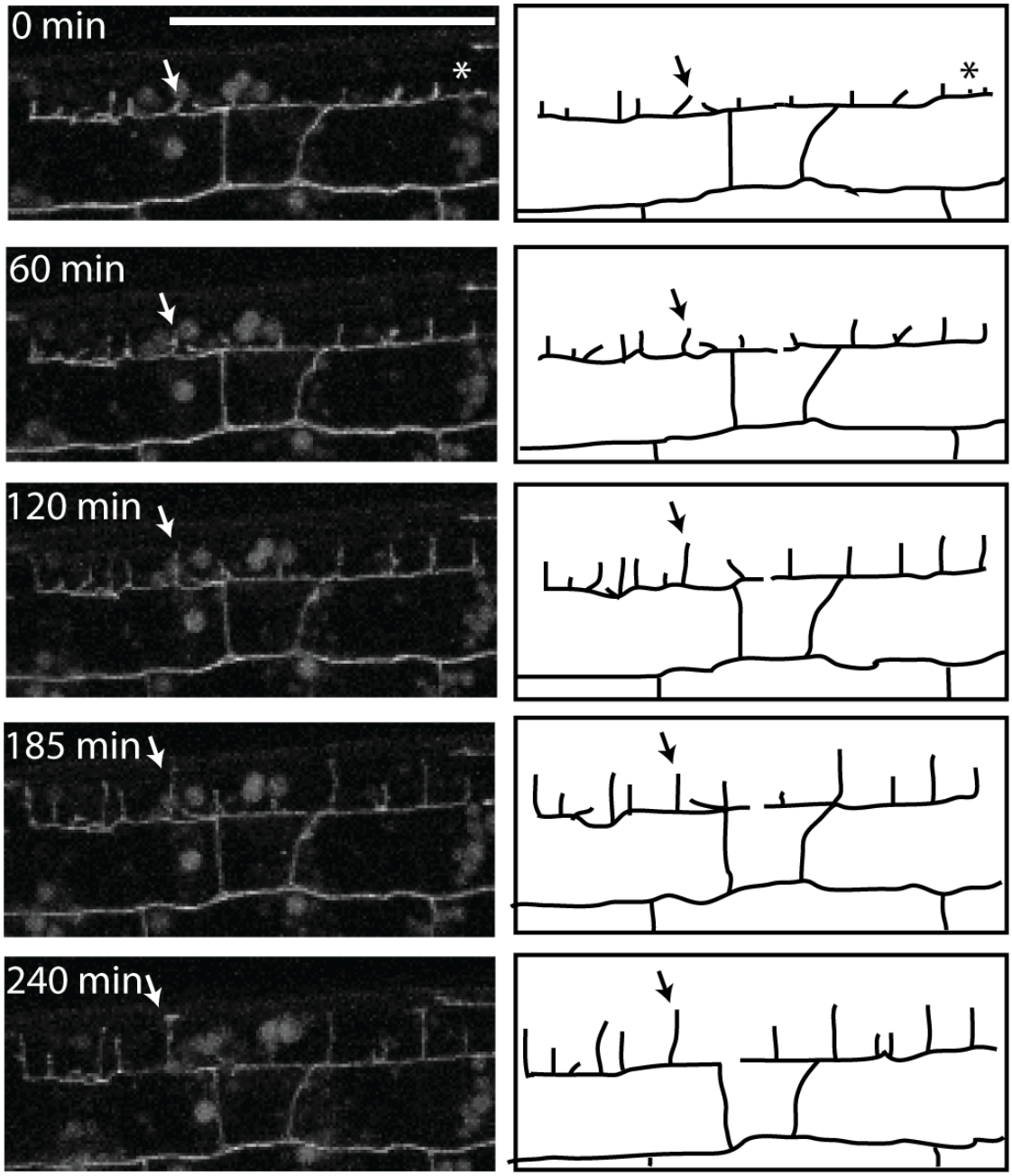

Figure 2.9. PVD 4^{O} branches exhibit dynamic growth. Time-lapse confocal images and schematic tracings of L4 larval stage (anterior left, ventral down) illustrating dynamic outgrowth of 4^{O} dendrites from established 3^{O} branches. Nascent 4^{O} branches (0 min) continue to grow throughout the L4 stage until they produce the mature menorah-like structures observed in the adult. Arrow denotes an example of a maturing 4^{O} branch. Asterisk (*, 0 min) indicates a nascent 4^{O} branch that ultimately retracts (60 min). Scale bar indicates 25 um. See supplemental movie 2.5.

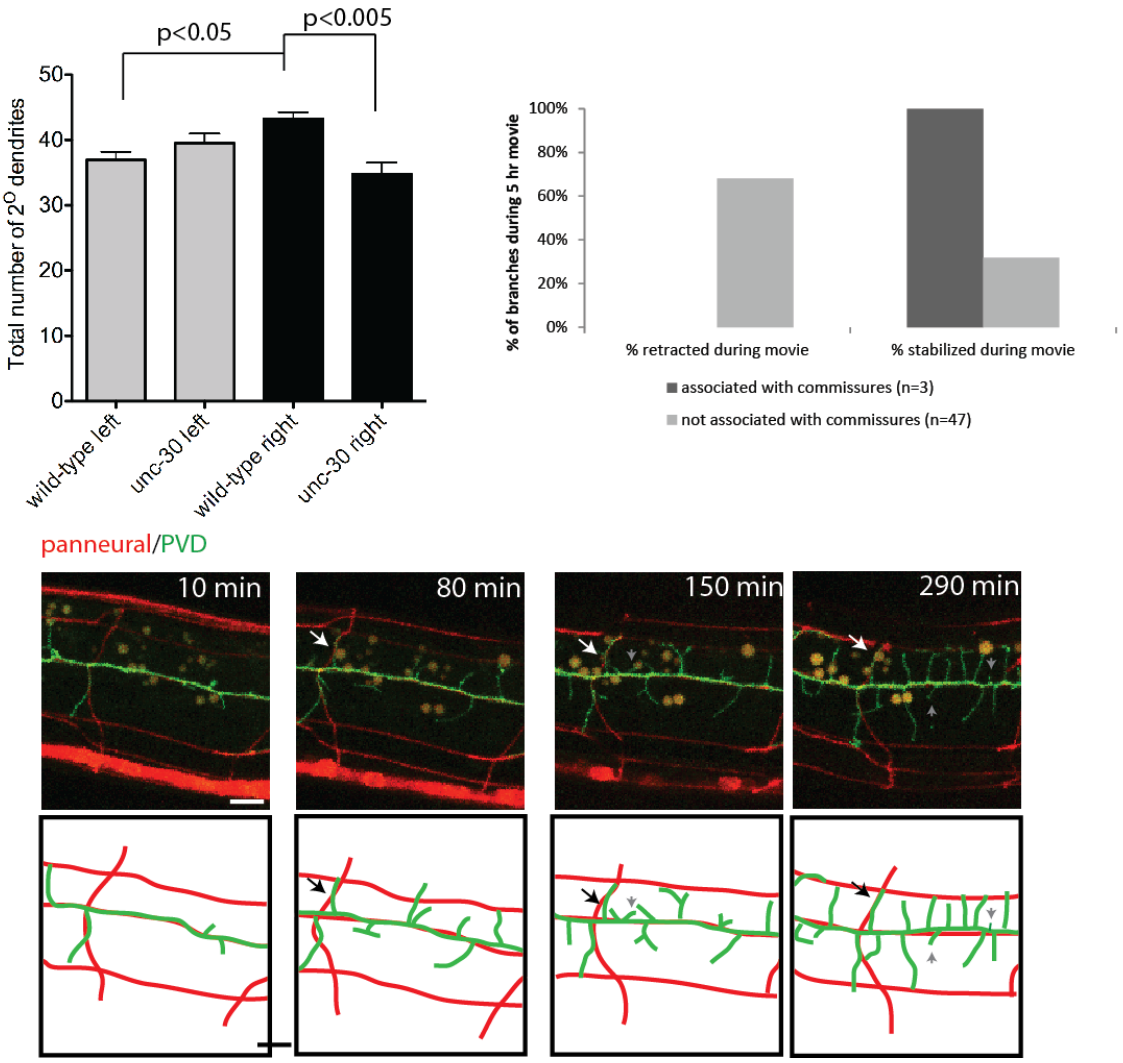

Figure 2.10 PVD 2^{O} dendrites are stabilized by commissures. Quantification of the number of 2^{O} dendrites in wildtype and *unc-30* mutants on the left and right side of the animal. Wild-type animals have more 2^{O} dendrites on the right side than the left side. In *unc-30* mutants, 2^{O} dendrites are reduced only on the right side where the majority of motor neuron commissures are located. Right, quantification of below data. The number of stabilized branches were scored in a 5 hour movie that either associated with commissures (dark grey bar) or did not contact commisssures (light grey bar). All branches that contacted motor neurons stabilized. Bottom, confocal time-lapse images of panneural::RFP (red) and PVD::GFP (green) during 2^{O} dendrite outgrowth. Arrows indicated 2^{O} dendrites that grew along commissures and became stabilized. Other branches that do not contact motor neurons initiated from the 1^{O} dendrite but do not stabilize.

commissures aid in the stabilization of 2^{O} dendrites. We conclude that 2^{O} dendrites utilize two modes of stabilization, one that is dependent on the commissure and a different pathway that is independent of commissures. Interestingly, 2^{O} dendrites were not stabilized when they contacted the sub-lateral nerve cord (Figure 2.10). This data suggests that although 2^{O} dendrite stabilization is influenced by motor neuron commissures the contact of PVD dendrites with the sub-lateral nerve cord does not elicit the same dendrite stabilization behavior.

Non-overlapping dendritic architecture of PVD is established by contact-dependent self-avoidance.

In the mature PVD neuron, 3^{O} branches from adjacent menorah-like structures point toward each other but do not touch (Figure 2.1). This feature of non-overlapping dendritic processes is a universal characteristic of sensory neurons [4, 169] and thus prompted us to consider a mechanism that could account for this outcome. Two possibilities seemed likely: either PVD 3^{O} processes (1) stop outgrowth upon reaching a fixed, mature location or (2) continue growing until contact with the tip of a neighboring 3^{O} branch induces withdrawal. We used time-lapse imaging to distinguish between these models. At the sub-lateral nerve cords, adjacent 3^{O} branches initially grow toward each other along the A/P axis. In fact, the tips of adjacent 3^{O} branches are frequently observed in closer proximity during larval development than in the adult (Figure 2.11, 0 min). Upon contact, these sister 3^{O} dendrites characteristically stop

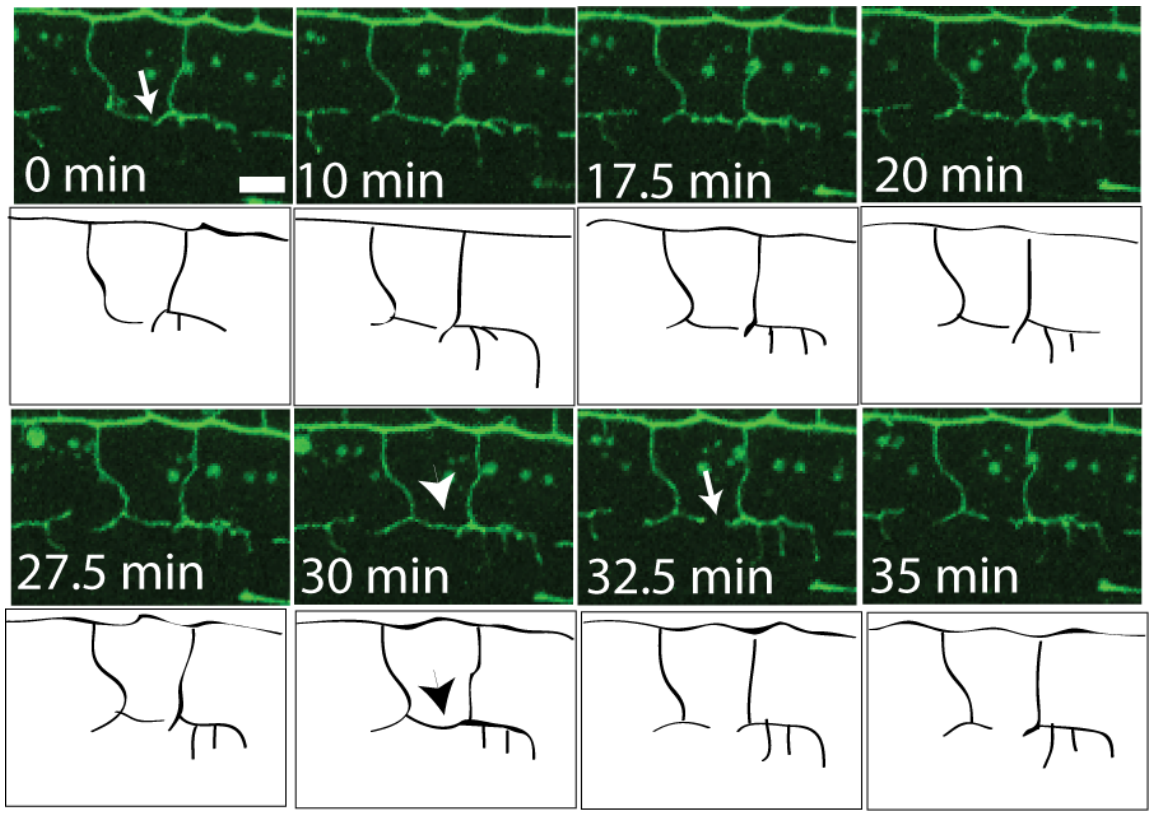

Figure 2.11. PVD tertiary branches demonstrate contact-dependent self-avoidance. Time-lapse confocal images of L3 larval stage (anterior left, ventral down) PVD 3^{O} branches growing toward each other (0-27.5 min, arrow indicates gap between branches), achieving contact (30 min, arrowhead) and then retracting (32.5-35 min) to leave intervening space (arrow). This spacing is preserved in the adult PVD dendritic network. Scale bar is 5 um.

outgrowth and withdraw (Figure 2.11, 30 min). Following retraction, 3^{O} dendrites remain separate and the gap between them is preserved in the mature PVD architecture. Our results are thus consistent with the second mechanism in which the final length of each 3^{O} branch is limited by contact with an adjacent sister dendrite. In fact, this phenomenon of self-avoidance was also observed for other transient dendritic extensions in which filopodia rapidly withdrew upon contact with each other or with previously established PVD branches. We therefore conclude that contact-dependent self-avoidance is likely to contribute to overall non-overlapping dendritic architecture of PVD. In chapter IV and V I discuss a signaling pathway that is required for PVD dendritic self-avoidance.

A gene expression profile of PVD nociceptive neurons

Having defined the detailed architecture and development of the PVD sensory network, we next generated a gene expression profile of PVD in order to identify transcripts with possible roles in PVD morphogenesis and function. For this purpose, we employed the mRNA tagging strategy in which an epitope-tagged poly-A-binding protein (FLAG::PAB-1) is used to co-immunoprecipiate cell-specific transcripts [156, 157]. Immunostaining with anti-FLAG confirmed specific expression in PVD and in OLL neurons (Figure. 2.12A) as predicted for the *ser2prom3* promoter used to construct our PVD mRNA tagging line [168]. Statistical analysis revealed 2,213 transcripts that are significantly enriched ($\geq$ 1.5 X) in the PVD/OLL profile vs all L3/L4 larval cells at a False Discovery Rate (FDR) $\leq$ 1 % (See Methods) (See file sup file in [12]). We also identified a larger

A

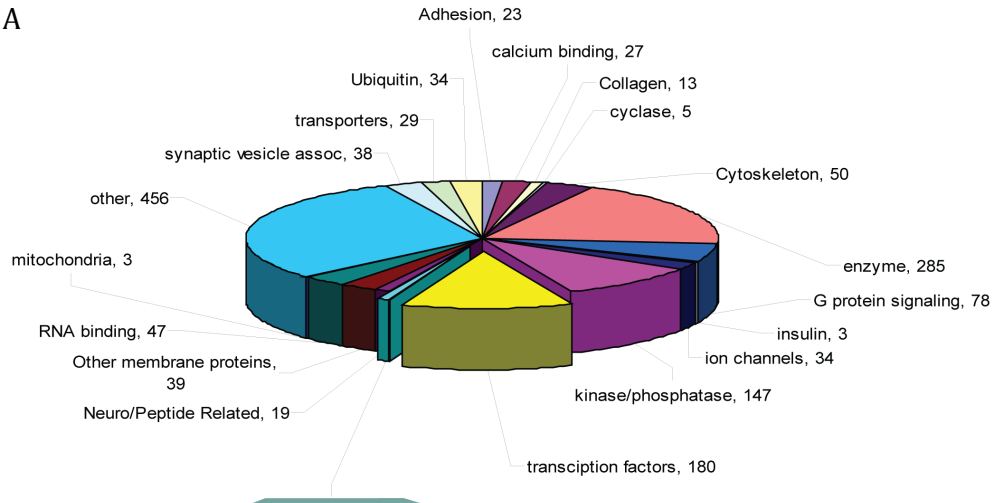

Cosmid	Gene	Protein	Fold change
C34B4.1b	*max-1*	PH/MyTH4/FERM domain	6.1x
F10E9.6c	*mig-10*	Lamellopodin	3.9x
C09B8.7b	*pak-1*	p21 activated kinase (PAK)	3.6x
Y38F1A.10a	*max-2*	p21 activated kinase (PAK)	3.2x
F32A7.3	*eva-1*	Slit Receptor	3.1X
B0273.4a	*unc-5*	UNC-5	2.9x
Y50D4C.1a	*unc-34*	Enabled/VASP	2.9x
K11D9.2b	*ced-10*	Rac1	2.7X
T19B4.7	*unc-40*	UNC-40/Frazzled/DCC	2.7x
ZK377.2	*sax-3*	Robo	2.5X
M79.1	*abl-1*	Abelson Kinase	2.4X

Figure 2.12. Expression profile reveals transcripts for PVD/OLL-enriched gene families. (A) Genes (with Wormbase annotation) encoding transcripts with elevated expression (1.5x) in the PVD/OLL microarray data set organized according to protein families or functional groups. Numbers denote genes in each group. (Table Inset) Enrichment of axon guidance proteins, including multiple UNC-6/Netrin pathway transcripts, enriched in the PVD/OLL microarray.

group of 4,977 “Expressed Genes” or “EGs” (see Methods) that are reliably detected by the PVD/OLL microarray profile but which may also be expressed at comparable levels in other cell types [157] (appendix File 2.2). Of genes previously described as expressed in PVD, 14/32 (~44%) are included in the enriched transcripts and 20/32 (~62%) are EGs. A smaller fraction of known OLL genes are detected with 8/43 (19%) enriched and 15/43 (35%) detected as EGs (appendix File 2.3). Previously noted PVD genes including the nicotinic acetylcholine receptor subunits (nAChRs) *deg-3* (18x) and *des-2* (17x), p21-activated kinase/PAK, *max-2* (3.1X) and the homeodomain transcription factors, *mec-3* (4.9x) and *unc-86* (2.6x) are especially prominent [123, 126, 171]. As an additional test of the specificity of the microarray profile, we scored *in vivo* expression of 18 promoter::GFP fusions for representative genes from the list of enriched transcripts (Table 2.2, Figure 2.7). Of the GFP reporters tested, 44% (8/18) are detected in PVD and 55% (10/18) are expressed in OLL with a total of 78% (14/18) expressed in either PVD or OLL (Table 2.2). For example, the promoter-GFP fusion for EGL-3, a proprotein convertase that functions to process neuropeptide precursors [172], is highly expressed in PVD where it outlines the dendritic network with strong GFP staining (Figure 2.13). *egl-3::*GFP is also expressed in the OLL neurons in the head (data not shown). Expression of the *egl-3* GFP reporter in the intestine and in many additional neurons underscores the sensitivity of the microarray analysis to differential expression. The broad range of enrichment (1.7x – 9.4X) of the PVD or OLL-expressed GFP reporters in this list provides a representative sample of transcripts with differing

Table 2.2. Expression of promoter-GFP reporters for transcripts enriched in PVD/OLL data set. + indicates expression, - indicates lack of expression and ND were not determined. GFP reporter genes were provided by the Genome BC *C. elegans* Gene Expression Consortium(Hunt-Newbury et al., 2007).

cosmid	GFP Strain	gene	Protein	Fold Change	PVD	OLL
C51E3.7	BC12649	*egl-3*	Proprotein convertase	4x	+	+
B0034.3	BC11525	*casy-1*	Calsyntenin	5.3x	+	+
F41E6.13	BC13515	*atgr-18*	Autophagy protein Atg18p	3.6x	+	+
C43G2.1	BC10234		Progestin and AdiopoQ Receptor	3.9x	+	+
C24A11.8	BC12301	*frm-4*	FERM domain	1.7x	+	ND
H09G03.2	BC13361	*frm-8*	FERM domain	2.9x	+	ND
C01G8.5	BC10874	*erm-1*	ERM family	1.7x	+	ND
C11D9.1	BC15697		TIAM1/CDC24 RhoGEF GTPase	2.6x	+	ND
C05D11.4	BC10312	*let-756*	Fibroblast Growth Factor (FGF)	6x	-	+
C24A8.1	BC13771		D2/D3 dopamine receptror	4.1x	-	+
F32F2.1	BC11367	*uig-1*	Cdc42 GEF	4.1x	-	+
F59B10.1	BC15924	*pqn-47*	Prion-like domain	9.4x	-	+
Y22F5A.3	BC13241	*ric-4*	SNAP-25	7.8x	-	+
T17H7.1	BC15671		Collagen	4.1x	-	+
T07G12.1	BC15622	*cal-4*	Calmodlin-like	6.9X	-	-
F13B10.1	BC11466	*tir-1*	Toll and interleukin-1 receptor domain	4.5x	-	-
ZK337.2	BC15709		Zinc Finger	5.2x	-	-
T04C9.6	BC16158	*frm-2*	FERM domain	2.9x	-	-

Hunt-Newbury, R., Viveiros, R., Johnsen, R., Mah, A., Anastas, D., Fang, L., Halfnight, E., Lee, D., Lin, J., Lorch, A.*, et al.* (2007). High-throughput in vivo analysis of gene expression in Caenorhabditis elegans. PLoS Biol *5*, e237.

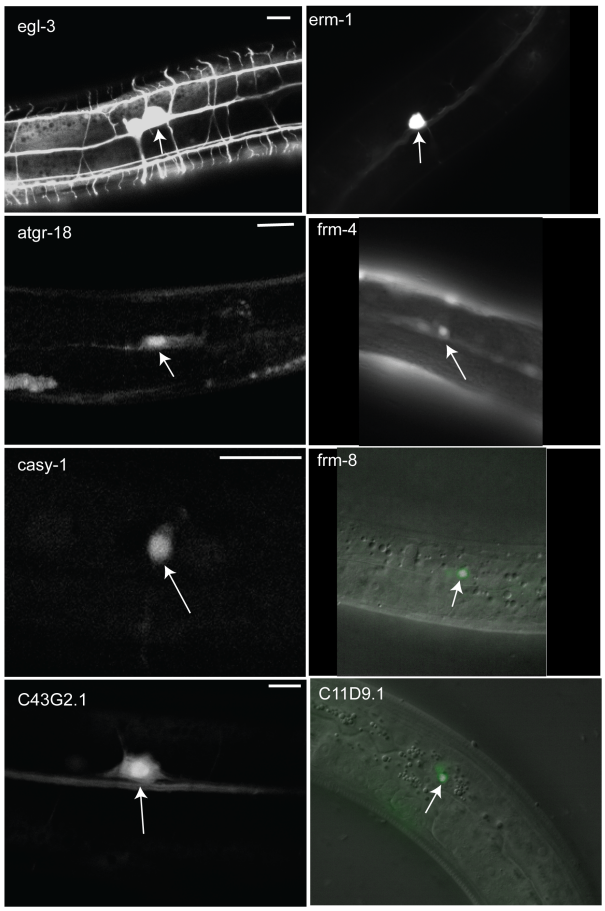

Figure 2.13. Cell specific microarray identifies transcripts expressed in PVD.
Promoter::GFP reporter genes for enriched transcripts show expression in PVD. Arrow indicates PVD cell soma. Scale bars = 5 um.

levels of expression. Together, these GFP reporter data validate the prediction that a majority of transcripts in this microarray data set are in fact expressed in either PVD or OLL neurons *in vivo*. Although a significant fraction of transcripts in this data set may be derived from OLL and not PVD, on the basis of these validation experiments we estimate approximately half of the genes in our enriched and EG data sets are expressed in PVD. Therefore, this list provides a useful compendium of candidate genes to test for potential roles in PVD morphogenesis and function.

Gene families enriched in the PVD/OLL profile.

Transcripts for a wide range of protein families are enriched in the PVD/OLL data set (Figure 2.12B)[12] and may be suggestive of specific functions. The coordinate enrichment of genes encoding known components of the UNC-6/Netrin axon guidance pathway is particularly striking, for example (Figure 2.12B). UNC-6/Netrin functions as an exogenous cue for cell migration, axon guidance, neuronal asymmetry and synaptogenesis [42, 56, 173-175]. The UNC-6/Netrin receptors, UNC-5 and UNC-40/DCC and several additional components with cytoplasmic roles in the UNC-6/Netrin signaling pathway are also highly enriched. In chapter IV-VI, I show that mutants for several of these components including *unc-6/Netrin, unc-5, unc-40/DCC, unc-34/Ena*, and *mig-10/lamellopodin* show similar defects in PVD morphology that are indicative of roles of a canonical UNC-6/Netrin signaling pathway that controls the elaboration of the PVD dendritic arbor (discussed in Chapters 4-6) [176, 177].

In addition to identifying genes that govern PVD morphogenesis, the microarray profile has also detected strong candidates for roles in PVD nociceptive function. For example, members of the DEG/ENaC family of cation channel subunit proteins have been implicated in pain sensation induced by either mechanical stimuli or low pH [122, 178]. The *C. elegans* genome encodes 28 predicted DEG/ENaC proteins [179]. Two of these, MEC-4 and MEC-10, are expressed in the "light touch" mechanosensory neurons (AVM, PVM, PLML, PLMR, ALML, ALMR) where they evoke an aversive response to physical contact [122, 180]. *mec-10* expression in PVD has been previously reported [181] and the *mec-10* transcript is enriched in the PVD/OLL profile. Three additional DEG/ENaC genes (*del-1, asic-1, F25D1.4*), but not *mec-4*, are also elevated [12]. Recent work has shown that one of these DEG/ENaC channel proteins, F25D1.4/DEGT-1, is required along with MEC-10 to mediate a PVD-dependent response to strong mechanical stimuli [124].

The MEC-3 homeodomain transcription factor is required for the initiation of PVD 2^{O} branch outgrowth

Extensive genetic studies have documented the key roles of transcription factors in sensory neuron morphogenesis [13, 14, 169] [20, 23]. As a first step toward identifying specific transcription factors that control PVD morphogenesis, we compiled a list of 112 transcription factor-encoding genes that are $\geq$ 2X enriched in the PVD/OLL data set (Table 2.3) [12]. This list includes a diverse array of transcription factor families with the largest groups represented by

Table 2.3. Transcription factor families. 112 Transcription factors that are ≥ 2X enriched in the PVD/OLL profile versus all larval cells. Transcription factors are grouped according to shared homology of function. General transcription refers to factors with broad roles in transcription. Other includes sequences with weak homology to transcription factor motifs. (Established by BLAST searches at NCBI)

Family/Domain	**# in PVD data set**
Nuclear Hormone receptors	27
Homeobox	16
General transcription	12
Basic region leucine zipper transcription factor	10
Zinc finger	6
SMAD	4
HMG	4
Forkhead	4
GATA-4/5/6 transcription factors	4
bHLH	4
ETS	2
Aryl-hydrocarbon receptor	1
Atrophin-like protein	1
CDK9 kinase-activating protein cyclin T	1
CREB/ATF	1
doublesex/MAB-3 domain	1
E2F-like protein	1
LIM domain	1
MADS box	1
Mlx interactors and related transcription factors	1
NGF1-A binding protein domain	1
Nuclear factor erythroid 2-realted factor 2	1
PAX and HOX domains	1
TBX2 and related T-box transcription factors	1
TEAD family	1
Other	5

nuclear hormone receptors and homedomain proteins. One of the most highly enriched (~5x) homeodomain proteins, MEC-3, is the only transcription factor in our data set that has been previously shown to affect PVD morphology. The complex PVD dendritic arbor is largely absent in *mec-3* mutants imaged with the *ser2prom3::*GFP reporter gene [11]. We have confirmed this result with our PVD::GFP marker which shows that the single PVD axon and 1^{O} dendritic process appear normal in *mec-3(e1338*) but higher order branches (2^{O}, 3^{O}, 4^{O}) are missing (Figure 2.6B). To explore the potential origin of the *mec-3* PVD branching defect, we initially used the pan neural RFP marker to visualize other neuronal processes that PVD dendrites contact during outgrowth. These images showed that the lateral nerve cord (fasciculates with PVD 1^{O} branch), motor neuron commissures (fasciculate with subset of PVD 2^{O} branches) and dorsal and ventral sublateral nerve cords (fasciculate with PVD 3^{O} branches) are intact in the *mec-3(e1338)* mutant (Figure 2.6A,B). These results are consistent with a cell-autonomous role for *mec-3* in promoting PVD dendritic branching. As reported above, in wild type animals, branches are actively extended and retracted along the length of the 1^{O} dendrite throughout the L2 and L3 larval stages. A subset of these nascent 2^{O} branches are stabilized and contact the sublateral nerve cords whereas others emerging from nearby regions during this time eventually collapse (Figure 2.6 C, D,). We therefore hypothesized that *mec-3* mutants are either (1) unable to stabilize 2^{O} branches or (2) are defective in 2^{O} branch initiation. We used time lapse imaging to distinguish between these alternative models. These experiments showed that the PVD 1^{O} dendritic

process is remarkably quiescent in *mec-3* mutants with virtually no saltatory branching even during extended periods (e.g., 10 hours) of observation (Figure 2.6E, F). This result supports the hypothesis that MEC-3 is required for the initiation of PVD 2^{O} dendrite outgrowth.

A targeted RNAi screen of transcription factors genes reveals regulators of PVD dendritic morphogenesis.

We used RNAi to test other $\geq$ 2X enriched transcription factors in our microarray data set for roles in PVD morphogenesis [12]. We selected late L4 larvae (F1 progeny of RNAi-treated parents) for screening with the idea that the appearance of the final structure could reveal transcription factors with roles at any stage of PVD morphogenesis. RNAi with empty vector served as a negative control and consistently resulted in a wildtype PVD dendritic architecture (Figure 2.14A,B). *mec-3* RNAi-treated animals displayed fewer dendritic branches after RNAi treatment (Figure 2.14E, F). As expected, the Mec-3 RNAi phenotype was less severe than that of *mec-3* mutants in which the 1^{O} process shows virtually no branching activity (Figure 2.6B). Of the 86 transcription factors screened via RNAi, nine resulted in PVD defects. In most cases, corresponding genetic mutants were examined to confirm the RNAi defect. Two additional transcription factor determinants of PVD morphology (*ahr-1* and *egl-46*) that did not produce RNAi phenotypes were detected in genetic mutants for a total of eleven transcription factor genes including *mec-3* that regulate some aspect of PVD differentiation or morphogenesis (Table 2.4) [12].

Table 2.4. Transcription factors that regulate PVD morphology. (DM=*D. melanogaster*, MM= *M. musculus*, HS=*H. sapiens*)

Gene	Family/Domain	enrichment	Orthologues	RNAi	mutant	phenotype
lin-39	HOX homeodomain	4.4	*Scr (DM)/Hox-B5 (HS)*	+	ND	no PVD
zag-1	homeodomain	3.4	*Afh-1 (DM)*	+	+	posterior defects, PVD duplicated on right side
unc-86	POU homeodomain	2.6	*Acj6 (DM)/ Brn3a (MM)*	+	+	unbranched 1^0 dendrite
dpl-1	E2F-like protein	2.8	*Dp (DM)*	+	ND	misguided 1^0 branch
mec-3	LIM homeodomain	4.9	*Lim-1 (DM) /Lhx5 (HS)*	+	+	unbranched 1^0 dendrite
unc-30	homeodomain	2.1	Pitx-1 (DM) /Pit1 (HS)	+	+	fewer 2^0 branches
ahr-1	aryl-hydrocarbon receptor	3	Spineless/SS (DM)	-	+	increased number of 2^0 branches
egl-46	Zinc Finger	3.6	nerfin 2A (DM)	-	+	fewer 2^0 branches
atf-2	bZip Superfamily	2.3		+	ND	overlapping 3^0 branches
thoc-2	General Transcription	2.0	*Tho2 (DM)*	+	ND	overlapping 3^0 branches
egl-44	TEAD	3.9	*Sd(DM)/TEF-3 (MM)*	+	+	ectopic branching

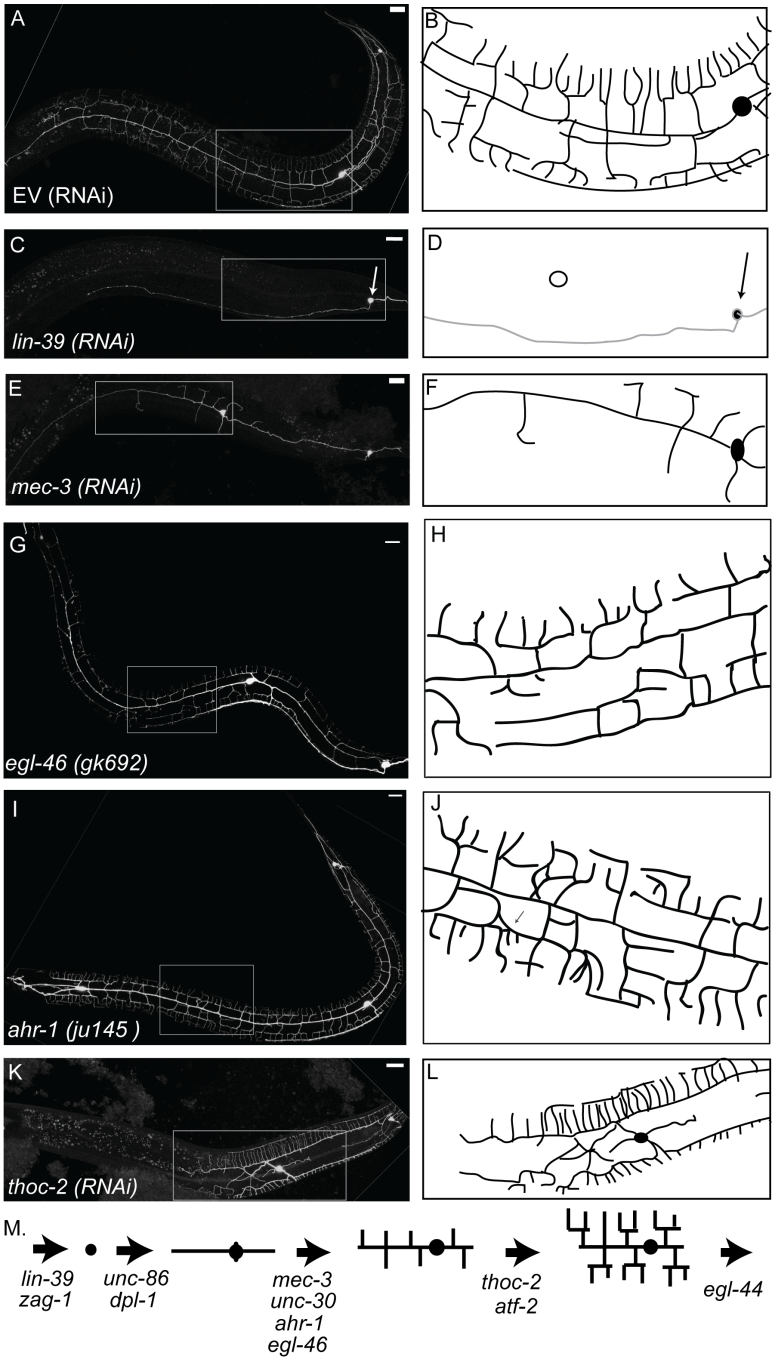

Figure 2.14. Transcription factors enriched in PVD expression profile control dendritic morphogenesis. Confocal images (left) and schematics (right) of RNAi-treated animals expressing PVD::GFP marker (anterior left, ventral down). (A,B) Empty vector (EV)-treated negative control. Positive control, *mec-3* RNAi (E-F), results in reduced 2^{O} and 3^{O} branches. *lin-39* RNAi-treated animals (C-D) do not show PVD neurons (open circle indicates location of wt PVD cell body, arrow points to tail neuron that also expresses PVD::GFP marker). Mutants *egl-46(gk692)* shows fewer 2^{O} branches (G,H) and ahr-1(ju145) displays increased numbers of 2^{O} branches (I,J) (Supplemental File 4). Proposed temporal order of transcription factor function during PVD morphogenesis (M). (Table 2.5).

lin-39, which encodes a conserved member of the HOX family of homedomain proteins, appears to have an early role as PVD is either not detected or shows an unbranched architecture in *lin-39* RNAi-treated animals (Figure. 2.14C). The Lin-39 PVD-defective phenotype is consistent with the established role of LIN-39 in the specification of cell fates in the mid body region of *C. elegans* [182]. RNAi knock down of *unc-86* (POU homeodomain) phenocopies the *mec-3* mutant with an unbranched 1^{O} dendrite. The *unc-86* mutant, however, is more severely affected; the PVD soma and axonal projection to the ventral cord are normal but the 1^{O} dendritic process fails to emerge (data not shown). This result indicates that UNC-86 is required for initiating dendritic outgrowth and is consistent with an earlier report that *unc-86* activates *mec-3* expression in PVD [183] (Table 2.4).

The ZAG-1 transcription factor (homeodomain) [184] displays a unique mutant phenotype in which two apparent PVDL neurons are consistently observed on the left side of the animal whereas PVDR on the right side is not duplicated. The striking asymmetry of the Zag-1 defect offers an explanation for a previous report of incompletely penetrant duplication of PVD in *zag-1* mutants [185]. The role of ZAG-1 in PVD morphogenesis is described further in Chapter 3. Other transcription factors detected in our screen appear to affect successive steps in the placement or elaboration of dendritic branches (Figure 2.14 M). To determine the developmental role of these transcription factors, we noted the larval stage at which the RNAi phenotype initially appeared. Misplacement of the 1^{O} branch in *dpl-1* RNAi-treated animals is observed during the L2 stage, which

suggests that DPL-1 (E2F-like protein) functions early in PVD morphogenesis to regulate targets that guide initial outgrowth along the lateral nerve cord. *dpl-1* mutants also lacked 4^{O} dendrites and therefore may have dual roles in PVD development. Other transcription factors appear to define the overall number of 2^{O} branches with *unc-30* (Pitx homeodomain)[186] and *egl-46* (Zn finger/Nerfin) [187] mutants showing fewer 2^{O} branches (Figure 2.14 G,H) (Figure 2.6) and *ahr-1* animals displaying an increased number of 2^{O} dendrites (Figure 2.14 I, J) (Figure 2.15). In Chapter 3 I characterize the *ahr-1* phenotype further and show that the conversion of another cell, AVM, into a PVD-like fate results in more 2^{O} dendrites on one side of the animal. The role of *ahr-1* (aryl-hydrocarbon receptor) in this case is intriguing because its *Drosophila* homolog, Spineless (SS), also controls the complexity of sensory neuron dendritic branching [23]. The importance of transcription to later stages of PVD morphogenesis is revealed by 3^{O} branch defects in *aft-2* (bZip superfamily) mutant and in *thoc-2* (general transcription) deficient animals. In both cases, 3^{O} branches are elongated and frequently overlap (Figure 2.14 K, L). The apparent failure of the contact-dependent self-avoidance mechanism indicates that *aft-2* and *thoc-2* may control downstream genes that mediate this characteristic feature of 3^{O} branch morphogenesis. *thoc-2* RNAi-treated animals also frequently show other PVD defects including misplaced 1^{O} processes and a general failure to elaborate dendritic branches anterior to the PVD soma. Lastly, one of the transcription factor mutants detected in our screen, *egl-44* (TEAD domain) [187] did not demonstrate any obvious PVD dendritic defects during early development but

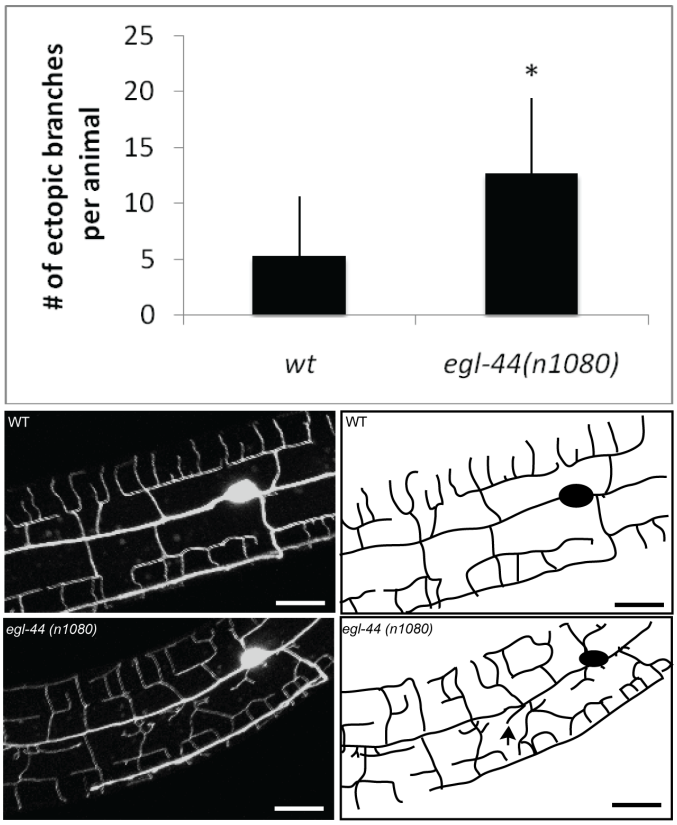

Figure 2.15. *egl-44* normally inhibits excess branching. Histogram shows ectopic branching in *egl-44 (n1080)* mutant animals (12.7±7, n=18) compared to that of wildtype control (5.3±5, n=16). Image and schematic tracing show ectopic branches radiating from the 1^{O} process (arrow head). Ectopic branches are defined as PVD outgrowths that terminate in the region with boundaries comprised of 1^{O} branch (medial) and 3^{O} branches (distal). Young adult animals were scored. Students t-test was used to detect significant differences. *p<0.001 wt vs. mutant. Scale bar = 15 um.

showed extensive ectopic branching in the adult stage (Figure 2.15). Thus, *egl-44* must normally act to limit excessive branching at later stages of development. We note that many of the ectopic branches observed in *egl-44* mutants appear to overlap which could mean that *egl-44* also regulates target genes that function in the self-avoidance mechanism that maintains the discrete sensory field for each dendritic branch in the PVD arbor.

DISCUSSION

Nociceptive function depends on elaborate networks of dendritic processes adjacent to the skin [188]. The complexity of this architecture and the general inaccessibility of sensory neurons to real time studies of morphogenesis have hindered the elucidation of cell biological mechanisms that govern dendritic branching. Here we describe a model nociceptor, the PVD neuron in *C. elegans*, that displays a complex but highly ordered sensory arbor and show that the generation of this network can be readily studied by dynamic imaging methods. This approach has revealed the step-wise emergence of PVD branches during development and identified external landmarks that correspond to key branch points. Our observations suggest that the final pattern of PVD branches also depends on an intrinsic mechanism of error correction in which sister dendrites avoid contact with each other. To identify genes with potential roles in dendritic morphogenesis, we generated a cell-specific expression profile that includes >2,000 PVD-enriched transcripts. Selected genes in this list were ablated by

RNAi or in mutants to identify eleven transcription factor proteins and representative members of other functional protein classes with a range of specific roles in PVD morphogenesis.

The PVD dendritic arbor is generated by a series of defined branching decisions.

Our observations show that the PVD dendritic arbor arises from a series of ordered branching decisions that correspond to specific stages of larval development. Dendritic outgrowth is initiated in late L2 larvae and continues throughout the L3 and L4 stages until the mature PVD morphology is achieved in the adult. Because PVD and its dendritic arbor are located near the surface, all of these branching events are readily observed in a live animal and can be catalogued by time-lapse imaging. A comparison of PVD morphology to the structure of the *C. elegans* nervous system showed that specific PVD dendrites are closely apposed to external nerve fascicles. These interactions are extensive and involve the 1^{O} PVD processes that extend along the lateral nerve cord, a subset of 2^{O} dendrites that fasciculate with motor neuron commissures and 3^{O} branches that are in contact with sublateral nerves throughout their length.

As we show, PVD 2^{O} dendrites develop in two micro-environments, either along commissures or not associated with commissures and show different stabilization properties depending on these two different growth substrates. The hypodermis is closely situated to aid in stabilization of commissure independent 2^{O} dendrites and therefore it seems likely that a protein expressed in PVD could

interact with a hypodermal protein to stabilize dendrites. Our work also shows that it is likely that a different protein localized on the commissures helps to aid in stabilization of PVD dendrites. Identification of proteins that aid in stabilization of 2^{O} dendrites and their spatial requirement will help to test this hypothesis. We also showed that 2^{O} dendrites are not stabilized by contact with the sub-lateral nerve cord. This data suggests that micro-environment on the commissural neuronal processes may be different than that present on the sublateral nerve cord neurons. An understanding of the consequence of ablating the entire sub-lateral nerve cord to PVD dendrite outgrowth could help to strengthen this hypothesis.

The cell biological mechanisms that drive PVD branching are unknown but could involve different components for separate branching events. This idea derives from the distinct spatial environments occupied by each of the branches and from the characteristic manner in which each arises. 1^{O} branches grow out from opposite sides of the PVD soma and project either anteriorly or posteriorly along the lateral nerve cord. In contrast, 2^{O} branches emerge at interstitial locations along the length of the 1^{O} process and grow in either the dorsal or ventral directions. The orthogonal switch in the geometry of these branching patterns is suggestive of a temporal change in either the intrinsic polarity of dendritic outgrowth and/or the responsiveness to external cues. The potential existence of diverse dendritic branching mechanisms is also suggested by the observation from time lapse imaging of two distinct modes of 3^{O} branch outgrowth. A 3^{O} process is initially generated as a 2^{O} branch that turns at the

sublateral nerve to extend in either the anterior or posterior direction. An additional branch then sprouts from the point of turning to grow in the opposite A/P direction and thus form the other arm of each 3^{O} dendrite (Figure 2.8). Although it seems likely that the turning and branching events may be triggered by a common signal, perhaps provided by the sublateral nerve cord, these cell biological responses are distinct and thus could employ subsets of unique components.

The overall shape and extent of the PVD sensory arbor may also depend on negative cues that constrain dendritic growth. We note, for example, that PVD processes do not extend into the head region occupied by the FLP neurons. FLP and PVD display dendritic arbors with similar branching patterns (Figure 2.2) and both mediate nociceptive responses to mechanical force [123, 170] [124]. The "tiling" pattern of dendritic arborization that PVD and FLP display in which sensory neurons of a given functional class occupy discrete topical domains is widely observed and may depend on mutual inhibition by outgrowing dendrites from adjacent neurons [4]. In *Drosophila*, the Ig protein, Turtle mediates homophilic interactions that maintain separate sensory fields for neighboring R7 photoreceptors [189]. An unknown negative cue also mediates this behavior in *C. elegans* and *Drosophila* in a shared signaling pathway involving the conserved components Furry/*sax-1* and Tricorner/*sax-2* [110, 111, 117]. We note that both Furry/*sax-1* and Tricorner/*sax-2* are enriched in the PVD microarray data set and are thus candidates for regulators of PVD dendritic outgrowth.

Additional evidence of negative regulation of dendritic outgrowth derives from our time lapse imaging results showing that PVD dendritic branches are actively repelled by contact with each other (Figure 2.11, Figure 2.7). This phenomenon of self-avoidance is commonly employed by sensory neurons and serves to prevent overlapping coverage of a given receptive field by sister dendrites from the same neuron [95, 190]. Studies in *Drosophila* have shown that the cell surface Ig superfamily proteins, Dscam and Turtle, mediate dendritic self-avoidance [100] [105]. Dscam is not encoded by the *C. elegans* genome and Turtle homolog does not appear to function in self-avoidance (see chapter 4), however, and thus alternative repulsive cues are likely utilized in PVD. These effectors of PVD dendritic self-avoidance could be potentially detected by genetic or RNAi ablation of candidate cell surface receptors (Figure 2.12) that are enriched in the PVD microarray data set [12]. In chapter 4 I identify that PVD transcripts of the UNC-6/Netrin signaling pathway are required for self-avoidance.

Having considered patterning mechanisms that involve extracellular cues or contact-dependent interactions among sister dendrites, we also suggest the possibility of internal cytoplasmic mechanisms for limiting dendritic outgrowth. Over half of the 2^{O} branches and most of the 4^{O} branches do not fasciculate with external nerve cords and thus are unlikely to follow specific paths defined by previously established external structures (Table 2.1). The regular spacing of 2^{O} and 4^{O} branches (Figure 2.16) could be indicative, however, of negative signals from established PVD processes that prevent the formation of additional stable

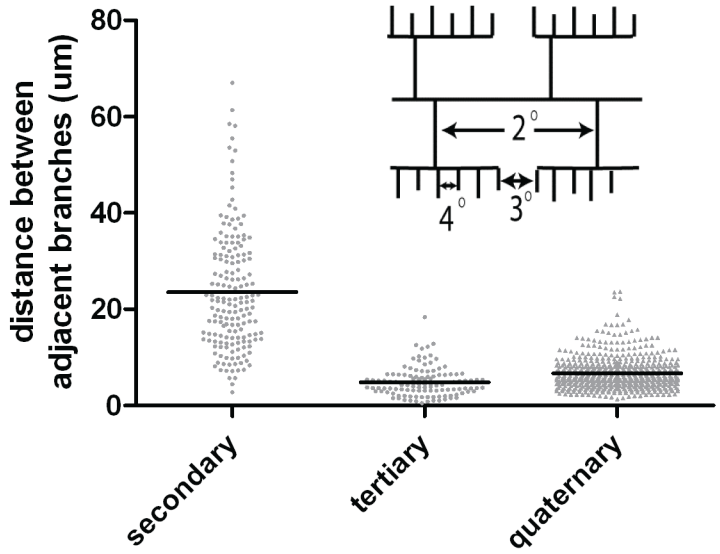

	secondary	tertiary	quaternary
Number of values	170	119	559
Maximum	67.00	18.34	23.69
Minimum	2.75	0.51	1.36
Median	21.49	4.40	6.02
Mean	23.56	4.85	6.70
Std. Deviation	12.47	2.95	3.37

Figure 2.16. The distance between PVD dendrites. The average distance between adjacent 2^0 branches is greater than distances separating adjacent 3^0 or 4^0 branches. Distances between adjacent 2^0 branches, between adjacent 3^0 branches and between adjacent 4^0 branches were measured in five animals. We note a slight but statistically significant bias with greater distances separating ventral 2^0, 3^0, and 4^0 branches than dorsal 2^0, 3^0, and 4^0 branches (See table below). This dorsal vs ventral bias is correlated with a larger number of 2^0 branches on the dorsal side (see **Table 2.1**). Students t-test was used to detect significant differences.

branches in flanking regions. Mutual contact-dependent withdrawal of adjacent branches that deviate from parallel outgrowth could also contribute to this final pattern as seen for the comb cell in the leech [191].

Transcription factors regulate specific steps in PVD dendritic morphogenesis.

RNAi and genetic ablation of transcription factors identified in the PVD microarray profile detected eleven genes with roles in PVD dendritic morphogenesis (Table 2.4). For two of these transcription factors, UNC-86 (POU homeodomain) and MEC-3 (LIM homeodomain), our results confirm earlier findings of PVD expression and necessary roles in PVD differentiation and function [123]. The PVD phenotypes of *unc-86* and *mec-3* mutants are consistent with a model in which *unc-86* acts first to promote 1^{O} branch outgrowth followed by *mec-3* which then initiates 2^{O} branching. The apparently sequential roles of *unc-86* and *mec-3* in PVD morphogenesis parallel their functions in the differentiation of the mechanosensory or touch neurons. In both cell types, *unc-86* is required for *mec-3* expression [123]. In the touch neurons, UNC-86 also functions with MEC-3 in a heterodimeric complex to co-regulate shared targets genes[192, 193]. The roles of *unc-86* and *mec-3* in PVD vs the touch neurons are also likely to differ (discussed in chapter 3). Only four of eleven canonical "mec" genes that *mec-3* regulates in the touch neurons to mediate mechanosensitive function [123, 194], *mec-3, mec-10*, *mec-12* and *mec-17*, are detected in the enriched PVD/OLL data set [12] (Table 2.5). Moreover, *mec-3*

Table 2.5. Specific *mec-3*-regulated genes are enriched in PVD

gene	protein	*mec-3*-dependent	PVD enriched
mec-1	Serine proteinase inhibitor	x	
mec-2	stomatin	x	
mec-3	homeodomain	x	4.9
mec-4	DEG/ENaC	x	
mec-6	paraoxonase		
mec-7	tubulin	x	
mec-8	RNA binding/splicing factor		4.2
mec-10	DEG/ENaC	x	1.7
mec-9	EGF/Kunitz repeat	x	
mec-12	tubulin	x	3.4
mec-14	Aldo-keto-reductase	x	
mec-17	uncharacterized	x	5.0
mec-18	Acyl-CoA synthetase	x	
unc-24	stomatin		

mec-3-dependent genes were compiled from (Zhang et al., 2002)

promotes dendritic branching in PVD [11] but clearly does not activate a comparable pathway in the touch neurons which normally adopt a simple, bipolar morphology [121]. This difference in the morphogenic roles of *mec-3* in distinct sets of *C. elegans* sensory neurons is also observed for the Spineless transcription factor in *Drosophila* which may either promote or inhibit dendritic branching in separate sensory neuron types [23]. These disparate outcomes are proposed to result from combinatorial interactions with other classes of transcription factors [195]. The key role of transcriptional control of dendritic branching is strikingly evident from the results of a genome wide RNAi screen in *Drosophila* that uncovered > 75 transcription factors that govern sensory neuron morphogenesis [196]. Our more limited RNAi screen revealed eleven transcription factors with morphogenic roles in PVD; experiments with mutants which typically display more penetrant phenotypes than RNAi knockdown are likely to detect additional transcription factors with necessary roles in PVD differentiation. The transcription factors that we have uncovered appear to act at different stages of PVD morphogenesis. This finding suggests that the generation of the PVD dendritic array is tightly regulated by an intricate genetic program and thus that the discovery of transcription factor targets in these pathways would provide a critical link between the regulation of gene expression and cell biological processes that control dendritic morphology. For example, the mechanisms that drive dendritic branch initiation are poorly understood. Our studies indicate that the MEC-3 transcription factor is required for the initiation of PVD branching and thus is likely to control target genes with direct roles in this

morphogenic event. The mRNA tagging method is well-suited to this problem and could be used to compare PVD microarray profiles of mutant (e.g., *mec-3*) vs wildtype to uncover these key downstream effector genes [157].

In addition to sharing morphological similarities with nociceptors in other organisms, PVD may also utilize common sets of genes for differentiation and function. At least two of the transcription factors uncovered in our RNAi screen for PVD morphogenic defects, *unc-86*/Brn3a/acj6 and *ahr-1*/Spineless, are also known to govern sensory neuron dendritic morphogenesis in other species (Figure 2.14) [23, 197, 198]. In addition, a significant fraction of ion channel components known to be expressed in mammalian nociceptors are also detected in the PVD microarray data set [199]. These shared proteins include members of the TRP family of ion channels with established roles in mechanosensation and nociception (appendix file 2.5). The striking contact-dependent mechanisms of error correction that we have documented for the PVD neuron in *C. elegans* are likely to be universally employed by sensory neurons in other species that characteristically establish non-overlapping dendritic fields [21, 95]. Taken together, these results indicate that the *C. elegans* PVD neuron affords an attractive model for defining fundamental mechanisms of nociceptor differentiation and function. This work provides a detailed structural, developmental, and molecular foundation for these studies.

Author Contributions

Joseph Watson performed the cell-specific microarray experiments and analyzed them with the help of W. Clay Spencer and Cody Smith. Tim O'Brien helped to confirm transcription factor mutants. All other experiments in this chapter were performed by Cody J. Smith. This work was published in Developmental Biology in 2010.

Acknowledgements

We thank Oliver Hobert for helpful advice on the manuscript; Sylvia Lee for the *mec-7::RFP* transgenic line; Chieh Chang and Sarah Kucenas for help with time-lapse imaging; Braden Boone, John Mote and Shawn Levy of the Vanderbilt Functional Genomics Shared Resource (FGSR) for help with microarray experiments; Shenglong Wang, Nurith Kurn and Joe Don Heath of NuGEN Technologies for help with RNA amplification; members of the Miller lab for technical advice and for comments on the manuscript. Some of the strains used in this work were provided by the *C. elegans* Genetic Center which is supported by NIH NCRR. This work was supported by U. S.-Israel Binational Science Foundation Grant 2005036 (MT), NIH R01 NS26115 (DMM), R21 NS06882 (DMM), NIH F31 NS49743 (JDW) and by NIH grants to Vanderbilt University: P30 CA68485, P60 DK20593, P30 DK58404, HD15052, P30 EY08126 and PO1 HL6744.

CHAPTER III

A GENETIC SWITCH SPECIFIES NOCICEPTOR MORPHOLOGY AND FUNCTION

INTRODUCTION

The human sensory system that innervates the skin can detect a variety of different stimuli including light skin brushes, robust temperature changes and injurious force [131]. The cells within this sensory circuit are thought to have specific roles for detecting specific environmental stimuli. Defects in these sensory cells can result in disease states that affect the sensitivity of sensory inputs [200, 201]. For example, genetic disorders have been linked to complete insensitivity to pain [202]. More commonly, humans experience varying sensitivity to touch and pain, which can change in disease states such as cancer [200-202].

In vertebrates, the dorsal root ganglia (DRG) contains a diverse population of sensory neurons. The skin alone can detect over twenty specific sensory modalities each of which can activate a particular neuronal subtype [131]. For example, c-fibre neurons originate from the DRG and are required for sensation of harsh touch. In contrast, Aβ fibre low-threshold mechanoreceptor (LTMR) neurons sense a variety of non-noxious stimuli such as light mechanical brush

[201]. *Drosophila* and *C. elegans* also have elaborate sensory neurons that are utilized to respond to mechanical stimuli [129] [3][140].

The diversity of these sensory neurons can arise from precise control of transcription factors that drive cell intrinsic programs [13, 14, 20, 23, 26, 112]. Transcription factors can influence neuronal cell fate either by exceeding a concentration threshold or by differential presence or absence of expression in a particular cell type. For example, the concentration of *Drosophila* Cut, a homeodomain transcription factor, specifies the fate of sensory neurons. Sensory neurons with low Cut levels adopt a simple neuronal morphology while those with high Cut level display complex dendritic arbors [18, 20, 196]. In contrast, the *Drosophila* Hamlet transcription factor specifies neuronal fate by exclusive expression in specific neurons [14]. These data support the hypothesis that by controlling the abundance and the differential expression of transcription factors, the animal can generate a complex network of sensory cells with differing morphologies and functions.

Another striking example is the *C. elegans* MEC-3 transcription factor [11, 183, 193]. In *C. elegans*, MEC-3 regulates transcriptional targets that are essential for light-touch neuronal fate [123, 183, 193]. Interestingly, MEC-3 also controls sensory fate of harsh-touch neurons [11, 12, 183]. It seems plausible that MEC-3 could regulate both light-touch and harsh-touch genes but that these genes are somehow differentially regulated in the respective cell-type. However, it has been difficult to test this hypothesis because the MEC-3 regulated harsh-touch genes that specify the elaborate nociceptive dendritic tree have been

largely elusive. In fact, the targets of transcription factors that are employed to generate elaborate dendritic arbors typical of sensory neurons are also mostly unknown [4].

Here we use *C. elegans* to characterize a transcriptional network that specifies sensory neuron function and morphology. We identify two transcription factors, AHR-1 and ZAG-1, which ensure that the animal can properly distinguish light mechanical stimulus from harsh touch. We show that AHR-1/Spineless does so by preventing light-touch neurons from acquiring a nociceptive sensory fate. For the first time, we identify MEC-3 harsh-touch transcriptional targets and show that they are inhibited by AHR-1/Spineless to prevent a nociceptive-like fate in light-touch neurons. Moreover, we show that the abundance of MEC-3 can further refine sensory cell fate. We hypothesize that expression of AHR-1 and the concentration of MEC-3 are utilized to generate the diverse network of mechanosensitive cells in *C. elegans*. This work, therefore, defines a transcriptional program which is employed to generate a sensory network that allows the animal to respond appropriately to their environment.

METHODS

Nematode strains and genetics.

The wild-type *C. elegans* Bristol strain N2 was used for all experiments and cultured as previously described [158]. Also used in this study were mutants: RB584 *zag-1 (ok214)*, SK86 *zag-1 (zd86),* VH4 *zag-1 (rh315),* CZ2485

ahr-1 (ju145), CB1338 *mec-3 (e1338),* RB1657 *hpo-30 (ok2047),* OH7193 *otIs181 (dat-1::mcherry),* OH8510 *otIs236 (asic-1*::GFP), AQ2145 ljEx19 (*egl-46*::YC2.6).

Additional strains that were generated for this study include: NC2440 [*ahr-1 (ju145); wdIs51; wdEx780 (pCJS04, F49H12.4::mcherry)*], NC2517 [*zag-1 (rh315); wdIs52; wdEx835 (pCJS04, F49H12.4::mcherry + ceh-22::GFP*)].

Visualization of AVM and PVM ectopic branching

Confocal images spanning the depth of the animal of wdEx835 (*F49H12.4*::mcherry); wdIs52 (*F49H12.4*::GFP) were taken. Single z-planes were used to identify overlap of adjacent neurons.

Tiling of FLP and converted PVD cell

F49H12.4::mcherry was used to visualize the ectopic PVD-like cell in the anterior while usIs22 (*mec-3*::GFP) was used to visualize FLP branches. Simultaneous imaging of both colors with a confocal microscope was used to visualize overlap. Terminal branches of FLP and PVD were identified in a single confocal plane. Overlap was identified as any two branches that overlap in the same plane.

Confocal Microscopy

Nematodes were immobilized with 15 mM levamisole on a 2% agarose pad in M9 buffer. Images were obtained in a Leica TCS SP5 confocal

microscope. Z-stacks were collected with either 40X (1 um/step) or 63X (0.75 um/step) objectives; single plane projections were generated with Leica Application Suite Advanced Fluorescence software.

Light-touch assay

Stationary animals were tapped just posterior of the pharynx with an eyelash pick. A positive response to touch was defined as any animal that initiated backward movement upon stimulus. All light touch assays were done blind to the experimenter. At least 50 animals were tested per strain.

Calcium Imaging and nociceptive modality

Optical recordings were performed on a Zeiss Axioskop 2 upright compound microscope equipped with a Dual View beam splitter and a Uniblitz Shutter. Filter-dichroic pairs were excitation, 400–440; excitation dichroic 455; CFP emission, 465–495; emission dichroic 505; YFP emission, 520–550. Individual adult worms (~24h past L4) were glued with Dermabond 2-Octyl Cyanoacrylate glue to pads composed of 2% agarose in extracellular saline (145 mM NaCl, 5 mM KCl, 1 mM CaCl2, 5 mM MgCl2, 20 mM d-glucose and 10mM HEPES buffer, pH 7.2). Worms used for calcium imaging had similar levels of cameleon expression in sensory neurons as inferred from initial fluorescence intensity.

Harsh stimuli were delivered using a glass needle with a sharp end (the outcome of these experiments was the same if a piece of platinum wire was

used), which was driven into the worm ~30 to 50 μm at speed of 2.8 μm s–1. Stimulus duration was ~50 ms.

For thermal stimulation, a rectangular metal stage (Microscope Thermal Stage MTS-1, Techne, Proton-Wilten) was fitted with two 100 W peltier elements controlled by a National Instruments controller and custom-made Labview software. A T-junction thermocoupler located inside the chamber where the worm is positioned provides a continuous stream of readings to the temperature controller and adjusts the temperature using a feedback system. A worm grown at 20 °C was glued on an agar pad (2%) in a buffer-filled chamber with an approximate volume of 0.5 ml. Temperature was shifted from 20°C to 15°C.

For the glycerol experiments Animals were glued on 2% agarose pads using Dermabond 2-Octyl Cyanoacrylate glue. The animals were placed under the microscope in a perfusion chamber (RC-26GLP,Warner Instruments) under constant flow rate (0.4 ml/min) of neuronal buffer using a perfusion pencil (AutoMate). Outflow was regulated using a peristaltic pump (Econo Pump, Biorad). Repellents were delivered using the perfusion pencil and manually controlled valves. Glycerol were dissolved in M13 buffer to a final concentration of 1M.

Images were recorded at 10 Hz using an iXon EM camera (Andor Technology) and captured using IQ1.9 software (Andor Technology). Analysis was done using a custom written Matlab (Mathworks) programme. A rectangular region of interest (ROI) was drawn surrounding the cell body and for every frame the ROI was shifted according to the new position of the centre of mass.

Fluorescence intensity, F, was computed as the difference between the sum of pixel intensities and the faintest 10% pixels (background) within the ROI. Fluorescence ratio $R=F_Y/F_C$ of the yellow and cyan channels after correcting for bleed through was used for computing ratio change, ΔR. ΔR for calcium traces was equal to $(R-R_0)/ R_0*100$, where R_0 is the average R within the first 3 sec of recording. For statistical quantification ΔR was computed as $(R_1-R_0)/ R_0*100$, where R_0 and R_1 are the average R over 10 sec prior and following nose touch stimulation. Where more than one comparison was made, an ANOVA followed by Bonferroni t-tests were used instead.

Microarray data analysis

Microarray data were quantile normalized and probe-specific effects were reduced by Robust-Multichip Average (RMA), omitting the background adjustment step (Irizarry RA, 2003; Bolstad BM, 2003). Differentially expressed genes were determined using a linear model and Bayes-moderated *t* statistic (Smyth GK, 2003; Smyth GK, 2004). Transcripts with $\geq$ 1.5-fold change and $\leq$ 1% False Discovery Rate (FDR) were called differentially expressed (summarized in Table 3.3). The PVD-specific transcripts isolated from *mec-3* mutant animals were compared to PVD-specific transcripts from wild-type animals. To control for potential sample preparation differences and transcriptional changes between wild-type and *mec-3* mutants at the whole animal level, we used the wild-type and *mec-3* whole animal RNA samples used for immunoprecipitation of PVD-specific transcripts to identify differentially expressed transcripts in whole animals. The significantly different whole animal

transcripts were filtered from the list of significantly different PVD-specific transcripts to produce the final list PVD-specific *mec-3* regulated transcripts (summarized in Table 3.3).

RESULTS

Mechanosensory neurons adopt distinct morphologies and sensory modalities

C. elegans responds to physical stimuli through a diverse array of mechanosensory neurons [118, 120]. Light touch to the body (posterior to pharynx) is mediated by six "touch neurons" (AVM, PVM, PLML, PLMR, ALMR, ALML) whereas a harsh mechanical stimulus to this region is detected by PVDL and PVDR (Figure 3.1)[183]. These neurons occupy unique locations and adopt distinct branching patterns. The touch neurons display a simple morphology with unbranched longitudinal processes emanating from the cell soma. In contrast, the "harsh-touch" PVD neurons are highly branched with an elaborate dendritic arbor that envelops the animal in a net-like array (Figure 3.1)[11]. FLP neurons in the head, which also respond to harsh mechanical force, show a similar PVD-like pattern of orthogonal dendritic branches [12]. PVD displays additional sensory responses to temperature and hyperosmolarity (see below)[124]. The members of this group of mechanosensory neurons are also distinguished by their developmental origins. The touch neurons ALMR, ALML, PLMR and PLML are generated in the embryo. AVM and PVM are each produced during the first larval

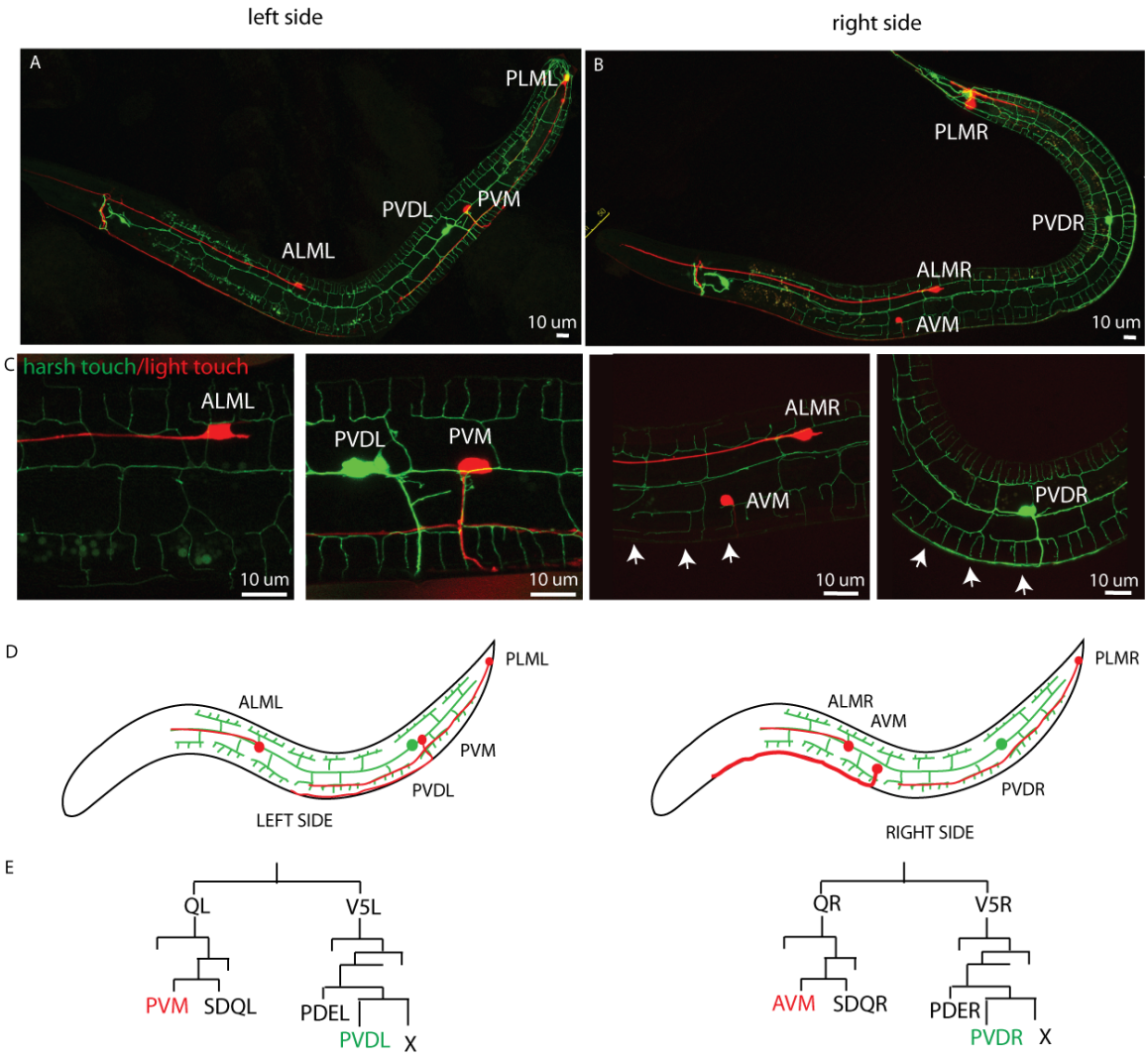

Figure 3.1. The *C. elegans* mechanosensitive network in the body. A,B. confocal z-projections of PVD::GFP and *mec-4*::mcherry labels the mechanosensitive neurons in the body on left (A) and right (B) sides. The large dendritic array of PVD neuron envelops the entire body. Light-touch neurons, ALML, PVM and PLML are located on the left, ALMR, AVM and PLMR on the right. C. Images of post-embryonic neurons PVM and PVD on the left side and PVD and AVM on the right. Note the simple morphology of light-touch neurons. D. Schematic of the mechanosensitive neurons in *C. elegans* on both the left and right side of the animal. E. Cell lineage of PVD and post-embryonic touch neurons AVM and PVM on the left and right sides.

(L1) stage by unique patterns of cell migration and division of Q-cell progenitors on the right (AVM) and left (PVM) sides of the body (Figure 3.1C). PVDL and PVDR arise from the ectodermal blast cell V5 during the second larval (L2) stage (Figure 3.1E)[119]; the highly branched PVD dendritic arbor emerges during later larval (L3-L4) development [12]. The proper development of these cells is essential for the animal to distinguish dangerous strikes from light mechanical brushes and thereby controls behaviors that are important for animal survival. To identify molecules required for the proper balance of this mechanical network we identified proteins required for the elaborate PVD branching pattern.

AHR-1/Spineless prevents AVM from adopting a PVD-like fate

On the basis of a genetic screen for transcription factors that regulate PVD morphology, we initially reported that PVD displays extra dendritic branches in an *ahr-1/spineless* mutant [12]. A closer examination of *ahr-1(ju145)* animals revealed, however, that the additional PVD-like branches actually arise from another cell soma that expresses the PVD marker, *F49H12.4::*GFP [163] (Figure 3.2). In most cases, this ectopic PVD-like cell is located anterior to the vulva whereas PVD is positioned in the posterior body (Figure 3.2B,C). In addition to mimicking the PVD pattern of dendritic branching, the extra PVD-like cell also expressed PVD-specific GFP markers for *ser2prom3* and *egl-46* (Table 3.1) [12, 124].

We hypothesized that the extra PVD-like cell may be generated by a lineage duplication of PVD. To test this we visualized a marker for PDE, a

Table 3.1. Molecular Markers for mechanosensitive cells. PVD markers *F49H12.4, asci-1, ser2prom3* are expressed in PVD in wild-type neurons. In *ahr-1* and *zag-1* mutants, PVD markers are expressed ectopically in AVM and PVM. An extra DAT-1 cell is not present in *ahr-1* and *zag-1* mutants. Light-touch marker *mec-4* is expressed in wild-type AVM and PVM but are not expressed in AVM of *ahr-1* or PVM of *zag-1*. MEC-3 expression is seen in all mechanosensitive cells in both wild-type and mutants backgrounds. However, levels of MEC-3::GFP are altered in *ahr-1* mutants (see figure 5). Numbers represent cells with marker/total number counted. The cAVM and cPVM also expressed *egl-46*.

Molecular marker	Genotype								
	wildtype			ahr-1 (ju145)			zag-1 (rh315)		
	AVM	PVM	PVD	AVM	PVM	PVD	AVM	PVM	PVD
F49H12.4	0/50	0/50	50/50	25/40	1/40	40/40	9/40	38/40	40/40
asic-1	0/20	0/20	20/20	--	--	--	0/20	17/20	20/20
ser2prom3	0/20	0/20	20/20	12/20	1/20	20/20	0/20	18/20	20/20
mec-3	20/20	20/20	20/20	20/20	20/20	20/20	30/30	30/30	30/30
dat-1	0/20	0/20	0/20	0/20	0/20	0/20	0/20	0/20	0/20
mec-4	20/20	20/20	0/20	1/7	7/7	0/7	21/21	1/21	0/21

lineage sister of PVD [119, 203]. However, we did not observe an additional PDE neuron in the anterior ruling out that the extra cell is from a lineage duplication (Table 3.1). We therefore considered the alternative possibility that the extra PVD-like cell could have arisen from a cell-fate conversion. The extra PVD-like neuron is located in an anterior lateral region normally occupied by AVM and its lineal sister SDQR (Figure 3.2I). To test this model we visualized a marker of AVM. We noted that the light touch neuron-specific marker *mec-4::mCherry* was expressed in only 5 cells in *ahr-1* mutants (86% of animals)(Table 3.1) whereas *mec-4::mCherry* marks 6 light touch neurons in the wild-type animals *[204]*. In a small fraction of cases (5%) an AVM cell of normal morphology expresses *mec-4*::mCherry and SDQR adopts a PVD-like morphology in the *ahr-1* mutant (data not shown). These results match the known expression of AHR-1/spineless in the Q-cell lineage and therefore suggest that AVM (and occasionally SDQR) has been converted to a PVD-like cell in the absence of *ahr-1/spineless* [205]. We therefore refer to the ectoptic PVD-like cell as “converted AVM” cell or “cAVM.”

The AVM cell arises in the early L2 larvae animals before PVD is generated [119]. We hypothesized that if cAVM generated PVD-like dendritic branches we would expect to see dendritic branching in animals before PVD arises. To characterize this, we visualized initiated branches in cAVM neurons in early L2 larvae animals (Figure 3.2D). We found that cAVM displayed dendritic branching in early L2 Larvae animals. We therefore conclude that cAVM generates dendritic branches similar to PVD in L2 larvae animals. We

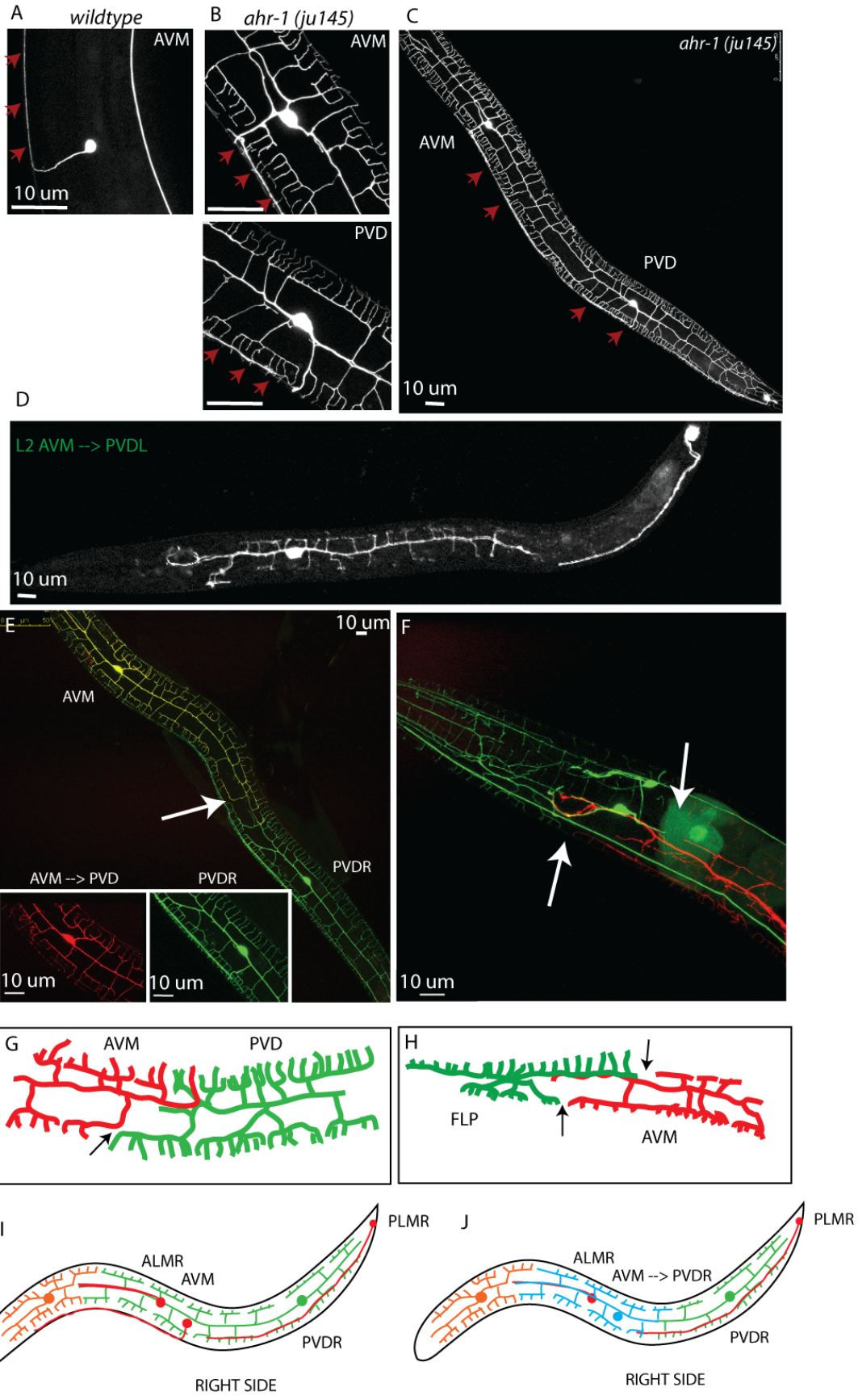
A
wildtype
AVM
10 um
B
ahr-1 (ju145)
AVM
PVD
C
ahr-1 (ju145)
AVM
PVD
10 um
D
L2 AVM --> PVDL
10 um
E
10 um
AVM
AVM --> PVD
PVDR
PVDR
10 um
10 um
F
10 um
G
AVM
PVD
H
FLP
AVM
I
PLMR
ALMR
AVM
PVDR
RIGHT SIDE
J
PLMR
ALMR
AVM --> PVDR
PVDR
RIGHT SIDE

Figure 3.2. AHR-1/Spineless restricts nociceptive fate. A. Confocal z-projection of wild-type AVM neurons display a simple morphology with a process that enters the ventral nerve cord and turns anterior in the nerve ring of the head. B,C. In *ahr-1 (ju145)* animals, AVM displays a large dendritic tree that contains an axon that enters the ventral nerve cord and navigates posterior. The dendritic tree of in cAVM (B, top) is similar to the PVD (B, bottom) array including an axon that projects toward the vulva. D. cAVM shows PVD-like lateral branches in the L2 stage. Arrow denotes newly generated PVD neuron that has not initiated branching at this stage. E,G. Confocal image and schematic showing this dendritic array is maintained in adult animals. The dendritic array of AVM appears to be truncated where PVD intersects it. F, H. Confocal image and schematic of AVM and FLP dendritic branches in *ahr-1 (ju145)* mutants. cAVM and FLP dendritic branches to not overlap (n=18/20 animals). I, J. Schematic of wild-type and the ahr-1 (ju145) mechanosensitive neurons on the right side shows an extra nociceptive cell in ahr-1 mutants that tile with FLP and PVD.

hypothesized that cAVM neuron maintained these PVD-like branches in the adult. To test this we visualized PVD and cAVM in adult animals. For simultaneous observation of cAVM and PVD, we combined a mosaic PVD::mcherry marker with the integrated PVD::GFP label (see methods). We visualized the individual morphology of each neuron in randomly occurring animals that retain the PVD::mCherry marker in cAVM (mCherry + GFP) but not PVD (GFP only). This analysis confirmed that cAVM retains a PVD-like branching pattern in the adult (Figure 3.2E,G) in contrast to the normal AVM morphology of a single process that exits the cell soma, enters the ventral nerve cord and projects anteriorly to the nerve ring (Figure 3.2A).

The combination of the stable PVD::GFP marker with the mosaic PVD::mCherry label also revealed that cAVM branches rarely overlap with the PVD dendritic arbor which appeared truncated and failed to enter the region occupied by cAVM in *ahr-1* mutants (Figure 3.2E). In contrast, in wild-type animals, PVD dendrites may touch AVM as they extend anteriorly to envelop the entire body region (Figure 3.1A). This feature is reminiscent of the tiling that is normally visualized in PVD and FLP neurons that rarely overlap in head of wild-type animals [12]. We therefore hypothesized that cAVM adopted the molecular identity to tile with nociceptive neurons. To ask this we simultaneously visualized cAVM and FLP by marking FLP with *mec-3::*GFP and cAVM with PVD::mcherry. In *ahr-1* mutant animals, the cAVM neuron consistently tiled with FLP (15/16 animals)(Figure 3.2F,H). Dendritic tiling is characteristic of sensory neurons that display similar sensory modalities [9, 95, 206]. Our results are therefore

consistent with a model in which the AVM touch neuron in *ahr-1* mutant animals is converted into a harsh touch mechanosensory neuron resembling PVD and FLP.

We noted an additional feature of cAVM morphology that is also indicative of this transformation. In wild-type animals, a single axon projects downward from the PVD cell soma to enter the nerve cord and extends anteriorly to terminate before reaching the vulval region [12, 121]. (Figure 3.1A,B). In the wild type, the AVM axon shows a similar downward trajectory but enters the ventral nerve cord anterior to the vulva and projects into the nerve ring in the head [121]. In *ahr-1* mutants, the PVD axon appears normal (Figure 3.2B). We hypothesized that if cAVM is converted to a PVD-like cell it may adopt a PVD axon guidance path. To ask this we visualized the axon of cAVM. In *ahr-1* mutants the cAVM axon now extends posteriorly in the ventral nerve cord and grows toward the region occupied by the PVD axon posterior to the vulva (Figure 3.2B). These results suggest that cAVM has adopted an identity that changes its axonal guidance program to that of PVD. Furthermore, the convergent outgrowth of the cAVM and PVD axons toward a common destination in the ventral nerve cord is suggestive of a potential guidance cue originating from this region. Together, our results suggest that AHR-1 normally functions in the Q-cell lineage to prevent AVM from adopting a PVD-like fate.

cAVM adopts sensory modalities normally displayed by PVD neurons

In the wild-type animal, AVM mediates a characteristic response to "light touch;" application of gentle physical stimulus (*e.g.,* with an eyelash) to the anterior body region occupied by AVM evokes a backward locomotory escape response [118]. We hypothesized that the extra branches and the change in the axonal guidance of the cAVM neuron in *ahr-1* mutants would impact the animal's behavior to a light mechanical stimulus. To test this we induced a light-touch behavioral response just posterior to the pharynx (Figure 3.4A). A majority (97%) of wild-type animals crawl backward after light touch to the anterior body (Figure 3.4B) whereas a significant fraction (~40%, $p < 0.05$) of *ahr-1* mutant animals failed to react to this stimulus (Figure 3.4B). To test the idea that cAVM is specifically defective in light touch, we used a cameleon marker to visualize calcium transients in cAVM. This experiment revealed that cAVM neurons in *ahr-1* mutant animals are less likely to respond to light mechanical stimuli than the wild-type AVM neuron (2/5 ahr-1 cAVM responded). Thus, these data are consistent with the defective behavioral response of *ahr-1* mutants in the light touch assay (Figure 3.4B). Since the cAVM cell strongly resembles PVD in *ahr-1* mutants we next asked if cAVM also adopts PVD-like sensory modalities. We first established that harsh-touch elicits a calcium transient in the cAVM cell similar to that of PVD neurons in wild type animals and in *ahr-1* mutants (Figure 3.4F). In wild-type animals the PVD cell responds to cold temperature whereas AVM does not. To ask if cAVM adopted PVD sensory modalities we visualized the cAVM response to cold temperature. cAVM displayed a similar cold

temperature response as PVD (Figure 3.4D). We also exposed *ahr-1* mutants to 1 M glycerol to confirm that cAVM responds to the newly discovered sensitivity of PVD to hyperosmolarity (Figure 3.4E). Thus in *ahr-1* mutants the proper AVM response to mechanical stimulus is lost. These data suggest that AHR-1/spineless not only controls AVM morphology and axon guidance but also defines AVM sensory function. We therefore conclude that cAVM cells are converted to a PVD-like fate in *ahr-1* mutant animals.

ZAG-1 prevents PVM from adopting a PVD-like fate

We quantified the percentage of animals with extra PVD-like cells in the anterior vs posterior regions that correspond to the locations of the two post-embryonic touch neurons, AVM and PVM. Extra PVD-like cells were never observed in wild-type animals (Table 3.2). A majority (63%) of *ahr-1* mutant animals show an ectopic PVD-like cell in the anterior region normally occupied by AVM (Table 3.2). Interestingly, the PVM cell also converted to a PVD-like morphology but at a much lower frequency (Table 3.2). We therefore considered the possibility that AHR-1 functions primarily to specify the AVM cell-fate but also exercises a minor parallel role in the PVM progenitor. This idea is substantiated by the finding that a null allele of the AHR-1 cofactor, AHA-1 [205], resulted in a similarly biased transformation of AVM vs PVM to a PVD-like fate (Table 3.2). Thus, we hypothesized that an additional transcription factor could be primarily required for specifying the PVM cell-fate. We have previously reported that a mutation in the conserved Zn finger/homeodomain transcription factor, ZAG-1,

Table 3.2. Genetic interaction between *ahr-1* and *zag-1* mutants. Extra PVD cells are seen in the location of AVM and PVM and *ahr-1* and *zag-1* mutants. Double mutants of *ahr-1; zag-1* have both cAVM and cPVM suggesting they function in different cells to restrict nociceptive fate.

Duplicated cell	Wild-type	*ahr-1*	*aha-1*	*zag-1*	*ahr-1; zag-1*
AVM only :	0/50	23/40	29/40	0/40	2/40
PVM only :	0/50	1/40	0/40	29/40	0/40
AVM and PVM:	0/50	2/40	4/40	9/40	38/40

results in an extra PVD cell on one side of the body [12](Chapter 2) and therefore considered the possibility that ZAG-1 could fulfill this role.

PVM is located on the left side of the animal and adjacent to the PVD cell soma [118, 121](Figure 3.1A,C,D,E). Mutants of *zag-1 (rh315)* showed an extra PVD-like cell in this location (Figure 3.3A,B). In addition to displaying the highly branched morphology that is characteristic of PVD, the extra PVD-like cell also expressed multiple PVD markers (Table 3.1). We considered the possibility that this PVD-like cell could have arisen from duplication of the PVD lineage (Figure 3.1E). However, the absence of an additional *dat-1*::mcherry-expressing PDE neuron in *zag-1(rh315)* ruled out this model (Table 3.1). Because the PVD sister cell, V5Rpaapp, normally undergoes programmed cell death (Figure 3.1E) we considered a model in which this cell survives in the *zag-1* mutant and gives rise to a duplicate PVD neuron. To test this we visualized *zag-1* mutants in conjunction with a mutant that blocks apoptosis. We ruled out this model by finding that a mutation in the *egl-1* gene that normally blocks V5Rpaapp apoptosis results in a third PVD-like cell on the left side in the *zag-1; egl-1* double mutant (~30% have 3 PVD cells). We next hypothesized that the extra PVD cell may arise from a cell fate conversion. We visualized PVM with *mec-4*::mcherry to test if the PVM cell could be converted. Expression of the light-touch neuron specific marker, *mec-4*::mcherry, was not detected in this region therefore suggesting that the normal PVM cell is missing in the *zag-1* mutant (Table 3.1). Based on these results, we conclude that the extra PVD neuron observed in *zag-*

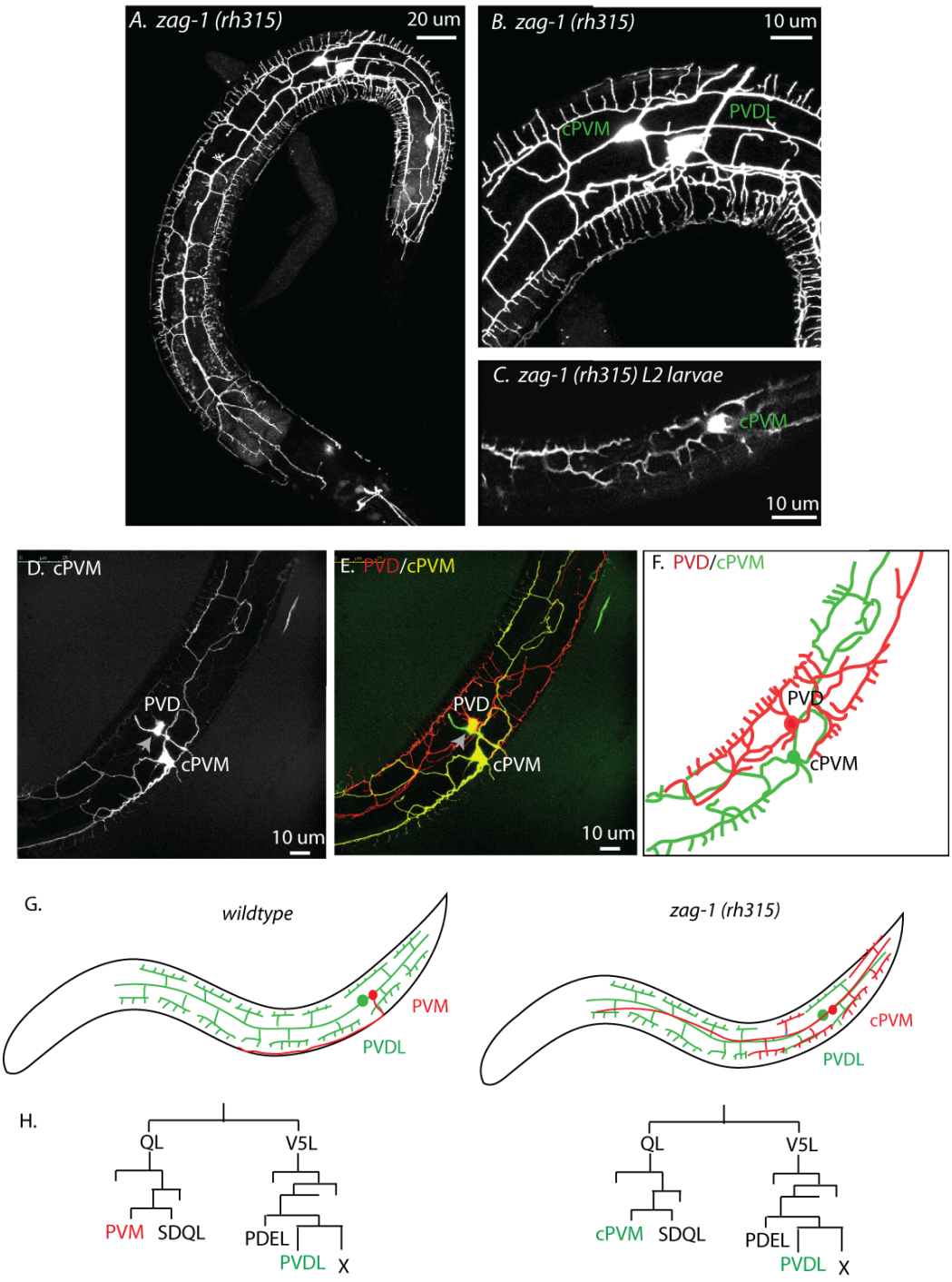

Figure 3.3. ZAG-1 is required to restrict nociceptive fate. A. Confocal image of the left side of the animal showing an extra PVD-like cell in *zag-1* mutants. B. Inset image shows cPVM neuron with PVD-like branches. C. cPVM shows lateral branches in the L2 stage before PVD initiates dendritic morphogenesis. D,E,F Confocal images of cPVM and PVD showing that dendritic branching is maintained in the adult animals although with less coverage. G. Schematic of the mechanosensitive cells on the left side in wild-type and zag-1 animals. ZAG-1 mutants lack the light-touch neuron PVM. H. Cell lineage of PVM in wildtype and *zag-1* mutants.

1 mutants arises from the conversion of PVM into a PVD-like cell. We refer to this converted PVM cell in *zag-1* mutants as cPVM.

We hypothesized that cPVM adopted PVD-like branching. The timing at which cPVM initiates lateral branching is consistent with the proposal that PVM is converted to a PVD-like fate in *zag-1* mutants. PVM normally arises soon after hatching in the wild type and cPVM was also initially observed in the first larval stage of *zag-1* mutant animals. As noted earlier for cAVM, the cPVM cell initiated a PVD-like branching pattern in L2 larvae in *zag-1* mutants whereas the PVD neuron, which first appears in L2 animals, does not display lateral branches until later, in the L3 larval stage (Figure 3.3C)[12] We hypothesized that this dendritic branching was maintained in adults. We used transgenic animals expressing the mosaic PVD::mCherry marker to distinguish PVD vs cPVM lateral branches in later larval stages and in the adult. Random loss of the mCherry marker from PVD but not cPVM confirmed that the PVD-like branching pattern of the cPVM cell is retained during larval development (Figure 3.3D). This analysis also revealed that PVD (marked with PVD::GFP) showed a reduced number of lateral branches in the *zag-1* mutant and that, in general, PVD and cPVM branches did not overlap (Figure 3.3D-F). This observation stands in contrast to wild-type animals in which PVD and PVM processes may contact one another (Figure 3.1D-F). The apparent tiling activity of PVD and cPVM is consistent with a model in which ZAG-1 normally functions to prevent PVM from adopting a PVD-like mechanosensitive fate.

cPVM neurons display PVD-like nociceptive responses

The transformation of PVM to a PVD-like neuron predicts that sensitivity to light touch, which depends in part on PVM, should be impaired by the *zag-1* mutation [118]. As previously noted for *ahr-1* mutants, *zag-1* animals showed a defective response in the light touch assay (Figure 3.4B). These data demonstrate that ZAG-1 function is required for a robust light-touch response. We hypothesized that like cAVM in *ahr-1* mutants, cPVM in *zag-1* mutants adopt a nociceptive modality. We used calcium imaging to confirm that cPVM neurons display a strong response to cold temperature stimuli that is not visualized in wild-type PVM (Figure 3.4D). cPVM also responded to other nociceptive sensory modalities (Figure 3.4D-F). These calcium transients were comparable to that of the PVD cell in *zag-1* mutants and to *wild-type* PVD cells. Interestingly, we did see some variation in the response of both the converted PVM and PVD cells in *zag-1* mutants (data not shown). We hypothesize that this is likely from the loss of branch coverage in *zag-1* mutants. Nonetheless, we conclude that *zag-1* controls the morphology and sensory modality of PVM.

AHR-1 and ZAG-1 function to maintain mechanosensitive balance

Our results indicate that most PVM neurons are converted into an extra PVD-like cell, cPVM, in *zag-1* mutants (Table 3.2). Close inspection revealed that a small fraction of AVM neurons are also transformed into a PVD-like cell in *zag-1* animals (Table 3.2). Because the *ahr-1* mutant shows a reciprocal effect in which the AVM adopts a PVD-like fate more frequently than PVM, we

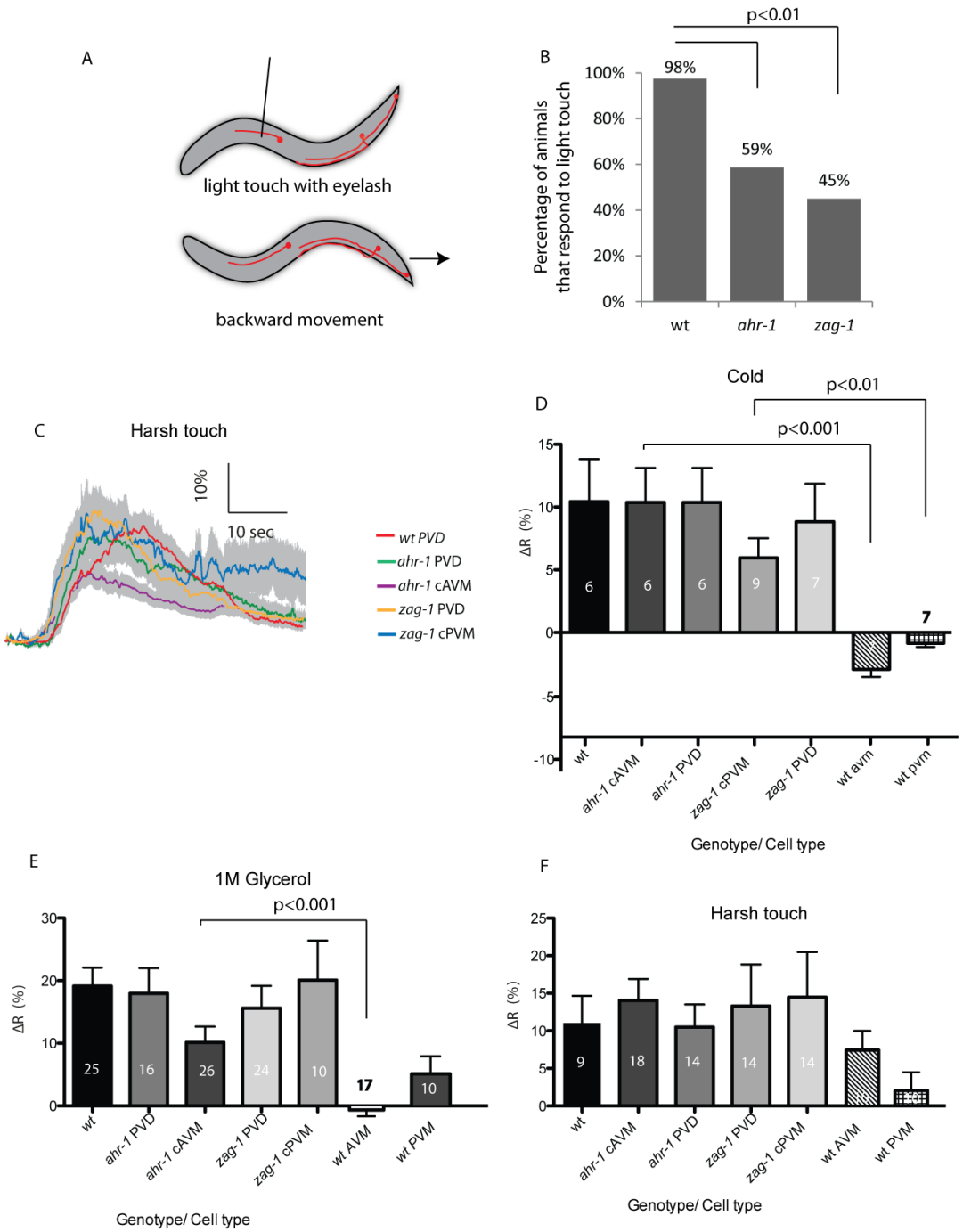

Figure 3.4. AHR-1 and ZAG-1 specify sensory neuron function. A. Experimental design of light-touch assay. B. Quantification of light-touch assay showing that 97% of wild-type animals responded. A significantly smaller fraction of *ahr-1* (59%) and *zag-1* (45%) animals are affected. C. Representative traces showing calcium transients in designated neurons. Note the similarity between the response. D. Quantification of calcium change showing cAVM and cPVM respond to cold temperature like PVD. E. Quantification of cameleon signal showing that hyperosmolarity (1 M glycerol) evokes a PVD-like response in cAVM and cPVM. F. Quantification of harsh touch shows that cAVM and cPVM respond to harsh touch. Numbers of animals examined are noted on histograms.

hypothesized that AHR-1 and ZAG-1 could function together to define the cell-fate of both post-embryonic light-touch neurons. To test this we visualized PVD::GFP in *zag-1;ahr-1* double mutants. In *zag-1; ahr-1* double mutants, 95% of animals showed conversion of both AVM and PVM into a PVD-like cell (Table 3.2). These results suggest that that AHR-1 is primarily required in AVM but also contributes to the PVM touch neuron fate. Conversely, ZAG-1 primarily defines the PVM fate but also functions with AHR-1 to specify AVM. Because AHR-1 and ZAG-1 are required in AVM and PVM to prevent the adoption of the PVD nociceptor fate, we next asked if they interact with MEC-3, a protein with dual roles in specifying both PVD and touch neuron fate.

AHR-1 functions with MEC-3 to specify light-touch mechanosensory neuron fate.

MEC-3 encodes a conserved LIM homeodomain transcription factor that is required for normal development of both PVD and light touch mechanosensory neurons [183]. Lateral branches are not generated in *mec-3* mutant PVD neurons which suggests that MEC-3 activates a transcriptional cascade that promotes dendritic branching [11, 12]. Because cAVM adopts a PVD-like morphology in *ahr-1* mutant animals, we wondered if MEC-3 was also required for this elaborate dendritic branching pattern. To test this idea, we generated a double mutant of *ahr-1; mec-3* and determined that cAVM neurons now resemble the simple, unbranched morphology of *mec-3* mutant PVD neurons (Figure 3.5H,I). This result confirms that MEC-3 function is necessary for cAVM branching in the *ahr-1*

mutant. Two potential models are consistent with this result: (1) AHR-1 normally limits *mec-3* expression in the touch neurons; (2) AHR-1 functions downstream to block expression of MEC-3-dependent targets that drive the creation of PVD-like branches. To address this question, we first asked if AHR-1 regulates *mec-3*.

In wild-type animals, *mec-3* is normally expressed in the 6 light touch neurons and in the FLP and PVD neurons [123, 207](Figure 3.5B). We noted that a *mec-3*::GFP reporter was strongly expressed in the touch neurons and in FLP but showed a weaker intensity in PVD. In the *ahr-1* mutant, *mec-3*::GFP expression was substantially reduced in cAVM in comparison to the wild type AVM neuron (Figure 3.5A,B). This finding argued against the idea that AHR-1 inhibits *mec-3* expression and favored the alternative possibility that AHR-1 actually activates *mec-3* to specify touch neuron traits. We tested this idea by examining the touch neuron-specific marker *mec-4*::mcherry which normally depends on *mec-3* function for expression in AVM [208]. *mec-4::*mCherry is not detected in cAVM neurons in *ahr-1* mutants but is restored by over-expression of MEC-3 in an *ahr-1* mutant (Table 3.1, Figure 3.5D,E). It is also important to note that over-expression of *mec-3* in *ahr-1* mutants did not prevent the formation of ectopic PVD-like branches or inhibit expression of the PVD-specific marker gene, *F49H12.4::*GFP in cAVM (Figure 3.5E). These results are consistent with a model in which MEC-3 must exceed a high threshold to activate expression of light touch neuron genes (*e.g., mec-4*) but that low levels of MEC-3 are sufficient to drive expression of transcripts that specify PVD-like traits (*e.g.,* lateral branching). We therefore considered the hypothesis that AHR-1 negatively

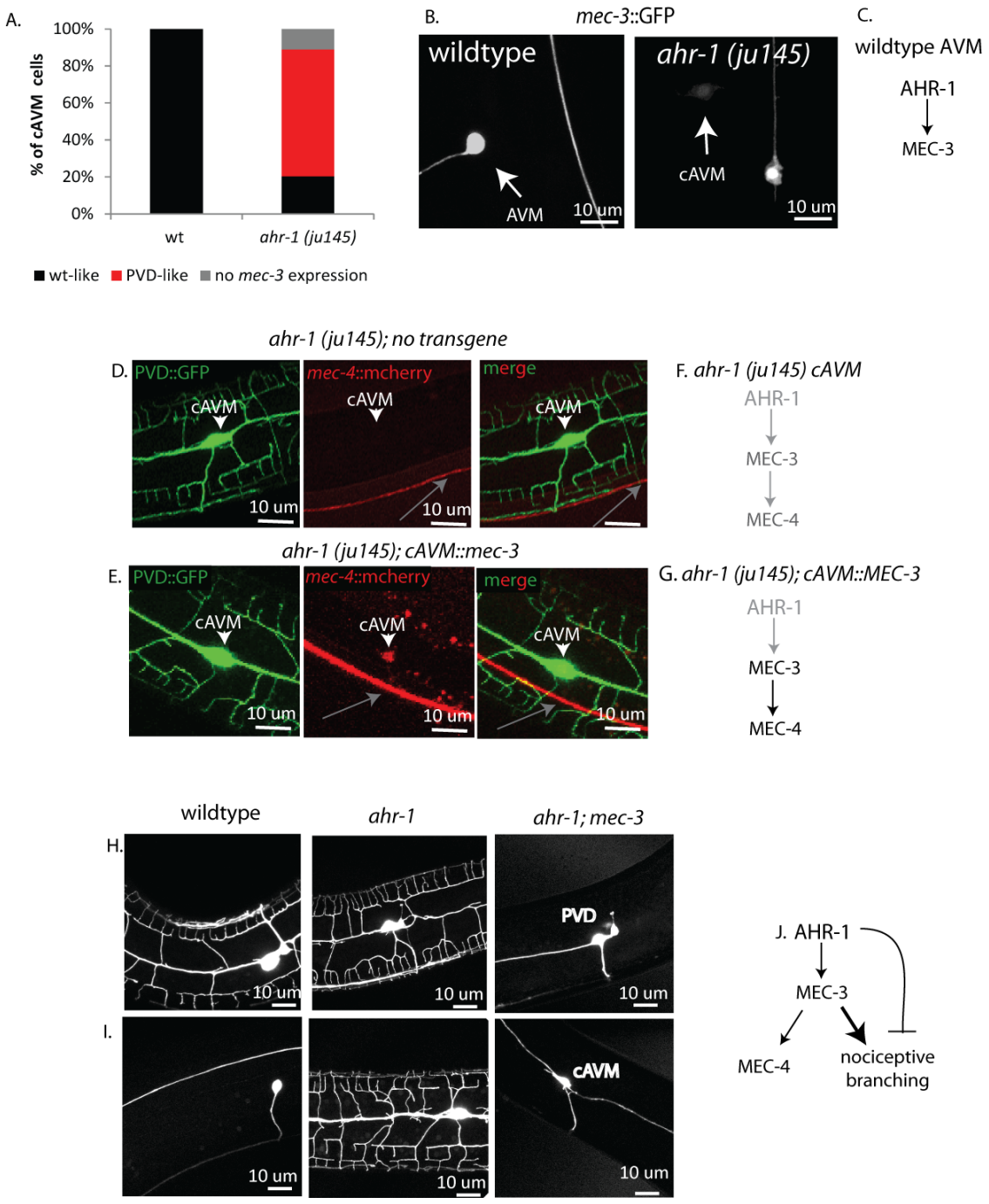

Figure 3.5. AHR-1 interacts with MEC-3 to control cellular fate. A. Quantification of *usIs22* (*mec-3*::GFP) in AVM in wild-type (wt) and *ahr-1*. Black represents strong *mec-3*::GFP expression, PVD-like (red) represents weak *mec-3*:GFP expression. B. Representative image of AVM in wild-type and cAVM in *ahr-1* mutants. Note that mec-3::GFP shows strong expression in ALM in both wt and *ahr-1*. D. PVD::GFP (green), *mec-4*::mcherry (red) and merge shows loss of *mec-4* expression in mutants. E. Overexpression of *mec-3* in cAVM restores *mec-4*:mcherry expression. F. Schematic of transcriptional pathway in *ahr-1* (F) and *ahr-1* with cAVM::MEC-3 (G). H,I. Confocal images reveal that *ahr-1* mutants display an extra PVD-like cell in the anterior that fails to develop lateral PVD-like branchines in *ahr-1; mec-3* double mutants. J. Transcriptional code for generation of AVM.

regulates PVD-like branching in AVM by inhibiting MEC-3 transcriptional targets and set out to identify these downstream genes.

MEC-3 regulated target genes are required for dendritic branching.

MEC-3 is likely to regulate different sets of transcripts in light touch vs PVD neurons because these two classes of mechanosensitive neurons adopt distinct morphologies and functions. We hypothesized, for example, that MEC-3-regulated targets in PVD should include genes that promote branching since PVD neurons show a branchless phenotype in *mec-3* mutants [11, 12]. To identify these genes, we used the mRNA tagging method to isolate PVD-specific transcripts from L2 stage larvae during the period in which PVD lateral branching is first observed [12]. A comparison of wild-type vs *mec-3* mutant PVD profiles revealed differentially expressed transcripts (See Methods). We focused on the list of 185 genes that were down regulated in the *mec-3* sample because MEC-3 is reported to function as a transcriptional activator [123, 194]. This analysis revealed several known MEC-3 regulated genes (*acp-2, des-2, deg-3, mec-7, mec-10, mec-18*) [194, 209]. Novel targets from this list encode a wide array of protein types including extracellular matrix proteins, transcription factors and cell-surface receptors (Table 3.3).

A MEC-3 harsh-touch target, *hpo-30*, is controlled by AHR-1

Our microarray revealed that HPO-30/Claudin was a potential MEC-3 harsh-touch transcriptional target (Table 3.3). To confirm this result we

Table 3.3. Summary of potential MEC-3 harsh-touch targets.. All the data represented in this table was collected by Tim O'Brien.

Protein Type	Enriched in microarray	Conserved	MEC-3 binding site	Screened for PVD defect	Hits	Conserved hits	Notable Gene Names
Acetylcholine receptor	2	2	1	1	0	0	
Enzyme	28	26	12	18	3	3	*pef-1, acp-2*
extracellular matrix	13	13	2	9	2	2	*col-159*
f-box protein	3	2	3	3	0	0	
Kinase	2	2	0	1	1	1	*T16G1.5*
Ligand	10	8	6	7	0	0	
Mechanosensation	4	4	2	0	0	0	
Metal Transfer	4	3	1	2	0	0	
Neuropeptide	3	2	2	1	0	0	
Receptor	7	7	2	4	2	2	*fukutin, hpo-30*
Secreted Molecules	4	3	1	1	0	0	
Transcription Factor	4	3	2	4	2	2	*zag-1, egl-46*
Transporter	4	4	4	2	0	0	
Uncharacterized protein	93	77	43	32	8	6	
Total	181	156	81	85	18	16	

visualized an *hpo-30* transcriptional reporter in the *mec-3* mutant. Consistent with our hypothesis that MEC-3 activated *hpo-30* transcription, *hpo-30*::GFP intensity was reduced in PVD of *mec-3* mutants compared to PVD of wild-type animals (Figure 3.6G,H). This result this consistent with the hypothesis that MEC-3 positively regulates *hpo-30* transcription in PVD.

Since MEC-3 is required for the elaborate branching and transcriptionally controls *hpo-30* we hypothesized that *hpo-30* may be important for PVD dendritic morphogenesis. To test this we visualized PVD in *hpo-30* mutants. This analysis showed that *hpo-30* is required for the elaborate dendritic pattern of PVD (Figure 3.6C). Since HPO-30 is required for branching of PVD, we hypothesized that it would also be required for branching of the extra PVD-like cell, cAVM, in *ahr-1* mutants. To test this hypothesis we generated an *ahr-1; hpo-30* mutant. Consistent with our hypothesis, *ahr-1; hpo-30* mutants had cAVM neurons that resembled PVD in *hpo-30* mutants (e.g. unbranched neuron)(Figure 3.6A-D). Based on these data we hypothesize that the extra branching that is generated in *ahr-1* mutants is dependent on ectopic *hpo-30* expression and thus AHR-1 normally inhibits *hpo-30* expression to prevent nociceptive-like dendritic branching in the light-touch neuron AVM (Figure 3.6E). If AHR-1 does negatively regulate *hpo-30* in AVM then *hpo-30*::GFP should be ectopically expressed in *ahr-1* mutants in AVM. Consistent with this hypothesis *hpo-30*::GFP was expressed in cAVM in *ahr-1* mutants (Figure 3.6F). In wild-type animals, *hpo-30*::GFP was never visualized in AVM (data not shown). These results therefore suggest that AHR-1 blocks a MEC-3 harsh-touch target, HPO-30 in AVM.

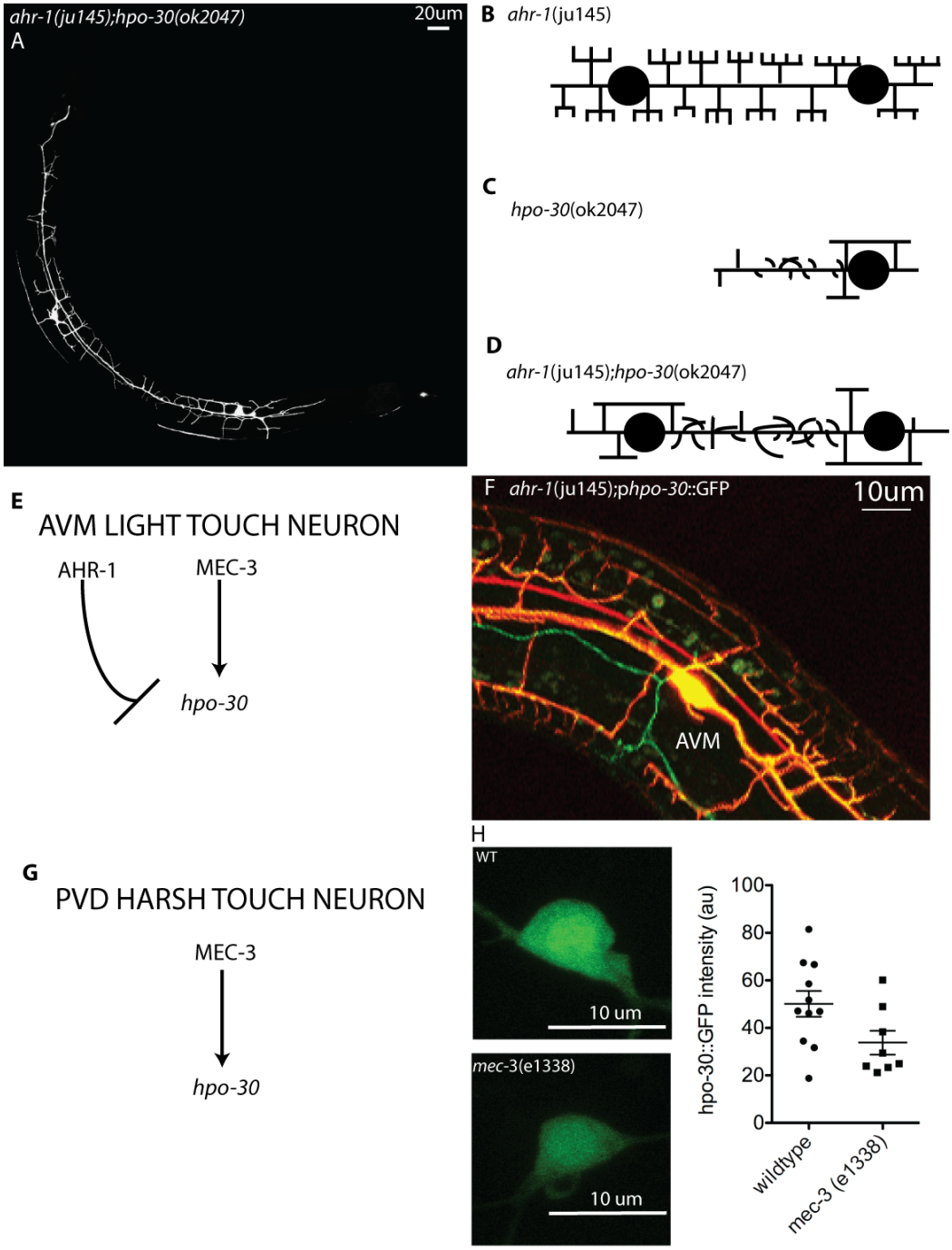

Figure 3.6 AHR-1 inhibits MEC-3 harsh-touch targets. A. Confocal image of PVD::GFP in *ahr-1 (ju145); hpo-30 (ok2047).* B-D. Schematic of PVD and AVM in *ahr-1 (ju145)* (B), *hpo-30 (ok2047)* (C) and *ahr-1 (ju145);hpo-30 (ok2047)* (D) that shows PVD (posterior) and cAVM (anterior) have reduced branching. Anterior to the left and ventral down. E. Model showing MEC-3 positively regulates *hpo-30* and AHR-1 negatively regulates *hpo-30*. F. Confocal image of PVD::mcherry and *hpo-30*::GFP showing ectopic expression of *hpo-30* in cAVM. G. Model for MEC-3 control of *hpo-30* in PVD. H Confocal images of *hpo-30*::GFP and quantification of its intensity in wild-type animals (wt) and *mec-3 (e1338)* mutants.

Model of a transcriptional cascade that maintains the mechanosensitive network

UNC-86 and MEC-3 have been shown to be required for differentiation of both light-touch and harsh-touch neurons [192]. However, based on the different morphology and function of these two cell types it is apparent that there must be a difference in the transcriptional identity that is activated by MEC-3. We propose that in light-touch neurons, a harsh-touch inhibitor is expressed (AHR-1 or ZAG-1) that inhibits MEC-3 targets that specify harsh-touch morphology (e.g. *hpo-30*) and function. In such a model, only light-touch genes can be activated. When the harsh-touch inhibitor is lost in light-touch cells, MEC-3 harsh-touch targets are ectopically activated and transform the cell into a nociceptive modality. In harsh-touch neurons, a mirror model may exist such that MEC-3 activates both harsh-touch and light-touch genes but that a light-touch inhibitor prevents expression of light-touch genes. However, we favor a model that elevated MEC-3 levels in light touch neurons controls light touch transcripts and this threshold is not reached in PVD.

DISCUSSION

The nervous system is crowded with neurons that have different morphologies and functions [7]. How a neuron specifies its morphology and function is likely controlled intrinsically by a transcriptional network and extrinsically by

environmental cues [4, 6]. In this study we identify an intrinsic molecular pathway that controls the dendritic morphology of two different neuronal types. We show that AHR-1/Spineless limits nociceptive fate by inhibiting harsh-touch targets. This prevents light-touch cells from generating large dendritic trees that respond to harsh stimuli. The tight regulation of MEC-3 targets provides the animal with the ability to make two distinct cell types with a single transcriptional activator.

A conserved role for AHR-1

Many transcription factors have been shown to be required for dendritic morphogenesis [12, 13]. Despite the extensive knowledge known about the transcription factors the targets of these proteins have been largely elusive. For example, AHR-1/Spineless is required to specify the complexity of *Drosophila* sensory neurons but does not seem to regulate key components that control dendritic branching such as abrut and cut [23]. For the first time, our study identifies that AHR-1 does regulate a key component of dendritic branching.

The AHR-1 transcriptional network we describe demonstrates that the AHR-1 requirement in dendritic development is conserved. In *Drosophila*, AHR-1/Spineless shares a common role such that it controls the complexity of sensory neurons [23]. The conservation of this role between nematodes and insects suggests that AHR-1 is likely to adopt a similar function in vertebrate sensory neurons. Our study also identifies many new aspects of the AHR-1 pathway. In *Drosophila*, the AHR-1 cofactor was not identified to be required [23]. In

contrast, the AHR-1 cofactor, AHA-1, is required to control dendritic morphogenesis in *C. elegans*. Our studies also demonstrate that loss of AHR-1 results in a neuron that responds to harsh touch stimuli. This suggests that AHR-1 not only controls branching genes but also other aspects of fate such as nociceptive mechanosensitive channels. Lastly, in *C. elegans*, it is plausible that AHR-1 does not control dendritic complexity of harsh touch neurons directly. Instead, the loss of branching that is visualized in harsh-touch neurons could be from gain of function tiling with newly specified harsh-touch neurons. We therefore hypothesize that AHR-1 also controls "identity" proteins that aid in tiling. The identification of such proteins will be important for future studies since proteins required for tiling have not been clearly identified. We note that in a small percentage of *ahr-1* mutants AVM does not appear to be fully converted and may retain light-touch sensitivity while also acquiring the ability to respond to harsh-touch. In these cases, AVM may represent a chimeric sensory neuron that has both light-touch and harsh-touch sensitivity.

MEC-3 transcription factor specifies multiple fates

MEC-3 has been shown to be a key determinant of light-touch neurons [123, 183]. Similarly, it is required for branching nociceptive neurons [11, 124, 183]. However, there is a clear difference between the light touch neurons that exhibit a simple morphology and the nociceptive neurons that display complex dendritic trees. This begs the question as to how MEC-3 is required to specify two distinct neuronal types. Our model suggests that the MEC-3 can activate

both harsh touch and light touch genes. However, in light touch neurons, AHR-1 inhibits harsh touch genes and thereby only light-touch genes are expressed. In harsh touch neurons there could be a similar transcription factor that instead inhibits light-touch targets. This idea is supported by work in the other *C. elegans* harsh-touch neurons, FLP. In FLP, EGL-46 and EGL-44 are required to prevent MEC-4 expression, a terminal light-touch protein [208]. Thus, EGL-46 and EGL-44 function as light-touch inhibitors in a harsh-touch neuron. However, we show that high levels of MEC-3 can induce expression of light-touch genes in PVD. These results suggest that as long as MEC-3 levels are low in PVD, light-touch genes will not be expressed. Thus it is plausible that controlling concentration of MEC-3 in light and harsh touch cells is sufficient to produce two different cell-types. These models provide an elegant solution to explain how MEC-3 could function in both harsh and light touch neurons to drive two different neural outcomes.

The finding that mRNAs from light-touch genes are expressed at low levels in the harsh-touch neuron FLP is also consistent with this model [207]. In other words, since MEC-3 is driving expression of both light-touch and harsh touch genes in FLP it seems plausible that light touch mRNAs would be detected in FLP. This detection of light-touch mRNAs could be from an imperfect inhibition at the transcriptional level from a light-touch inhibitor, likely EGL-44 and EGL-46. The combination of both a light-touch inhibitor preventing transcription and a protein (i.e ALR-1) inhibiting translation from imperfect control of

transcription [210] limits FLP neurons from becoming light touch neurons. This therefore provides a two-tier control to tightly regulate FLP neuronal fate.

ZAG-1 may function similar to AHR-1 but in PLM. It would intriguing to determine the control of MEC-3 harsh-touch targets by ZAG-1. For example, visualizing *hpo-30* expression in ZAG-1 mutants would help to resolve the hypothesis that ZAG-1 controls MEC-3 harsh-touch targets.

The results reported in this work reveal an intrinsic transcriptional network that specifies neuronal fate. Through a precise transcription factor code, the nervous system can generate a myriad of different neurons with varying morphologies and functions. Interestingly, a switch in a single factor within this code can result in an animal that has an imbalance of mechanosensitive cells that can alter behavior induced by environmental stimuli.

Author Contributions

Tim O'Brien and I collaborated in most experiments in this chapter. Tim specifically generated the *mec-3* PVD microarray profile and identified HPO-30 as a MEC-3 regulated determinant of dendritic morphogenesis. Lani Feingold-Link generated the *ahr-1;zag-1* mutant. Clay Spencer completed the analysis of the microarray profile. Marios Chatzigeorgiou performed the calcium imaging experiments.

Acknowledgements

We thank JoAnne Powell-Coffman for providing *ahr-1* reagents, Harald Hutter for *zag-1* reagents, Oliver Hobert for *dat-1*::mcherry and other PVD molecular markers and members of the Miller lab for advice. Some of the strains used in this work were provided by the *C. elegans* Genetics Center which is supported by NIH NCRR. This work was supported by NIH R01 NS26115 (DMM), NIH R21 NS06882 (DMM), NIH F31 NS071801 (CJS)

CHAPTER IV

NETRIN (UNC-6) MEDIATES DENDRITIC SELF-AVOIDANCE

INTRODUCTION

Sensory neurons form highly branched networks of dendritic processes. Despite the complexity of these structures, dendrites arising from a given neuron rarely overlap. This phenomenon of self-avoidance is widely observed and is presumptively employed to maximize coverage of the receptive field [4, 206, 211]. Studies in *Drosophila* have revealed that the cell surface proteins Dscam, turtle and Flamingo can mediate self-avoidance and thus suggest that physical contact between sister dendrites is sufficient to trigger mutual repulsion [99, 100, 105, 106, 212]. Differential expression of the large number of available Dscam isoforms offers an elegant solution to the problem of distinguishing self *vs* non-self by providing unique combinations of markers for specific neuron types. A much smaller array of distinct Dscam isoforms is produced in mammals, however, and thus is unlikely to account for the majority of self-avoidance decisions in vertebrate neural development [109].

Overall, the molecular roles of other determinants of dendritic architecture are also poorly understood[4]. In contrast, the outgrowth of axons have been linked to a wide array of guidance cues and receptors. For example, the extracellular protein, UNC-6/Netrin, is secreted from specific donor cells to

generate a graded signal that directs axon outgrowth [45, 47, 173]. UNC-6/Netrin can also function as a short-range cue on either the membrane of the secreting cell or after capture by distal guidepost cells to direct local axon trajectory [54, 56-59]. The axon guidance function of UNC-6/Netrin is evolutionarily conserved and depends on interaction with specific receptor proteins including UNC-40/DCC and UNC-5 [45, 47, 173].

Here we exploit the morphological simplicity of the PVD nociceptive neuron [11, 12, 124] in the model organism *C. elegans* and its accessibility to live cell imaging to detect a new function for UNC-6/Netrin in dendritic self-avoidance. We also show that this mechanism depends on physical contact between sister dendrites. Our finding provides the first example of a diffusible cue in this role and therefore expands the repertoire of potential self-avoidance components to include other established extracellular signaling molecules and the pathways that they control.

METHODS

Nematode Strains and Genetics

The wild-type *C. elegans* Bristol strain N2 was used for all experiments and cultured as previously described [158].

Mutants used in this study

unc-6 (ev400); unc-6 (rh46); unc-5 (e152); unc-40 (e271); unc-129 (ev554); slt-1 (eh15); sax-3 (ky123); vab-2 (ju1); ptp-3 (ok244); madd-2 (ok2266);

nid-1 (cg119). Some strains were provided by the *Caenorhabditis Genetics* Center, which is funded by the NIH National Center for Research Resources (NCRR). All studies in this work used *C. elegans* hermaphrodites.

Additional strains

NC1686 [*wdIs51* (*F49H12.4*::GFP + *unc-119*)][12], NC1687 [*wdIs52* (*F49H12.4*::GFP + *unc-119*)][12]; CX6488 [*kyIs299*, *hsp16.2::unc-6*::HA + *ord-1*::RFP][174], YC149 [*unc-6 (ev400); ghIs9 (unc-6*::venus + *odr-1*::RFP)][213]; CZ1200 [*juIs76 (unc-25*::GFP)]; NW1454 [*unc-5 (e53); dpy-20 (e1282); evIs105* (pU5::HA delta ZO-1)]; NW1151 [*unc-5 (e53); evIs906* (pU5::HA Ig # 1m + dpy-20)]; NW1180 [*unc-5 (e53); evIs91* (pU5::HA delta BamH1 + dpy-20)]; NW1137 [*unc-5 (e53); evIs886* (pU5::HA + dpy-20)][214]

Transgenic strains generated by microinjection:

NC2099 [*pha-1 (e2123ts); wdEx682* (MVC119 (*rig-3*::unc-6) + *pBx (pha-1)* + *dat-1*::mcherry)]; NC2099 [*pha-1 (e2123ts); wdEx682* (MVC119 (*rig-3::unc-6*) + pBx (*pha-1*) + *dat-1*::mcherry); NC2182 [*pha-1 (e2123ts); wdEx692* (pCJS28, *F49H12.4::unc-6*::HA + *pBx, pha-1* + *dat-1*::mcherry)]; NC1893 [*pha-1 (e2132ts); wdEx640 (F49H12.4*::unc-40::mcherry + *pBx (pha-1)* + *odr-1*::mcherry)]; NC2059 [*pha-1 (e2123ts); wdEx662* (pCJS52 (*ser2prom3*::unc-40::mcherry) + *pBx (pha-1)* + *dat-1*::mcherry)]; NC2098 [*pha-1 (e2123ts); wdEx681* (pCJS68 (*unc-25*::unc-40::mRFP) + *pBx (pha-1)* + *dat-1:*::mcherry)]; TV1788 [*unc-40 (e271); wyIs45; wyEx650* (*unc-40* minigene w/ mcherry injected at 20 ng/ul has co-

selector marker GFP in coelomocytes)]; NC2301 [*pha-1 (e2123ts); wdEx746* (pCJS93, *F49H12.4::*unc-40::GFP + *pBx, pha-1* + pCJS85*, dat-1*::mcherry)]; N2315 [*pha-1 (e2123ts); wdEx748* (pCJS98, *F49H12.4*::unc-40deltaECTO::mcherry + *dat-1::*mcherry + *pBx, pha-1*)]; NC2044 [*pha-1 (e2123ts)*; *wdEx660* (pCJS65 (*unc-5::*unc-5::CFP) + *dat-1::*mcherry + *pBx (pha-1*))]; NC2247 [*pha-1 (e2123); lon-2 (e678); wdEx716* (pCJS72, *unc-25::*unc-5::mRFP + *dat-1*::mcherry + *pBx)*];

Molecular Biology

UNC-40, UNC-6 and UNC-5 expression plasmids were constructed using conventional cloning and gateway recombinase technology as previously described [51, 173-175]. See appendix table 1 for more detailed description.

Confocal Microscopy

Nematodes were immobilized with 15 mM levamisole on a 2% agarose pad in M9 buffer [12]. Images were obtained in a Leica TCS SP5 confocal microscope. Z-stacks were collected with either 40X (1 um/step), 63X (0.75 um/step) or 100x (0.75 um/step) objectives; single plane projections were generated with Leica Application Suite Advanced Fluorescence software. Brightness and contrast were enhanced using Adobe Photoshop CS5.

Time-Lapse Imaging

Nematodes were imaged as previously described [12]. For each time point, the 40X, 63X or 100X objective was used to collect a Z-stack (0.75 um/step) spanning the focal depth of the PVD neuron and its dendritic branches. Dendritic branch outgrowth at each time point was evaluated from a Z-projection. Larval stages were identified from morphological features: L2 (postdeirid); L3, L4, and young adult (vulval development) [119]. At least three independent movies verified each example of dynamic dendritic growth described in this report.

Measuring 3^O dendrites length

Images from L4 larval animals were measured using the vector tool in ImageJ.

Scoring self-avoidance defects

Each genotype was visualized in a PVD::GFP reporter line (*wdIs51* or *wdIs52*). At least 20 animals ($\geq$ 600 of 3^O gaps) were visualized for each genotype. Confocal images were collected in a z-stack to span the depth of PVD with a step size of 1 um. PVD morphology was scored from Z-stack projections. A self-avoidance defect is identified as any two adjacent 3^O branches that lack an intervening gap between them. Adjacent 3^O branches are defined as physically linked to 2^O branches that project from flanking locations on the PVD 1^O branch. The number of self-avoidance errors (*i.e.*, absence of intervening space between 3^O branches of adjacent menorahs) was divided by the total number of potential

3^{O} branch gaps per animal (*i.e.*, number of 2^{0} branches – 2]) to provide the fraction of overlapping 3^{O} branches per animal. The average fraction of overlapping 3^{O} branches for each genotype was calculated for histograms summarizing these results. An unpaired Student's t-test was used to calculate statistical significance between different strains.

Heat Shock Experiments

Animals were heat shocked at the appropriate age as previously described [174]. All animals were imaged at the late L4 larval stage after PVD development is complete.

Temporal requirement for UNC-6/Netrin

unc-6 (rh46) worms were maintained at the appropriate temperature [215] and treated with hypochlorite to release embryos for overnight incubation in M9 buffer. Synchronized L1s were placed on a bacterial lawn to initiate larval development and then shifted to either the permissive (15C) or restrictive (25C) temperature at specific larval intervals (L2/L3 larval transition, L3/L4 larval transition, end of L4 larval stage) for growth until the late young adult stage for imaging. Animals grown at either the permissive or restrictive temperature throughout development were used as controls.

RESULTS

PVD neurons exhibit dendritic self-avoidance.

PVD neurons display a highly branched network of sensory processes in which a collection of dendritic trees or "menorahs" is rooted in a common 1^0 dendrite (Figure 4.1a, b)[12, 125, 216, 217]. This well-ordered and non-overlapping array of PVD dendrites is generated by a combination of defined branching events and an error correction mechanism in which sister dendrites are repelled by mutual contact[12, 216]. The patterning role of self-avoidance is strikingly evident in the outgrowth of 3^O dendrites. In each menorah, paired 3^O dendrites project along a sublateral nerve cord in either an anterior or posterior direction (Figure 4.1a,b). We used time-lapse imaging to establish that growth continues until the tip of one 3^O dendrite contacts another 3^O branch pointing in the opposite direction[12]. Touch evokes rapid withdrawal that results in an eventual gap between 3^O dendrites from adjacent menorahs. This mechanism readily accounts for the observation that the inter-tip gap distance is constant between flanking 3^0 dendrites but that adult branch length and termination points are highly variable for PVD neurons in different animals (Figure 4.1c).

As an additional test of a self-avoidance model, we used a mutant of the *egl-46/Zn finger/Nerfin* transcription factor to reduce the overall number of PVD menorahs[12]. This genetic background effectively widens the spacing between the branch initiation points of adjacent 3^0 dendrites (Figure 4.1d). Thus, this approach uses a genetic strategy to answer the question: If repulsion specifies the regular layout of PVD dendrites, what is the consequence of branch ablation?

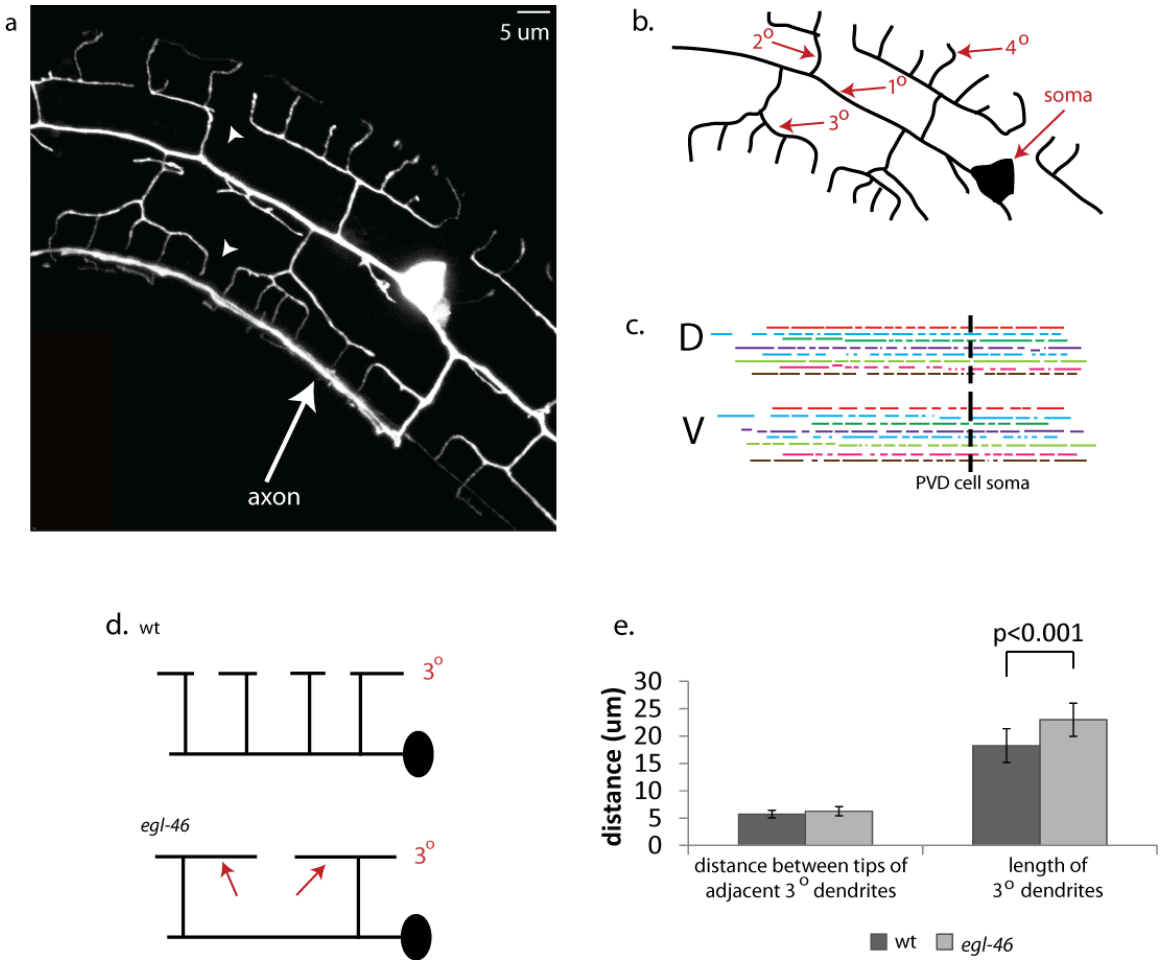

Figure 4.1. UNC-6/Netrin signaling is required for contact-dependent self-avoidance. (a) Fluorescent image of PVD neuron labeled with GFP to show the non-overlapping pattern of PVD dendrites. Arrowheads denote gaps between 3^0 dendrites of adjacent menorahs. The single PVD axon (arrow) marks the location of the ventral nerve cord. **(b)** Tracing of PVD branches to show numbering scheme. **(c)** Tracings of 3^O dendrites from dorsal (D) and ventral (V) regions of ten individual PVD neurons are denoted with matching colors. Note that 3^O dendrites do not terminate at specific anatomical regions or exhibit a single length as would be expected if outgrowth were governed by external landmarks or limited by an intrinsic mechanism of length determination. **(d)** *egl-46* mutants show fewer 2^O branches and longer 3^O dendrites (arrows). **(e)** PVD neurons have fewer 2^O branches in *egl-46 (n1076)* mutants (32.3 $\pm$ 5.3) than wild type (wt) (38.9 $\pm$ 5.4). Despite the consequent reduction in the overall number of 3^O branches in *egl-46* mutants, the normal distance between the tips of adjacent 3^O dendrites is maintained by extending the average outgrowth length of 3^O dendrites.

Our results show that 3^0 branches are significantly longer in the *egl-46* mutant but that the inter-tip gap is maintained (Figure 4.1e)[12]. Thus, these observations rule out models in which branch length is determined by a fixed yardstick or defined by external landmarks but favor the idea that the non-overlapping PVD dendritic architecture is achieved through a contact-dependent mechanism of self-recognition.

UNC-6 signaling is required for dendritic self-avoidance.

We generated a PVD expression profile[12] and used genetic analysis of known axon guidance molecules suggested by this list to test for potential roles in dendritic morphogenesis (Table 4.1). We noted that genetic ablation of the UNC-6 receptors UNC-40/DCC and UNC-5 altered several aspects of PVD morphology (Figure 4.2[12, 217]) including the aberrant occurrence of overlaps between flanking menorahs in the adult (Figure 4.3a). We used time-lapse imaging to establish that this mutant phenotype arises from a self-avoidance defect. In the wild type, 3^O dendrites from adjacent menorahs grow toward each other but quickly retract with over > 50% regressing within 3 minutes of contact and < 13% still touching at the 10 min mark; ultimately, less than 1% of wild-type 3^O dendrites overlap with each other (Figure 4.4b, d). In contrast, in *unc-40 (e271)* mutants, a majority (76%) of adjacent 3^O dendrites failed to withdraw within 10 min of contact and almost one third (29%) never regressed (Figure 4.3 a,c,e) (Figure 4.4). Similar defects were captured in time-lapse movies of *unc-5 (e152)* (Figure 4.4). Motivated by these results, we examined the mutant *unc-6*

Table 4.1. Self-avoidance requires specific axon guidance molecules in the UNC-6/Netrin signaling pathway. Mutants of known axon guidance molecules were tested for PVD 3^0 branch self-avoidance defects with the PVD::GFP reporter. Transcripts enriched ($\geq$1.5X , FDR $\leq$ 1%) in PVD (Smith et al., 2010) are denoted with bold lettering. Only mutants of the UNC-6/Netrin signaling pathway showed self-avoidance defects that were significantly different from wt (+ indicates $p<0.01$, Student's t-test). N $\geq$ 20

Function	Gene	Self-avoidance defect
Ligand	*unc-6/Netrin*	+
	unc-129/TGF beta family	-
	vab-1/Ephrin	-
	slt-1/Slit	-
Receptor	***sax-3/Robo***	**-**
	vab-2/Eph	-
	ptp-3/Lar	**-**
	unc-5/Unc-5H	**+**
	unc-40/DCC	**+**
	madd-2/NetrinR	-
ECM component	*nid-1/Nidogen*	-

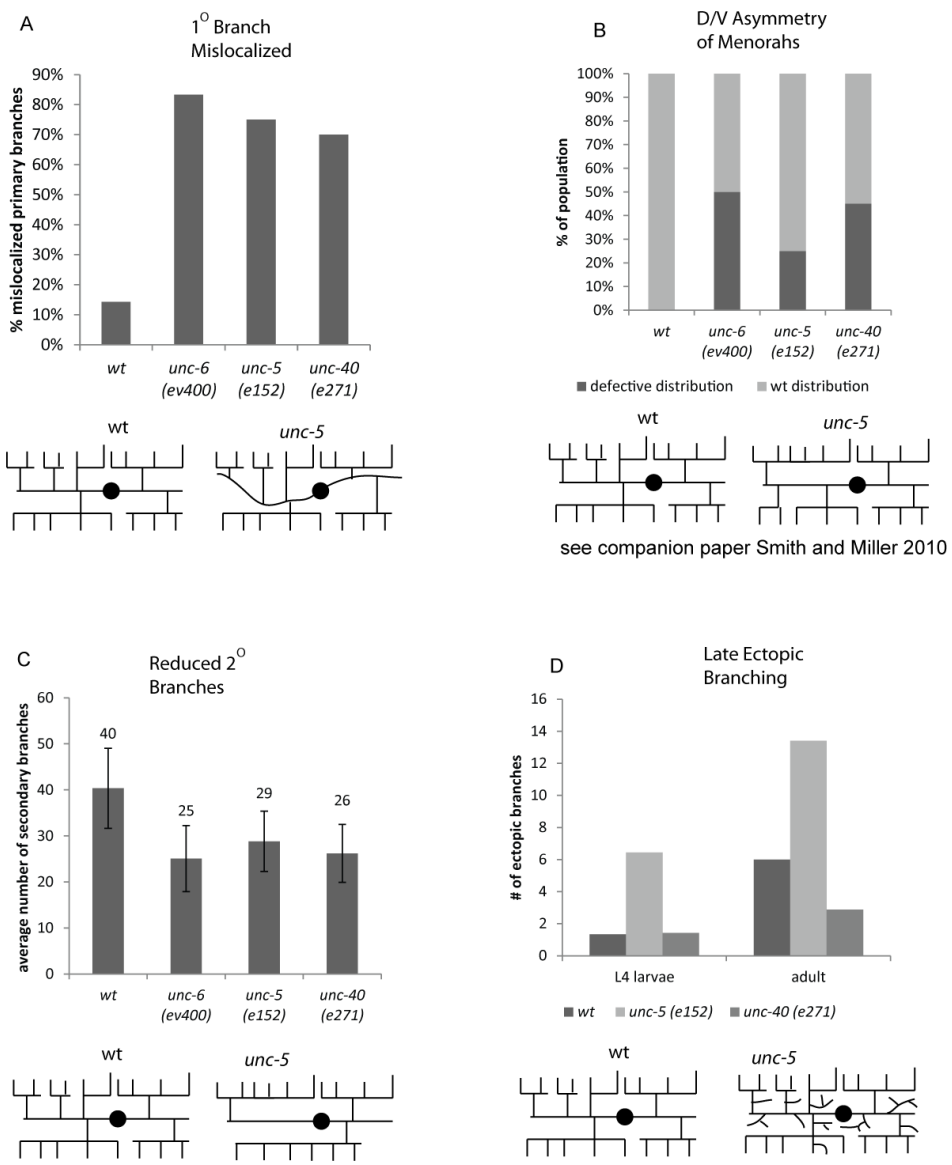

Figure 4.2. Mutants of *unc-40, unc-5* and *unc-6* show a range of dendritic morphogenesis phenotypes in addition to the self-avoidance defect. (a) PVD 1^{O} processes project along the lateral nerve cord in the wild type but deviate from a strict A/P trajectory in >75% of *unc-40, unc-5* or *unc-6* mutants. **(b)** Wild-type (wt) PVD neurons show an asymmetric pattern of lateral branching that results in more dorsal than ventral menorahs in 100% of cases examined (n > 15) (wild-type distribution). In UNC-6/Netrin pathway mutants, this asymmetry is disrupted resulting in PVD neurons that have more ventral menorahs than dorsal menorahs or an equal number of menorahs on each side ~50% of the time (defective distribution), an outcome that is consistent with a randomized probability of dorsal vs ventral initiation of 2^{0} branches (CJ Smith and DM Miller, manuscript in preparation). **(c)** The average number of 2^{O} dendrites/PVD neuron in *unc-6, unc-5* and *unc-40* mutants is reduced in comparison to wild-type PVD neurons. **(d).** Ectopic branching in adults is more frequent in unc-5(e271) than in either wild type (wt) or *unc-40(e271).*

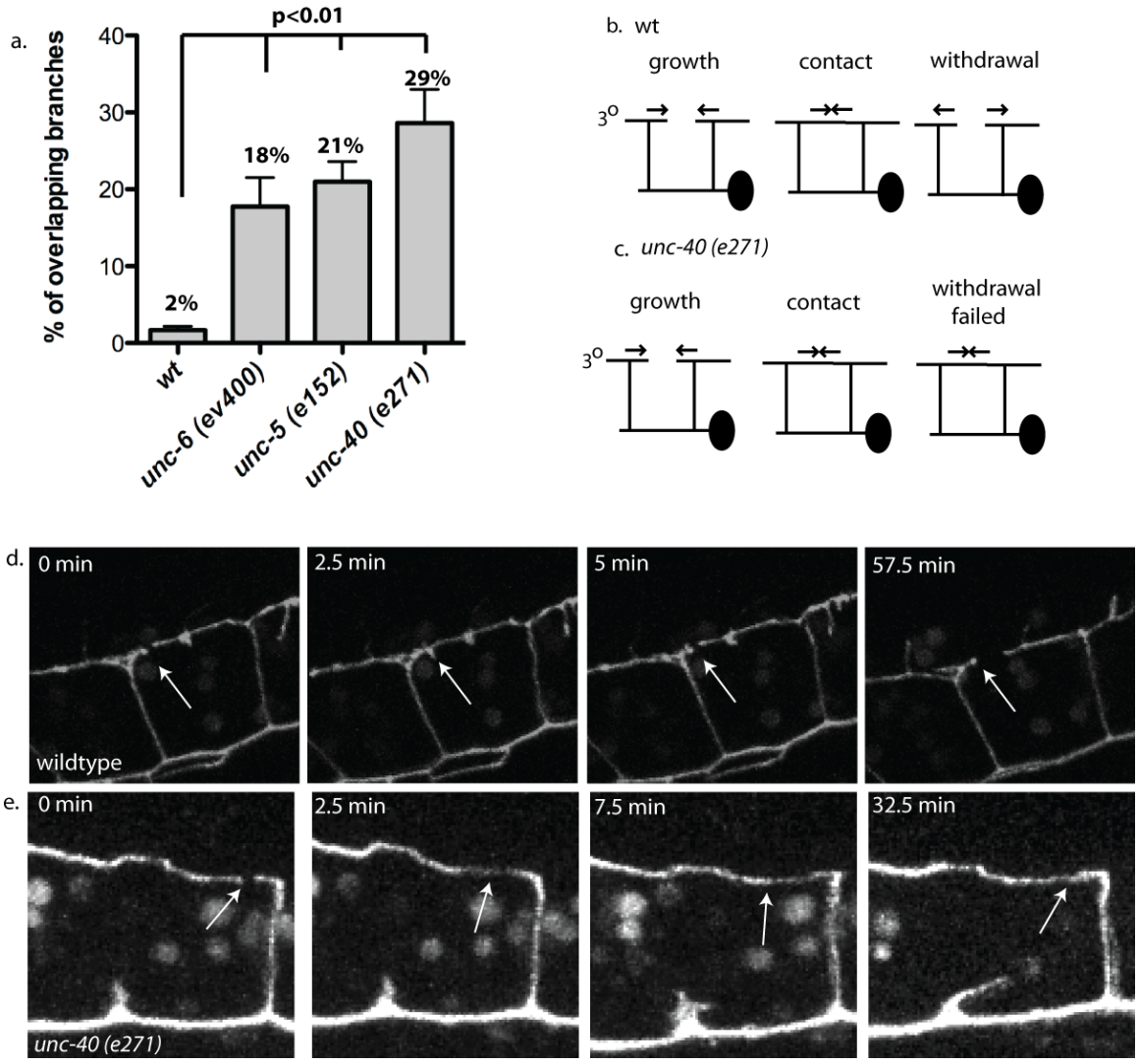

Figure 4.3. UNC-6/Netrin signaling is required for contact-dependent self-avoidance. (**a**) 3^{O} branches from adjacent menorahs overlap in *unc-6 (ev400), unc-5(e152)* and *unc-40 (e271)* mutants more frequently than in wild type (wt)(student's t-test, p<0.01). **(b)** Schematic showing 3^{O} outgrowth, contact and retraction in wild type (wt). **(c)** 3^{O} branches fail to withdraw after contact in an *unc-40* mutant. **(d)** Images captured from a time-lapse movie showing contact then rapid withdrawal (< 2.5 min) (arrow) of 3^{O} branches in wild type**. (e)** Successive images showing that 3^{O} branches fail to withdraw within 30 min of mutual contact in *unc-40(e270)* (arrow).

(ev400) and detected 3^{O} self-avoidance defects resembling those of *unc-40/DCC* and *unc-5* mutants (Figure 4.3a).

If these genes function in a common pathway, double mutants between *unc-6* and each of its receptors should fail to enhance the self-avoidance defect of either single mutant. This prediction is confirmed for the self-avoidance defect arising from the combination of *unc-5* and *unc-6* which is comparable to that of either *unc-5* or *unc-6* alone (Figure 4.5). However, the *unc-40* mutation enhances both the Unc-5 and Unc-6 single mutant self-avoidance phenotypes. These results are consistent with model in which *unc-40* exercises a role in self-avoidance that is independent of *unc-6* signaling through *unc-5*. In addition, because neither *unc-5* nor *unc-6* enhance the Unc-40 self-avoidance defect (Figure 4.5), we conclude that *unc-40* also functions in the *unc-6*- and *unc-5*-dependent pathway. Here we describe experiments designed to establish the mechanism whereby UNC-6/Netrin and its receptors, UNC-40/DCC and UNC-5, mediate dendritic self-avoidance.

Self-avoidance requires UNC-6 but not a graded UNC-6 signal

UNC-6 is secreted from ventral cells to direct axonal outgrowth and cell migration along the D/V body axis [43, 173]. When this ventral source of UNC-6 is removed in *unc-6 (ev400)* mutants, 18% of PVD 3^{O} branches overlap per animal (Figure 4.6a,d). This defect is complemented by UNC-6 expression with the native *unc-6* promoter (Figure 4.6d). Transgenic expression of UNC-6 in a ventral neuron (AVA) with the *rig-3* promoter[218] also improves the self-

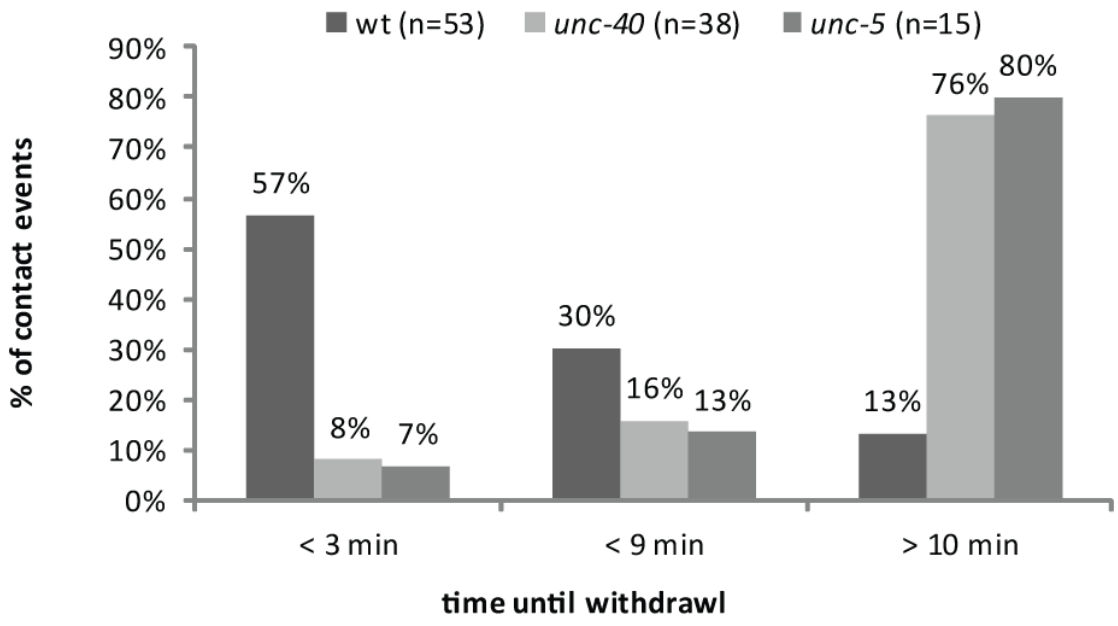

Figure 4.4. *unc-40* and *unc-5* mutants show defects in contact-dependent self-avoidance. Quantification from movies of self-avoidance events in wild type (wt), *unc-5 (e152)* and *unc-40 (e271)* show that 3^{O} branches in *unc-5 (e152)* and *unc-40 (e271)* do not retract as quickly as in wild-type animals; a majority (>75%) of 3^{O} branches have failed to retract up to 10 minutes after initial contact in *unc-40* and *unc-5* mutants whereas only 13% of 3^{O} dendrites are still overlapping at this time point in wild type.

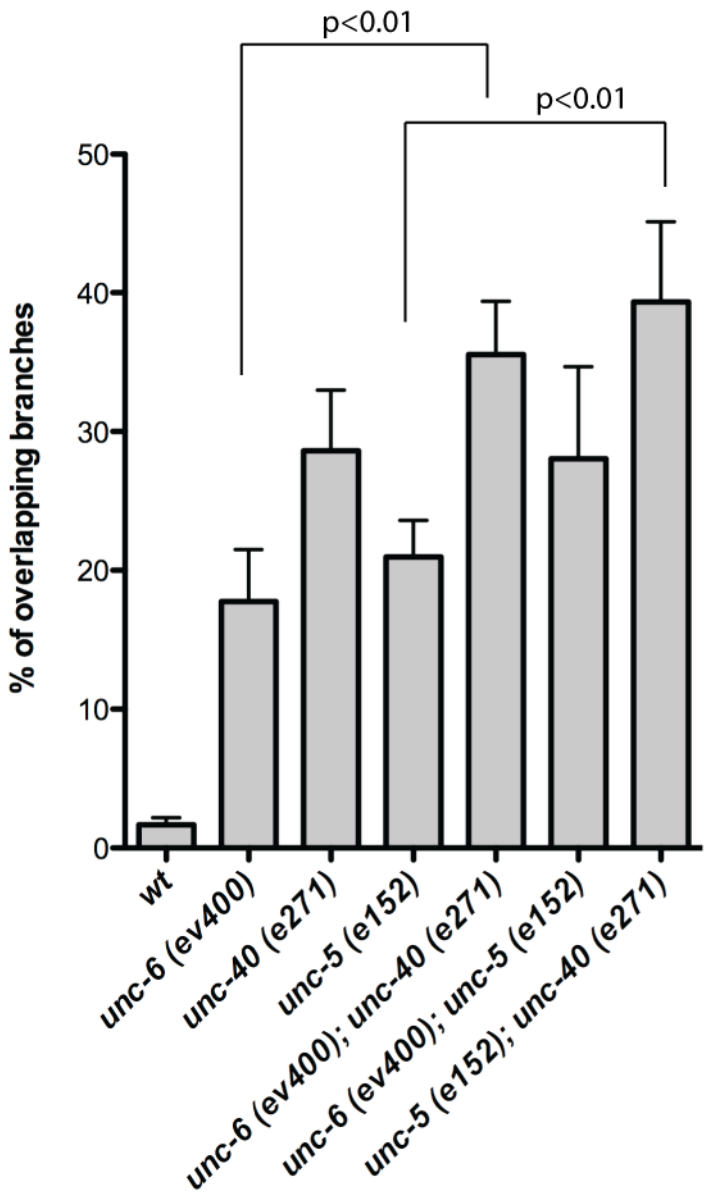

Figure 4.5. Genetic interactions of *unc-40, unc-5* and *unc-6*. Single mutants of *unc-5 (e152), unc-40 (e271)* and *unc-6 (ev400)* show comparable self-avoidance defects that are not statistically different from each other. The self-avoidance defect of the double mutant *unc-5 (e152); unc-6 (ev400)* is not significantly different from either *unc-5 (e152)* or *unc-6 (ev400)* single mutant which suggests that unc-5 and unc-6 function in a common pathway. *unc-40 (e271); unc-5 (e152)* double mutants do not show enhancement of the PVD self-avoidance defect vs *unc-40 (e271)* but do show a more severe self avoidance defect than *unc-5 (e152)* alone ($p < 0.01$, n= 20, Students t-test). *unc-40 (e271); unc-6 (ev400)* double mutants show enhancement of self-avoidance defects compared to *unc-6 (ev400*) but not to *unc-40 (e271)* (p=3E-3 vs unc-6 (ev400)). These results suggest that *unc-40* fulfills an additional *unc-5/unc-6*-independent role in self-avoidance.

avoidance response (8% overlapping branches, p=0.02 vs *unc-6*) and thus indicates that UNC-6 expression from ventrally located cells is sufficient to mediate PVD 3^O branch self-avoidance (Figure 4.6d).

Although extracellular UNC-6 protein is presumptively distributed in a ventral to dorsal gradient, we did not observe a significant difference in the extent of self-avoidance errors in ventral vs. dorsal 3^O branches in *unc-6 (ev400)* (Figure 4.7). We next used a heat shock promoter (*hsp16.2*) to drive expression of UNC-6 in all cells[174] and thereby directly determine if a ventral to dorsal gradient of UNC-6 is required for self-avoidance. Although global expression of UNC-6 is known to disrupt axon guidance along the D/V axis[174], ubiquitous UNC-6 expression in a wild-type background during multiple larval stages did not perturb PVD 3^O branch self-avoidance (Figure 4.6b,d).

We reasoned that UNC-6/Netrin might function as a permissive cue in this case such that a specific source or gradient of UNC-6/Netrin is not necessary provided sufficient ligand is available. This idea is substantiated by our finding that global expression of UNC-6/Netrin in *unc-6 (ev400)* with the heat shock promoter before the L3 larval stage rescues 3^O branch self-avoidance (9% overlapping branches, p=0.04 vs *unc-6*) (Figure 4.6c,d). In addition, we showed that expression of UNC-6/Netrin in PVD, with the *F49H12.4* promoter[163], also rescued *unc-6 (ev400)* self-avoidance defects (7% overlapping branches, p=0.01 vs *unc-6*) (Figure 4.6d).

Based on these results, we conclude that PVD dendritic self-avoidance is independent of the UNC-6/Netrin gradient and therefore that UNC-6/Netrin does

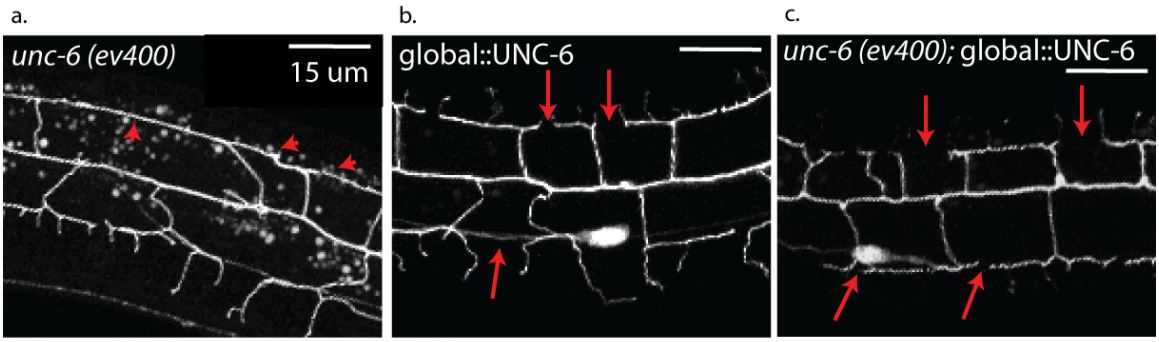
a.
unc-6 (ev400)
15 um
b.
global::UNC-6
c.
unc-6 (ev400); global::UNC-6

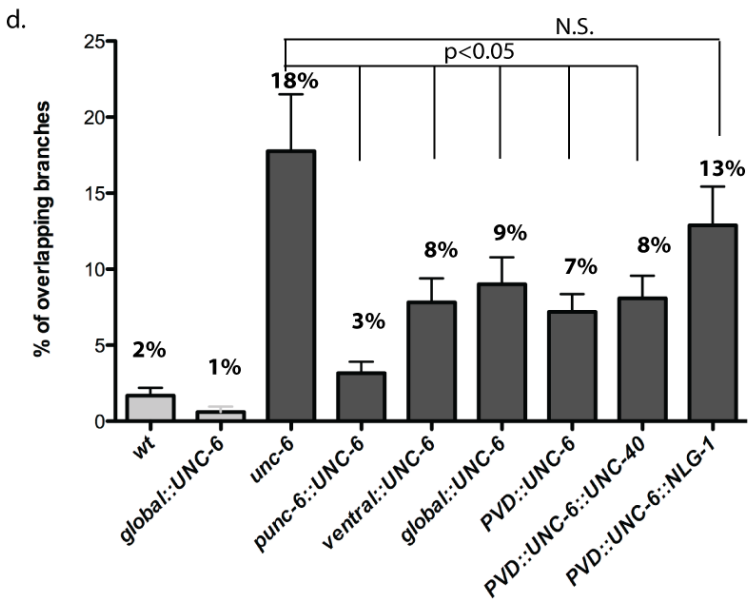
d.
% of overlapping branches
N.S.
p<0.05
2%
1%
18%
3%
8%
9%
7%
8%
13%
wt
global::UNC-6
unc-6
punc-6::UNC-6
ventral::UNC-6
global::UNC-6
PVD::UNC-6
PVD::UNC-6::UNC-40
PVD::UNC-6::NLG-1

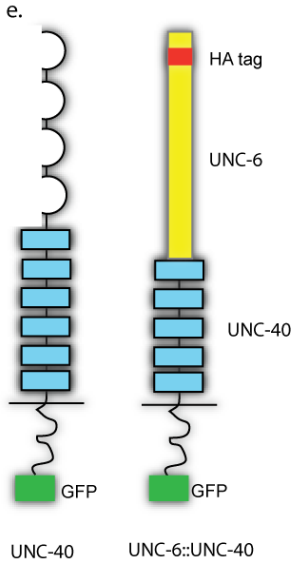
e.
HA tag
UNC-6
UNC-40
GFP
GFP
UNC-40
UNC-6::UNC-40

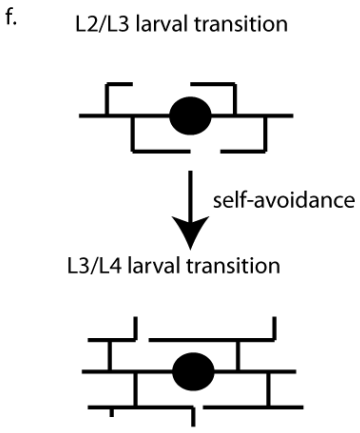
f.
L2/L3 larval transition
self-avoidance
L3/L4 larval transition

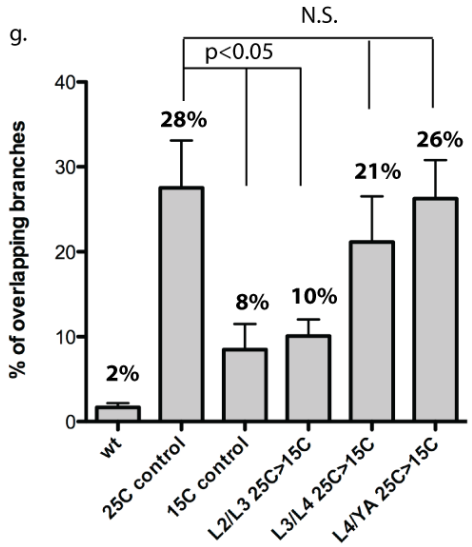
g.
N.S.
p<0.05
% of overlapping branches
2%
28%
8%
10%
21%
26%
wt
25C control
15C control
L2/L3 25C>15C
L3/L4 25C>15C
L4/YA 25C>15C

Figure 4.6. UNC-6/Netrin functions as a permissive cue to prevent dendritic branch overlap during the larval period in which self-avoidance normally occurs. **(a, d)** *unc-6(ev400)* shows overlapping 3^{O} PVD branches (arrowheads) **(b, d)** Expression of UNC-6 with a heat shock promoter (global::UNC-6) restores PVD self-avoidance (arrows) to *unc-6 (ev400)* but **(c, d)** does not induce PVD dendritic outgrowth defects in a wild-type background. (d) UNC-6 expression with the native *unc-6* promoter (*unc-6*::UNC-6), a ventral neuron-specific promoter (ventral::UNC-6) or the PVD promoter (PVD::UNC-6) rescues *unc-6(ev400)* PVD self-avoidance defects (see Methods). Expression of UNC-6 fused to the extracellular domain of UNC-40 (PVD::UNC-6::UNC-40) restores self-avoidance but UNC-6 fused to the membrane protein neuroligin (PVD::UNC-6::NLG-1) does not rescue 3^{O} branch self-avoidance defects in *unc-6(ev400)*. Genetic backgrounds are wild type (wt) (light grey boxes) or *unc-6(ev400)* (dark gray boxes). **(e)** Schematic of UNC-40 protein (Ig domain = loops, Fibronectin domains = rectangles, intracellular domain and GFP tag = dark rectangle) and UNC-6::UNC-40 chimera (UNC-6 contains HA tag). (**f**) Schematic of PVD development showing that 3^{O} branch self-avoidance occurs during the L3 larval stage. **(g)** The temperature sensitive allele *unc-6 (rh46*) was shifted from restrictive (25C) to permissive temperature (15C) at successively later stages (L2/L3, L3/L4, L4/adult transitions) during larval development. Temperature shift from 25C to 15C at the L2/L3 transition rescues the 3^{O} branch self-avoidance defect ($p<0.01$) but downshifts at later developmental stages do not restore self-avoidance. Continuous growth at 25C (25C control) results in a higher fraction of overlapping branches than continuous growth at 15C (15C control). PVD 3^{O} branch overlap was scored in the adult.

not provide a directional signal to repel dendritic outgrowth. We considered an alternative model in which the mere availability of UNC-6/Netrin is sufficient to trigger repulsion and next asked the question of when this function is required.

UNC-6 is required during the period when dendrites self-avoid

Time-lapse imaging established that PVD 3^{O} branch self-avoidance occurs during the L3 larval stage[12]. If UNC-6 is directly involved in self-avoidance then UNC-6 function should be required during this period. We used a conditional *unc-6* allele *(rh46)* to test this idea in temperature shift experiments that regulate temporal UNC-6 activity [215].

unc-6(rh46) mutants grown at the restrictive temperature (25C) display a self-avoidance defect (28% of overlapping 3^{O} branches, Figure 4.6g) comparable to that of the *unc-6(ev400)* null allele *(p=0.14 ev400 vs rh46)* which therefore suggests that the *rh46* point mutation results in a dysfunctional UNC-6 protein at restrictive temperature [215]. The self-avoidance defect is weaker but still significant at 15^{O}C (Figure 4.6g, 8% of overlapping 3^{O} branches, p =0.006 *vs* 25C control, p=0.047 vs N2) indicating that the *rh46* mutant UNC-6 protein is only partially active at permissive temperature. We shifted *unc-6(rh46)* from restrictive temperature (25^{O}C) to permissive temperature (15^{O}C) at succeeding developmental stages (Figure 4.6f,g). *unc-6(rh46)* animals downshifted at the L2/L3 transition and then maintained at permissive temperature until the adult, showed a self-avoidance defect comparable to that of control animals grown continuously at 15^{O}C (Figure 4.6g, 10% overlapping branches, p = 0.007 *vs*

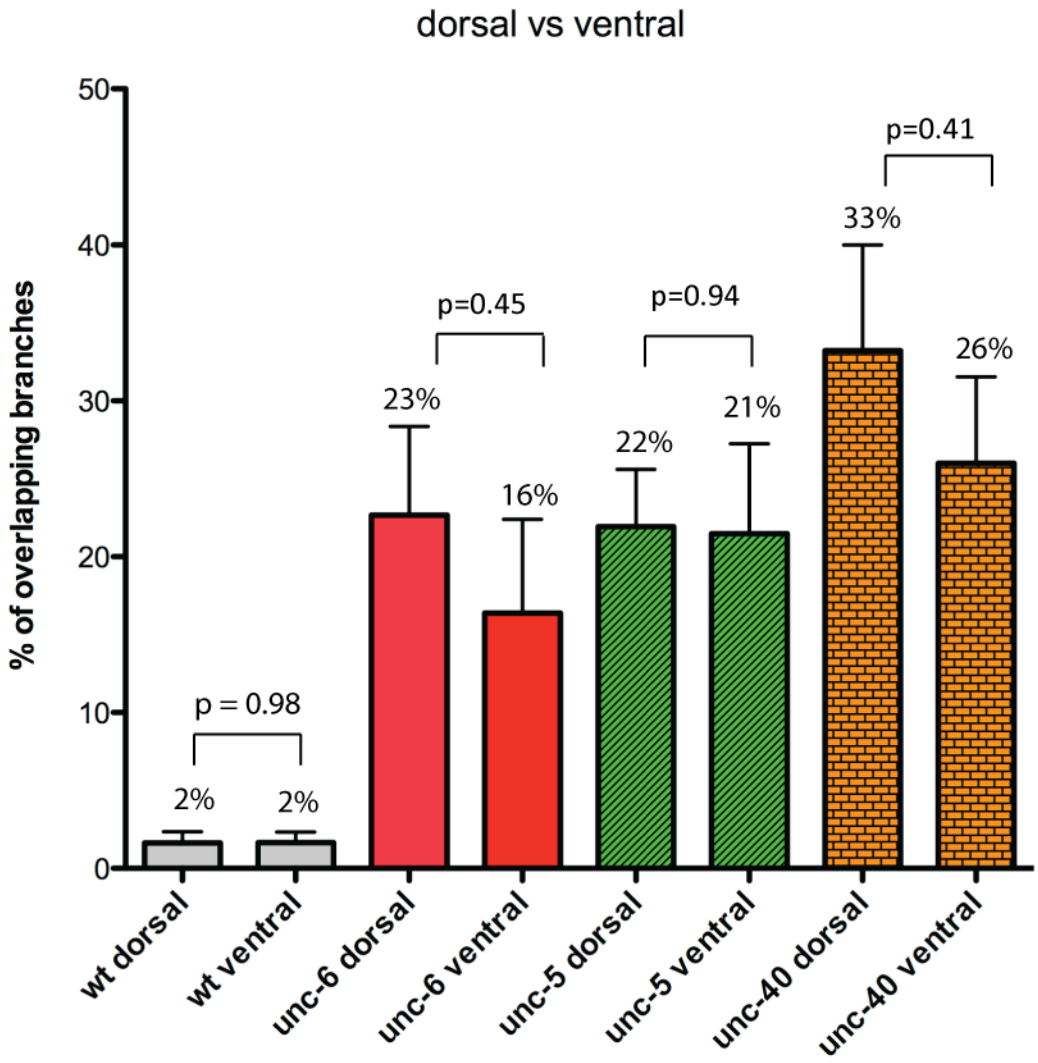

Figure 4.7. UNC-6/Netrin signaling mutants do not show differences in dorsal vs. ventral 3^0 dendrite self-avoidance phenotypes. The fraction of overlapping 3^O branches in dorsal vs ventral regions was scored for *unc-6(ev400), unc-5(e152)* and *unc-40(e271).* N = 20 animals

25^{O}C control). In contrast, downshifts to permissive temperature (*i.e.,* restoration of UNC-6 activity) after the L2/L3 transition resulted in a self-avoidance defect as severe as *unc-6(rh46)* animals grown continuously at the restrictive temperature (Figure 4.6g, p = 0.42 for L3/L4, p = 0.86 for L4/YA *vs* 25^{O}C control). These results indicate that self-avoidance does not depend on UNC-6 function during embryonic and early larval development but that UNC-6 is required after the beginning of the L3 stage. Similar temperature upshift experiments confirmed that loss of UNC-6 function during the L3 larval period enhances the *rh46* self-avoidance defect but later shifts to restrictive temperature (*i.e.,* L3/L4 or L4/YA) after 3^{0} branch outgrowth is complete do not result in a severe branch overlap phenotype (Figure 4.8).

Thus, our results are consistent with a model in which UNC-6/Netrin function is required for self-avoidance during a brief developmental window in the L3 larval stage in which 3^{0} dendrites are actively engaged in outgrowth and contact-dependent repulsion. This finding is important because it argues against the possibility that UNC-6/Netrin signaling fulfills an earlier, indirect role in which it primes PVD dendrites for self-avoidance by regulating expression [219], for example, of an alternative set of interacting components.

UNC-40/DCC and UNC-5 function cell-autonomously in PVD

Genetic ablation of UNC-5 and UNC-40 resulted in significant overlap of 3^{O} dendrites (Figure 4.3a). Because UNC-5 and UNC-40 have been previously shown to function as receptors for UNC-6/Netrin and because UNC-5 and UNC-

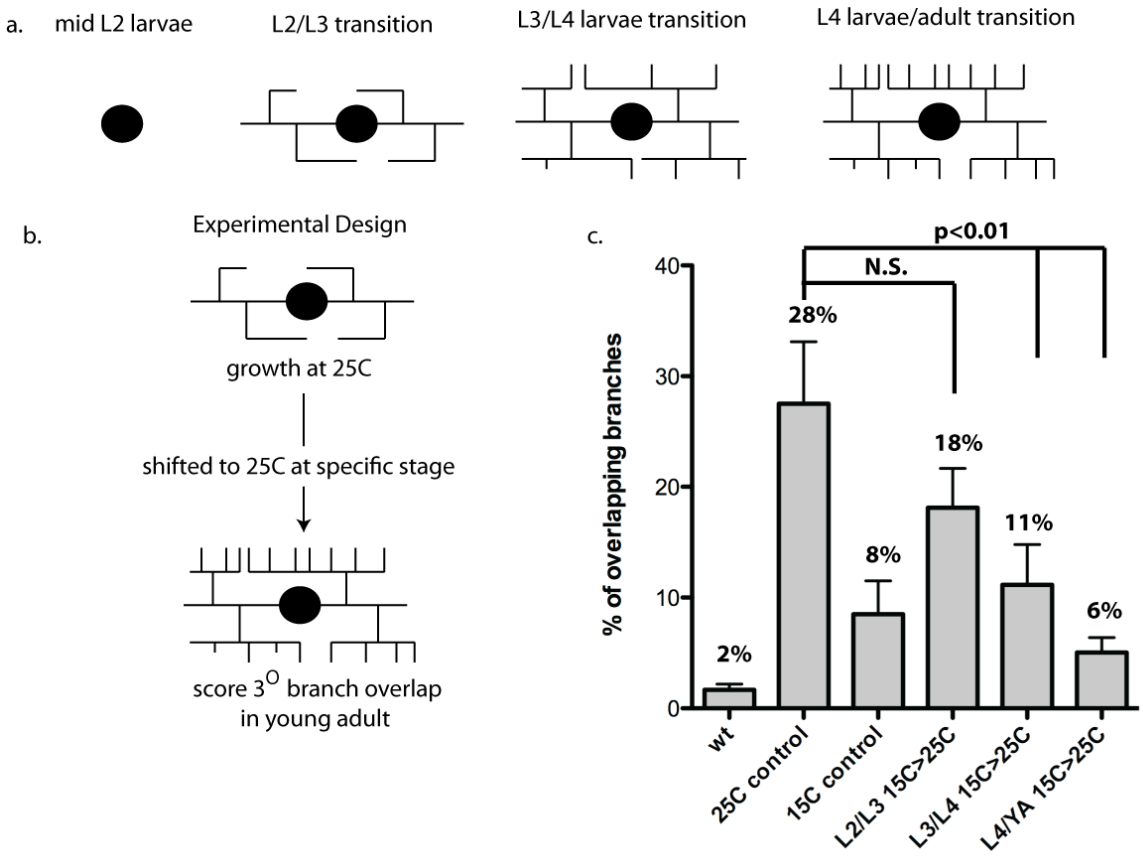

Figure 4.8. UNC-6/Netrin is required for self-avoidance during the L3 larval stage. **(a)** Schematic of PVD development showing the elaboration of dendritic branches during larval development. **(b)** Experimental design for temperature shifts with the temperature sensitive mutant *unc-6(rh46)* to determine the temporal requirement for UNC-6 in PVD 3^0 dendritic branch self-avoidance. **(c)** Histogram showing fraction of overlapping 3^0 branches resulting from maintenance at either the permissive (15C) (15C control) or restrictive (25C) (25C control) temperatures and from upshift experiments (15C>25C) in which animals grown at permissive temperature are shifted to growth at the restrictive temperature. Note that the extent of overlapping 3^0 branches after shifting to restrictive temperature at the L2/L3 larval transition is not significantly different from the self-avoidance defect resulting from continuous exposure to 25 C whereas shifts to restrictive temperature at later developmental periods (*i.e.*, L3/L4 transition, L4/adult transition) result in a significantly lower fraction of overlapping 3^0 dendritic branches that is not significantly different from the PVD self-avoidance defect from 15C control animals. These results indicate that UNC-6/Netrin function is required before the L3 larval stage for 3^0 branch self-avoidance but is not necessary in older animals.

40 transcripts are enriched in our PVD microarray data set [12], we reasoned that UNC-5 and UNC-40 are likely to act in PVD to prevent overlap of 3^O dendrites. This model predicts that expression of UNC-5 and UNC-40/DCC in PVD should be sufficient to restore self-avoidance to the corresponding *unc-5* or *unc-40* mutants.

Expression of UNC-40 with its endogenous promoter in *unc-40 (e271)* reduced the frequency of overlapping branches from 29% to 5% ($p = 3E^{-5}$ *vs unc-40*) (Figure 4.9d). UNC-40 expression with the PVD promoters, *F49H12.4 [163]* or *ser2prom3[12]* , also showed significant rescue (8% overlapping 3^O branches, $p=5E^{-7}$ vs *unc-40*) (Figure 4.9c,d). Thus, these results are indicative of the cell-autonomous function of UNC-40 in PVD. We have previously noted that a significant fraction of PVD 2^0 branches fasciculate with motor neuron commissures that also project from the ventral to dorsal side of the animal [12]. To determine if PVD dendritic self-avoidance is indirectly compromised by commissural axon guidance defects in *unc-40(e271)[48]*, we restored UNC-40 expression to ventral cord motor neurons with the *unc-25* promoter [220]. Motor neuron expression of UNC-40 largely rescued commissural axon outgrowth to the dorsal cord, as expected[48] (Fig 4.10) but did not restore PVD self-avoidance (Figure 4.9d).

In similar experiments, expression of UNC-5 under its endogenous promoter resulted in a significantly reduced fraction of overlapping branches in the *unc-5 (e152)* mutant (Figure 4.11d) (7%, p = 8.56E-5 vs *unc-5*). A cell autonomous role for UNC-5 in PVD is consistent with our finding that UNC-5

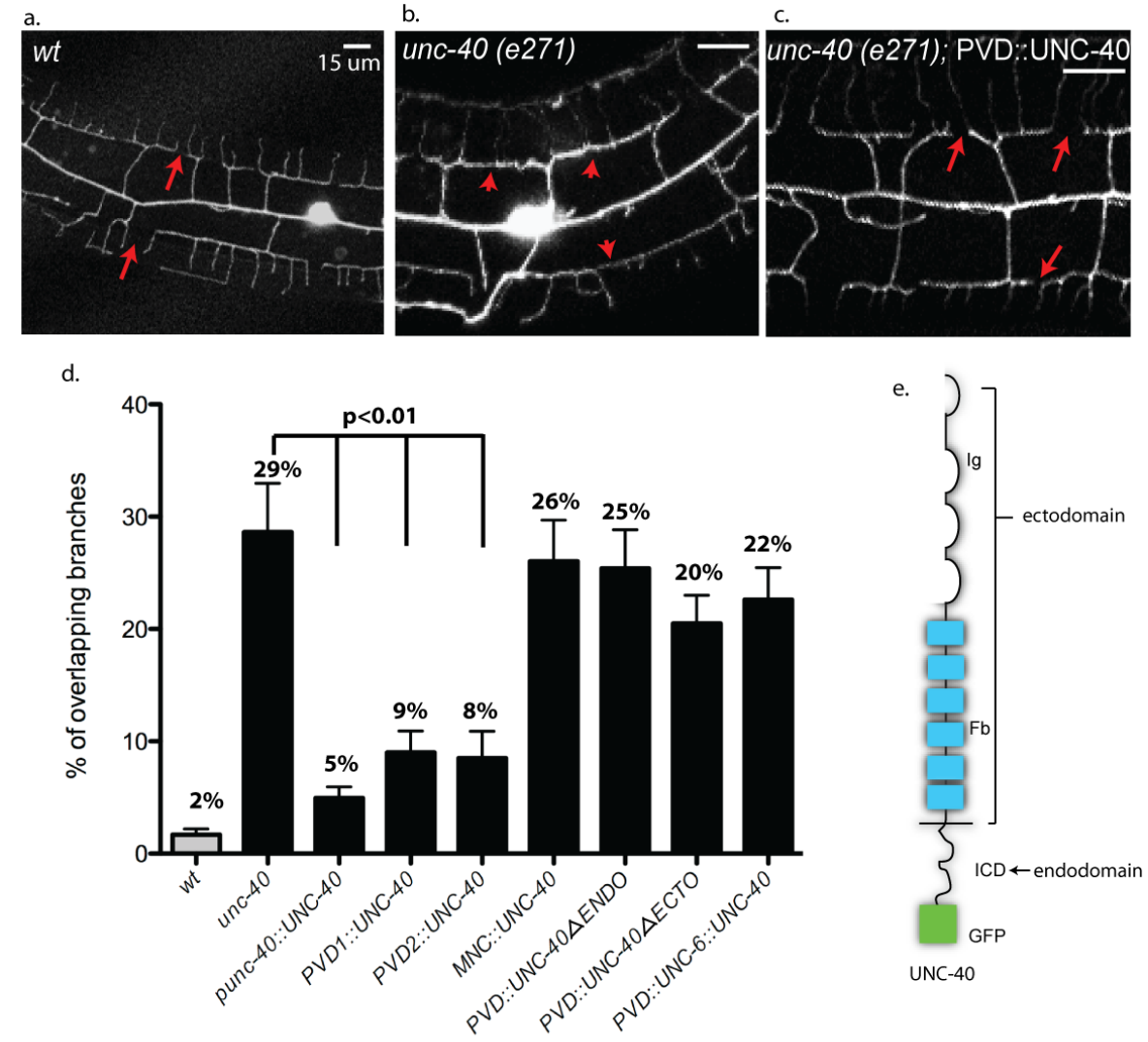
a.
wt
15 um
b.
unc-40 (e271)
c.
unc-40 (e271); PVD::UNC-40
d.
% of overlapping branches
p<0.01
29%
2%
5%
9%
8%
26%
25%
20%
22%
wt
unc-40
punc-40::UNC-40
PVD1::UNC-40
PVD2::UNC-40
MNC::UNC-40
PVD::UNC-40ΔENDO
PVD::UNC-40ΔECTO
PVD::UNC-6::UNC-40
e.
Ig
ectodomain
Fb
ICD
endodomain
GFP
UNC-40
f.
PVD::UNC-40::GFP
10 um
g.
punc-6::UNC-6::YFP
h.
UNC-6
UNC-40
MERGE

Figure 4.9. UNC-40/DCC functions in PVD to mediate self-avoidance and captures exogenous UNC-6/Netrin at the PVD cell surface. (a) PVD 3^{O} dendrites do not overlap in wild-type (wt) adults (arrows). **(b, c)** Expression of UNC-40 (PVD::UNC-40) in *unc-40 (e271)* rescues (arrows) the Unc-40 self-avoidance defect (arrowheads). (**d**) Quantification confirms that expression of UNC-40/DCC with the native *unc-40* promoter (*unc-40*::UNC-40) and with two different PVD promoters (PVD1::UNC-40, PVD2::UNC-40) restores PVD dendritic self-avoidance whereas expression with a motor neuron-specific promoter (MNC::UNC-40) does not. PVD expression of UNC-40/DCC lacking either the extracellular UNC-6 binding domain (PVD::UNC-40deltaECTO) or intracellular signaling domain (PVD::UNC-40deltaENDO) fails to rescue self-avoidance. Genetic backgrounds are wild type (wt) (grey box) or *unc-40(e271)* (black boxes). **(e)** Schematic of UNC-40 protein (Ig domain = loops, Fibronectin domains = rectangles, intracellular domain and GFP tag = dark rectangle). **(f)** PVD expression of GFP labeled UNC-40 (PVD::UNC-40::GFP) results in GFP puncta in PVD processes (arrows) and at tips of growing dendrites (arrowheads). **(g)** YFP-labeled UNC-6 expressed from its native promoter in ventral cells (*unc-6*::UNC-6::YFP) decorates PVD neurons (arrowheads) expressing UNC-40::mCherry. Arrow denotes UNC-6::YFP labeling of ventral nerve cord. (**h**) UNC-6::YFP (UNC-6, green) labeling of PVD expressing UNC-40::mCherry (UNC-40, red). Merged image showing co-localization of UNC-6::YFP and UNC-40::mCherry puncta (arrows).

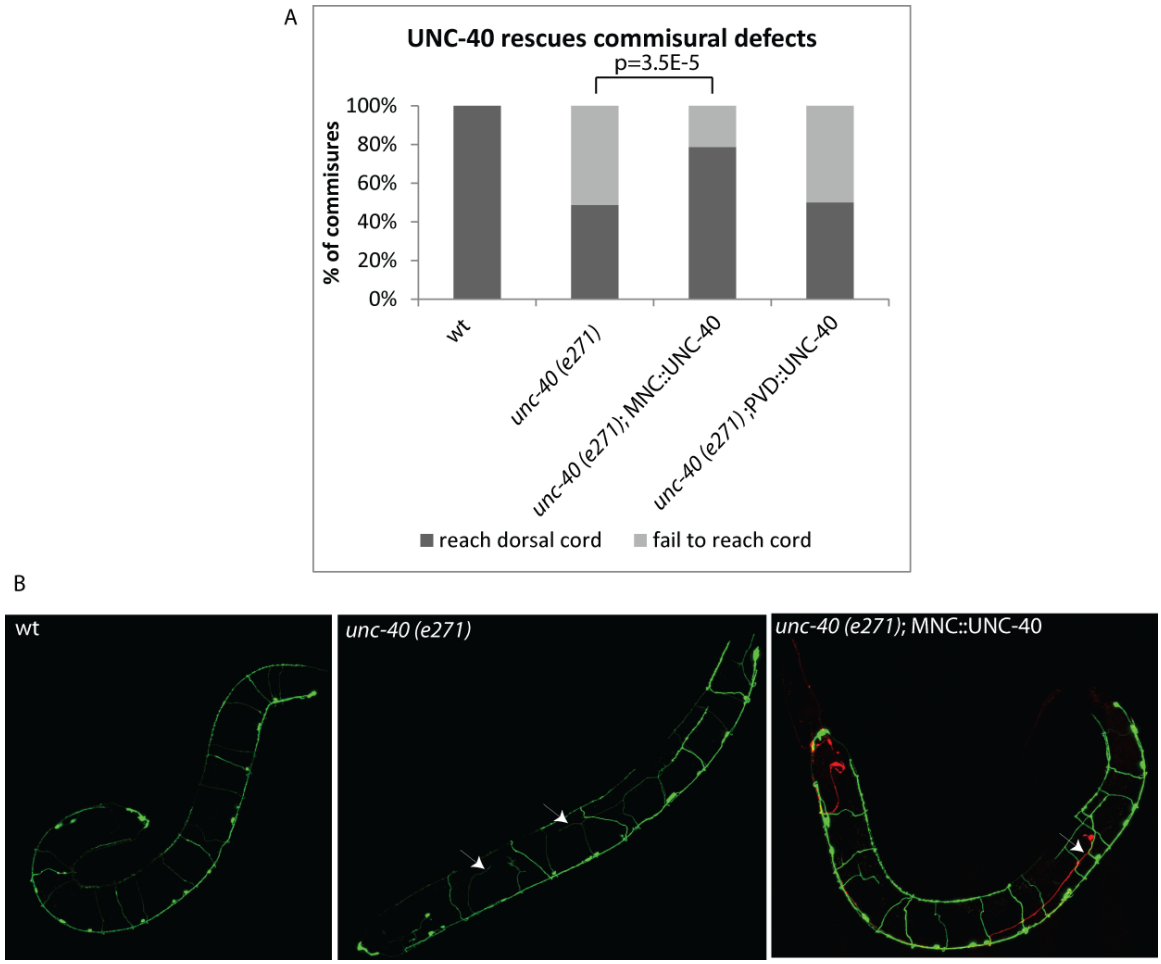

Figure 4.10. Expression of UNC-40/DCC in ventral cord motor neurons rescues motor axon guidance defects. (a) Histogram showing that 100% of *unc-25*::GFP-labeled GABAergic motor neurons extend circumferential commissures (MNCs) to the dorsal cord whereas only ~45% of MNCs reach the dorsal nerve cord in *unc-40 (e271)* (n = 20). MNC guidance defects are largely rescued by expression of UNC-40 in ventral cord motor neurons with the *unc-25* promoter (MNC::UNC-40). **(b)** Representative confocal images of wild type (wt), *unc-40 (e271)* and *unc-40 (e271*); MNC::UNC-40 adults. Arrows point to MNCs that fail to reach the dorsal nerve cord in *unc-40(e271)*. Axon guidance defects are not rescued in the PDE neuron that is labeled by a co-injected marker (*dat-1::mcherry*) in which expression of UNC-40 is not restored (arrow in MNC::UNC-40)

expression with the *F49H12.4* promoter also rescues the Unc-5 self-avoidance defect (Figure 4.11b,d, p = 1.8E-4 *vs unc-5*). Restoration of UNC-5 expression in motor neurons did not complement *unc-5 (e152)* PVD self-avoidance errors (Figure 4.11d) but does repair the uncoordinated phenotype that arises from misguided motor axon outgrowth (data not shown)[51, 214]. The results of these cell-specific rescue experiments show that UNC-5 function is required in the PVD dendrites to prevent overlap of 3^{O} branches.

UNC-40/DCC localizes UNC-6/Netrin to PVD dendrites

Consistent with the hypothesis that UNC-40/DCC function is required in PVD dendrites, PVD expression of a functional GFP-tagged UNC-40 protein (UNC-40::GFP)[174] resulted in distinct GFP puncta in PVD processes (Figure 4.9f). Moreover, UNC-40::GFP puncta can be readily seen at the tips of 3^{O} dendrites where contact-dependent self-avoidance occurs (Figure 4.9f,h).

We considered the possibility that UNC-6 functions as a contact-dependent repellent and tested this idea with an experiment designed to detect UNC-6 at the surface of PVD dendrites. We used the endogenous UNC-6 promoter to drive expression of UNC-6::YFP[213]. Although this transgenic line rescues Unc-6 axon guidance defects and therefore must secrete a functional UNC-6::YFP protein, UNC-6::YFP is too diffuse to detect in a wild-type animal outside of the ventral cells in which it is expressed (Figure 4.12)[213]. To enhance the sensitivity of this assay, we expressed mCherry-labeled-UNC-40/DCC in PVD. In this background, UNC-6::YFP is strikingly evident as YFP

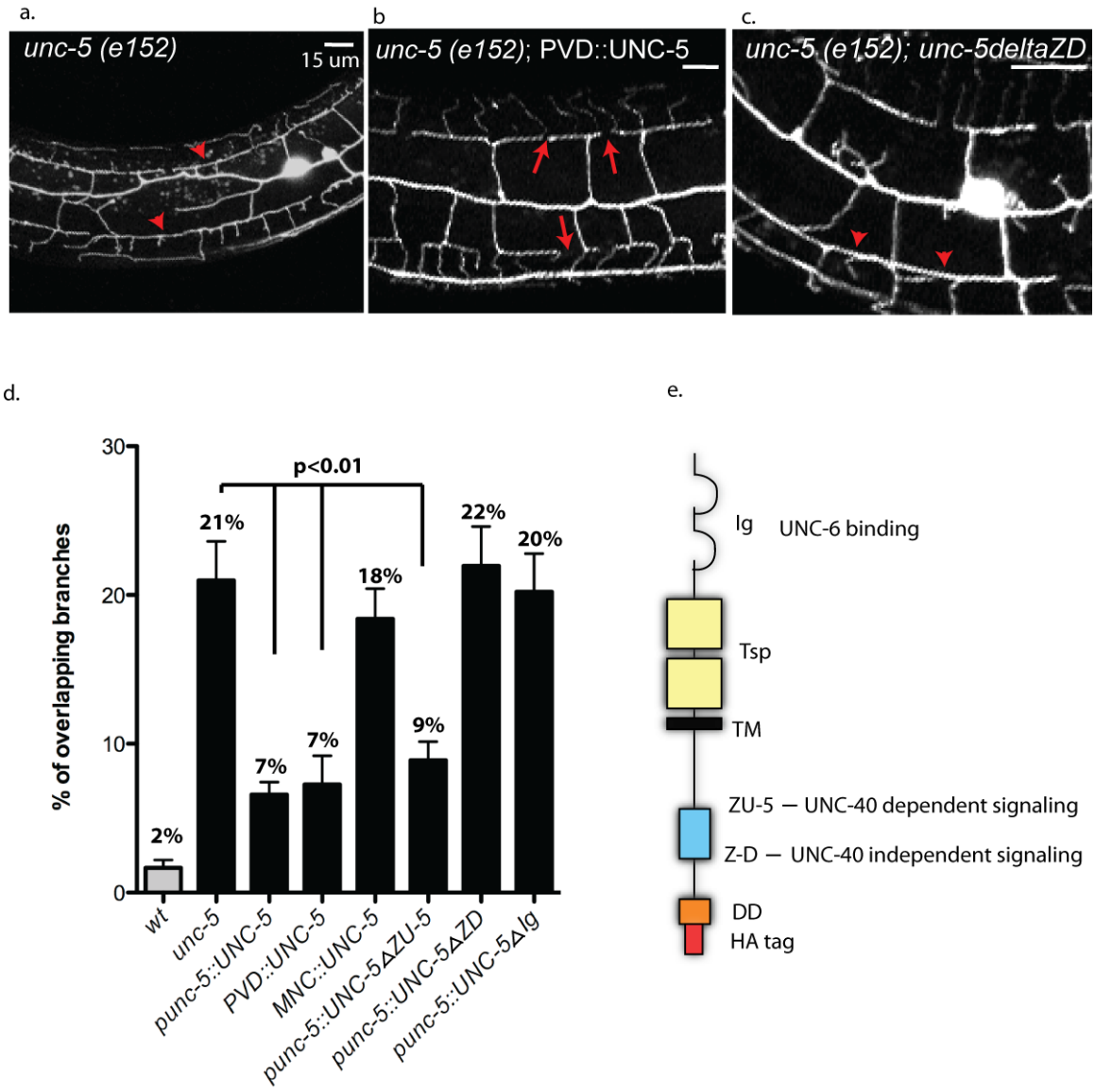

Figure 4.11. UNC-5 is required in PVD and utilizes UNC-40-independent signaling to mediate self-avoidance. **(a, d)** *unc-5(e152)* shows PVD self-avoidance defects (arrowheads) **(b)** Expression of UNC-5 with the PVD promoter (PVD::UNC-5) prevents 3^{O} branch overlap in *unc-5 (e152)* but **(c)** UNC-5 lacking the Z-D domain does not rescue. **(d)** Expression of UNC-5 with the native *unc-5* promoter (*unc-5*::UNC-5) or with the PVD promoter (PVD::UNC-5) restores PVD self-avoidance but expression of the UNC-5 with the motor neuron promoter (MNC::UNC-5) does not. Expression of UNC-5 proteins lacking either an UNC-40-independent cytoplasmic signaling domain (*unc-5*::UNC-5deltaZD) or UNC-6-binding domain (*unc-5*::UNC-5deltaIg) fails to rescue self-avoidance in *unc-5 (e152)* mutants whereas expression of an UNC-5 protein lacking an UNC-40-dependent signaling domain (*unc-5*::UNC-5deltaZU-5) prevents 3^{O} branch overlap. Genetic backgrounds are wild type (wt) (grey box) or *unc-5(e151)* (black boxes). **(e)** Schematic of UNC-5 protein showing functional regions (Ig domain = loops, Thrombospondin domain (Tsp) = square, TM = transmembrane domain, and ZU-5, Z-D, Death domain (DD) intracellular domains and C-terminal HA tag).

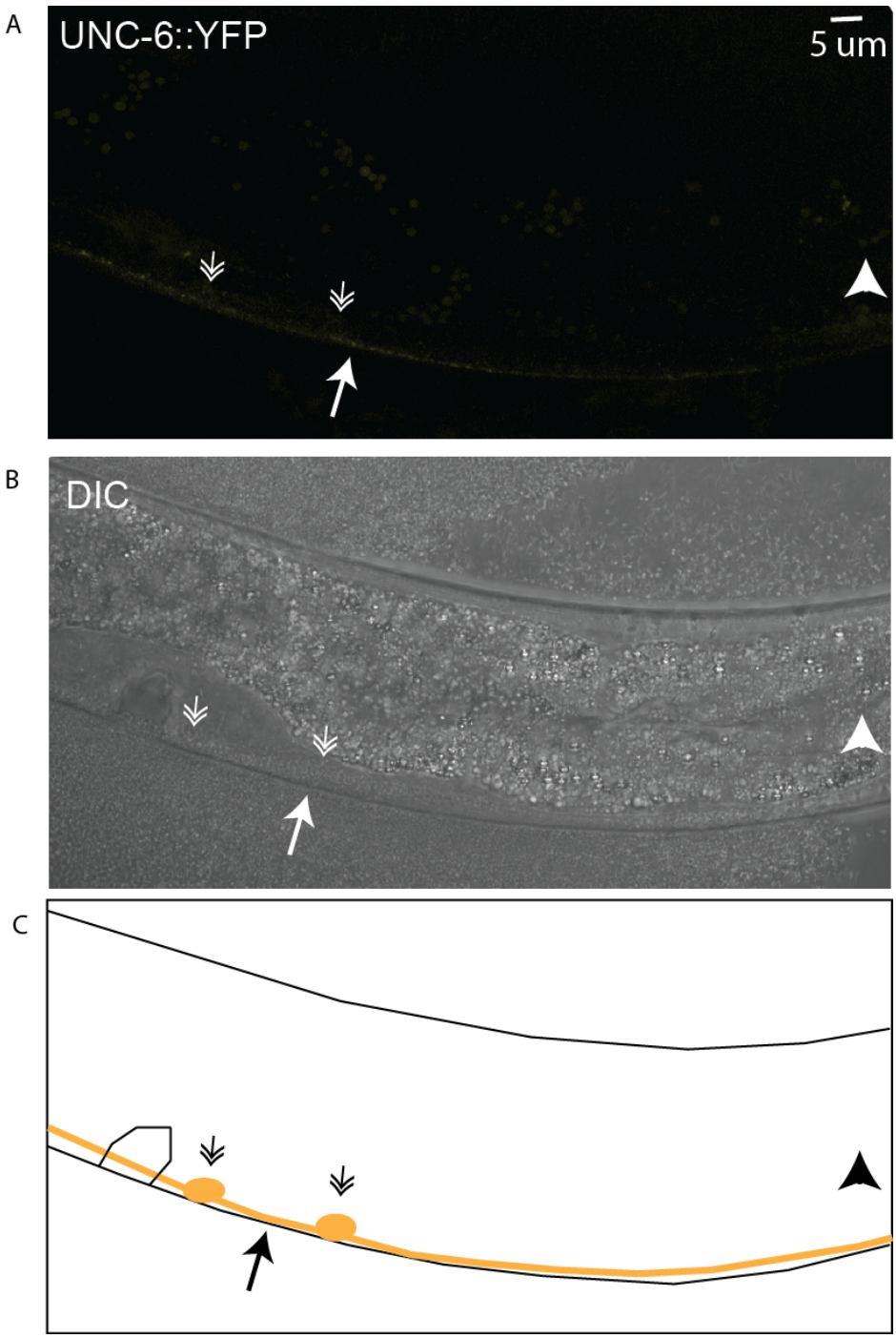

Figure 4.12. Expression of UNC-6::YFP in ventral motor neurons labels the ventral nerve cord but is not detected at the wild-type PVD neuron. (a,b) In a wild-type animal, YFP-labeled UNC-6 (UNC-6::YFP) is detected in the cell body of ventral cord motor neurons (double-headed arrowheads) where it is expressed (*unc-6* promoter) and in the adjoining ventral nerve cord (arrow) but is not detectable in posterior lateral region in which the wild-type PVD neuron (arrowhead) and it dendritic arbor reside. **(c)** Schematic representation of UNC-6::YFP localization.

puncta that overlap with mCherry::UNC-40 (Figure 4.9g,h). In contrast, expression of UNC-5 in PVD rescued the Unc-5 self-avoidance defect (Figure 4.11d) but did not result in detectable localization of UNC-6::YFP on PVD (data not shown). These results are consistent with a model in which UNC-40/DCC, but not the UNC-5 receptor, captures UNC-6 from the extracellular space at the surface of PVD dendrites. This idea is supported by our finding that PVD expression of a truncated UNC-40 protein lacking the UNC-6-binding extracellular domain (PVD::UNC-40deltaECTO) fails to restore 3^{O} branch self-avoidance in *unc-40 (e271)* (20% overlapping dendrites, p=0.23 *vs unc-40*) whereas PVD expression of intact UNC-40/DCC protein is sufficient (Figure 4.9 d). To rule out the possibility of a dominant negative effect, we determined that the PVD::UNC-40deltaECTO protein does not disrupt self-avoidance in a wild-type background (data not shown).

UNC-6 bound to UNC-40 functions as a short-range cue

Our results show that UNC-6/Netrin secreted from a ventral source can be captured by UNC-40/DCC at the surface of PVD dendrites. Because PVD sister dendritic repulsion depends on direct contact, we wondered if UNC-6 bound to UNC-40 at the tips of touching 3^{0} dendrites could trigger this response. In this model, UNC-40/DCC might adopt a role in which it positions UNC-6/Netrin at this critical location to activate withdrawal of an apposing dendrite. This idea mirrors the observation that *Drosophila* UNC-40/Fra/DCC can sequester exogenous NetrinB at the surface of guidepost cells to steer local axon outgrowth in a

contact-dependent mechanism[59]. This model predicts that UNC-6/Netrin protein tethered to the UNC-40/DCC receptor can function as a short-range cue. To test this idea, we used a chimeric protein in which UNC-6 is fused to the extracellular region of UNC-40 and expressed it in PVD. This membrane bound form of UNC-6/Netrin (PVD::UNC-6::UNC-40) rescued the dendritic self-avoidance defects of *unc-6 (ev400)* (8% overlapping 3^{O} branches, p=0.02 *vs* *unc-6*) (Figure 4.6 d). Expression in AVA interneurons in the ventral nerve cord with the *rig-3* promoter [218] (ventral::UNC-6::UNC-40), however, fails to restore self-avoidance to *unc-6(ev400)* and therefore confirms that the UNC-6::UNC-40 fusion protein is not released from the cell surface (Figure 4.13). Thus, our results are consistent with a model in which UNC-40/DCC localizes exogenous UNC-6/Netrin to the surface of PVD dendrites where it functions as a short-range cue to trigger self-avoidance. This configuration may be specifically required because PVD expression of UNC-6 fused to the N-terminus of a different transmembrane protein, NLG-1/Neuroligin (PVD::UNC-6::NLG-1),[58] did not rescue self-avoidance in *unc-6 (ev400)* (Figure 4.6d). The next problem to consider was how apposing PVD dendrites might detect this local UNC-40-bound, UNC-6/Netrin ligand. Because of the well-established role of UNC-5 in mediating repulsive responses to UNC-6/Netrin[51, 52, 54], and our finding that UNC-5 expression in PVD is necessary for self-avoidance, we imagined that UNC-5 could provide this function

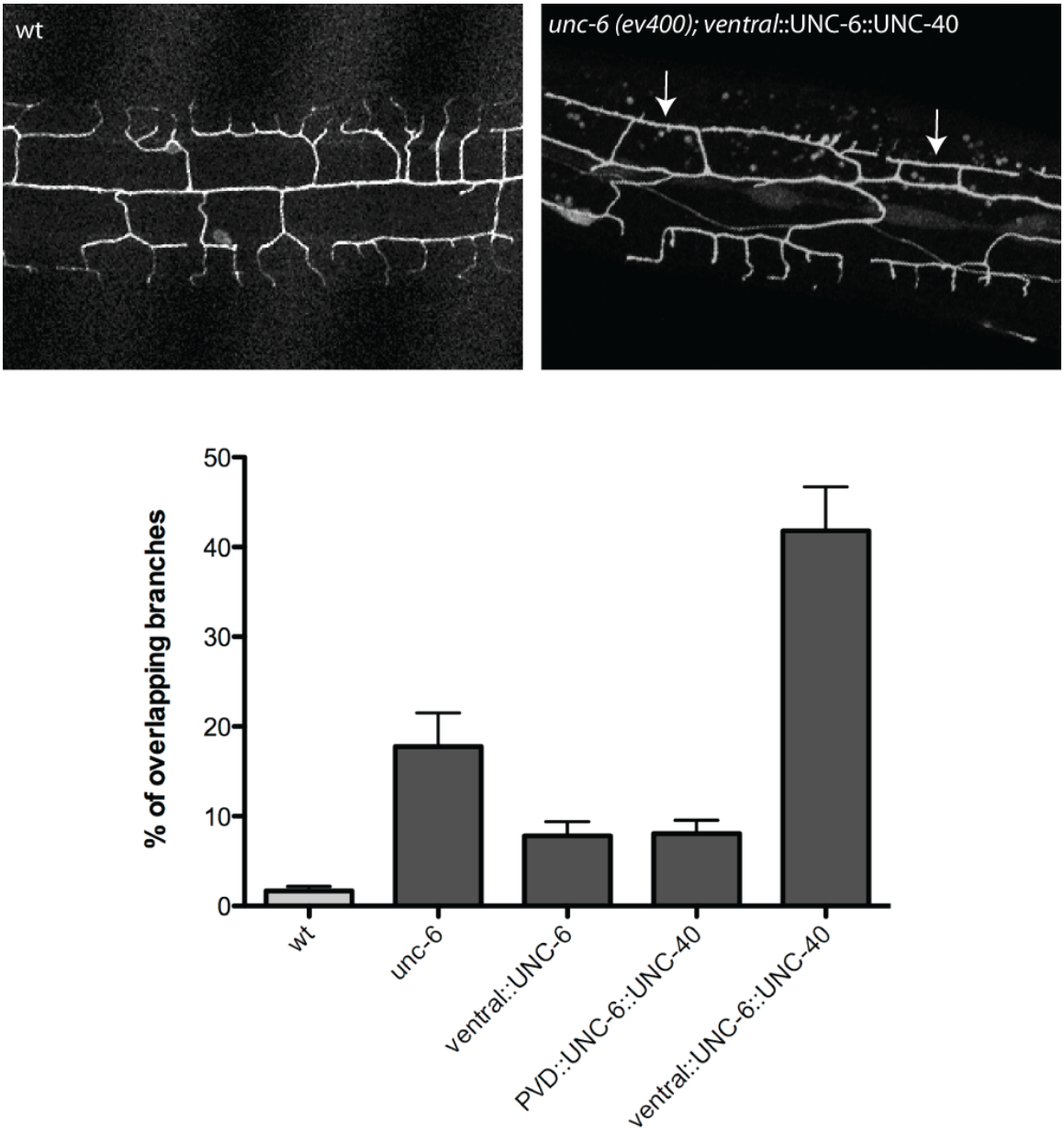

Figure 4.13. Expression of the UNC-6::UNC-40 chimeric protein in ventral neurons does not rescue the Unc-6 PVD self-avoidance defect. Expression of ventral::UNC-6::UNC-40 in *unc-6 (ev400)* does not restore self-avoidance (*unc-6* vs ventral::UNC-6::UNC-40) whereas expression of a secreted form of UNC-6 in ventral neurons (ventral::UNC-6) or membrane-tethered UNC-6 in PVD (PVD:UNC-6::UNC-40) does rescue the Unc-6 self-avoidance defect. We note that expression of UNC-6::UNC-40 in ventral neurons enhances the PVD self avoidance defect of *unc-6(ev400)*; the mechanism of this effect is unclear. For histogram, genetic backgrounds are wild type (wt) (light grey box) or *unc-6(ev400)* (dark grey boxes).

Self-avoidance is mediated by UNC-5 signaling

A mutation in the UNC-5 extracellular Ig domain that disrupts UNC-6/Netrin binding fails to rescue self-avoidance when expressed in *unc-5 (e152)* (Figure 4.11d, 20% overlapping branches, p=0.83 vs *unc-5*). This finding is consistent with genetic results (Figure 4.5) showing that *unc-5* and *unc-6* function in a common pathway to mediate self-avoidance and with the proposal that UNC-6 binding to UNC-5 is necessary for this interaction. Genetic analysis in *C. elegans* has shown that UNC-5 can mediate UNC-6-mediated repulsion either in concert with UNC-40 or independently[214]. These UNC-5 functions depend on specific conserved cytoplasmic domains; the Z-D sequence is necessary for UNC-40-independent signaling whereas the ZU-5 region is required for UNC-40-dependent activity[214]. To distinguish between these models, we tested mutant versions of the UNC-5 protein that lack either the ZU-D region (UNC-40-independent signaling) or the ZU-5 domain (UNC-40-dependent signaling). Previous work has shown that UNC-5 localization is not disrupted by these mutations[214]. Transgenic expression of the UNC-5 protein lacking the Z-D domain (UNC-5deltaZD) did not restore self-avoidance to an *unc-5 (e152)* mutant (Figure 4.11c,d 22% overlapping branches, p=0.79 vs *unc-5*). In contrast, deletion of the ZU-5 region (UNC-5deltaZU-5) that is required for UNC-40-dependent signaling significantly improved the frequency of self-avoidance in comparison to the *unc-5 (e152)* mutant alone (Figure 4.11d, 9% overlapping branches, $p=3E^{-4}$). These results are consistent with a model in which UNC-5-mediated repulsion does not depend on interactions *in cis* with the UNC-40

protein but that UNC-40 function is required for localizing UNC-6/Netrin for binding *in trans* to UNC-5 at the apposing tip of the adjacent 3^0 dendrite.

UNC-40/DCC signaling is required for self-avoidance.

Although the UNC-6::UNC-40 fusion protein rescues the *unc-6* mutant (Figure 4.6d) and therefore likely functions as a membrane-bound cue to trigger dendrite repulsion, UNC-6:UNC-40 does not restore self-avoidance to *unc-40(e271)*(Figure 4.9d). One explanation for this result is that *unc-40* signaling is not active in the UNC-6::UNC-40 fusion protein and that this UNC-40 function is necessary for self-avoidance. We tested this idea with a modified UNC-40 protein that lacks the intracellular domain (ICD) that mediates UNC-40/DCC downstream signaling[221]. Interestingly, PVD expression of this truncated UNC-40/DCC protein (PVD::UNC-40deltaENDO) in *unc-40(e271)* fails to rescue dendrite repulsion (Figure 4.9d). Thus, our results indicate that UNC-40 provides the dual roles of capturing UNC-6 at the PVD cell surface for interaction with UNC-5 as well as activating a downstream pathway to mediate self-avoidance.

DISCUSSION

Dendrites from a single neuron may be highly branched but rarely touch one another[109, 206]. The absence of overlap arises from a mechanism in which sister dendrites are mutually repelled by transient encounters during outgrowth. The necessity of physical contact for self-avoidance is indicative of

interaction between surface markers that trigger repulsion[206]. This model is substantiated by the recent discovery that membrane proteins can mediate self-avoidance in *Drosophila* sensory neurons[99, 100, 105, 106]. Here we describe a novel mechanism in the nematode, *C. elegans*, in which this self-recognition function is provided by a diffusible cue (Figure 4.14).

Our results show that UNC-6/Netrin is secreted from ventral cells to modulate self-avoidance of PVD sensory neuron dendrites in distal, lateral locations (Fig 4.14). We propose that UNC-6/Netrin is sequestered at the surface of PVD dendritic branches by the canonical receptor UNC-40/DCC where it is positioned to trigger a repulsive response upon contact with UNC-5 on the apposing dendrite. PVD self-avoidance also depends on UNC-40/DCC function in a separate pathway that does not require *unc-5* and *unc-6* (Fig 4.14).

In some respects, our model parallels an earlier finding in *Drosophila* in which UNC-40/Frazzled/DCC functions in guidepost cells to capture Netrin to provide a local guidance cue for nearby axons[59, 222, 223]. In this setting, however, the Netrin receptor in the responding cells is unknown and this signaling event occurs between separate cells. In the model that we have proposed, UNC-5 mediates a negative response to UNC-6 between spatially distinct membrane regions of the same cell. Netrin has also been shown to function as a short-range signal for axonal and dendritic guidance in other contexts and for defining the placement of synapses between specific neurons[54, 56-58]. The phenomenon of self-avoidance that we have detected includes additional features that point to a complex mechanism. In addition to the

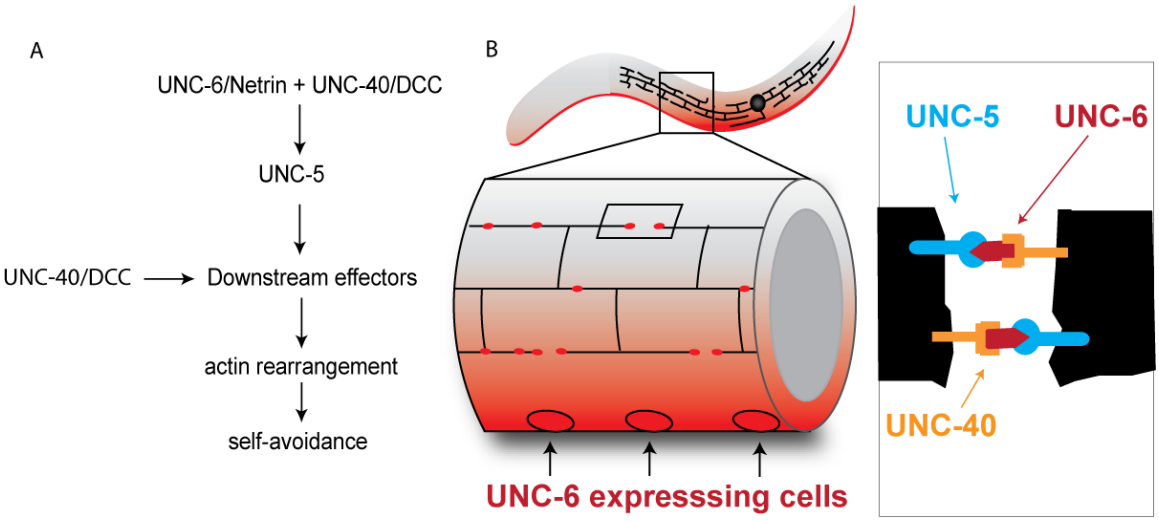

Figure 4.14. Model: UNC-40/DCC captures UNC-6/Netrin at the tips of growing dendrites to mediate UNC-5-dependent mutual repulsion. (a) UNC-6/Netrin functions with UNC-40 and UNC-5 through downstream effectors to reorganize the actin cytoskeleton for self-avoidance. UNC-40 also signals through an UNC-6/Netrin-independent pathway (**b**) Schematic showing distribution of UNC-6/Netrin expressed from ventral cells and focal UNC-6/Netrin localization to PVD dendritic branches. Inset depicts the tips of adjacent sister dendrites where UNC-40/DCC captures UNC-6/Netrin for contact with UNC-5 and mutual repulsion.

proposed role for UNC-40/DCC of sequestering UNC-6/Netrin for interaction with UNC-5, our genetic evidence (Fig 4.5) indicates that UNC-40/DCC also functions in a parallel self-avoidance pathway that does not involve *unc-5* and *unc-6*. UNC-6-independent signaling by UNC-40/DCC has been previously observed[48, 219, 224] and is suggestive of additional UNC-40/DCC activating ligands. Previous work has shown that UNC-5 and UNC-40 can signal independently of each other to mediate repulsion to UNC-6/Netrin[48, 54, 225, 226] but our findings include the additional observation that this activity requires physical contact between apposing dendrites.

In addition to expanding the repertoire of self-avoidance proteins, our discovery that UNC-40/DCC and UNC-5 are involved suggests that other established UNC-6/Netrin signaling proteins could also be utilized to trigger repulsion[12]. The significance of this possibility is underscored by the fact that little is known of the downstream mechanisms that reorganize the dendritic cytoskeleton to effect mutual repulsion [206]. For example, the intracellular proteins tricornered (trc) and furry (fry) are required for dendritic self-avoidance in a subset of *Drosophila* sensory neuron but mechanisms that activate these components are poorly defined[106, 111]. In addition, the cytoplasmic domain of Dscam is necessary for self-avoidance but no downstream effectors have been identified [100].

We have established that UNC-6/Netrin is required for self-avoidance of PVD dendrites. However, our results also point to additional mechanisms for regulating iso-neuronal repulsion. We note that most (~ 65%) of PVD 3^0

dendrites undergo normal self-avoidance in strong loss-of-function alleles of UNC-6/Netrin pathway genes (Figure 4.3). This result parallels the observation that mutants in self-avoidance genes in *Drosophila* (*e.g.*, Dscam, Turtle) and *C. elegans* (*e.g., eff-1)* are also incompletely penetrant[100, 105, 216].

Although our results reveal a new role for UNC-6/Netrin signaling in dendritic self-avoidance, the model that we have proposed involving a single cue and its receptors is unlikely to provide a general solution to the problem that individual neurons face of distinguishing self from non-self. The cell surface markers Dscam and protocadherins which can be expressed in many different alternative forms, are proposed to fulfill this role by providing unique combinations of labels for marking single neuron types in complex neural environments[109]. However, our discovery of a mechanism whereby an exogenous cue can be utilized to pattern dendritic self-avoidance suggests that other extracellular signals and their receptors could be similarly employed. This possibility significantly expands the potential utility of this self-avoidance strategy.

Author Contributions

Joseph Watson helped in the original characterization of UNC-6/Netrin signaling mutants. All other experiments were performed by Cody Smith. This work was published in Nature Neuroscience in 2012.

CHAPTER V

ACTIN POLYMERIZING PROTEINS TRIGGER RETRACTION IN DENDRITIC SELF-AVOIDANCE

INTRODUCTION

The precise control of neuronal process outgrowth drives the formation and maintenance of functional circuits. Mechanisms that control neuronal morphogenesis require both attractive and repulsive cues which are thought to control the cytoskeleton of developing neurons [2].

Actin polymerization regulates cell motility and axon guidance [227]. In axonal growth cones actin-based protrusions respond to attractive signals with striking precision. Repellents can also guide axons to their proper targets [2]. Interestingly, repulsive cues can induce instantaneous switches from growing to retractive states [228-231]. It is not clear how this switch is generated but has been proposed to require retrograde flow [83] and actin depolymerization [227].

Interestingly, many molecules that are required for attraction also appear to function in repulsion. For example, UNC-34/Enabled is thought to promote actin-polymerization at the tip of the growth cone in growing axons [232-235] but is also required for axonal repulsion [234, 236, 237]. Similarly, the F-actin promoting component MIG-10/Lamellipodin has been reported to function in both attractive and repulsive events [75, 76, 78]. Because repulsion has been

proposed to depend on actin disassembly it has been difficult to explain the role of UNC-34/Ena and MIG-10/Lpd in this process. In fact, the molecular understanding of how neuronal branches retract is poorly understood compared to how branches grow.

Active extension and retraction of neuronal processes is also a characteristic of dendritic morphogenesis. One particular example of branch retraction is activated to prevent overlap of sister dendrites [95, 96, 206, 238]. This phenomenon is known as self-avoidance and is widely observed during the development of sensory circuits. Cell surface receptors (*i.e.* Dscam, Turtle, Flamingo) have been shown to mediate self-avoidance [105, 106, 239, 240]. Although the cytoplasmic domains of these membrane proteins are required for self-avoidance, the intracellular mechanisms that rearrange the cytoskeleton to drive dendrite retract have remained a mystery [4][99, 105].

We have recently shown that dendritic self-avoidance can also depend on the diffusible axon guidance cue UNC-6/Netrin and its membrane receptors UNC-5 and UNC-40/DCC (Chapter 4)[241]. Here we identify components of a downstream signaling cascade that links UNC-6/Netrin signaling to the cytoskeleton. We show that dendritic self-avoidance requires the actin-polymerizing proteins UNC-34/Enabled and MIG-10/Lamellipodin. Our results show that UNC-34/Ena accumulates with actin near the tips of sister dendrites as they contact one another. The conserved protein DAB-1/Disabled functions in the UNC-6/Netrin pathway to ensure UNC-34/Ena can freely traffic to the site of contact. MIG-10/Lpd, specifically the C isoform, localizes with UNC-34/Ena but

appears to function in an independent pathway to promote contact-dependent self-avoidance. Together, these results suggest that actin polymerization is controlled by a cell-surface signal to effect dendritic retraction in a self-avoidance mechanism. We provide additional genetic evidence that myosin II is required for dendrite retraction. Together our results favor a model in which dendrite retraction is driven by retrograde flow and that this mechanism depends on polymerization of new actin filaments near the tips of sister dendrites as they touch. In addition to identifying the first cytoplasmic effectors of a known self-avoidance receptor our work also provides a new model for neurite retraction that appears to resolve a long-standing mystery of how UNC-6/Netrin signaling could drive axonal repulsion. We believe, therefore, that these findings reach beyond the scope of self-avoidance.

METHODS

Nematode strains and genetics

The wild-type N2 Bristol strain was used for all experiments and cultured as previously described [158].

Mutant Strains

unc-34 (gm104), mig-10 (ct41), dab-1 (gk291), unc-6 (ev400), unc-5 (e152), wsp-1 (gm324), pfn-1 (ok808), unc-73 (e936), ced-10 (n1993), max-2 (ok1904), unc-40 (e271), ced-5 (n1812), unc-115 (ky275), madd-2 (ok2226), mig-

2 (ok2273), rac-2 (ok326), daf-18 (ok480), epac-1 (ok655), src-1 (ok2685), pak-1 (ok448), pak-2 (ok332), abl-1 (ok171), unc-60 (e723), nmy-2 (ne3409), nmy-1 (sb115), nmy-1 (sb113), spe-15 (hc75), hum-2 (ok596), let-502 (ok1283), hum-7 (ok3054).

Transgenic Strains

NC1687 [wdIs52 (*F49H12.4*::GFP + *unc-119*)],

NC1686 [wdIs51 (*F49H12.4*::GFP + *unc-119*)],

NC2422 [wdEx775 (pCJS78, *F49H12.4*::UNC-34::mcherry + coel::RFP + *dat-1*::mcherry)],

NC2463 [wdEx794 (pCJS91, *F49H12.4*::utrophin::GFP + *ceh-22*::GFP + pCJS04, *F49H12.4*::mcherry)],

NC2462 [wdEx773 (pCJS94, *F49H12.4*::MIG-10C::GFP + coel::RFP + pCJS85, *dat-1*::mcherry)]

NC2261 [*pha-1 (e2123ts); lon-2; wdEx726 (*pCJS96*, F49H12.4::MIG-10a::GFP* + pCJS85*, dat-1::mcherry* + pCJS04*, F49H12.4::mcherry + pBx)]*

NC2436 [wdIs52 (*F49H12.4::GFP* + *unc119); wdEx777 (*pCJS88*, F49H12.4::mig-10b::YFP* + pCJS85*, dat-1::mcherry + coel::RFP)*]

NC2257 [*pha-1 (e2123ts); lon-2; wdEx722 (*pCJS95*, F49H12.4::ced-10::GFP* + pCJS85*, dat-1::mcherry* + pCJS04*, F49H12.4::mcherry + pBx*)]

NC2496 [*wdEx819 (*pCJS78*, F49H12.4::mcherry::UNC-34* + pCJS94*, F49H12.4::MIG-10C::GFP + dat-1::mcherry + coel::RFP*)]

Generating transgenic strains

All transgenic animals in this study were generated by microinjection. Plasmids were injected at 30 ng/ul into the N2 or NC1687. In some cases a co-injectable marker coel::RFP (30 ng/ul) or *ceh-22*::GFP (15 ng/ul) was used to identify potential transgenic strains. At least two strains were generated from each plasmid.

Molecular Biology

CED-10, UNC-34, MIG-10A and MIG-10C plasmids were modified from gifts from D.C.R [242]. Sph1 and Asc1 were used to swap in the *F49H12.4* promoter from pCJS04. MIG-10B was a gift from C.B., the promoters were swapped using SphI and XmaI. DAB-1 cDNA was amplified from cDNA from the animal with primers that contained XmaI and AgeI and placed into pCJS93.

Time-lapse TIRF microscopy

Animals were prepped for imaging on a slide as previously described [12]. A Nikon Eclipse TiE TIRF microscope equipped with a Photometrics Roper Evolve EM-CCD camera and Coherent Sapphire 488 and 561 was used for all TIRF experiments. All images were taken with a 100X ApoFluor Nikon lens (1.49 NA). The TIRF angle was manually adjusted to image into the sample at a point where the 3^{O} dendrites were illuminated but the surrounding medial tissue was not. Nikon Elements 3.2 was used to optimize imaging settings. For contact

events, images were taken every 10 sec for 1 hr. To visualize trafficking of UNC-34, images were taken ~15 frames/second. For each TIRF tiff image the scale was 0.16 um/pixel.

Confocal Microscopy

Nematodes were immobilized with 15 mM levamisole as previously described [12]. Images were obtained in a Leica TCS SP5 confocal microscope. Z-stacks were collected with either 40X (1 um/step), 63X (0.75 um/step) or 100x (0.75 um/step) objectives. Brightness and contrast were enhanced using Adobe Photoshop CS5.

Quantifying UNC-34::mcherry puncta

Z-stacks spanning the depth of the PVD neuron were imaged with a 100X objective on a Leica TCS SP5 microscope. All images were taken with the exact laser power and image settings (see settings below). Z-stacks were collapsed to provide a projection of the PVD neuron. Images were then converted to 8-bit grayscale using ImageJ software. The 3D object counter was used to count the number of puncta. Puncta above an arbitrary intensity setting of 24 were used to define individual puncta. 10 animals were counted for each genotype. An unpaired students t-test was used to determine statistical significance.

Leica TCS SP5 settings for counting UNC-34::mcherry

Pinhole: 144.5 um
Step Size: 0.76 nm
Scan Direction: 2
Scan Speed: 400 Hz
Excitation Beam Splitter DD 488/561
Resolution: 8 bits

Channels:	488	561
Laser Power:	28%	NA
Laser Line Visible:	20%	50%
Emission Bandwidth:	500 nm - 550 nm	570 nm - 700 nm
Active Gain:	700	712
Offset:	0	0

Generating Kymographs

The vector tool in ImageJ was used to draw a trace of the PVD dendrite. The kymograph function in ImageJ was used to generate a kymograph [243]. Kymograph were pseudocolored by manual tracing of the two branches in Adobe Illustrator. The pseudocolors were overlaid with the original gray scale kymograph.

Scoring Self-avoidance Defects

Each genotype was scored using PVD::GFP. Confocal images spanning the PVD depth were used to quantify self-avoidance defects. Confocal stacks were collapsed into a single plane. Overlap was designated as any two adjacent 3^{O} dendrites that do not have an intervening space between. The total number of 3^{O} dendrites was determined by the number of 2^{O} dendrites as previously described [241]. An unpaired Student's t-test was used to determine statistical significance. Because *nmy-2* null mutants are embryonic lethal we utilized a viable temperature sensitive allele [244]. To bypass embryonic lethality we

scored *nmy-2* mutant animals that laid eggs at 15C, the permissive temperature but were shifted during early L1 larval stage before PVD is generated to the restrictive temperature, 25C. All self-avoidance errors were scored in young adults.

RESULTS

The *C. elegans* PVD neuron envelops the worm in a non-overlapping net-like array [12]. The lack of overlap is driven by a mechanism that utilizes UNC-6/Netrin and receptors UNC-5 and UNC-40/DCC (Chapter 4)[241]. As a first step toward defining the downstream signaling cascade that drives PVD self-avoidance we first sought to characterize the cytoskeletal composition of the PVD dendrite.

F-actin is enriched in retracting dendrites

In *Drosophila*, actin filaments fill the entire dendritic array of sensory neurons. In contrast, static images of microtubule binding proteins shows that microtubules are limited to the 1^{O} dendrite and do not extend into higher order dendrites [245]. In PVD, microtubules are also limited to the 1^{O} dendrite [246]. We, therefore, hypothesized that actin is the primary cytoskeletal component in the 3^{O} dendrites that self-avoid. To characterize the actin cytoskeleton of the PVD dendrite we built transgenic animals to visualize the localization of fluorescent proteins that are tagged with specific actin-binding domains in PVD.

moesin::mCherry [247, 248] and *utrophin*::GFP [249] both showed striking subcellular localization within the PVD dendritic tree (Figure 5.1A,B). In static images, *utrophin*::GFP was notably enriched at newly synthesized branches (*i.e.* 4^{O} branches in the L4) (Figure 5.1A,B). We conclude that actin is likely the predominant cytoskeletal component of 3^{O} dendrites.

Given the abundance of actin in lateral PVD dendrites, we hypothesized that dynamic rearrangement of actin could drive PVD dendrogenesis. Because the fluorescence intensity of *utrophin*::GFP was dim in immature PVD neurons it was not possible to use time-lapse imaging to visualize these markers by conventional confocal microscopy (data not shown). Since the PVD neuron is located near the surface of the animal we considered using TIRF microscopy to observe the subcellular localization of actin and other components during PVD morphogenesis. With TIRF images we could collect images at near video rates (*e.g.* $\geq$ 30 frame per second) at high signal to noise ratios (Figure 5.2A,B). With this approach it was possible to observe temporal changes in the localization of growing dendrites. *utrophin*::GFP was typically concentrated near the tip of a growing dendrite (Figure 5.1, D arrow 0 sec). With the initiation of retraction, *utrophin*::GFP intensity initially increased in the area behind the tip of the dendrite and filled the entire dendrite as it withdrew (Figure 5.1D,E 190 sec). As a control, cytosolic mcherry intensity did not increase in the retracting branch (Figure 5.1D). The enhanced intensity of the *utrophin*::GFP in the dendrite remained until retraction stopped (n=4) (Figure 5.1D, E). These results are consistent with a model in which increased actin assembly at the area just

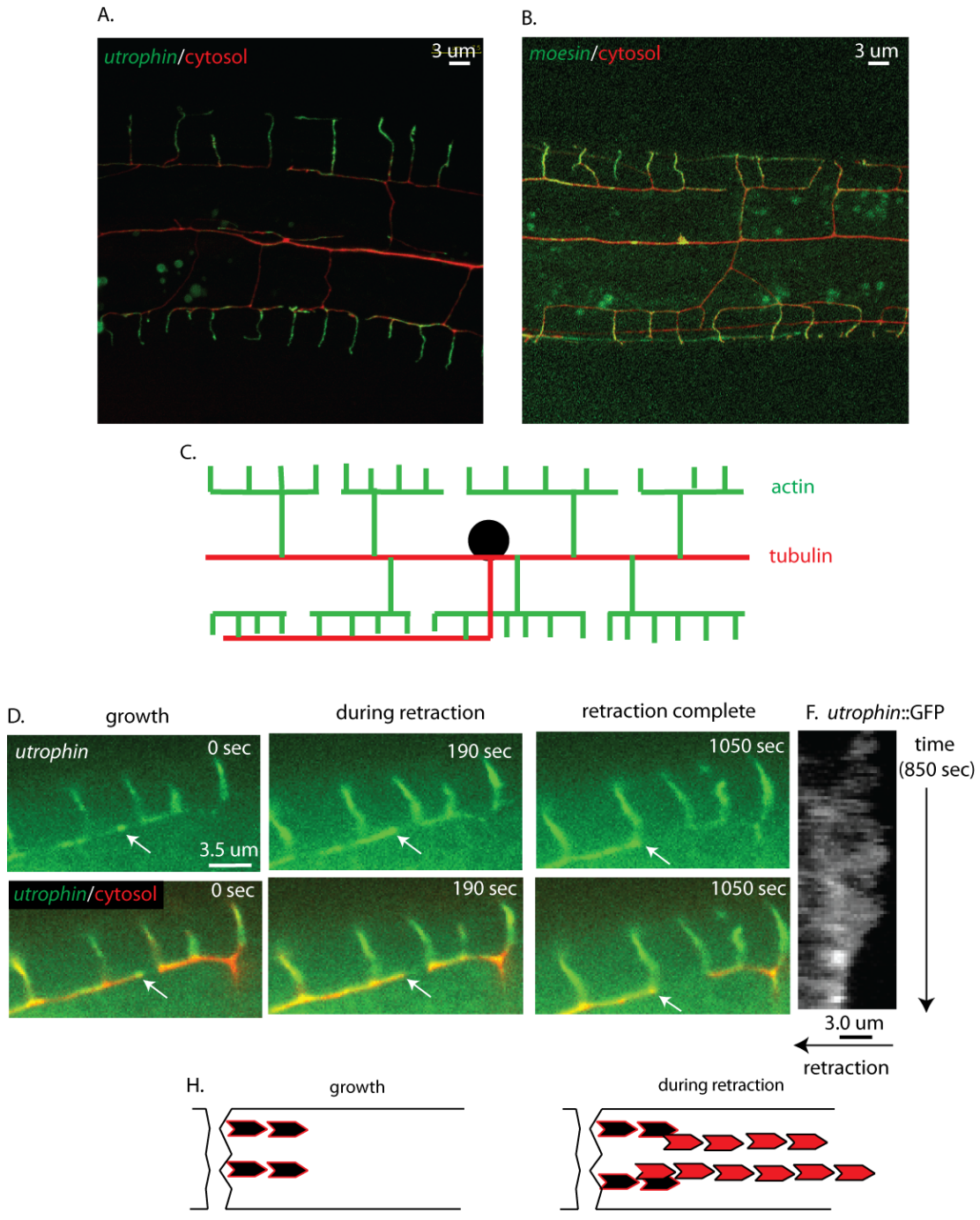

Figure 5.1 Actin is enriched near tips of retracting dendrites. A. Confocal image of Utrophin::GFP and cytosolic::mcherry in the PVD neuron. Utrophin::GFP is strongly localized at newly formed branches in L4 larvae. B. Confocal image of moesin::mcherry and cytosolic GFP in PVD displays a similar pattern as utrophin. C. Schematic of the cytoskeletal composition of PVD with actin localized to higher order dendrites and microtubules in the 1^{O} dendrite and axon. D. Time-lapse TIRF microscopy of utrophin::GFP and cytosolic mcherry in a 3^{O} dendrite. In retracting branches, utrophin::GFP is enriched(arrow). F. Kymograph of utrophin::GFP during dendrite retraction. H. Model of time-lapse results showing actin (black hexagon) at the tip during growth. Additional actin (red hexagon) accumulate in the retracting dendrite.

proximal to the tip of the dendrite could drive retraction and thus proteins that are utilized to promote actin assembly could be key players in self-avoidance. We next sought to identify these likely downstream components.

Actin-Polymerizing components are required for self-avoidance

In previous work we collected confocal stacks every 160 sec to establish that self-avoidance is mediated by a contact-dependent event[12, 241]. Here we obtained TIRF images at 10 sec intervals to confirm that contact events last about 140 sec (Figure 5.2C,D). These results, therefore, validate our earlier findings with confocal microscopy and also provide a higher temporal resolution of contact-dependent self-avoidance.

To identify downstream signaling components that are required for self-avoidance we used PVD::GFP to screen specific genetic mutants for overlapping 3^{O} dendrites. Our analysis focused on proteins that either interact with the actin cytoskeleton or that have been shown to function in UNC-6/Netrin signaling pathways. Mutants of 35 genes were examined to identify 10 candidate downstream components that are required for self-avoidance (Table 5.1). Many of these mutants displayed PVD dendritic defects strikingly similar to those of *unc-6, unc-5* and *unc-40 [241]*. Interestingly, our approach revealed multiple proteins that are normally employed during actin polymerization. For example, MIG-10/Lpd, UNC-34/Ena, PFN-1/Profilin and WSP-1/WASP have all been shown to promote actin polymerization. Other components revealed by our screen, UNC-73/Trio, CED-10/Rac, CED-5/Dock180, and MAX-2/p21 kinase

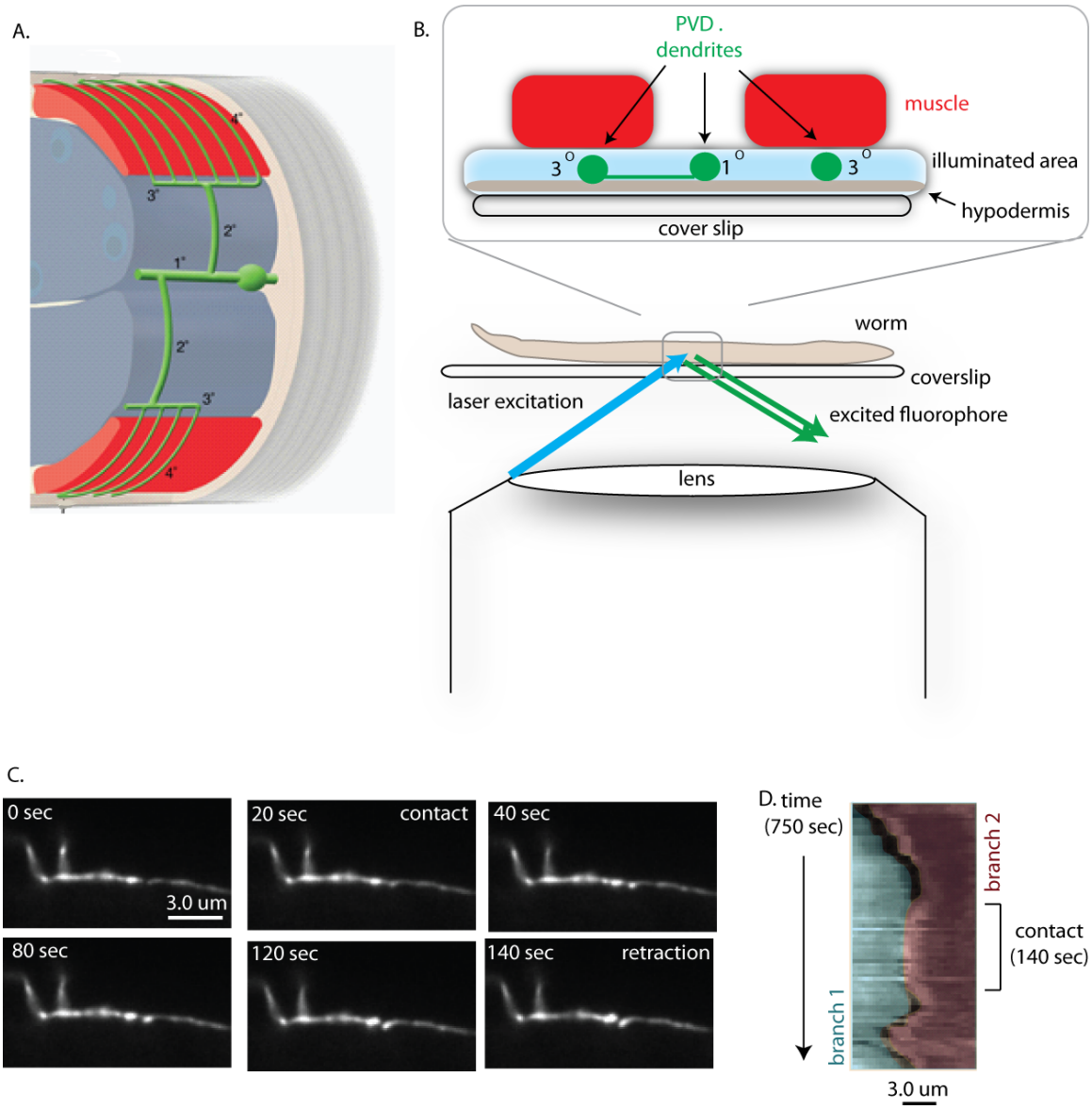

Figure 5.2. TIRF microscopy to image PVD dendritic growth. A. Schematic of PVD dendrites (green), muscle (red), and hypodermis (light grey) showing the proximity of PVD branches to the surface of the animal (from Albeg et. al 2011). B. Schematic of TIRF microscopy setup. Upper section shows a sagittal cross section of a nematode on its side next to a coverslip. PVD dendrites (green) are sandwiched between the hypodermis (beige) and the muscle (red) close to the cover slip. TIRF illumination (glue) evokes fluorescent signals from PVD region immediately beneath the hypodermis. Bottom cartoon shows the lens limits the laser angle to excite only the region close to the cover slip and the excited fluorophore in this region is the only collected signal. Worm (beige) is sitting on the coverslip. C. TIRF imaging of PVD::GFP during a contact event. Images were taken every 10 sec. D. Kymograph (750 sec total) of the contact event of branch 1 (green) with branch 2 (red). Branches were pseudocolored. Contact represents the area of the kymograph with no black space between the two branches. Contact lasted for about 140 sec (~2.5 min).

Table 5.1 Mutants that were screened for PVD defects.
* significance from wt, # described in Chapter 6
all with numbers were scored. Those without numbers were screened via visual screen for overlapping branches.

Gene	3° dendrite overlap (%)	2° dendrite asymmetry#
unc-5	21*	
unc-40/DCC	29*	Yes
unc-6/Netrin	18*	Yes
unc-34/Enabled	34*	Yes
dab-1/Disabled	31*	
mig-10/Lpd	22*	Yes
unc-73/Trio	21*	Yes
wsp-1/WASP	18*	
max-2/p21 kinase	12*	
pfn-1/Profilin	7*	
ced-10/Rac	6*	
ced-5/Dock180	4*	
unc-115/Limatin	4	
madd-2/Tri	3	
mig-2/Rac	3	
rac-2/Rac	2	
nmy-1/myosin II	20*	
daf-18/PTEN	No overlap	
nid-1/Nidogen	No overlap	
epac-1/epac	No overlap	
src-1/Src	No overlap	
ccb-1	No overlap	
gON-2	No overlap	
cca-1	No overlap	
egl-19	No overlap	
pkc-1	No overlap	
pak-1/p21 kinase	No overlap	
pak-2/p21 kinase	Lethal	
igcm-2/turtle	No overlap	
abl-1/Abelson	No overlap	
ptp-3/LAR	No overlap	
unc-60/cofilin	No overlap	
nmy-2/myosin II	No overlap	
spe-15/myosin VI	No overlap	
hum-2/myosin XII	No overlap	
let-502/Rho Kinase	No overlap	
hum-7/myosin IX	No overlap	
hum-1/myosin I	No overlap	

have all been shown to function downstream of UNC-6/Netrin to promote UNC-34/Ena and/or MIG-10/Lpd mediated actin polymerization [69, 76, 78, 171, 234, 242, 250]. Based on these results we considered the hypothesis that actin polymerization drives contact-dependent self-avoidance. We thus sought to characterize how these components are utilized during self-avoidance.

UNC-34/Ena triggers self-avoidance

UNC-34/Ena has been shown to function downstream of UNC-6/Netrin signaling in axon guidance to mediate either attraction or repulsion [233]. In PVD, UNC-5 functions as the receptor of UNC-6. We hypothesized that UNC-34/Ena also functioned with UNC-6/Netrin and UNC-5 to drive self-avoidance. If this model is correct, then a genetic strain bearing mutations in *unc-34* and in other *unc-6* pathway mutants should show self-avoidance defects comparable to that of either single mutant. To test this idea we generated an *unc-34;unc-5* double mutant. The double mutant of *unc-34; unc-5* phenocopied self-avoidance errors of both the *unc-5* and *unc-34* single mutants (Figure 5.3A). These data are consistent with the hypothesis that *unc-34/Ena* function is in the same pathway as *unc-5* to trigger self-avoidance (Figure 5.3B).

UNC-34/Ena has been shown to function in many different developmental processes. We hypothesized that UNC-34/Ena function in self-avoidance was cell-autonomous in PVD. To test UNC-34/Ena cell-autonomy, we generated a transgenic animal that expressed UNC-34 specifically in the PVD neuron. Restoration of UNC-34 to the PVD neuron rescued self-avoidance defects of the

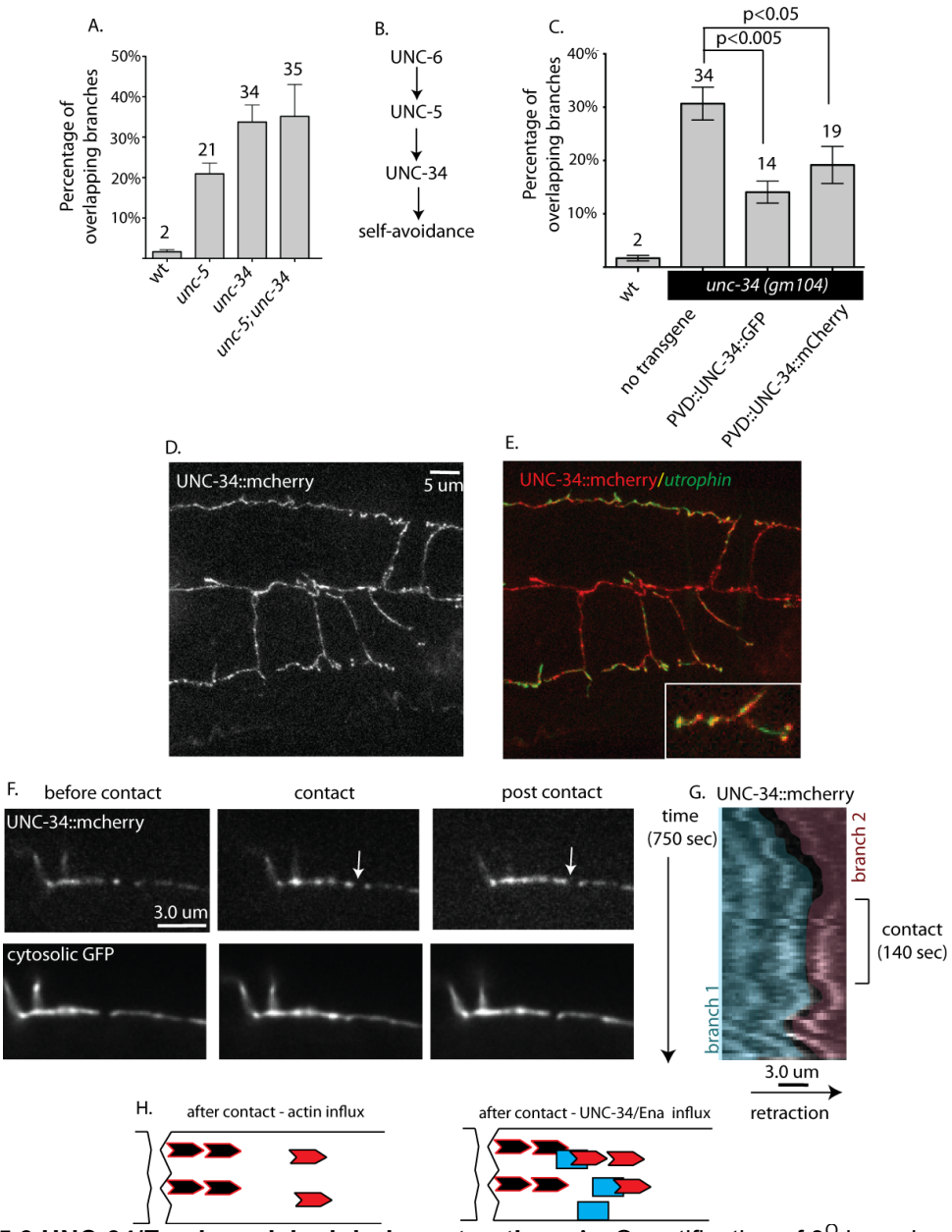

Figure 5.3 UNC-34/Ena is enriched during retraction. A. Quantification of 3^{O} branch overlap. *unc-5, unc-34* and *unc-5;unc-34* are not significantly different. B. Self-avoidance pathway. C. Quantification of overlapping dendrites when UNC-34::GFP or UNC-34::mcherry specifically expressed in PVD. Both PVD::UNC-34::GFP and PVD::UNC-34::mcherry are significantly different then the *unc-34 (gm104)* with no transgene. D. Confocal images of UNC-34::mcherry shows punctate localization throughout the dendrites. E. Confocal images of Utrophin::GFP and UNC-34::mcherry shows colocalization of UNC-34 and F-actin in the dendrites. Inset shows overlap. E. Images from time-lapse TIRF micrscopy of UNC-34::mcherry and cytosolic GFP during a contact event. UNC-34::mcherry becomes enriched after contact and remains enriched during retraction is complete. F. Kymograph of UNC-34 during contact. Branch outline detected by PVD::GFP were overlayed and pseudocolored. Branch 2 is the retracting branch. H. Model of UNC-34 (blue rectangle) influx into the area of contact to induce retraction via actin (pointed red hexagon) polymerization.

unc-34 null allele *gm104* (Figure 5.3C). These data indicate that UNC-34 functions in PVD to trigger self-avoidance.

If UNC-34/Ena is utilized to trigger repulsion in self-avoidance, then it should be localized in the dendrite. To detect the subcellular localization of UNC-34 in PVD, we first visualized functionally tagged versions of the protein in static images with the confocal microscope. Both UNC-34::mCherry and UNC-34::GFP showed a punctate pattern throughout PVD dendrites (Figure 5.3D). In both cases, we observed UNC-34 at the tip of dendrites where it could be available to modulate contact-dependent retraction (Figure 5.3D).

We hypothesized that UNC-34/Ena may become specifically enriched at the contact site to promote actin polymerization and thereby induce self-avoidance. To address this possibility, we visualized UNC-34::mcherry during a contact-induced retraction event with time-lapse TIRF microscopy. Upon contact between neighboring 3^{O} dendrites, UNC-34 intensity increased near dendritic tips and remained in these locations until retraction was complete (Figure 5.3F,G). UNC-34::GFP intensity was highest in a proximal region approximately 3 um behind the dendritic tip (Figure 5.3F,G). This region coincided with the area in which the actin-binding protein Utrophin is also enriched during retraction. Based on these results we considered the hypothesis that UNC-34 is recruited in self-avoidance to induce actin polymerization at the area just distal to the tip of the dendrite.

To ask if UNC-34 could potentially be trafficked to the site of contact we visualized UNC-34::mCherry movement at ~15 frames per second in the PVD

dendrite. Interestingly, these movies revealed rapid movement of UNC-34::GFP puncta in the PVD dendrites (Figure 5.4F). Both anterograde and retrograde movement was observed (Figure 5.4F). Based on this evidence it seems plausible that UNC-34 could traffic to the site of contact to induce retraction.

To test this idea that UNC-34 was trafficked to the site of contact to promote actin polymerization, we generated a transgenic line that allowed us to visualize both UNC-34 and Utrophin in the PVD neuron. Consistent with our hypothesis that UNC-34 could be utilized to drive actin polymerization, UNC-34 and utrophin co-localized in the PVD dendrite (Figure 5.3E). We also visualized dynamic colocalization of these components using TIRF microscopy (data not shown). Thus, these data are consistent with the hypothesis that UNC-34/Ena is recruited to the site of contact to promote actin polymerization (Figure 5.3H). Because UNC-34/Ena localization was dynamic and was enriched near sites of dendritic contact we hypothesized that self-avoidance would also require proteins that control UNC-34/Ena localization. We thus sought to identify these molecules.

DAB-1/Disabled is required for self-avoidance

Drosophila Disabled has previously been shown to regulate Enabled localization in epithelial cells [251]. We therefore examined UNC-34::mCherry localization in *dab-1* mutants to ask if DAB-1/Disabled functioned similarly in the *C. elegans* PVD neuron. In wild-type animals, UNC-34::mCherry is broadly distributed in the dendrites in a punctate pattern (Figure 5.4D). In *dab-1* mutants,

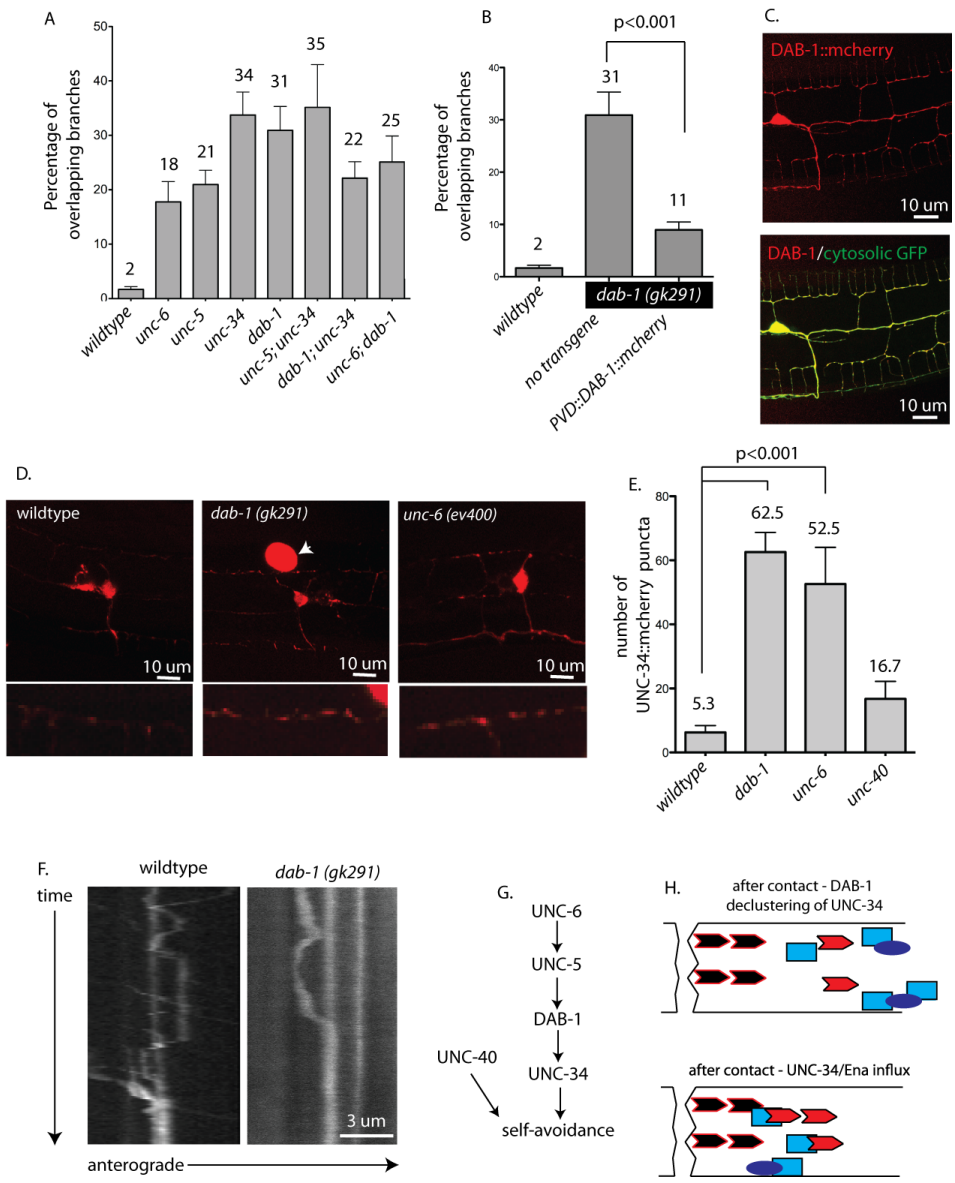

Figure 5.4 DAB-1 controls the localization of UNC-34. A. Quantification of PVD::GFP in Double mutants are not significantly different from single mutants. B. Quantification of PVD::GFP in *dab-1 (gk291)* that either have no transgene or express DAB-1::mcherry only in PVD. The no transgene *dab-1* animal is significantly different than when DAB-1 is expressed in PVD. C. Confocal image of DAB-1::mcherry and cytosolic GFP shows punctate localization of DAB-1::mcherry in the higher order PVD dendrites. D. Confocal images of UNC-34::mcherry in wild-type, *dab-1* and *unc-6* mutants. Insets show increased numbers of DAB-1::mcherry puncta in *dab-1* and *unc-6* mutants (arrow denotes coelomocyte mcherry marker). E. Quantification of UNC-34::mcherry shows higher number of puncta in *dab-1* and *unc-6* mutants compared to *wildtype*. F. Kymograph of time-lapse TIRF microscopy of UNC-34::mcherry in the 1^{O} dendrite of wild-type and *dab-1* mutants. G. Summary of the molecular pathway that is activated to promote retraction in dendritic self-avoidance. H. Model suggesting that DAB-1 (purple oval) ensures UNC-34 (blue rectangle) localization to the contacting dendrite to polymerize actin (red pointed hexagon).

however, these UNC-34::mCherry puncta were significantly brighter and more abundant (Figure 5.4D,E). These results are consistent with the hypothesis that DAB-1 controls UNC-34 sub-cellular localization in neuronal dendrites.

We considered a potential mechanism in which DAB-1 aids in the trafficking of UNC-34 to ensure that it can reach the site of dendritic contact. To test this possibility, we visualized UNC-34 trafficking at ~15 frames per second in wild-type and *dab-1* mutant animals. In wild-type animals, UNC-34 puncta are highly mobile. In particular we noted that migrating UNC-34::mCherry do not stall upon contact with stationary UNC-34::mCherry puncta (Figure 5.4F). In *dab-1* mutants however, UNC-34 puncta appear to aggregate upon contact (Figure 5.4F). Based on these observations we propose that DAB-1 ensures free trafficking of UNC-34, which allows UNC-34 to become enriched at the contact site during retraction. Because of the role of DAB-1 in UNC-34 localization we hypothesized that DAB-1 would be required for self-avoidance.

To ask if DAB-1 is required for self-avoidance we used PVD::GFP to score self-avoidance errors in *dab-1* mutants. Consistent with our hypothesis, *dab-1* mutants exhibit self-avoidance defects strikingly similar to those of the *unc-34* mutant (Figure 5.4A). Because UNC-34 is downstream of UNC-6, we considered the possibility that DAB-1 could be activated by UNC-6 to control UNC-34 localization. This model would suggest that DAB-1 functions in a common pathway with UNC-6 and UNC-34. To test this idea we first generated the *unc-34;dab-1* double mutant. The *dab-1; unc-34* double mutant showed comparable self-avoidance errors to each single mutant suggesting that DAB-1 functions in

the same pathway as UNC-34 (Figure 5.4A). To ask if DAB-1 functioned in the UNC-6 pathway, we generated an *unc-6;dab-1* double mutant. Consistent with the hypothesis that DAB-1 is in the same pathway as UNC-6, the double mutant phenocopied both single mutants (Figure 5.4A). We conclude that DAB-1 function in a common genetic pathway with UNC-34 and UNC-6. Thus, our data establishes for the first time that DAB-1/Disabled functions in UNC-6/Netrin signaling. In this case, DAB-1/UNC-6 signaling is utilized in dendritic self-avoidance (Figure 5.4G).

We proposed that DAB-1 functions with UNC-6 to control UNC-34 sub-cellular localization during self-avoidance. To test this hypothesis we visualized UNC-34 subcellular localization in UNC-6 mutants. Consistent with the idea that UNC-6 activates a pathway that controls UNC-34 localization, the number and intensity of UNC-34 puncta were greatly increased in *unc-6 (ev400)* (Figure 5.4E). The subcellular localization of UNC-34::mCherry in *unc-6 (ev400)* was strikingly similar to *dab-1 (gk291)*. Given these results, we propose that UNC-6 functions with DAB-1 to enrich UNC-34/Ena at the site of contact to drive actin polymerization (Figure 5.4H).

Our model suggests that DAB-1/Disabled functioned cell-autonomously in the PVD neuron. This model was confirmed by our finding that expression of DAB-1 cDNA in the PVD neuron in *dab-1* mutants significantly rescued self-avoidance defects (Figure 5.4B). If DAB-1 functions in self-avoidance we also expected to see DAB-1 localized in the 3^{O} dendrites. To test this idea we tagged the c-terminus of DAB-1 with mCherry and showed this functional tagged version

of DAB-1 was localized in the PVD dendrites (Figure 5.4C). These data support the hypothesis that DAB-1 functions in self-avoidance with the UNC-6/Netrin pathway to drive contact-induced retraction.

Thus far each of the components that we have determined as necessary for self-avoidance also are required for axon guidance. Since the role of DAB-1 in *C. elegans* axon guidance has not been previously examined we tested its requirement in commissural axon guidance by visualizing commissures in *dab-1* mutants. Interestingly, commissures were normal in *dab-1* mutants (data not shown). This result suggests that DAB-1 may not be utilized in axon guidance of motor neuron commissures and thus may activate a task-specific pathway to trigger contact-dependent repulsion.

A specific isoform of MIG-10 is required for self-avoidance

Having established that UNC-34 controlled contact-dependent self-avoidance, we sought to characterize its interaction with other downstream components from our screen. We started with *mig-10*, which has previously been shown to interact with *unc-34*. We could not generate an *unc-34; mig-10* double mutant because this combination is embryonic lethal. Thus, we looked at *mig-10* interactions with other components of the UNC-34 self-avoidance pathway. To do this we generated the *mig-10;dab-1* double mutant and scored self-avoidance defects. MIG-10 mutants displayed 20% overlapping branches whereas the *dab-1* and *unc-34* mutants displayed 30% overlap (Figure 5.5A). Interestingly, the *mig-10; dab-1* double mutants displayed significantly more

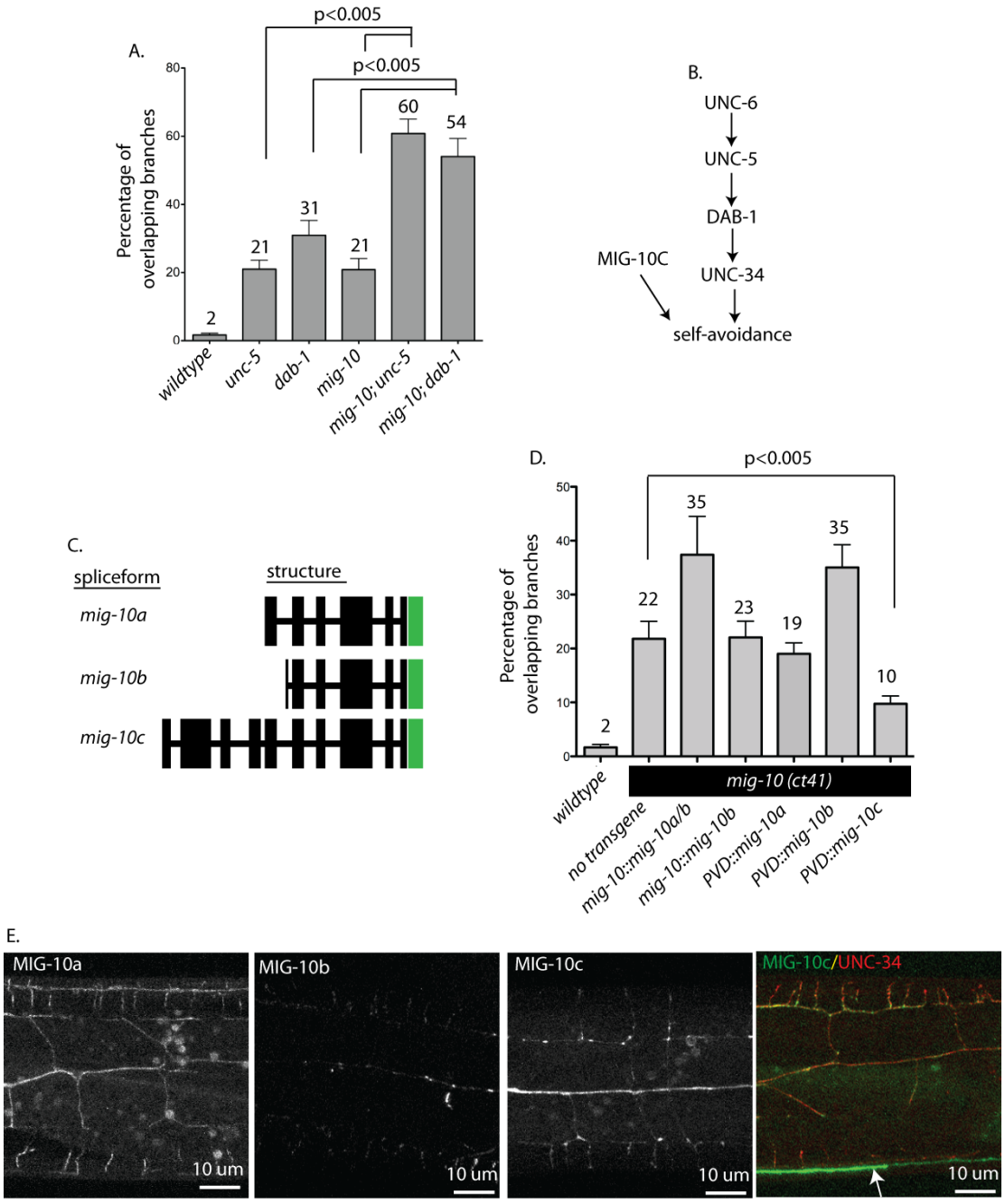

Figure 5.5 MIG-10C is required for self-avoidance. A. Graph showing quantification of genetic mutants. Note that double mutants (*mig-10; unc-5 and mig-10; dab-1*) were significantly different than single mutants. B. Molecular pathway of downstream components based on double mutant analysis. C. Summary of *mig-10* spliceforms. Large boxes represent exons. Green bar shows the location of GFP tag for MIG-10 localization studies. D. Defects of self-avoidance quantification of *mig-10* mutants with rescuing constructs. Expression of *mig-10a/*b or *mig-10b* fosmids did not rescue self-avoidance. Expression of MIG-10b *or* MIG-10a under the PVD promoter also did not rescue self-avoidance. PVD expression of MIG-10c did rescue PVD self-avoidance defects. P value determined by students t-test. E. Confocal images of *mig-10* spliceforms tagged with GFP. Far right shows a confocal image of MIG-10C::GFP (green) and UNC-34::mcherry (red) in the same PVD dendrite.

overlap (60%) than either single mutant (Figure 5.5A). These data suggest that *mig-10* functions in parallel to the *dab-1* pathway in self-avoidance. To confirm that *mig-10* functions in parallel to the UNC-34 pathway we tested the genetic interaction of *mig-10* and *unc-5*. Consistent with our hypothesis, *mig-10;unc-5* animals also showed enhanced self-avoidance defects than either single mutant (Figure 5.5A). Thus, we conclude that *mig-10* functions in an independent pathway than the UNC-5/DAB-1/UNC-34 pathway to promote self-avoidance and sought to further characterize its role (Figure 5.5B).

The *mig-10* genomic region encodes three *mig-10* spliceforms (Figure 5.5C). We hypothesized that the different spliceforms may acquire different functions in PVD development. To test this model we restored specific isoforms of *mig-10* in *mig-10* mutants and tested the ability of these transgenes to rescue self-avoidance errors. We first used fosmids that contain the genomic region of either *mig-10a/b* or just *mig-10b*. When we restored *mig-10b* or *mig-10 a/b* expression in *mig-10 (ct41)* we could not rescue self-avoidance errors (Figure 5.5D). These data suggest that *mig-10a or mig-10b* are not sufficient to induce self-avoidance. To confirm that *mig-10a* or *mig-10b* are not required for self-avoidance we restored *mig-10a* or *mig-10b* cDNA in PVD in *mig-10* mutants. Consistent with our fosmid rescue, restoration of *mig-10a* or *mig-10b* cDNA also did not rescue Mig-10 self-avoidance defects. We therefore hypothesized that *mig-10C* may be uniquely required in self-avoidance. To ask if *mig-10c* was sufficient to restore self-avoidance we expressed *mig-10c* specifically in the PVD neuron in *mig-10 (ct41)*. Expression of *mig-10c* in PVD in *mig-10 (ct41)* did

rescue self-avoidance defects (Figure 5.5D). These results are therefore consistent with the hypothesis that a specific spliceform of *mig-10*, the C isoform, is utilized during self-avoidance.

If *mig-10c* is required for self-avoidance we predicted that it would be localized in the 3^O dendrites. To test this possibility we visualized a functional GFP-tagged MIG-10C (MIG-10C::GFP) in PVD. Interestingly, MIG-10C localization was punctate in the 3^O dendrite (Figure 5.5E). We therefore conclude that MIG-10C could function in self-avoidance of the 3^O dendrites. Our rescue data suggests that other MIG-10 spliceforms may have different functions in the PVD dendrite. To address this possibility we visualized the localization of MIG-10B and MIG-10A in the 3^O dendrite. MIG-10B localization differed from that of MIG-10C in that it was punctate in all dendritic branches (1^O-4^O) and was most highly abundant in younger animals (Figure 5.5E). MIG-10A localization was also different as it was mostly diffuse throughout the dendrites (Figure 5.5E). Thus, we conclude each *mig-10* spliceform has a different localization pattern in the PVD 3^O dendrite. These data are consistent with the hypothesis that MIG-10 spliceforms may be differentially required during PVD development.

Because the localization of MIG-10C was strikingly similar to the localization of UNC-34 we considered the possibility that MIG-10C functioned in similar areas as UNC-34 and thus may co-localize with UNC-34. To test this we generated a transgenic line that expressed both UNC-34::mcherry and MIG-10C::GFP. Interestingly, MIG-10C and UNC-34 were co-localized in the dendrites (Figure 5.5E). We also generated a transgenic line to score the co-

localization of MIG-10A and UNC-34 but did not visualize obvious co-localization (data not shown). These data support the hypothesis for the differential roles of MIG-10 spliceforms in neurodevelopment and suggests there may be different interacting components. Together our genetic data is consistent with the model that MIG-10C and UNC-34 function in different molecular pathways. The subcellular co-localization of these proteins, however, suggests UNC-34 and MIG-10C may function at the same site to drive self-avoidance.

Additional downstream components

Our limited screen identified a role for CED-10 in contact-induced self-avoidance. The PVD microarray profile detected enrichment of the CED-10 transcript (Chapter 2). We therefore hypothesized that CED-10 functioned in the PVD cell to promote self-avoidance. To test this we expressed a functional CED-10::GFP in PVD in *ced-10* mutants and scored the ability of this transgene to rescue Ced-10 self-avoidance defects. Consistent with our hypothesis that CED-10 functions cell-autonomously in PVD, expression of CED-10 in PVD in *ced-10* mutants rescued self-avoidance defects (Figure 5.6A). Additionally, if CED-10 functioned in self-avoidance, we expected to see CED-10::GFP in the dendrite where self-avoidance occurs. Consistent with this idea, CED-10::GFP was localized in the 3^{O} dendrites (Figure 5.6B). Based on these data we conclude that CED-10 functions in the PVD neuron to drive contact-induced dendritic retraction.

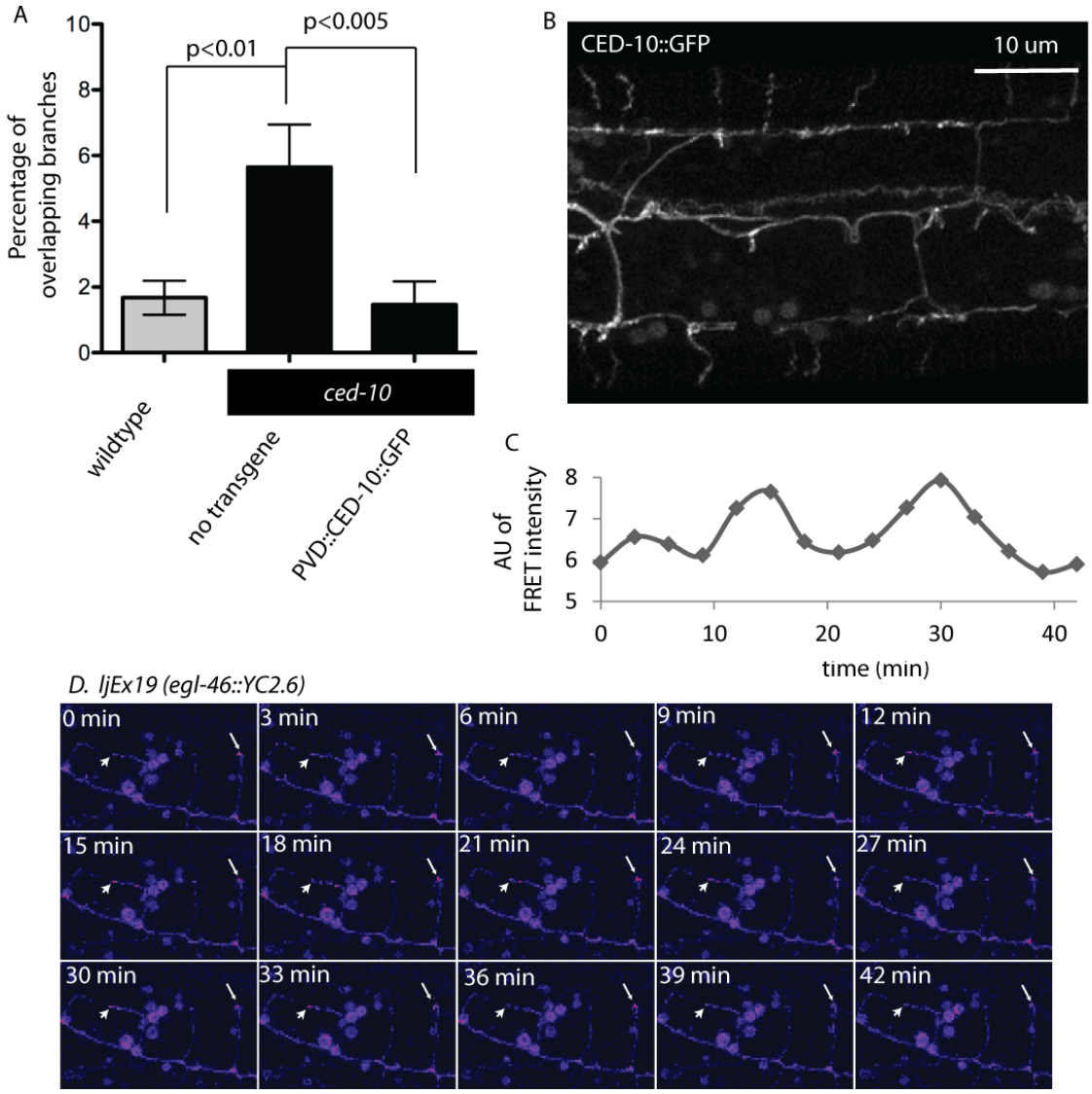

Figure 5.6 CED-10 and calcium in PVD. (A) Quantification of overlapping dendrites which are visualized with PVD::GFP in wildtype, *ced-10* and *ced-10* with PVD::CED-10::GFP. Note significant rescue from *ced-10* no transgene vs. *ced-10* with PVD::CED-10::GFP. N > 15. (B) Confocal micrograph of CED-10::GFP in the PVD neuron. CED-10::GFP puncta are localized in all dendritic branches. (C) Graph of the mean intensity of the ratio of CFP/YFP (FRET insensity) from calcium indicator YC2.6 at the tip of the 3^{O} dendrites demarcated by the arrowhead in (D). Note the change in calcium levels that occurs in a growing 3^{O} dendrite. (D) Confocal micrograph of the FRET signal in a growing dendrite. Arrowhead marks growing 3^{O} dendrite that shows changes in a FRET signal. Arrow demarcates a turning 2^{O} branch that also undergoes changes in calcium.

In axon guidance, changes in cytoplasmic calcium are visible in migrating growth cones. This change in calcium has been proposed to interact with UNC-6/Netrin signaling to drive either attraction or repulsion. We therefore hypothesized that calcium signaling may function in contact-induced self-avoidance. To ask if cytoplasmic calcium levels changed during PVD outgrowth we visualized a calcium indicator in PVD branches as the dendrites grew. Interestingly, the YFP signal of the chameleon calcium indicator increased during states of dendritic growth and repulsion at the tips of the dendrites (n=1) (Figure 5.6C). These results are consistent with the idea that levels of cytoplasmic calcium may change in the dendrite during growth or retraction. It should be noted that only one time-lapse movie of the chameleon reporter was visualized and more movies would need to be acquired to confirm these results. Moreover, the chameleon reporter strain displays PVD dendritic arrays with reduced branching and thus these results must be analyzed cautiously. If calcium signaling were required for self-avoidance then proteins that detect cytoplasmic calcium levels or that function in calcium signaling should be required to prevent overlap. Unfortunately, a limited screen of mutants that correspond with these proteins did not identify animals that display self-avoidance defects. Thus, the hypothesis that calcium imaging is required for self-avoidance remains to be substantiated.

A screen for myosin proteins

Our data are consistent with the model that MIG-10 and UNC-34 contribute to self-avoidance by promoting actin polymerization at the site of contact. We considered the hypothesis that actin polymerization could aid in retraction through retrograde flow, which can be mediated by myosins, specifically class II myosins [252-255]. Based on this knowledge, we screened the *C. elegans* non-muscle myosins by scoring PVD::GFP in different genetic mutants for defects in self-avoidance (Table 5.2). *C. elegans* have two Class II myosins, *nmy-1* and *nmy-2*, which function redundantly in *C. elegans* embryogenesis [244]. *nmy-2* mutants did not display self-avoidance errors (Figure 5.7A). We hypothesized that the other non-muscle myosin II may be the predominant motor for self-avoidance. To test this idea we visualized overlapping dendrites with PVD::GFP in *nmy-1* mutant animals [244]. Interestingly, *nmy-1* mutants displayed self-avoidance defects that were comparable to *dab-1* and *unc-34* mutants (Figure 5.7A). We therefore propose that *nmy-1* is required for contact-induced retraction.

We predicted that myosin might function with the actin-polymerizing component UNC-34 to drive contact-induced retraction. To test this we visualized the genetic interaction between *nmy-1* and *unc-34*. Double mutants of *nmy-1 (sb113); unc-34 (gm104)* did not show significantly more overlap than either single mutant *nmy-1 (sb113)* or *unc-34 (gm104)* (Figure 5.7). Based on this data we propose that *nmy-1* functions with *unc-34* to induce retraction.

Table 5.2 Non-muscle myosins in *C. elegans*. List of non-muscle myosins in *C. elegans* and their respective class. Table generated from wormbase descriptions.

Class Myosin	*C. elegans* myosin
I	*hum-1* *hum-5*
II	*nmy-1* *nmy-2*
VI	*hum-8* *spe-15*
VII	*hum-6*
IX	*hum-7*
XII	*hum-2* *hum-4*

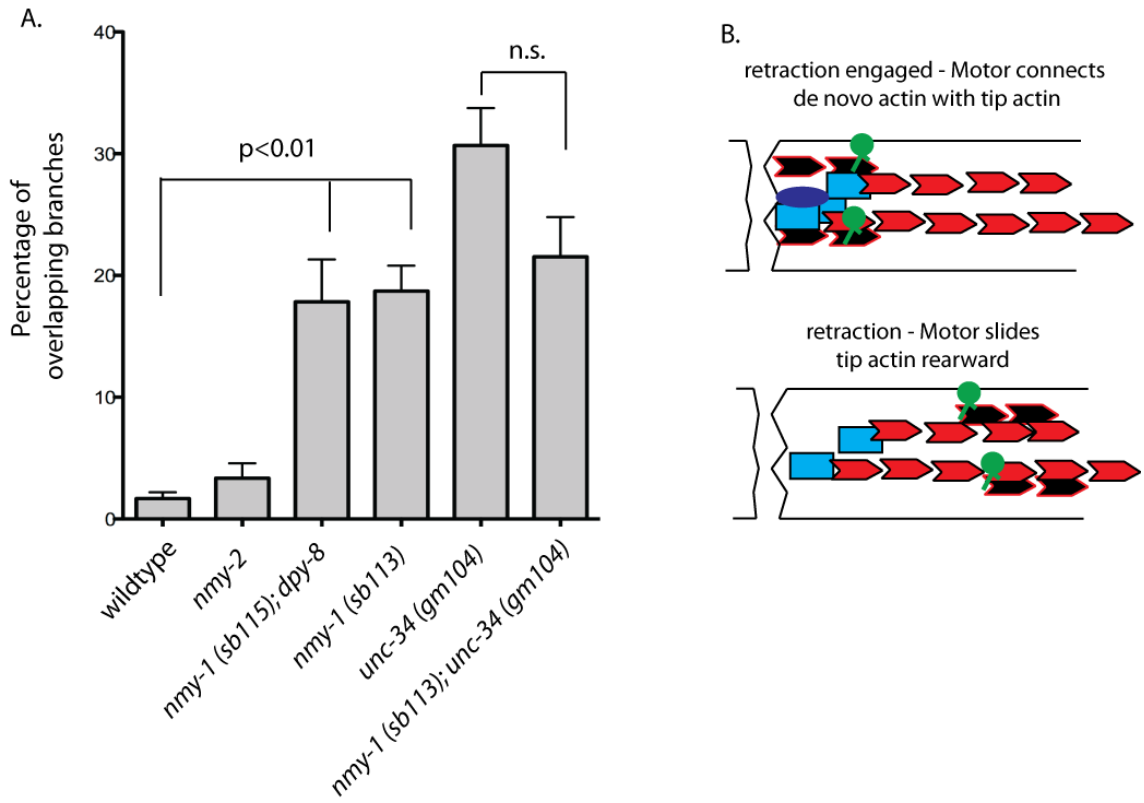

Figure 5.7 Myosin is required for self-avoidance. A. Quantification of overlapping branches in different mutants. *nmy-1 (sb115);dpy-8 and nmy-1 (sb113)* animals show significantly more overlap than wt . *nmy-2* mutants do not show overlap. Double mutants *nmy-1 (sb113); unc-34 (gm104) are* not significantly different than *unc-34 (gm104)* or *nmy-1 (sb113*). B. Model for myosin in retraction of dendrites. Myosin (green) is utilized to provide work to move actin (black) or membrane components away from the tip.

It is worth noting that NMY-1 and NMY-2 function is redundant in the embryo and thus our analysis may underestimate the general contribution of myosins to self-avoidance. Unfortunately, we could not test this hypothesis because the *nmy-1; nmy-2* double mutant died embryonically [244]. Nonetheless, these data are consistent with the hypothesis that *nmy-1* is required for self-avoidance of the PVD neuron (Figure 5.8B).

Myosins are activated by myosin light chain kinases, which are activated by Rho kinases. *C. elegans* has one known Rho Kinase, *let-502* [244]. We hypothesized that *let-502* could activate *nmy-1* to induce self-avoidance. Interestingly, *let-502* mutants did not show self-avoidance defects.

DISCUSSION

Actin Polymerization promotes self-avoidance via UNC-34/Ena

This study shows that actin-polymerizing components UNC-34 and MIG-10 are required to drive contact-dependent dendritic retraction. During retraction, actin becomes enriched and localized with UNC-34/Ena. UNC-34/Ena is trafficked to the site of contact to induce retraction. This UNC-34/Ena trafficking is dependent on DAB-1/Disabled and UNC-6/Netrin. These data are consistent with a model in which actin polymerization is required for contact-induced retraction (Figure 5.8). We propose that UNC-6 activates the UNC-5 receptor upon contact. UNC-5 functions with DAB-1, which ensures UNC-34 can localize to the site of contact. Once localized, UNC-34 can then promote actin

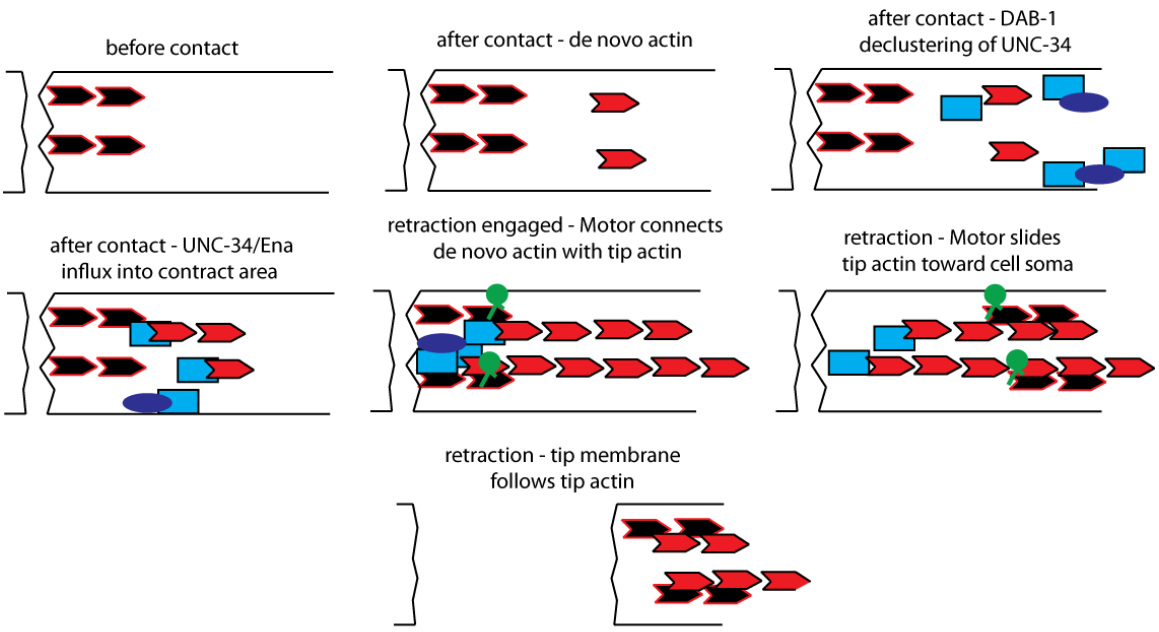

Figure 5.8 Model of contact-induced retraction during self-avoidance. Before contact, tip actin (black pointed hexagon) is localized at the tip of the dendrite. After contact, *de novo* actin (red pointed hexagon) forms just distal to the tip. DAB-1 (purple oval) declusters UNC-34 (blue square) and allows for influx of UNC-34 into the contact site to polymerize actin. This rearward movement of the tip actin may require a motor (e.g. myosin) (green probe) to provide work. Tip actin movement toward the cell soma drives the membrane rearward and results in dendrite retraction.

polymerization just distal to the tip of the dendrite (Figure 5.8). This actin polymerization then induces dendrite retraction. It seems likely that the new actin filaments that are assembled by UNC-34 can be utilized by motors, potentially non-muscle myosin II, NMY-1, to drive retrograde flow to pull the actin cytoskeleton at the very tip of the dendrite backward resulting in rearward movement of the branch (Figure 5.8). We also propose that MIG-10 functions in a similar location as UNC-34 but in a parallel pathway to induce dendritic retraction of self-avoiding branches.

UNC-34/Ena functions in attraction and repulsion

UNC-34/Ena has canonically been shown to be an actin-polymerizing component [71]. This hypothesis is supported by *in vitro* evidence that shows Enabled aids in actin polymerization [256-258]. *In vivo* data both in migrating cells and axon growth cones also established a clear role of actin polymerization via Enabled [232-234, 236]. For example, it is thought that actin polymerization by Enabled drove growth cones toward attractive guidance molecules such as Netrin [233, 234].

UNC-34/Ena has also been shown to function in repulsive axon guidance [259]. In *C. elegans*, UNC-34/Ena is required for commissural axon outgrowth away from the Netrin source [260]. In *Drosophila*, Ena also functions in repulsive guidance to steer motor axons to their proper target [232, 236]. In each of these examples, it was not clear how Enabled via its canonical actin polymerization role could be required for a repulsive event because repulsion is proposed to be

mediated through an actin depolymerization mechanism that prevents active extension of filopodia [227]. Retrograde flow may also function in repulsion [83]. In this study we provide another example for the role of UNC-34/Ena in neuronal branch repulsion. However, we propose that UNC-34/Ena functions as it has canonically been described to polymerize actin. This hypothesis is supported by our data that shows that at the site of contact, actin becomes enriched in PVD with UNC-34. It seems plausible that Ena may function in a similar manner in axonal repulsion.

The dual role of Ena in both attraction and repulsion is also seen in other actin polymerizing components. For example, MIG-10/Lamellipodin also functions in repulsive and attractive axon guidance[75, 76, 78]. It seems plausible that the function of these proteins is the same in both attraction and repulsive but the site of activation may be different. In attraction, actin polymerization at the tip of the growth cone could drive filopodia like growth. In repulsion, actin polymerization may be shifted to a more distal location. In this case, polymerization would not push against the membrane but would rather establish a road that can be utilized for repulsion or drive retrograde flow. It is conceivable that a protein that controls localization of actin polymerizing components could mediate this directional switch. We show that DAB-1 with UNC-6 functions to ensure UNC-34 localization. Repulsion and attraction can also be delineated by the receptors that are activated by axon guidance ligands [2]. For example, UNC-5 is utilized to promote repulsion but does not function in attraction [51, 173]. Perhaps UNC-5 activates proteins that shift the location of

actin polymerization. In the case of self-avoidance, this UNC-5 activated protein may be DAB-1.

It is not clear if contact-dependent dendritic retraction via retrograde flow is a passive or active process. In an active process, actin polymerization may be coupled to the membrane and the active pulling of the actin filament may in turn tug the dendritic membrane into a retractive state. In such a model, a protein would be required to couple the actin filament to the membrane. However, it seems plausible that the removal of the actin filament may simply result in the collapse of the membrane. In this passive model, the actin filaments function more as supports for the dendritic membrane and when the supports are removed so does the surrounding membrane structure.

MIG-10 in dendritic retraction

Our data establishes a role for MIG-10/Lpd in dendritic retraction. MIG-10 has been shown to interact with F-actin and can localize F-actin binding proteins at the membrane where actin assembly occurs in migrating cells [75, 76, 78, 242]. It seems plausible that MIG-10 may share similar function in PVD to localize F-actin binding proteins to promote actin assembly at the site of contact. However, MIG-10 likely recruits components other than UNC-34/Ena to mark the site of actin assembly since UNC-34 and MIG-10 appear to be in different genetic pathways. Interestingly, the MIG-10C isoform is specifically required for self-avoidance suggesting it may interact with a particular set of proteins to promote

contact-induced retraction. Identifying these MIG-10 spliceform-specific interacting components could reveal key proteins required for self-avoidance.

Actin Polymerization in Dendrite Outgrowth

Interestingly, we tested mutants of multiple proteins that function in actin polymerization but never observed animals in which PVD dendritic outgrowth as disabled. Moreover, actin markers such as utrophin did not show enriched localization in dendrites that were stabilized and were only localized at the tip of dendrites during growth (Figure 5.1). Thus, it is not clear how PVD dendrites grow. Microtubules could aid in the growth of dendrites but previous evidence showed that tubulin is limited to the 1^{O} dendrite of PVD [246]. It will be interesting in the future to determine the requirements of dendrite growth and reveal the cytoskeletal composition of these growing dendrites.

Controlling the cytoskeleton in self-avoidance

Self-avoidance is a universally observed phenomenon across phylogeny [4]. Cell surface proteins that function to prevent contact-dependent overlap mediate self-avoidance. For example, Dscam and Turtle both have been described as self-avoidance receptors and both require the intracellular domain to prevent overlap [105, 239]. These findings suggest that these cell-surface proteins activate an intracellular signaling cascade but to date this pathway has not been identified. In *Drosophila*, Flamingo also functions in self-avoidance [106]. Cytosolic proteins such as Tricorned and Furry have been shown to

interact with Flamingo but the link to the cytoskeleton remains to be unclear [110, 111]. In PVD, we show that the self-avoidance receptor UNC-5 interacts with cytosolic components that control the cytoskeleton. These components are required to trigger retraction during self-avoidance. Because retraction is a universal characteristic of contact-dependent self-avoidance the downstream components of other self-avoidance receptors could be similar to what we have identified in PVD. Thus, it will be interesting in the future to determine if any of the components that we described in this report also function downstream of other self-avoidance receptors. This work provides foundation for understanding how a neuron controls the cytoskeleton in the dendrite to ensure non-redundant coverage of a receptive area. We believe insight gained from this study could also be applied to other cases of neurite retraction that are observed during the developing nervous system.

Author Contributions

Andrea Stavoe, Jessica Nelson and Daniel Colón -Ramos provided reagents and Matthew Tyska helped with TIRF microscopy. Cody J. Smith completed all the experiments in this chapter.

Acknowledgements

Thank you to C. Bargmann (Rockefeller) who provided *mig-10b* and *unc-34* plasmids for this study and members of the D. Colón -Ramos (Yale), Matt Tyska (Vanderbilt) and D. Miller III (Vanderbilt) labs for advice on the manuscript.

Some of the strains used in this work were provided by the *C. elegans* Genetics Center which is supported by NIH NCRR. This work was supported by NIH R01 NS26115 (DMM), NIH R21 NS06882 (DMM), NIH F31 NS071801 (CJS), NIH R00 NS057931 (DCR), and Klingenstein Foundation and the Alfred P. Sloan Foundation fellowship (DCR)

CHAPTER VI

AN UNC-6/NETRIN GRADIENT DRIVES DENDRITIC ASYMMETRY IN A SOMATOSENSORY NEURON

INTRODUCTION

Neurons throughout the nervous system exhibit dendritic arrays with varying complexity [98]. The morphology of these dendritic trees defines the receptive field and demarcates potential connectivity for the neuron, which is required for proper signaling of neuronal circuits [261]. One aspect of dendritic morphogenesis that is widely seen in areas of the mammalian brain is dendritic asymmetry. [262, 263]. In fact, it has been proposed that most neurons in the visual system display some form of dendritic asymmetry [264]. For example, retinal ganglion cells have asymmetric dendritic arrays that arise from early dynamic branching events [265]. The molecular underpinning or functional significance of this asymmetry, however, is not known.

Cajal first predicted that development of neuronal branches could be regulated by a neurotropic mechanism and it is well known that asymmetry can be shaped from similar factors [98]. The neurotropic factor Netrin has diverse roles in branch morphogenesis and can have different temporal requirements. For example, in *C. elegans,* Netrin can define the initiation site of axon outgrowth by establishing an early asymmetry on the HSN neuron. Once the axon initiates,

this ventral UNC-6/Netrin source also helps to guide the axon growth cone to the ventral side via its receptor UNC-40/DCC [43, 45, 47]. Netrin can also regulate dendritic outgrowth. Netrin guides dendritic branches toward its source in a role that is reminiscent of its function in axonal outgrowth[57, 67, 266]. These studies highlight the versatility of the Netrin signaling cascade and emphasize that even within the same cell, Netrin can function at two distinct time points to properly pattern the nervous system.

It is assumed that for the same neurotropic factor to regulate different aspects of neuronal morphogenesis it must activate “task-specific” downstream effectors [57]. This hypothesis is underscored by the recent discovery that Netrin signaling utilizes distinct downstream signaling pathways to properly pattern *C. elegans* motor neurons [57]. The DA9 motor neuron first utilizes Netrin during embryonic development via the UNC-5 receptor to control axon outgrowth. Later in development, Netrin, controls the presynaptic machinery via the UNC-5 receptor but also controls dendritic outgrowth via the UNC-40 receptor. Thus Netrin has distinct roles even in the same neuronal compartment and these diverse tasks can be controlled by different receptors and downstream effectors. A better understanding of the downstream effectors of neurotropic factors and their role in neuronal morphogenesis would strengthen this hypothesis.

In this report we describe a model to study the conserved phenomenon of dendritic asymmetry. In *C. elegans*, the PVD somatosensory neuron exhibits dendritic asymmetry. During development, branches are initiated more on the dorsal side than the ventral side, resulting in a mature neuron that is asymmetric.

Disruption of the UNC-6/Netrin signaling pathway caused defects in asymmetric dendritic distribution. This dendritic asymmetry requires a gradient of UNC-6/Netrin that radiates from the ventral side and is dependent on the UNC-40/DCC receptor, downstream components UNC-34/Ena and UNC-73/Trio and a specific isoform of MIG-10/Lpd. We show that the role of Netrin in dendritic asymmetry is mechanistically different from its role in self-avoidance. The conservation of dendritic asymmetry in the mammalian nervous system and of the UNC-6/Netrin signaling pathway suggests this pathway may also function similarly in higher organisms. Thus, this report can provide foundation for future studies in dendritic asymmetry and for understanding how Netrin can temporally control different aspects of dendritic development by utilizing distinct downstream components.

METHODS

Nematode strains and genetics

The wild-type *C. elegans* Bristol strain N2 was used for all experiments and cultured as previously described [158]. All analysis was completed on hermaphrodites.

Mutants used in this study

unc-6 (ev400); unc-40 (e271); unc-5 (e152); unc-5 (e53); unc-34 (gm104), unc-34 (e315), mig-10 (ct41), unc-73 (e936), madd-2 (ok2226), ced-10 (n1993), unc-115 (ky275), max-2 (ok1904), mig-2 (ok2273), rac-2 (ok236), dab-1 (gk291),

ced-5 (n1812), pfn-1 (ok808), daf-18 (ok480), nid-1 (cg119), epac-1 (ok655), src-1 (ok2685), pak-1 (ok448), abl-1 (ok171), unc-60 (e723), *nmy-2 (ne3409), wsp-1 (gm324).* Some strains were provided by the *Caenorhabditis Genetics* Center, which is funded by the NIH National Center for Research Resources (NCRR).

Additional Published Transgenics

NC1686 [*wdIs51* (*F49H12.4*::GFP + *unc-119*)]; NC1687 [*wdIs52* (*F49H12.4*::GFP + *unc-119*)]; CX6488 [*kyIs299*, *hsp16.2::unc-6*::HA + *ord-1*::RFP], NC2099 [*pha-1 (e2123ts); wdEx682* (MVC119 (*rig-3*::*unc-6*) + *pBx (pha-1) + dat-1*::mcherry)]; NC2099 [*pha-1 (e2123ts); wdEx682* (MVC119 (*rig-3::unc-6*) + pBx (*pha-1*) + *dat-1*::mcherry); NC2182 [*pha-1 (e2123ts); wdEx692* (pCJS28, *F49H12.4::unc-6*::HA + *pBx, pha-1* + *dat-1*::mcherry)]; NC1893 [*pha-1 (e2132ts); wdEx640 (F49H12.4*::*unc-40*::mcherry + *pBx (pha-1) + odr-1*::mcherry)]; NC2098 [*pha-1 (e2123ts); wdEx681* (pCJS68 (*unc-25*::unc-40::mRFP) + *pBx (pha-1) + dat-1*::mcherry)]; TV1788 [*unc-40 (e271); wyIs45; wyEx650* (*unc-40* minigene w/ mcherry injected at 20 ng/ul has co-selector marker GFP in coelomocytes)]; NC2301 [*pha-1 (e2123ts); wdEx746* (pCJS93, *F49H12.4::unc-40*::GFP + *pBx, pha-1* + pCJS85*, dat-1*::mcherry)]; N2315 [*pha-1 (e2123ts); wdEx748* (pCJS98, *F49H12.4*::*unc-40*deltaECTO::mcherry + *dat-1*::mcherry + *pBx, pha-1*)]

Transgenic Strains generated by microinjection

NC1822 (*unc-119; wdEx633 (F49H12.4::mig-10B::YFP* + *unc119*), NC2261 (*pha-1 (e2123); wdEx726 (*pCJS96*, F49H12.4::mig-10a::GFP* + pCJS85*, dat-1::mcherry* + pCJS04*, F49H12.4::mcherry* + *pBX*), NC2462 (wdEx773 (pCJS94, *F49H12.4::mig-10c::GFP* + pCJS04*, F49H12.4::mcherry* + pCJS85*, coel::RFP*)), NC2420 (wdEx773 (pCJS78, *F49H12.4*::mcherry::UNC-34 + pCJS85, *dat-1*::mcherry + coel::RFP)). All strains were generated by microinjection. pCJS96, pCJS85, pCJS94, pBX, pCJS04 and coel::RFP were all injected at 30 ng/ul. Two stable transgenic lines were visualized for each injection.

Molecular Biology

MIG-10 and UNC-34 expression plasmids were constructed using conventional cloning. The *F49H12.4* promoter was digested using AscI and SphI from pCJS04 and combined with MIG-10 and UNC-34 expression plasmids.

Confocal Microscopy

Nematodes were immobilized as previously described [12]. Images were collected on a Leica TCS SP5 confocal microscope. Z-stacks were collected with a 40X (1 um/step) or 100X (0.75 um/step) objectives. Single plane projections were generated using Leica Application Suite Advanced Fluorescence Software. Brightness and contrast was enhanced with Adobe Photoshop CS5.

Time-Lapse Imaging

Nematodes were imaged as previously described [12]. Confocal z-stacks spanning the depth of the PVD neuron were taken every 2.5 min.

Quantification of Time-lapse imaging

Confocal z-stacks were collapsed into a single projection. All dendritic branches were marked in each timeframe. An initiation event was scored as any branch that was not present in a time-frame (e.g. t=0) and appeared from the 1^{O} dendrite in the next timeframe (e.g. t=2.5min). A retraction event was scored as any branch that was present at one time frame (e.g. t=0) and lost in the text time frame (e.g. t=2.5). All time frames were averaged over a 2-hour movie. Each genotype was imaged three times. A students t-test was used to determine statistical significance.

Scoring Dendritic Asymmetry

Each genotype was visualized with *wdIs52* or *wdis51* (PVD::GFP). At least 15 animals were visualized for each genotype. Confocal images were collected in a z-stack to span the depth of the PVD neuron. 2^{O} dendrites were characterized as a branch that connected the 1^{O} dendrite to the 3^{O} dendrite. A normal dendritic distribution was defined as a neuron that contained more dorsal branches than ventral branches. Defective distribution was defined as a neuron that contained equal number of branches on the dorsal and ventral side or a

neuron that contained more ventral than dorsal branches. Circular representation of dendritic asymmetry was drawn manually. The difference in ventral vs dorsal branches was calculated and drawn in the appropriate direction of asymmetry. Barnard's exact probability test was used to determine statistical significance.

Temporal Requirement of UNC-6/Netrin

kyIs299 animals were treated with hypochlorite to release embryos for overnight synchronization. Animals were grown to the appropriate age and heat-shocked as previously described. Morphological markers L2 (posteirid), L3, L4 and young adult (vulval development) were used for aging the animals. Non-heat shocked animals were used as a control. Branches were counted on young adult animals that were heat-shocked at appropriate ages.

RESULTS

PVD exhibits an asymmetric dendritic structure

The *C. elegans* PVD neuron exhibits a non-overlapping dendritic pattern that envelops the animal between the muscle and the hypodermis [12, 125, 140, 216]. The architecture of PVD dendrites is achieved by a series of orthogonal branching decisions [12]. We previously described the detailed description of the PVD dendritic array using time-lapse imaging [12]. Further characterization revealed a dorsal/ventral asymmetry in the mature dendritic array. The mature

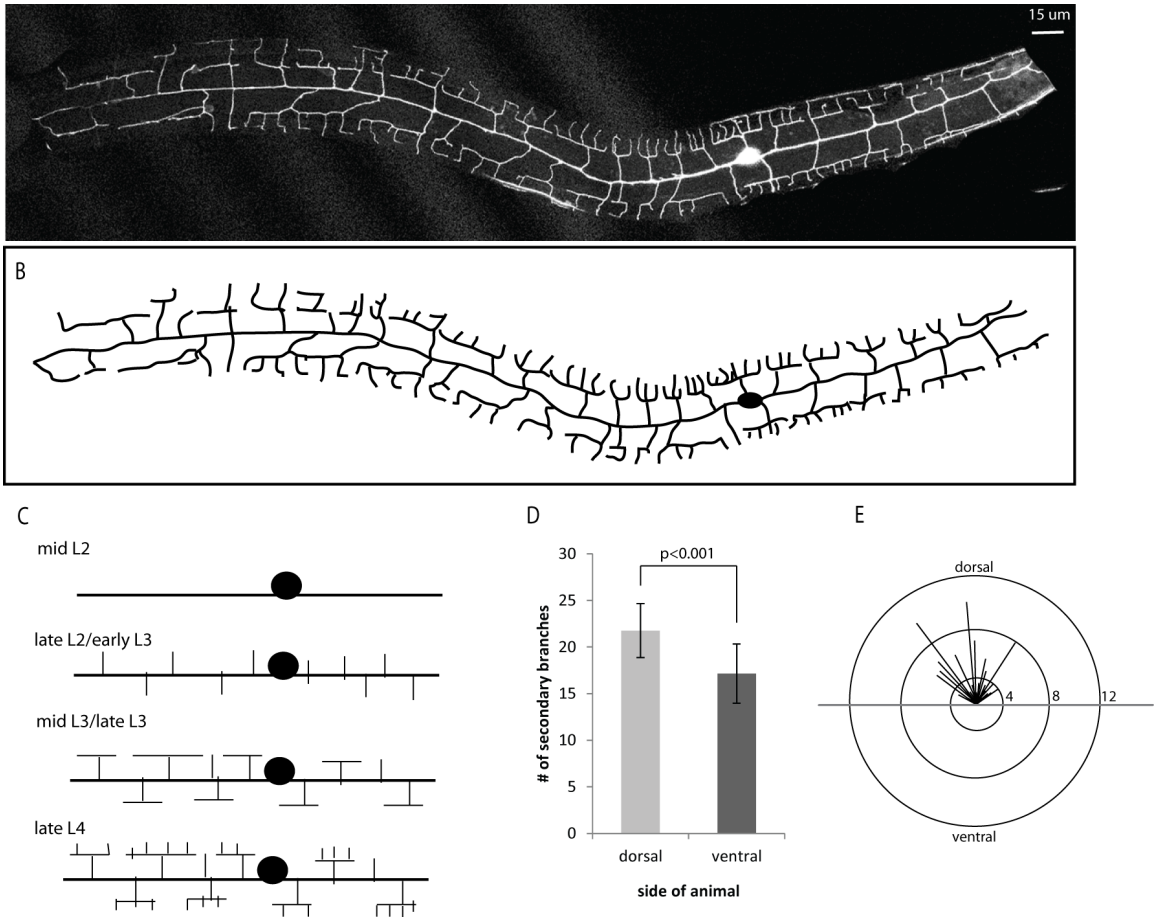

Figure 6.1. PVD neurons display dendritic asymmetry. (A) Image of PVD neuron and traced (B) schematic displaying the non-overlapping dendritic array that envelop the animal. (C) Schematic of PVD development. Note that 2^{O} dendrites grow out during the late L2/Early L3 larval stage. 2^{O} dendrite growth is complete by the early L4 larval stage. (D) In a population of animals the number of 2^{O} dendrites on the dorsal is significantly different ($p>0.001$) than those on the ventral side. (E) Plot showing that in single animals the number of dorsal branches is always greater than the number of ventral branches. Each line segment corresponds to a single animal and denotes increased number of dorsal vs ventral 2^{O} branching in PVDR. Each concentric ring (4, 8, 12) denotes difference (dorsal vs ventral) in number of PVDR 2^{O} dendrites. N>20 PVDR for each genotype.

PVD neuron always exhibits more dorsal branches (21.8 branches) than ventral branches (17.1 branches). Though the total number of branches can vary from neuron to neuron, the number of dorsal branches in a given neuron is always more than the number of ventral branches (Figure 6.1A,B,D,E, wt 100% dorsal asymmetric distribution). The consistent asymmetry of PVD 2^{O} dendrites and the conservation of dendritic asymmetry across phylogeny led us to seek potential molecules required to set up this phenomenon.

UNC-6/Netrin signaling is required for dendritic asymmetry

To determine molecules required for the dendritic asymmetry, we utilized a PVD cell-specific microarray profile [12]. Interestingly, molecules with known asymmetry roles [174] were enriched in PVD, including transcripts required for UNC-6/Netrin signaling (i.e. UNC-40/DCC, UNC-5 and UNC-34/Ena). To test the requirement of these proteins in the distribution of PVD 2^{O} dendrites we looked at PVD::GFP in different genetic mutants. Because motor neuron commissures aid in 2^{O} dendrite outgrowth (Smith and O'Brien et. al. unpublished data, Chapter 2) we visualized the PVDL neuron that has limited interaction with neuronal commissures compared to PVDR [12]. Genetic ablation of the UNC-6/Netrin receptor UNC-40 and the ligand UNC-6, revealed a requirement for UNC-6/Netrin signaling in establishing the dorsal/ventral dendritic asymmetry in PVD. *unc-40 (e271)* and *unc-6 (ev400)* mutants exhibited PVD neurons with more ventral branches than dorsal branches (Figure 6.2A,B,D). In *unc-40 (e271)* and *unc-6 (ev600)* animals, ~50% of PVD neurons showed dendritic asymmetry

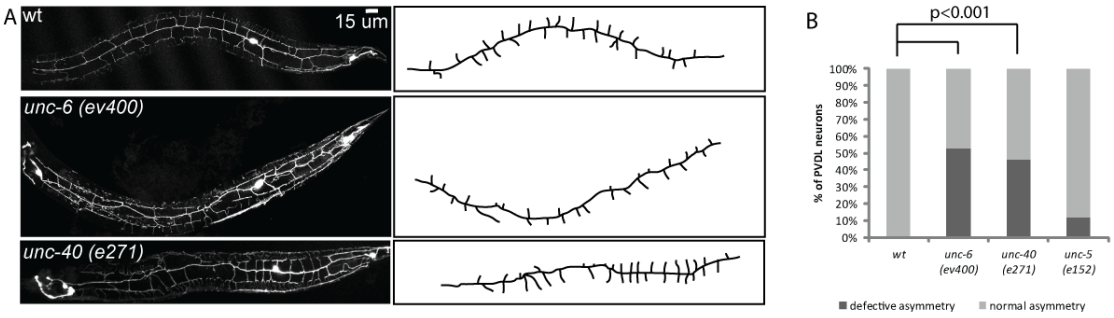
A
wt
15 um
unc-6 (ev400)
unc-40 (e271)
B
p<0.001
% of PVDL neurons
100%
90%
80%
70%
60%
50%
40%
30%
20%
10%
0%
wt
unc-6 (ev400)
unc-40 (e271)
unc-5 (e152)
defective asymmetry
normal asymmetry

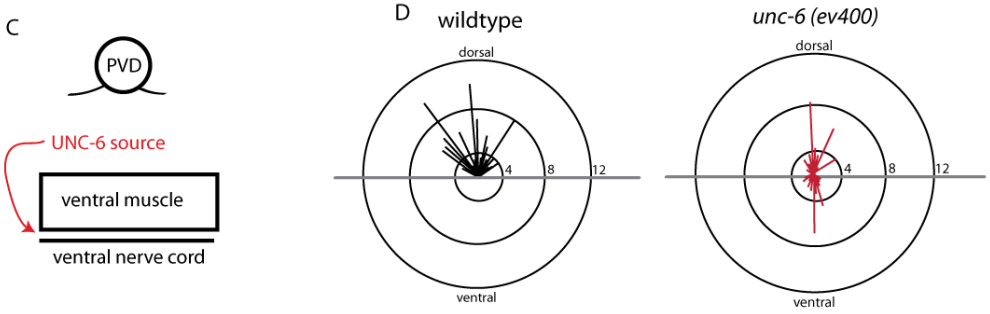
C
PVD
UNC-6 source
ventral muscle
ventral nerve cord
D
wildtype
unc-6 (ev400)
dorsal
ventral
4
8
12

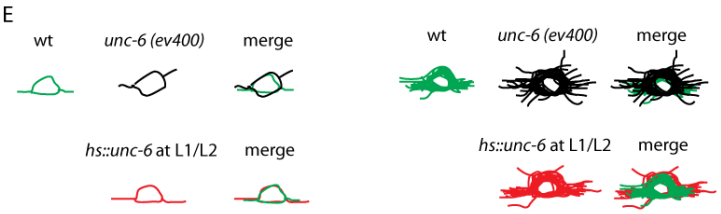
E
wt
unc-6 (ev400)
merge
hs::unc-6 at L1/L2
merge

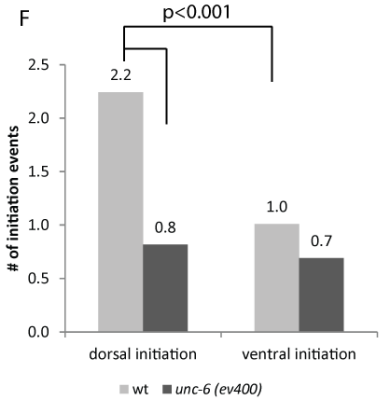
F
p<0.001
# of initiation events
2.5
2.0
1.5
1.0
0.5
0.0
2.2
0.8
1.0
0.7
dorsal initiation
ventral initiation
wt
unc-6 (ev400)

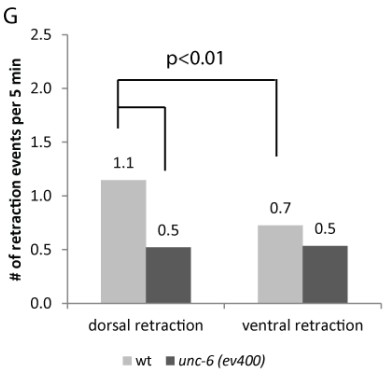
G
p<0.01
# of retraction events per 5 min
2.5
2.0
1.5
1.0
0.5
0.0
1.1
0.5
0.7
0.5
dorsal retraction
ventral retraction
wt
unc-6 (ev400)

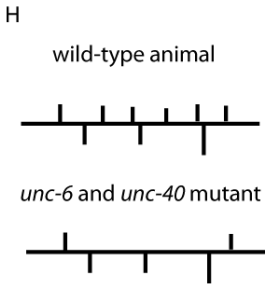
H
wild-type animal
unc-6 and unc-40 mutant

Figure 6.2. Netrin is required for dendritic asymmetry. (A) Image of a wild-type, *unc-6 (ev400)* and *unc-40 (e271)* and schematic of 2^{O} dendrites showing Netrin. (B) Graph scores the percentage of animals in a population that have defective asymmetry of 2^{O} dendrites (more ventral than dorsal branches) and normal distribution (more dorsal than ventral branches). Light bar indicates normal distribution. Dark bar indicates defective distribution. (C) Schematic showing the PVD neuron and UNC-6 expressing cells on the ventral side. (D) Plot showing in wild-type animals the number of dorsal branches is always greater than the number of ventral branches. Some PVD neurons are ventrally asymmetric in *unc-6 (ev400)* animals. Each line presents a single animal in the population. Each ring represents the difference in branches (dorsal vs ventral, quantity of distance is listed on right side) on the side of the animal. (E) Tracings of the PVD cell soma and the exit of the 1^{O} dendrite showing 1^{O} dendrite that exits the ventral portion of the wt cell soma. This is defective in *unc-6 (ev400)* but not defective when the gradient and dendritic asymmetry is disrupted suggesting cell soma polarity does not cause dendritic asymmetry. Bottom tracings represent merges of 20 animals showing wild-type animals always have 1^{O} dendrites that sit on the ventral side of the cell where *unc-6* mutants this is defective. (E) Graph of initiation events in wild-type animals and *unc-6 (ev400*) shows more initiation on the dorsal side than the ventral side in wild-type animals. This initiation bias is lost is *unc-6 (ev400)*. (F) Graph of retraction events shows a slight decrease in the retraction of dorsal branches in wildtype compared to *unc-6 (ev400).* (G) Schematic summary of genetic ablation of Netrin signaling shows randomization of the dendritic asymmetry of PVD neurons.

defects. Thus in the absence of these transcripts, the dendritic asymmetry of PVD dendrites is essentially random. Interestingly, genetic ablation of the repulsive UNC-6 receptor, *unc-5*, did not cause significant dendritic asymmetry defects (Figure 6.2B).

To determine the origin of this phenotype we sought to characterize the developmental time point when a dorsal/ventral asymmetry could first be visualized in the PVD neuron. First we noted that in wild-type neurons, the anterior and posterior 1^{O} branches projected from the cell soma on the ventral side, displaying a cell soma that appeared to be sitting on the 1^{O} branch (Figure 6.2C). We hypothesized that the asymmetry in 2^{O} dendrites could be dependent on an initial polarity that is established on the 1^{O} dendrite. We noted that the 1^{O} branch polarity was disrupted in *unc-6* mutants (Figure 6.2C). Based on this observation we concluded that UNC-6 is required to polarize the outgrowth of the 1^{O} dendrite on the ventral side. To ask if the polarity established on the 1^{O} branch is coupled to the asymmetry observed in 2^{O} dendrites we attempted to disrupt *unc-6* signaling after the 1^{O} branch was established. To do this we used a transgene that expressed UNC-6 under a heat shock promoter. This transgene provided us with the ability to disrupt the normal UNC-6 ventral gradient at a particular time. Disrupting the UNC-6 gradient after 1^{O} branch outgrowth did not disrupt 1^{O} branch polarity but did affect 2^{O} dendrite asymmetry (Figure 6.2C). This data is consistent with the model that the UNC-6/Netrin gradient functions at two uncoupled stages during development, initially to polarize 1^{O} dendrite outgrowth and later to administer 2^{O} dendrite asymmetry.

We next considered the possibility that 2^{O} dendrite outgrowth was defective in *unc-6 (ev400)* mutants, resulting in the defect of the dorsal/ventral asymmetry. Using time-lapse imaging, we visualized the dynamic growth of 2^{O} branches in *wildtype* and *unc-6 (ev400).* As previously published in wild-type animals, 2^{O} dendrites dynamically initiated and retracted from the 1^{O} branch. Upon quantifying the amount of initiation and retraction events, we noted on average 2.24 dorsal initiation events vs. 1.01 ventral events per 5 min interval (Figure 6.2E). There was a smaller significant dorsal/ventral bias in the number of retraction events. Since branch initiation on the dorsal side is different from that on the ventral side we hypothesized that the difference of 2^{O} dendrites in the mature neuron could be a result of differential branch initiation.

To test this we visualized *unc-6* mutants via time-lapse microscopy. Interestingly, time-lapse imaging of 2^{O} branch outgrowth in *unc-6 (ev400)* mutants showed a loss of dorsal/ventral bias in branch initiation, both sides contained about 0.70 initiation events (Figure 6.2E). We, therefore, hypothesize that the biased initiation of branches on the dorsal side in wild-type neurons results in an asymmetric mature neuron and the loss of this initiation bias in *unc-6* signaling mutants results in neurons that are not dorsally asymmetric.

A ventral UNC-6/Netrin gradient is required to polarize dorsal/ventral outgrowth

In axon guidance, an UNC-6/Netrin gradient is required to spatially orient growing axons [43, 45, 47]. We reasoned that the ventral gradient could function

similarly in the distribution of 2^{O} dendrites to expose the ventral side to a higher concentration of UNC-6/Netrin than the dorsal side. To determine if the ventral source of UNC-6/Netrin is sufficient to polarize dorsal/ventral outgrowth we spatially restored UNC-6 expression in the *unc-6 (ev400)* mutant using a transgene that drove *unc-6* under a ventral specific marker. In *unc-6 (ev400)* mutants, 53% of PVD neurons are defective in dorsal/ventral asymmetry. When UNC-6 expression was restored ventrally in the *unc-6 (ev400)* mutant background, the Unc-6 defect was significantly rescued to 22% defective neurons (Figure 6.3). Therefore, we conclude that ventral UNC-6 expression is sufficient to properly polarize 2^{O} dendrite outgrowth.

We recently showed that UNC-6/Netrin could function as a permissive cue in dendritic branch self-avoidance [12]. We considered the possibility that UNC-6/Netrin could function similarly in 2^{O} branch distribution, in which the spatial distribution of the gradient was not essential but only the presence of the ligand was required. To test this, a heat shock promoter was used to globally express UNC-6 in an *unc-6 (ev400)* mutant. In agreement with the hypothesis that a specific source of UNC-6/Netrin is required for the asymmetric distribution of dendrites, we did not see rescue of 2^{O} branch asymmetry when UNC-6 was globally expressed (50% defective neurons) in an *unc-6 (ev400)* mutant (Figure 6.3). Based on these results we hypothesize that a specific source of UNC-6 is required for dendritic asymmetry. We therefore conclude that UNC-6 signaling not only has different temporal requirements in PVD development but also has mechanistic differences between dendritic asymmetry and self-avoidance.

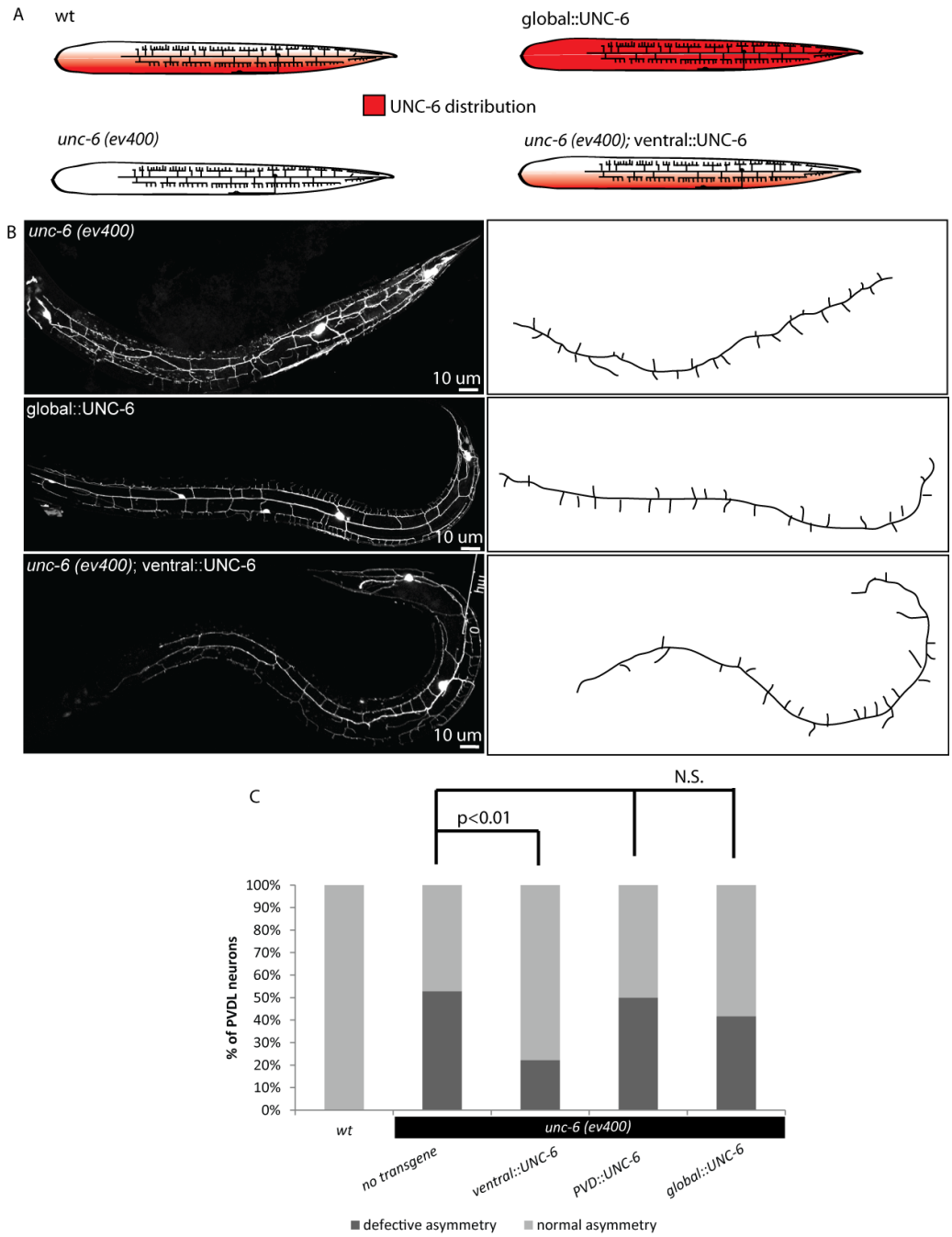

Figure 6.3. A ventral source of UNC-6 defines dendritic asymmetry. (A) Schematics showing distribution of UNC-6 protein in specific genetic backgrounds. UNC-6 is expressed from the ventral cells in wt and globally expressed with heatshock of hs::UNC-6 transgene. The ventral::UNC-6 transgene restores ventral expression of UNC-6 to *unc-6*. (B) Images and schematic tracings of PVD neurons in *unc-6 (ev400), global::UNC-6 and unc-6 (ev400); ventral::UNC-6 animals*. (C) Graph shows population of animals that have normal or defective distribution of 2^{O} dendrites. Expression of *unc-6* ventrally (ventral::UNC-6) restores dendritic asymmetry *unc-6 (ev400)* mutants whereas expression of UNC-6 in PVD (PVD::UNC-6) or globally with the heat shock promoter (global::UNC-6) does not rescue the dendritic asymmetry defect. Light bar indicates normal distribution. Dark bar indicates defective Distribution.

In self-avoidance the wild-type UNC-6/Netrin gradient is not required for self-avoidance. To test whether the UNC-6/Netrin ventral gradient was necessary for PVD dendritic distribution of 2^{O} dendrites, we heat shocked UNC-6 globally in a wild-type background to disrupt the endogenous UNC-6/Netrin ventral gradient. 50% of the neurons were defective when the gradient was disrupted by globally expressing UNC-6/Netrin in a wild-type background, essentially randomizing dendritic outgrowth (Figure 6.4). Thus disruption of the UNC-6 gradient is sufficient to perturb asymmetry in an otherwise wild-type background. To further test the hypothesis that an UNC-6/Netrin gradient determines dendritic asymmetry we attempted to reverse the gradient by expressing UNC-6 dorsally with the *unc-129* promoter in the *unc-6* mutant background. Unfortunately, as described before, *unc-6* mutants with this transgene die embryonically and thus we could not test if reversal of the gradient results in complete reversal of dendritic asymmetry [174]. Nonetheless, our results are consistent with a model in which a ventral source of UNC-6/Netrin distributes a gradient (with a high ventral concentration and low dorsal concentration) that patterns 2^{O} dorsal/ventral dendritic asymmetry. These data further support our hypothesis that the UNC-6 signaling during 2^{O} dendrite asymmetry is mechanistically different than self-avoidance.

We propose that PVD dendritic outgrowth utilizes the UNC-6/Netrin molecule twice; early in development, as presented in this report, as an instructive cue in which a ventral gradient is required and later in development

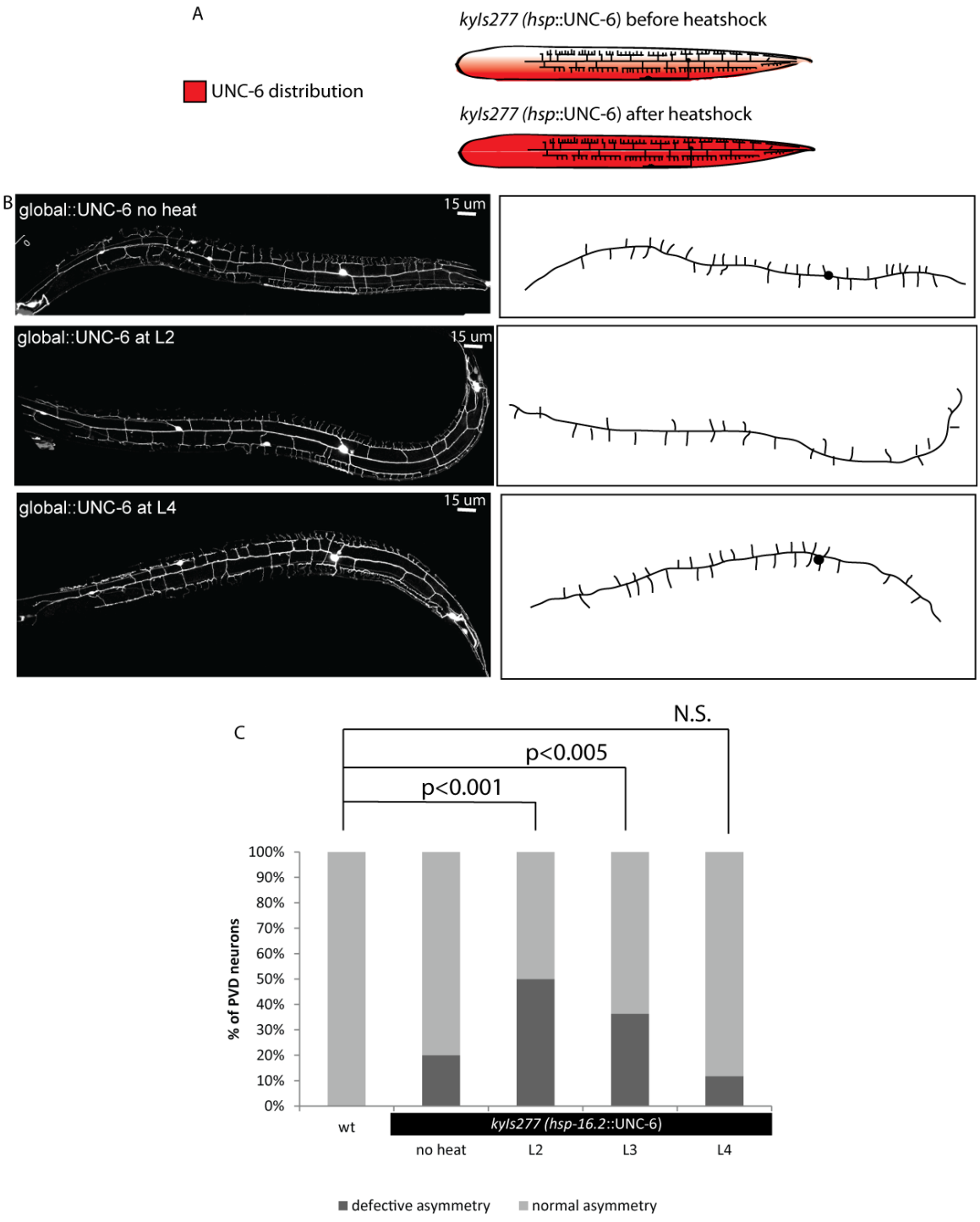

Figure 6.4. An UNC-6/Netrin gradient is required during 2^{O} dendrite outgrowth. (A) Schematic of UNC-6 expression before and after induction by heat shock *kyIs277 (hsp*::UNC-6) corresponds to a heat shock inducible transgene. (B) Confocal images and traced schematic of PVD neurons shows that global expression of UNC-6 at the L2 stage disrupts dendritic asymmetry whereas global expression at the L4 larval stage does not. (C) Quantification of PVD branching asymmetry shows that global expression of UNC-6 at the L2 stage induces the most severe asymmetry defect with weaker effects for L3 expression and no significant effect with L4 expression. Light bar indicates normal distribution. Dark bar indicates defective distribution.

during self-avoidance as a permissive cue in which a specific source is not required but merely the presence of the ligand is essential [12].

UNC-6/Netrin is required during 2^{O} branch outgrowth to control asymmetry

Having established that an UNC-6/Netrin ventral gradient is required, we next sought to understand the temporal requirement of the gradient in 2^{O} dendritic polarity. We reasoned that since UNC-6/Netrin is required for MNC axon guidance [43] then guidance defects could be indirectly disrupting PVD dendritic distribution. This model is plausible since MNCs function during PVD branch development to stabilize branches (Chapter 2). In this model the ventral gradient would be required in the early L2 larval stage during commissural guidance and before 2^{O} branch outgrowth begins. In contrast, the ventral gradient could be required to control branch outgrowth directly in PVD as we proposed based on our time-lapse imaging results. In this model, the gradient would be required after commissural growth in the late L2 larval stage during PVD branch outgrowth. To distinguish which of these two models is more likely we used a heat shock promoter that drove UNC-6 expression globally [174] in a wild-type background to temporally disrupt the endogenous UNC-6/Netrin gradient. Disruption of the ventral gradient during 2^{O} branch outgrowth (L2 and L3 larval stage, after MNC outgrowth) resulted in PVD neurons that exhibited more ventral branches than dorsal branches, randomizing the PVD dorsal/ventral distribution of 2^{O} dendrites (Figure 6.4). Heat shock during the L2 stage, however, did not disrupt MNC outgrowth (data not shown). The dorsal/ventral

asymmetry of PVD was not disrupted if UNC-6 was heat-shocked after 2^{O} outgrowth (L4 larval stage). These results and our time-lapse imaging analysis are consistent with the model in which a ventral UNC-6/Netrin gradient patterns the dorsal/ventral asymmetry of PVD dendrites during 2^{O} branch outgrowth.

The UNC-6/Netrin receptor, UNC-40/DCC, is required cell-autonomously in PVD to direct dorsal/ventral asymmetry.

Recently, we demonstrated a cell-autonomous role in PVD of UNC-40 and UNC-5 in dendritic self-avoidance [241]. We reasoned UNC-40 could be required cell-autonomously in PVD, as it is in self-avoidance, to direct dorsal/ventral dendritic asymmetry. To test this hypothesis we expressed UNC-40 cDNA with a PVD cell-specific promoter in *unc-40 (e271)* mutants. Expression of UNC-40 in PVD in an *unc-40* mutant resulted in 16% defective neurons, which was a significant rescue from the 46% defective neurons seen in the *unc-40 (e271)* mutant (Figure 6.5A,C). The other *unc-6/Netrin* receptor, UNC-5, is also required cell-autonomously in PVD for self-avoidance. However, as noted above, UNC-5 did not appear to be required in PVD for dendritic distribution (Figure 6.2B). These data support a role of UNC-6/Netrin signaling in PVD via the UNC-40 receptor to direct dorsal/ventral asymmetric outgrowth and again emphasizes the hypothesis that UNC-6 signaling during 2^{O} dendrite outgrowth is mechanistically different than self-avoidance.

We hypothesized that UNC-40 interacted with UNC-6 during 2^{O} dendrite outgrowth to properly distribute dendrites. To test if the interaction of UNC-6 and

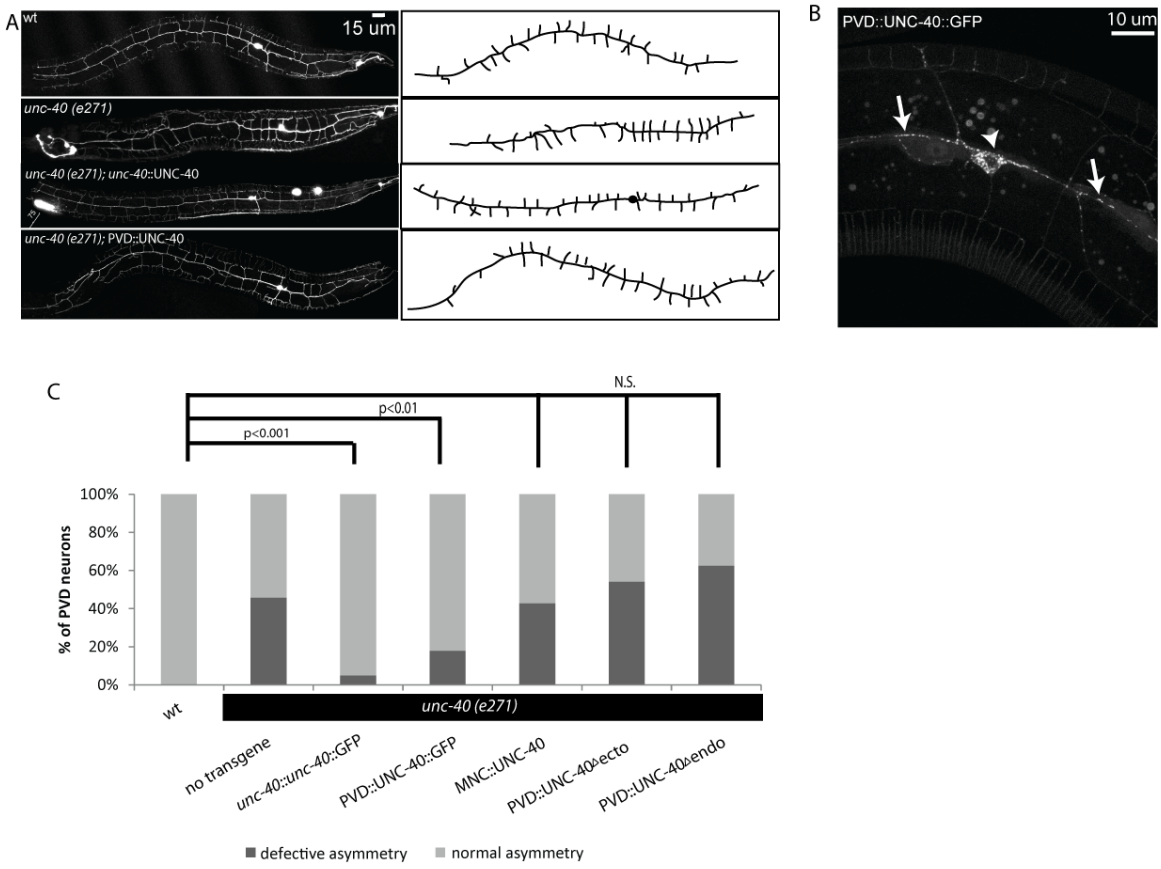

Figure 6.5. UNC-40 is required cell-autonomously in PVD. (A) Images and schematic tracings of PVD lateral branches show that UNC-40 expression from its endogenous promoter (*unc-40::unc-40::*GFP) or in PVD (PVD::UNC-40::GFP) rescues the *unc-40 (e271)* branching asymmetry defect whereas expression of UNC-40 in the motorneurons (MNC::UNC-40) does not. (B) Confocal image showing punctate localization of UNC-40::GFP 2^{O} (arrowheads) dendrites. Arrow head denotes PVD cell body (C) Graph shows that expression of *unc-40* in PVD restores dendritic asymmetry of *unc-40 (e271)* mutants. Expression of *unc-40* lacking an ectodomain or an intracellular domain does not rescue asymmetry defects. Light bar indicates normal distribution. Dark bar indicates defective distribution.

UNC-40 was required we deleted the extracellular domain of UNC-40 and scored its ability to rescue defects in *unc-40 (e271)*. Consistent with our hypothesis that the UNC-40/UNC-6 interaction was important, this truncated UNC-40 protein failed to rescue dendritic distribution defects in *unc-40 (e271)* (Figure 6.5C). Our hypothesis also suggested that UNC-40 signaling was required and thus the intracellular domain of UNC-40 would be essential to properly distribute dendrites. This hypothesis was confirmed when an *unc-40* transgene lacking the intracellular domain also failed to rescue *unc-40* mutant defects (Figure 6.5C).

We hypothesized that if UNC-40 was required for dendritic asymmetry it should be localized in the 1^{O} and 2^{O} dendrites were dendritic asymmetry is established. In support of the hypothesis that UNC-40 is required for asymmetry of 2^{O} dendrites, a functional UNC-40::GFP fusion was localized in puncta along the 1^{O} and 2^{O} branches (Figure 6.5B). Interestingly, later in development UNC-40 was also localized at the 3^{O} and 4^{O} dendrites, consistent with the hypothesis that it also plays a role after 2^{O} outgrowth in self-avoidance [241].

Netrin downstream components function in 2^{O} branch asymmetry

Multiple downstream components of UNC-6/Netrin signaling have been identified. However, the role of these components downstream of Netrin in dendritic development is largely unknown. To identify UNC-6/Netrin downstream components required for 2^{O} dendrite distribution we screened 38 cytosolic proteins via genetic mutants or RNAi for asymmetry defects using PVD::GFP (Table 5.1). This analysis identified three downstream components that were

required for dendritic asymmetry. Genetic ablation of *unc-34, mig-10* and *unc-73* resulted in dendritic asymmetry defects that phenocopied *unc-6* and *unc-40 (*Figure 6.6A*)*.

The *mig-10* genomic region produces three different spliceforms [76]. These spliceforms have been shown to be required differently in specific cells (Stavoe and Colón-Ramos unpublished data)(Chapter 5). We asked which MIG-10 spliceform was required in PVD to establish dendritic asymmetry. To do this we utilized a MIG-10 fosmid that did not encode the *mig-10c* spliceform and tested its ability to rescue dendritic asymmetry defects of *mig-10 (ct41)*. Restoration of *mig-10a/b* with this fosmid rescued dendritic asymmetry defects of *mig-10 (ct41)* animals suggesting *mig-10a* and *mig-10b* were sufficient to function in dendritic asymmetry and that *mig-10c* was not essential to establish asymmetry (Figure 6.6). To further test the requirement of the different spliceforms we utilized a fosmid that only expressed *mig-10b*. This fosmid rescued dendritic asymmetry defects of *mig-10 (ct41)* mutants (Figure 6.6A). Thus, *mig-10b* alone is sufficient to establish PVD dendritic asymmetry. To test if *mig-10b* function was sufficient in PVD to establish dendritic asymmetry we used the PVD promoter to drive expression of *mig-10b* only in the PVD neuron in *mig-10 (ct41).* Expression of *mig-10b* in PVD rescued dendritic asymmetry defects of *mig-10 (ct41)* suggesting that *mig-10b* functions cell-autonomously in PVD (Figure 6.6A). We also tested the ability of *mig-10c* to rescue asymmetry defects but consistent with our fosmid data *mig-10c* expression in PVD did not rescue dendritic asymmetry defects of *mig-10* mutants (Figure 6.6A). Lastly, we

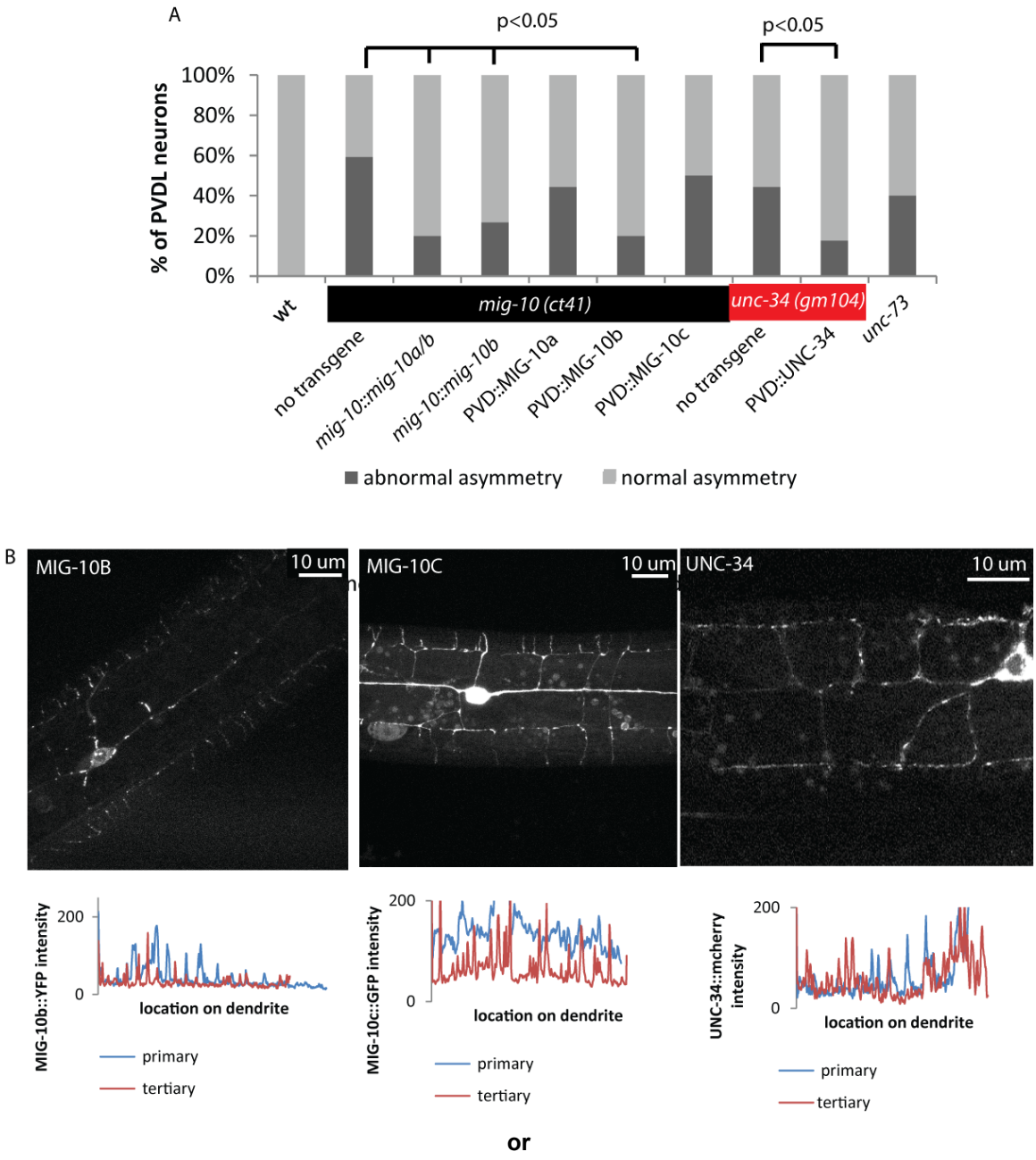

Figure 6.6. Specific downstream components are required for PVD branch asymmetry. (A) Graph showing that *mig-10 (ct41), unc-34 (gm104)* and *unc-73* disrupt dendritic asymmetry. Restoration of *mig-10a/b* and *mig-10b* with the *mig-10* promoter in *mig-10 (ct41)* mutants restores dendritic asymmetry. Expression of *mig-10b (PVD::mig-10b)* specifically in PVD rescues asymmetry defects whereas expression of *mig-10c (PVD::MIG-10C)* or *mig-10a* (PVD::MIG-10a) does not. Expression of *unc-34* in PVD (*PVD::unc-34*) rescues asymmetry defects of *unc-34 (gm104)*. Light bar indicates normal distribution. Dark bar indicates defective distribution. (B) Image of MIG-10B::YFP in PVD shows YFP puncta in the 1^{O} dendrite. MIG-10C::GFP in PVD shows diffuse localization in the 1^{O} dendrite but punctate localization in higher order branches. UNC-34::GFP shows punctate localization pattern similar to that of MIG-10B. Graphs below show line scans of intensity of the corresponding fluorescent proteins in the 1^{O} (blue) and 3^{O} (red) dendrite. Note that MIG-10b is punctate throughout while MIG-10c is diffuse in the 1^{O} dendrite but punctate in the 3^{O} dendrite. UNC-34 puncta are seen in all dendrites.

expressed MIG-10a specifically in PVD to determine if it was sufficient to rescue *mig-10 (ct41)* asymmetry defects. Interestingly, restoration of *mig-10a* cDNA in PVD did not rescue asymmetry defects. These results are consistent with the model that *mig-10b* is uniquely sufficient in PVD to confer dendritic asymmetry of PVD neurons. We therefore conclude that *mig-10b* is utilized to establish dendritic asymmetry.

Because the different *mig-10* spliceforms appear to be uniquely required during dendritic development we asked if they were localized differently in the dendrites. To characterize this we expressed functional GFP tagged versions of each spliceform and monitored their sub-cellular localization in the 1^{O} and 2^{O} dendrites. Interestingly, MIG-10B and MIG-10A puncta were located throughout the dendrites, including obvious puncta in the 1^{O} dendrite (Figure 6.6B). In contrast, MIG-10C was diffuse in the 1^{O} dendrite and puncta were only visible at higher order branches (Figure 6.6B). This data is consistent with specific roles of MIG-10 spliceforms in dendritic development. We conclude that *mig-10b* is specifically required for dendritic asymmetry and is localized in puncta where 2^{O} dendrite outgrowth occurs.

Mutants of *unc-34* also displayed PVD defects that were striking similar to *unc-40* and *unc-6*. Since we detected *unc-34* transcripts in a PVD cell-specific microarray profile [12] we considered the hypothesis that *unc-34* functioned in PVD to establish dendritic asymmetry. To test this we restored UNC-34 specifically in the PVD neuron in *unc-34 (gm104)* and tested its ability to rescue dendritic asymmetry defects. Expression of UNC-34 specifically in PVD in *unc-*

34 (gm104) rescued dendritic asymmetry defects (Figure 6.6A). These results are therefore consistent with the hypothesis that UNC-34 and MIG-10B function cell-autonomously in PVD to establish dendritic asymmetry.

Because MIG-10B and UNC-40 were localized in punctate patterns in the 1^{O} dendrite we asked if UNC-34 also displayed punctate subcellular localization along the 1^{O} dendrite. Consistent with the role of UNC-34 in 2^{O} dendrite distribution we visualized UNC-34 puncta in 1^{O} and 2^{O} dendrites (Figure 6.6B). Together these data are consistent with a model in which UNC-6/Netrin signals through UNC-40 and downstream components UNC-34, MIG-10B and UNC-73 to properly distribute dendrites.

DISCUSSION

Model for UNC-6/Netrin signaling in dendritic outgrowth

The mature dendritic architecture of PVD exhibits an asymmetric structure that contains more dorsal branches than ventral branches. Time-lapse imaging data suggests this difference is a result of differential initiation of dorsal branches than ventral branches. We propose a model in which a higher concentration of UNC-6/Netrin on the ventral side establishes dendritic asymmetry via the UNC-40/DCC receptor (Figure 6.7). When the UNC-6/Netrin gradient is lost, asymmetry defects arise from the loss of initiation bias in PVD. One potential model is that UNC-6/Netrin signaling establishes polarity that asymmetrically distributes branch initiation machinery in the PVD 1^{O} branch.

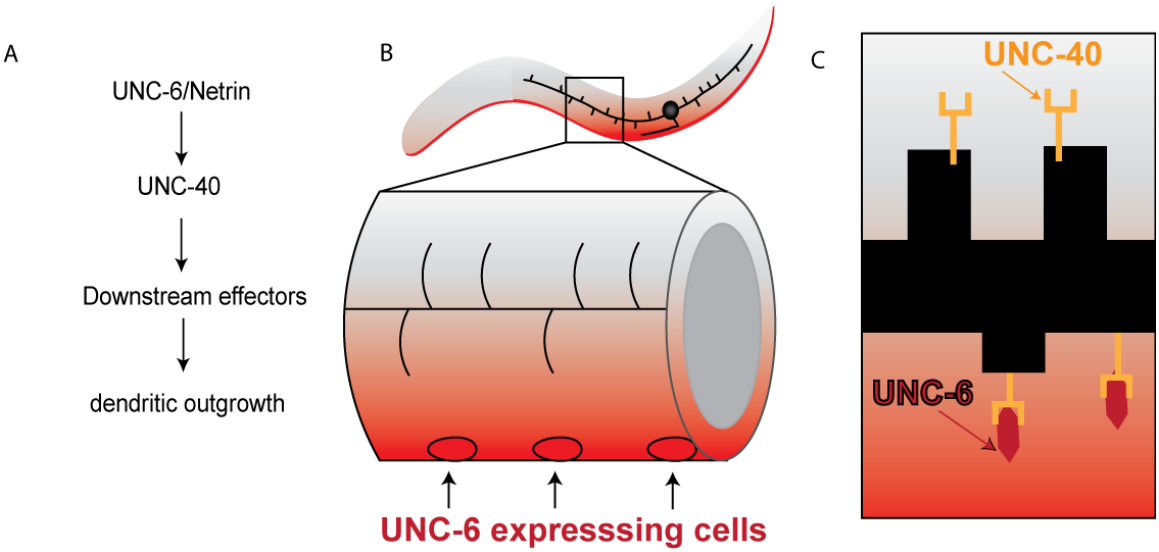

Figure 6.7. Model for the role of UNC-6/Netrin signaling in dendritic asymmetry. (A) UNC-6/Netrin signaling pathway in dendritic asymmetry. UNC-6 functions through the UNC-40 receptor and downstream effectors to control dendritic outgrowth. (B) UNC-6 expressing cells produce a ventral gradient. (C) Inset schematic of the PVD neuron (black) showing higher concentration of UNC-6/Netrin on the ventral side of the 1^{O} dendrite.

UNC-6/Netrin dual roles: Dendritic distribution and self-avoidance

We previously described that UNC-6/Netrin was utilized on the surface of the PVD dendrite as a cell-surface repellent (Chapter 4) [241]. In this report we identified that UNC-6/Netrin is also required to properly distribute dendrites. These two different roles for UNC-6/Netrin share some common aspects. In self-avoidance and dendritic asymmetry, a ventral source of UNC-6/Netrin is a sufficient source of the neurotropic ligand [241]. In addition, both self-avoidance and dendritic asymmetry require proper signaling of the UNC-40/DCC receptor and for the ability of the UNC-40/DCC receptor to interact with UNC-6/Netrin.

However, the role UNC-6/Netrin in dendritic distribution is clearly different from its role in self-avoidance. Firstly, a Netrin gradient radiating from a ventral location is required to properly distribute dendrites. In self-avoidance, however, the gradient is not essential. In addition, self-avoidance requires signaling of the UNC-5 receptor [241]. In dendritic asymmetry, UNC-5 appears to be dispensable. Thus though Netrin is used twice during dendritic development the signaling receptors of the two pathways are clearly different. Lastly, dendritic asymmetry and self-avoidance require different downstream components. For example, MIG-10B functions to properly distribute dendrites but does not seem to function similarly in self-avoidance (Chapter 5). These data are consistent with the hypothesis that Netrin activates two independent pathways during dendritic development to pattern different aspects of the nociceptive dendritic tree.

It was initially surprising that a diffusible molecule was required for a contact-dependent self-avoidance event. However, this is less surprising now that we have identified in this report that UNC-6/Netrin is utilized earlier in PVD development to distribute dendrites. It seems plausible that UNC-6/Netrin is first used to distribute dendrites and then conveniently recycled later in development for a contact event. In this model, UNC-6/Netrin is captured by the UNC-40 receptor to activate an UNC-40 dependent signal for dendritic asymmetry and then later the UNC-6/UNC-40 complex activates UNC-5 for contact-dependent self-avoidance. This model allows the cell to control different aspects of development without having to generate a new set of molecules for each role. Interestingly, Netrin's ability to function in different aspects of development in the same cell has been described in other neuronal cells [57, 174].

This report shows a requirement for specific downstream components in dendritic asymmetry. Why are these specific components employed to establish dendritic asymmetry? MIG-10/Lamellipodin and UNC-34/Enabled have both been implicated in asymmetry in other neuronal cells [174]. For example the asymmetric sub-cellular localization of MIG-10/Lamellipodin in response to Netrin has been previously described in HSN neurons of *C. elegans* [174]. This MIG-10/Lpd asymmetric localization is utilized to establish the initiation site of the axon. Interestingly, in the absence of MIG-10/Lpd, axons still initiated but in the incorrect direction, suggesting MIG-10/Lpd is specifically required to mark the initiation site. UNC-6/Netrin has also been shown to define the site of synaptogenesis. In AIY neurons in *C. elegans*, UNC-6 from a specific ventral

source marks the synaptic site of AIY and RIA [56]. Interestingly, the AIY and RIA synapse form on the side of the neuron that is not in contact with the UNC-6/Netrin source. Thus UNC-6/Netrin does not directly drive synaptogenesis but rather marks the site of its formation. MIG-10 and UNC-34 are also required for AIY synaptogenesis [242]. We hypothesize that MIG-10/Lpd and UNC-34/Ena could have similar function to define an asymmetry in the PVD neuron and could be used to mark the site of initiation of dendritic branches. It will be intriguing to identify the components of dendritic initiation as they may show asymmetric dendritic localization that is dependent on MIG-10/Lpd and UNC-34/Ena.

Netrin has been shown to control branching in other contexts similar to what we see in PVD [267]. For example, in axons of retinal ganglion cells Netrin mediates axonal branching through the DCC receptor. Interestingly, this effect of axonal branches of RGC neurons seemed to be specific to the initiation of branches [267]. This data is consistent with our findings in *C. elegans*. In PVD, loss of UNC-6/Netrin effects the initiation of neuronal branches. Also similar to RGCs, the PVD neuron requires the UNC-40/DCC protein to properly initiate branches. In our present study we uncover additional components of Netrin induced neuronal branching. For example, in RGCs it is not clear if there is biased outgrowth (i.e. on one side of the axon) of axonal branches as we saw in PVD. We also identified additional components downstream of the UNC-40/DCC that are required to properly distribute dendrites including UNC-34/Ena, MIG-10/Lpd and UNC-73/Trio. It will be intriguing in the future to visualize the spatial

requirement of Netrin in RGC axonal branch development and to identify the downstream molecules required to establish RGC branches.

A gradient establishes asymmetry

In dendritic asymmetry a Netrin gradient is used to bias initiation of dendritic branches. It is noteworthy that ventral and dorsal branch initiation is only separated by the width of the 1^{O} branch (~100-200 nm in diameter) [12]. Interestingly, a small bacterial cell can recognize a graded difference during chemotaxis [268]. Similarly, a growth cone can detect differences of gradient across the cone [269]. In PVD, it is possible that the UNC-6/Netrin protein is captured by the UNC-40 receptor where it first interacts with the 1^{O} dendrite, which would be the ventral side. This capture on the ventral side may reduce the UNC-6/Netrin concentration that is exposed to the dorsal side and thus steepen the gradient. The combination of the diameter of the 1^{O} dendrite and the ventral side limiting UNC-6/Netrin protein that can reach the dorsal side may be sufficient to provide a difference of UNC-6/Netrin between the ventral and dorsal side of the 1^{O} dendrite. To test this model it would be interesting to determine how the UNC-6/Netrin gradient is distributed and whether this plays a role in dendritic outgrowth.

In an alternative model, the growth of 2^{O} dendrites away from the 1^{O} dendrite could result in differential exposure to the Netrin protein concentration, which may influence dendrite stabilization. We note that time-lapse imaging is limited by the sampling interval and thus unstable branches could have quickly

initiated and retracted within our 2.5 minute imaging interval. We, therefore, cannot definitively rule out the model that PVD dendritic branches sense differences in Netrin as the branches grow. Nonetheless, our data is consistent with the model that the Netrin gradient is required to asymmetrically affect 2^{O} dendritic branch outgrowth of the PVD neuron.

Dendritic distribution of other neuronal cells

Interestingly, retinal ganglion cells in zebrafish display dendritic asymmetry that arises during developmental branching. Moreover, mislocalization of these RGCs caused defects in this stereotypical dendritic asymmetry [265]. Based on our current study it seems possible that these RGCs have lost the ability to respond to extracellular signaling cues such as Netrin. It would be interesting in the future to determine the molecular foundation of RGC asymmetric morphology.

It is worth noting that previous evidence has suggested that dendritic asymmetry can be established independent of external cues [270]. However, in the PVD neuron our study shows that the extracellular cue UNC-6 is required to properly distribute dendrites. These findings, are therefore consistent with Ramon y Cajal hypothesis that dendritic development is controlled by a neurotropic mechanism [98]. The careful characterization of dendritic arrays and the molecules used to generate asymmetric dendritic trees will be an exciting aspect of dendritic morphogenesis in the future.

Author Contributions

Andrea Stavoe, Jessica Nelson and Daniel Colón Ramos provided unpublished reagents to test the cell-specific requirement of UNC-40, UNC-34, and MIG-10 and helpful advice. Cody Smith did all the experiments in this chapter.

Acknowledgments

We thank Cori Bargmann (Rockefeller) for CX6488 and A. Hardaway (Vanderbilt), members of the Miller (Vanderbilt) and Colón -Ramos (Yale) Labs for comments on the manuscript. Some of the strains used in this work were provided by the *C. elegans* Genetics Center which is supported by NIH NCRR. This work was supported by NIH R01 NS26115 (DMM), NIH R21 NS06882 (DMM), NIH F31 NS071801 (CJS), NIH R00 NS057931 (DCR), and Klingenstein Foundation and the Alfred P. Sloan Foundation fellowship (DCR)

CHAPTER VII

DISCUSSION AND FUTURE DIRECTIONS

Sensory neurons across phylogeny share fundamental features

This thesis addresses two key processes that are conserved in evolution from nematodes to human: 1) Sensory neurons are specialized to detect specific stimuli and 2) Sensory neurons adopt complex arbors that innervate the area just below the hypodermis. Sensory neurons allow animals to respond to specific stimuli from their surrounding environment [145, 271]. Although the network of sensory neurons is more complex in humans, sensory neurons in insects and nematodes maintain striking morphological and functional similarity to their evolutionary descendants [3, 4, 12, 112, 140].

Defining polymodal determinants

Sensory circuits in insects and vertebrates contain specialized cells to sense specific environmental stimuli and many of these sensory neurons detect multiple sensory stimuli [9, 10, 132, 145, 271]. Emerging evidence shows that polymodal sensory neurons also exist in the *C. elegans* sensory circuit [124, 183]. For example, PVD can detect harsh touch, cold temperature and hyperosmolarity (Chapter 3). The molecular understanding of how these polymodal neurons are defined, however, is not well understood. It would therefore be interesting to determine the factors that specify the different sensory

modalities of functionally distinct neurons. Defining the ion channels that are used to detect these different sensory stimuli may aid in describing the generation of these neurons [124]. A screen for mutants that perturb expression of a given ion channel could reveal proteins that transcriptionally control sensory modalities. Because of the conservation of sensory neuron function across phylogeny it seems likely that the molecules that generate these conserved cell types in the nematodes may exercise similar functions in mammals [4, 6]. Thus, the identification of such molecules in nematodes and insects should help to characterize the development of the vertebrate sensory circuit. This approach offers exciting opportunities for the future.

Transcription factor codes specify dendritic diversity

Transcription factors are utilized to drive cell intrinsic programs that define cellular identity. The key roles of transcription factors in dendritic morphogenesis have been well-documented in the *Drosophila* peripheral nervous system (PNS) [3, 4, 6]. Some PNS neurons display simple, unbranched morphology whereas others adopt extensively branched dendritic trees. Multidendritic neurons in *Drosophila* are classified according to the complexity of their arbors with class I being simple branched neurons and class IV displaying highly branched dendritic arbors that resemble many sensory neurons that are seen in vertebrates [4]. Abrupt, a zinc-finger transcription factor functions in class I neurons to prevent excess branching [15]. This model is reminiscent of the role we have identified for *ahr-1/spineless* in *C. elegans* (Chapter 3). In our studies, AHR-1 is expressed

in an unbranched neuron, AVM, to prevent elaborate branching typically reserved for nociceptive neurons, PVD and FLP.

AHR-1/Spineless has also been shown to function in dendritic morphogenesis of *Drosophila* PNS neurons [23]. In *Drosophila*, AHR-1/spineless appears to be expressed in all PNS neurons and functions either to restrict dendritic branching in unbranched neurons or to promote branching in highly branched neurons. In *C. elegans*, an AHR-1 promoter reporter did not show expression in PVD but was detected in an unbranched neuron, AVM [205](Chapter 3). However, PVD specific microarray data did detect the *ahr-1* transcript in PVD (Chapter 2). Thus it seems plausible, that as in *Drosophila*, *C. elegans ahr-1* is expressed in both unbranched and highly branched neurons. In our studies, however, it is still not clear if AHR-1 has a direct role in PVD morphogenesis. The reduced number of PVD branches in *ahr-1* mutants is likely the result of tiling with newly formed nociceptive neurons (cAVM and cPVM) (Chapter 3). Nonetheless a common theme persists; AHR-1 directs dendritic morphogenesis.

Many questions remain about the role of AHR-1/Spineless in dendritic morphogenesis. The mechanisms that activate AHR-1/Spineless function in *Drosophila* is largely unknown. In *C. elegans*, previous work has shown that AHR-1 is controlled by UNC-86 [205]. It would, therefore, be interesting to determine if the *Drosophila* UNC-86 homolog exercises a similar role in dendritic morphogenesis. In both *C. elegans* and *Drosophila*, the targets of AHR-1 are mostly unknown [23, 205]. Besides *hpo-30*, other targets of AHR-1/Spineless

have not been defined (Chapter 3). Since the *hpo-30* mutant does not fully suppress the *ahr-1* mutant phenotype it seems likely that *ahr-1* controls additional targets (unpublished data). Identification of these targets would provide important clues to the determinants of dendritic diversity. Lastly, the role of AHR-1/spineless in vertebrate dendritic morphogenesis is not known. As mentioned before, the similar role of this transcription factor in nematodes and insects suggests that AHR-1/Spineless may represent an ancient transcriptional program that is present in vertebrate neuronal development.

Similar to *ahr-1*, Cut is expressed in all *Drosophila* PNS neurons [19, 20]. However, Cut abundance differs between the different classes of neurons with class I neurons showing no Cut expression and class IV neurons displaying high levels of Cut expression [20]. These observations lead to the hypothesis that differential levels of Cut expression define the neuronal complexity. My work did not detect dendritic morphogenesis defects in *cut* mutants in *C. elegans* (Chapter 2). However, our work has revealed comparable roles for the LIM-homeodomain protein, MEC-3, which shows dose-dependent roles in mechanosensory neuron differentiation. MEC-3 is expressed in mechanosensitive sensory neurons including both unbranched and branched neurons. My work has shown that MEC-3 is expressed at lower levels in branched neurons, PVDs, and this lower expression limits transcripts that are normally reserved for unbranched neurons (Chapter 3). Once MEC-3 exceeds a higher threshold, light-touch specific genes are expressed.

It is not clear how the concentration of a given transcription factor is directly related to dendritic complexity. Perhaps transcription factor binding affinity varies for different groups of targets. Thus, at lower concentrations of a given transcription factor only high affinity DNA-binding sequences will be occupied and those genes are selectively activated whereas targets with weaker binding affinities will not be expressed. Competition by other transcription factors could also limit expression of transcripts. In the future, it would be exciting to determine the mechanism by which varying concentrations of transcription factors (e.g. Cut, MEC-3) drive different dendritic morphologies. The identification of binding sites of these transcription factors and biochemical characterization of the chromatin structure of their targets in each cell-type could be an interesting direction. With the advancement of cell isolation techniques in *C. elegans,* it seems plausible that specific chromatin profiles of each cell type could be obtained [272]. Identification of transcription targets and binding sites in specific cell-types is certainly an interesting direction for the future and could provide us with the potential to further understand the diversity of dendritic arbors [273, 274].

Netrin has multiple roles in neuronal development

Recent studies have revealed that Netrin has several different roles during neuronal development [43, 56, 57, 59]. Netrin was first identified as a diffusible molecule that functioned at a distance from its source [43, 45]. However, the immunohistochemistry staining pattern of Netrin does not show a gradient-like

pattern [59, 173]. Instead, Netrin appears in localized clusters in the nervous system [59]. It seems plausible that Netrin may be primed in these locations to function as a short-range cue. This idea is supported by emerging evidence in insects and nematodes that have established that Netrin can function as a short-range cue [54, 55, 57, 58, 112]. This short-range potential expands the use of the molecule as it can now function at long-range as well as for contact-dependent events. For example, in PVD, Netrin is initially used as a graded signal to define PVD branch asymmetry along the dorsal/ventral axis (Chapter 6). Later in development Netrin/UNC-6 functions as a short-range molecule to trigger contact-dependent retraction of sister dendrites (Chapter 4). How then does PVD distinguish the two Netrin signals? I hypothesize that distinct combinations of downstream signaling molecules define these different roles for Netrin. This suggests that a "task-specific" pathway may be activated. For example, asymmetry requires UNC-34, MIG-10B and UNC-73. These proteins could be used to asymmetrically mark one side of the cell (e.g. dorsal vs ventral) as they have been described to do in axon initiation [174]. Self-avoidance utilizes actin-polymerizing components UNC-34 and MIG-10C and also proteins that can generate force such as NMY-1 to trigger retraction. Thus, the components of each pathway have roles that are relevant to the specific cellular phenomenon. This hypothesis of "task-specific" components is also supported in studies describing the development of a *C. elegans* motor neuron [57]. Future work to clarify the signaling details of Netrin will likely strengthen this hypothesis.

Interestingly, work in *C. elegans* and *Drosophila* has identified that UNC-40/DCC has a Netrin-independent function [48, 219, 224][223]. For example, Netrin functions with the UNC-40/DCC homolog, Frazzled, to guide longitudinal pioneering axons in *Drosophila* [223]. However, as with self-avoidance, Frazzled/DCC appears to have a Netrin independent function in addition to its role with Netrin. Interestingly, both migrating longitudinal axons in *Drosophila* and self-avoiding dendrites in *C. elegans* respond to Netrin that is captured by DCC [223, 241]. Identification of the UNC-40 interacting components in self-avoidance may provide insight into the missing component that guides pioneering axons. This molecule would likely function with UNC-40/DCC in the UNC-6/Netrin independent pathway in *C. elegans* self-avoidance and function cell-autonomously in migrating longitudinal axons as an interacting partner with Frazzled/DCC. Because both these phenomena utilize short-range captured Netrin, it may represent another task-specific component that is employed during neuronal development.

Actin Polymerization is required for retraction

My work on the PVD neuron has shown that contact-dependent dendrite retraction requires actin-polymerizing components (Chapter 5). These findings are consistent with the observation that actin appears enriched at the tips of dendrites as they initiate retraction. It therefore seems plausible that actin polymerization is a potential attribute of retraction. Studies in the literature clearly demonstrate a role for actin-polymerizing components in axonal repulsion

[232-235]. However, the cell biology of how actin-polymerizing components drive retraction is not clear.

I hypothesis that actin polymerization drives dendrite retraction in a mechanism that depends on newly generated actin filaments for retrograde movement. One potential mechanism that could describe this is the presence of a protein that forms a bridge between the actin cytoskeleton and the cell membrane [275]. Treadmilling of actin in conjunction with myosin-dependent retrograde flow would drive this bridge protein in the direction of actin flow and thus also pull the membrane rearward. Actin polymerization would be required in such a model to first generate a road for treadmilling and then also be required to maintain that road for full retraction. Myosin in this case would be utilized to enhance treadmilling. In an alternative model, a bipolar myosin filament may connect two parallel actin filaments both with plus end orientation toward the dendritic tip. With the myosin anchored, plus end directional movement of the myosin motor on the actin filament would drive the actin filaments away from the tip resulting in rearward movement of the dendrite. Such a filament orientation would resemble a folded sarcomere so that the plus end of both actin filaments is near the tip. Newly formed actin filaments may be utilized to generate actin filaments that engage pre-existing tip actin filaments. This model represents a more passive mode of retraction that does not require a protein that actively links the cytoskeleton to the dendritic membrane; instead the actin filament maintains the dendritic architecture and removal of the filament would therefore collapse the dendritic architecture to drive retraction. It is also possible that the actin

arrangement of the dendrite is similar to a sarcomere in which bipolar actin filaments form contractile machinery. Bipolar myosin filaments would function similar to myosin in sarcomeres to pull the two actin populations together to generate contraction. A closer look at the actin population with EM or by visualizing the localization of a plus-end directed marker with advanced super-resolution light microscopy techniques such as PALM could help to distinguish these models. Nonetheless, it remains interesting that actin polymerizing components function in neuronal branch retraction. This mechanism of branch retraction could also be applied to axonal growth cone guidance, which as described before, is thus far poorly understood.

Recognizing Self from Non-Self

To date, four potential cell-surface molecules have been implicated in self-avoidance [99, 100, 105, 106, 241]. The model involving alternative spliceforms of Dscam provides an intriguing solution for self-avoidance because it suggests only one gene is required to prevent overlap [99, 100]. The other additional self-avoidance molecules, Netrin, Turtle and Flamingo do not appear to adopt alternative spliceforms and thus are unlikely to offer a general solution for self-avoidance in complex neural environments [105, 106, 241]. However, the role of Turtle and Flamingo in contact-dependent self-avoidance are now controversial due to a recent paper that could not reproduce the effect of a *turtle* mutant on self-avoidance and findings that the Tri/Fry pathway that is presumably linked to flamingo regulates insertion into adjacent epithelial cells [106, 107].

Nevertheless, there are a wide array of extracellular ligands and receptors in the nervous system that could potentially function in self-avoidance similar to Netrin [2]. In axon guidance, neurons respond to a unique code of guidance molecules that steers outgrowth along specific trajectories [2]. It seems possible that a combinatorial code could also define the capacity of individual dendrites to distinguish self from non-self.

Thus far, all the self-avoidance mutants that have been identified display incomplete phenotypes [99, 100, 105, 106, 241]. These findings suggest that other molecules are likely to function in self-avoidance. For example, in PVD, the majority of dendrites do not overlap in Netrin/UNC-6 pathway mutants [241]. Moreover, in time-lapse movies of these mutants, branches sometimes retract upon contact. This observation suggests that additional pathways are likely to function in self-avoidance. It will be interesting in the future to identify additional self-avoidance molecules in PVD. The PVD microarray profile includes likely candidate molecules [12]. A targeted screen of transmembrane proteins with extracellular domains that are common in receptors that activate retraction, such as immunoglobin or fibronectin domains, (28 enriched in PVD vs all cells), for example, could help to identify such molecules.

Work in leeches has shown that detachment of a neurite from the cell body results in the failure of the severed neurite to recognize self from non-self [276]. These results are suggestive of an additional cytoplasmic signal. Perhaps electrical coupling or calcium influx is triggered when two branches contact one another and the coincident occurrence of this in the same cell could identify self.

In this model, branches that are severed from one another or from a separate neuron would not produce this shared signal and thus would not retract after mutual contact. Such a model would provide a general solution to self-avoidance. In this case, an additional molecule such as Netrin could be used to activate the downstream retraction machinery. For example, the shared calcium (Ca^{++}) transient could identify self while Netrin would activate retraction machinery. Each of these signals would depend on the other to fully prevent overlap. Interestingly, calcium (Ca^{++}) influx/efflux has been linked to Netrin signaling in axon guidance [79]. A laser could be used to sever PVD lateral branches for a direct test of this possible interpretation of the mechanism of UNC-6/Netrin dependent self-avoidance.

Tiling, which ensures non-redundant coverage of dendrites from two different cells is also universally observed across phylogeny [4]. As with self-avoidance, the molecular mechanism of tiling is also poorly understood. Interestingly, some self-avoidance molecules are dispensable for tiling [4]. This finding suggests that a different set of molecules could function to prevent heterodendritic interactions. My work has shown that the two nociceptive neurons in *C. elegans,* FLP and PVD, tile to ensure the nematode body is completely covered with nociceptive arbors [12, 125]. A screen for tiling molecules seems plausible in *C. elegans* since FLP and PVD can be differentially labeled with cellular markers (Chapter 3) and because of the ease of forward or reverse genetic screens. It would be interesting in the future to identify mutants that cause overlap of the two neurons, FLP and PVD. Such studies could serve as

foundation for identifying tiling molecules that function in the vertebrate body plan.

The Functional Consequence of Overlap

Self-avoidance is a universally conserved phenomenon and although the function of self-avoidance is not understood, the appearance of non-overlapping dendritic trees across phylogeny suggests it may be important for neuronal function. In sensory neurons, self-avoidance may be utilized to efficiently cover the receptive area. The non-redundant coverage of the receptive area not only ensures that the entire area can receive input but it could also prevent one particular area from receiving too much input. Overlapping coverage of nociceptive dendrites could, therefore, cause excess pain sensation in the animal. Interestingly, neurons in the brain also display non-overlapping arbors [98]. Non-redundant coverage in the brain may help to ensure proper connectivity of the neuronal circuit. It will be interesting in the future to determine the functional consequence of overlap in the nervous system, as this is a significant unanswered question in the field. Recording responses to noxious stimuli in mutant backgrounds that only have defects in self-avoidance could help determine the functional consequence of overlap. *dab-1* mutants would be an excellent candidate to test.

Time-lapse imaging as a tool for studying development in *C. elegans*

Time-lapse imaging in other model organisms such as zebrafish has been highly useful for characterizing the cell biology of development. Developing a time-lapse imaging protocol was also imperative for my studies. The careful analysis of PVD development with time-lapse imaging defined fundamental aspects of PVD dendritic development that would not have been easily described with static images. For example, time-lapse imaging showed that PVD dendrites develop through an error correction mechanism in which more dendrites are produced during development than are present in the adult (Chapter 2)[12].

Live time-lapse confocal microscopy has also provided invaluable information for my studies of self-avoidance (Chapter 4). Although static images of PVD helped to define the Unc-6 phenotype, it was time-lapse imaging that allowed me to observe the defect in contact-dependent repulsion [241]. In the future it will be important to visualize not only the PVD dendrite during development but also the proteins within the cell. The *C. elegans* PVD neuron is close to the surface of the animal and thus is accessible to TIRF microscopy (Chapter 5). This attribute of PVD has thus far been unique to *in vivo* systems for studying dendritic development. Cell culture models have been useful for studying dendritic morphogenesis but may not accurately replicate *in vivo* dendritic behavior. This caveat does not apply to the PVD neuron which can offer a new and highly useful model for *in vivo* studies of dendritic morphogenesis.

Other studies in neuronal development can also utilize time-lapse imaging. Because *C. elegans* is transparent, all neurons in the animal are accessible to confocal microscopy. Similarly, just as many aspects of PVD development are dynamic, so likely are other neuronal developmental phenomena. Preliminary results with our collaborator suggests that the NSM neuron in *C. elegans* also exhibits dynamic branching during a specific developmental period (Daniel Colón-Ramos and Smith, unpublished data). This dynamic branching, as with PVD, was not appreciated in static images of the neuron during development.

Watching the remodeling of *C. elegans* neurons is an additional intriguing use of time-lapse imaging. A subset of GABAergic neurons remodel during development of *C. elegans [277]*. Synapses normally form on the ventral side early in development. In adults, these synapses are absent from the ventral side and are dorsally located instead. Interesting, the morphology of the neuron remains unchanged during this process. Are synapses removed from the ventral side, trafficked along the commissures and then placed on the dorsal side? Alternatively, synapses on the ventral side could be degraded and new synapses could be built on the dorsal side. Time-lapse imaging would be invaluable in understanding this phenomenon. In fact, time-lapse imaging was recently utilized to show that some proteins from ventral synapses are recycled to the dorsal side [278]. The detailed description of GABAergic remodeling with time-lapse imaging could be helpful to characterize potential phenotypes that arise in genetic mutants.

Thus, it is clear that the transparency of *C. elegans,* the ease of producing transgenic animals and the sophisticated fluorescent tagging of cellular components makes *C. elegans* an ideal system for using time-lapse imaging to define and characterize development. It will be important to utilize these techniques for future studies.

BIBLIOGRAPHY

1. Tahirovic S, Bradke F: Neuronal polarity. *Cold Spring Harbor perspectives in biology* 2009, 1:a001644.

2. Kolodkin AL, Tessier-Lavigne M: Mechanisms and Molecules of Neuronal Wiring: A Primer. *Cold Spring Harbor perspectives in biology* 2011, 3:a001727-a001727.

3. Jan Y, Jan L: The control of dendrite development. *Neuron* 2003, 40:229-242.

4. Corty M, Matthews B, Grueber W: Molecules and mechanisms of dendrite development in Drosophila. *Development* 2009, 136:1049-1061.

5. Horton AC, Ehlers MD: Neuronal polarity and trafficking. *Neuron* 2003, 40:277-295.

6. Gao F: Molecular and cellular mechanisms of dendritic morphogenesis. *Curr Opin Neurobiol* 2007, 17:525-532.

7. Garcia-Lopez P, Garcia-Marin V, Freire M: The histological slides and drawings of cajal. *Frontiers in neuroanatomy* 2010, 4:9.

8. Masland RH: Neuronal cell types. *Current biology : CB* 2004, 14:R497-500.

9. Grueber WB, Jan LY, Jan YN: Tiling of the Drosophila epidermis by multidendritic sensory neurons. *Development* 2002, 129:2867-2878.

10. Sweeney NT, Li W, Gao FB: Genetic manipulation of single neurons in vivo reveals specific roles of flamingo in neuronal morphogenesis. *Developmental Biology* 2002, 247:76-88.

11. Tsalik E: LIM homeobox gene-dependent expression of biogenic amine receptors in restricted regions of the C. elegans nervous system. *Developmental Biology* 2003, 263:81-102.

12. Smith CJ, Watson JD, Spencer WC, O'brien T, Cha B, Albeg A, Treinin M, Iii DMM: Time-lapse imaging and cell-specific expression profiling reveal dynamic branching and molecular determinants of a multi-dendritic nociceptor in C. elegans. *Developmental Biology* 2010, 345:18-33.

13. Parrish J, Kim M, Jan L, Jan Y: Genome-wide analyses identify transcription factors required for proper morphogenesis of Drosophila sensory neuron dendrites. *Genes Dev* 2006, 20:820-835.

14. Moore AW, Jan LY, Jan YN: hamlet, a binary genetic switch between single- and multiple- dendrite neuron morphology. *Science* 2002, 297:1355-1358.

15. Li W, Wang F, Menut L, Gao FB: BTB/POZ-zinc finger protein abrupt suppresses dendritic branching in a neuronal subtype-specific and dosage-dependent manner. *Neuron* 2004, 43:823-834.

16. Crozatier M, Vincent A: Control of multidendritic neuron differentiation in Drosophila: the role of Collier. *Developmental Biology* 2008, 315:232-242.

17. Hattori Y, Sugimura K, Uemura T: Selective expression of Knot/Collier, a transcriptional regulator of the EBF/Olf-1 family, endows the Drosophila sensory system with neuronal class-specific elaborated dendritic patterns. *Genes to cells : devoted to molecular & cellular mechanisms* 2007, 12:1011-1022.

18. Jinushi-Nakao S, Arvind R, Amikura R, Kinameri E, Liu A, Moore A: Knot/Collier and cut control different aspects of dendrite cytoskeleton and synergize to define final arbor shape. *Neuron* 2007, 56:963-978.

19. Blochlinger K, Bodmer R, Jan LY, Jan YN: Patterns of expression of cut, a protein required for external sensory organ development in wild-type and cut mutant Drosophila embryos. *Genes & development* 1990, 4:1322-1331.

20. Grueber WB, Jan LY, Jan YN: Different levels of the homeodomain protein cut regulate distinct dendrite branching patterns of Drosophila multidendritic neurons. *Cell* 2003, 112:805-818.

21. Sugimura K, Yamamoto M, Niwa R, Satoh D, Goto S, Taniguchi M, Hayashi S, Uemura T: Distinct developmental modes and lesion-induced reactions of dendrites of two classes of Drosophila sensory neurons. *The Journal of neuroscience : the official journal of the Society for Neuroscience* 2003, 23:3752-3760.

22. Cubelos B, Sebastian-Serrano A, Beccari L, Calcagnotto ME, Cisneros E, Kim S, Dopazo A, Alvarez-Dolado M, Redondo JM, Bovolenta P, et al: Cux1 and Cux2 regulate dendritic branching, spine morphology, and synapses of the upper layer neurons of the cortex. *Neuron* 2010, 66:523-535.

23. Kim MD, Jan LY, Jan YN: The bHLH-PAS protein Spineless is necessary for the diversification of dendrite morphology of Drosophila dendritic arborization neurons. *Genes & Development* 2006, 20:2806-2819.

24. Sulkowski MJ, Iyer SC, Kurosawa MS, Iyer EP, Cox DN: Turtle functions downstream of Cut in differentially regulating class specific dendrite morphogenesis in Drosophila. *PLoS ONE* 2011, 6:e22611.

25. Ainsley JA, Pettus JM, Bosenko D, Gerstein CE, Zinkevich N, Anderson MG, Adams CM, Welsh MJ, Johnson WA: Enhanced Locomotion Caused by Loss of the Drosophila DEG/ENaC Protein Pickpocket1. *Current Biology* 2003, 13:1557-1563.

26. Gaudilliere B, Konishi Y, de la Iglesia N, Yao G, Bonni A: A CaMKII-NeuroD signaling pathway specifies dendritic morphogenesis. *Neuron* 2004, 41:229-241.

27. Aizawa H, Hu SC, Bobb K, Balakrishnan K, Ince G, Gurevich I, Cowan M, Ghosh A: Dendrite development regulated by CREST, a calcium-regulated transcriptional activator. *Science* 2004, 303:197-202.

28. Kidd T, Brose K, Mitchell K, Fetter R, Tessier-Lavigne M, Goodman C, Tear G: Roundabout controls axon crossing of the CNS midline and defines a novel subfamily of evolutionarily conserved guidance receptors. *Cell* 1998, 92:205-215.

29. Li HS, Chen JH, Wu W, Fagaly T, Zhou L, Yuan W, Dupuis S, Jiang ZH, Nash W, Gick C, et al: Vertebrate slit, a secreted ligand for the transmembrane protein roundabout, is a repellent for olfactory bulb axons. *Cell* 1999, 96:807-818.

30. Brose K, Bland KS, Wang KH, Arnott D, Henzel W, Goodman CS, Tessier-Lavigne M, Kidd T: Slit proteins bind Robo receptors and have an evolutionarily conserved role in repulsive axon guidance. *Cell* 1999, 96:795-806.

31. Kidd T, Bland KS, Goodman CS: Slit is the midline repellent for the robo receptor in Drosophila. *Cell* 1999, 96:785-794.

32. Zallen JA, Yi BA, Bargmann CI: The conserved immunoglobulin superfamily member SAX-3/Robo directs multiple aspects of axon guidance in C. elegans. *Cell* 1998, 92:217-227.

33. Hao JC, Yu TW, Fujisawa K, Culotti JG, Gengyo-Ando K, Mitani S, Moulder G, Barstead R, Tessier-Lavigne M, Bargmann CI: C. elegans slit acts in midline, dorsal-ventral, and anterior-posterior guidance via the SAX-3/Robo receptor. *Neuron* 2001, 32:25-38.

34. Wang KH, Brose K, Arnott D, Kidd T, Goodman CS, Henzel W, Tessier-Lavigne M: Biochemical purification of a mammalian slit protein as a

positive regulator of sensory axon elongation and branching. *Cell* 1999, 96:771-784.

35. Sabatier C, Plump AS, Le M, Brose K, Tamada A, Murakami F, Lee EY, Tessier-Lavigne M: The divergent Robo family protein rig-1/Robo3 is a negative regulator of slit responsiveness required for midline crossing by commissural axons. *Cell* 2004, 117:157-169.

36. Stein E, Tessier-Lavigne M: Hierarchical organization of guidance receptors: silencing of netrin attraction by slit through a Robo/DCC receptor complex. *Science* 2001, 291:1928-1938.

37. Yazdani U, Terman JR: The semaphorins. *Genome Biology* 2006, 7:211.

38. Kolodkin AL, Matthes DJ, O'Connor TP, Patel NH, Admon A, Bentley D, Goodman CS: Fasciclin IV: sequence, expression, and function during growth cone guidance in the grasshopper embryo. *Neuron* 1992, 9:831-845.

39. Luo Y, Raible D, Raper JA: Collapsin: a protein in brain that induces the collapse and paralysis of neuronal growth cones. *Cell* 1993, 75:217-227.

40. Tran TS, Kolodkin AL, Bharadwaj R: Semaphorin regulation of cellular morphology. *Annual review of cell and developmental biology* 2007, 23:263-292.

41. Tamagnone L, Comoglio PM: Signalling by semaphorin receptors: cell guidance and beyond. *Trends in Cell Biology* 2000, 10:377-383.

42. Hedgecock E, Culotti J, Hall D: The unc-5, unc-6, and unc-40 genes guide circumferential migrations of pioneer axons and mesodermal cells on the epidermis in C. elegans. *Neuron* 1990, 4:61-85.

43. Ishii N, Wadsworth W, Stern B, Culotti J, Hedgecock E: UNC-6, a laminin-related protein, guides cell and pioneer axon migrations in C. elegans. *Neuron* 1992, 9:873-881.

44. Kennedy TE, Serafini T, de la Torre JR, Tessier-Lavigne M: Netrins are diffusible chemotropic factors for commissural axons in the embryonic spinal cord. *Cell* 1994, 78:425-435.

45. Serafini T, Kennedy T, Galko M, Mirzayan C, Jessell T, Tessier-Lavigne M: The netrins define a family of axon outgrowth-promoting proteins homologous to C. elegans UNC-6. *Cell* 1994, 78:409-424.

46. Harris R, Sabatelli LM, Seeger MA: Guidance cues at the Drosophila CNS midline: identification and characterization of two Drosophila Netrin/UNC-6 homologs. *Neuron* 1996, 17:217-228.

47. Mitchell K, Doyle J, Serafini T, Kennedy T, Tessier-Lavigne M, Goodman C, Dickson B: Genetic analysis of Netrin genes in Drosophila: Netrins guide CNS commissural axons and peripheral motor axons. *Neuron* 1996, 17:203-215.

48. Chan S, Zheng H, Su M, Wilk R, Killeen M, Hedgecock E, Culotti J: UNC-40, a C. elegans homolog of DCC (Deleted in Colorectal Cancer), is required in motile cells responding to UNC-6 netrin cues. *Cell* 1996, 87:187-195.

49. Keino-Masu K, Masu M, Hinck L, Leonardo ED, Chan SS, Culotti JG, Tessier-Lavigne M: Deleted in Colorectal Cancer (DCC) encodes a netrin receptor. *Cell* 1996, 87:175-185.

50. Kolodziej P, Timpe L, Mitchell K, Fried S, Goodman C, Jan L, Jan Y: frazzled encodes a Drosophila member of the DCC immunoglobulin subfamily and is required for CNS and motor axon guidance. *Cell* 1996, 87:197-204.

51. Leung-Hagesteijn C, Spence A, Stern B, Zhou Y, Su M, Hedgecock E, Culotti J: UNC-5, a transmembrane protein with immunoglobulin and thrombospondin type 1 domains, guides cell and pioneer axon migrations in C. elegans. *Cell* 1992, 71:289-299.

52. Leonardo E, Hinck L, Masu M, Keino-Masu K, Ackerman S, Tessier-Lavigne M: Vertebrate homologues of C. elegans UNC-5 are candidate netrin receptors. *Nature* 1997, 386:833-838.

53. Hong K, Hinck L, Nishiyama M, Poo M, Tessier-Lavigne M, Stein E: A ligand-gated association between cytoplasmic domains of UNC5 and DCC family receptors converts netrin-induced growth cone attraction to repulsion. *Cell* 1999, 97:927-941.

54. Keleman K, Dickson B: Short- and long-range repulsion by the Drosophila Unc5 netrin receptor. *Neuron* 2001, 32:605-617.

55. Brankatschk M, Dickson BJ: Netrins guide Drosophila commissural axons at short range. *Nature Neuroscience* 2006, 9:188-194.

56. Colon-Ramos D, Margeta M, Shen K: Glia promote local synaptogenesis through UNC-6 (netrin) signaling in C. elegans. *Science* 2007, 318:103-106.

57. Teichmann HM, Shen K: UNC-6 and UNC-40 promote dendritic growth through PAR-4 in Caenorhabditis elegans neurons. *Nature Neuroscience* 2010:1-9.

58. Park J, Knezevich PL, Wung W, O'Hanlon SN, Goyal A, Benedetti KL, Barsi-Rhyne BJ, Raman M, Mock N, Bremer M, Vanhoven MK: A conserved juxtacrine signal regulates synaptic partner recognition in Caenorhabditis elegans. *Neural development* 2011, 6:28.

59. Hiramoto M, Hiromi Y, Giniger E, Hotta Y: The Drosophila Netrin receptor Frazzled guides axons by controlling Netrin distribution. *Nature* 2000, 406:886-889.

60. Klein R: Eph/ephrin signaling in morphogenesis, neural development and plasticity. *Current Opinion in Cell Biology* 2004, 16:580-589.

61. Feldheim DA, O'Leary DD: Visual map development: bidirectional signaling, bifunctional guidance molecules, and competition. *Cold Spring Harbor perspectives in biology* 2010, 2:a001768.

62. Marquardt T, Shirasaki R, Ghosh S, Andrews S, Carter N, Hunter T, Pfaff S: Coexpressed EphA receptors and ephrin-A ligands mediate opposing actions on growth cone navigation from distinct membrane domains. *Cell* 2005, 121:127-139.

63. Shen K, Cowan CW: Guidance molecules in synapse formation and plasticity. *Cold Spring Harbor perspectives in biology* 2010, 2:a001842.

64. Polleux F, Morrow T, Ghosh A: Semaphorin 3A is a chemoattractant for cortical apical dendrites. *Nature* 2000, 404:567-573.

65. Komiyama T, Sweeney LB, Schuldiner O, Garcia KC, Luo L: Graded expression of semaphorin-1a cell-autonomously directs dendritic targeting of olfactory projection neurons. *Cell* 2007, 128:399-410.

66. Furrer M, Kim S, Wolf B, Chiba A: Robo and Frazzled/DCC mediate dendritic guidance at the CNS midline. *Nat Neurosci* 2003, 6:223-230.

67. Suli A, Mortimer N, Shepherd I, Chien C: Netrin/DCC signaling controls contralateral dendrites of octavolateralis efferent neurons. *The Journal of neuroscience : the official journal of the Society for Neuroscience* 2006, 26:13328-13337.

68. Dent EW, Gupton SL, Gertler FB: The Growth Cone Cytoskeleton in Axon Outgrowth and Guidance. *Cold Spring Harbor perspectives in biology* 2011, 3:a001800-a001800.

69. Fleming T, Chien S-C, Vanderzalm PJ, Dell M, Gavin MK, Forrester WC, Garriga G: The role of C. elegans Ena/VASP homolog UNC-34 in neuronal polarity and motility. *Developmental Biology* 2010, 344:94-106.

70. Breitsprecher D, Kiesewetter AK, Linkner J, Vinzenz M, Stradal TEB, Small JV, Curth U, Dickinson RB, Faix J: Molecular mechanism of Ena/VASP-mediated actin-filament elongation. *The EMBO journal* 2011.

71. Krause M, Dent E, Bear J, Loureiro J, Gertler F: Ena/VASP proteins: regulators of the actin cytoskeleton and cell migration. *Annu Rev Cell Dev Biol* 2003, 19:541-564.

72. Liebl EC, Forsthoefel DJ, Franco LS, Sample SH, Hess JE, Cowger JA, Chandler MP, Shupert AM, Seeger MA: Dosage-sensitive, reciprocal genetic interactions between the Abl tyrosine kinase and the putative GEF trio reveal trio's role in axon pathfinding. *Neuron* 2000, 26:107-118.

73. Li X, Meriane M, Triki I, Shekarabi M, Kennedy TE, Larose L, Lamarche-Vane N: The adaptor protein Nck-1 couples the netrin-1 receptor DCC (deleted in colorectal cancer) to the activation of the small GTPase Rac1 through an atypical mechanism. *The Journal of biological chemistry* 2002, 277:37788-37797.

74. Shekarabi M, Moore SW, Tritsch NX, Morris SJ, Bouchard JF, Kennedy TE: Deleted in colorectal cancer binding netrin-1 mediates cell substrate adhesion and recruits Cdc42, Rac1, Pak1, and N-WASP into an intracellular signaling complex that promotes growth cone expansion. *The Journal of neuroscience : the official journal of the Society for Neuroscience* 2005, 25:3132-3141.

75. Chang C, Adler C, Krause M, Clark S, Gertler F, Tessier-Lavigne M, Bargmann C: MIG-10/lamellipodin and AGE-1/PI3K promote axon guidance and outgrowth in response to slit and netrin. *Current biology : CB* 2006, 16:854-862.

76. Quinn C, Pfeil D, Chen E, Stovall E, Harden M, Gavin M, Forrester W, Ryder E, Soto M, Wadsworth W: UNC-6/netrin and SLT-1/slit guidance cues orient axon outgrowth mediated by MIG-10/RIAM/lamellipodin. *Current biology : CB* 2006, 16:845-853.

77. Krause M, Leslie J, Stewart M, Lafuente E, Valderrama F, Jagannathan R, Strasser G, Rubinson D, Liu H, Way M, et al: Lamellipodin, an Ena/VASP

ligand, is implicated in the regulation of lamellipodial dynamics. *Dev Cell* 2004, 7:571-583.

78. Quinn C, Pfeil D, Wadsworth W: CED-10/Rac1 mediates axon guidance by regulating the asymmetric distribution of MIG-10/lamellipodin. *Current biology : CB* 2008, 18:808-813.

79. Round J, Stein E: Netrin signaling leading to directed growth cone steering. *Curr Opin Neurobiol* 2007, 17:15-21.

80. Wu X, Suetsugu S, Cooper LA, Takenawa T, Guan JL: Focal adhesion kinase regulation of N-WASP subcellular localization and function. *The Journal of biological chemistry* 2004, 279:9565-9576.

81. Lee J, Li W, Guan K: SRC-1 mediates UNC-5 signaling in Caenorhabditis elegans. *Mol Cell Biol* 2005, 25:6485-6495.

82. Drees F, Gertler FB: Ena/VASP: proteins at the tip of the nervous system. *Current Opinion in Neurobiology* 2008, 18:53-59.

83. Mallavarapu A, Mitchison T: Regulated actin cytoskeleton assembly at filopodium tips controls their extension and retraction. *The Journal of Cell Biology* 1999, 146:1097-1106.

84. Kubo T, Endo M, Hata K, Taniguchi J, Kitajo K, Tomura S, Yamaguchi A, Mueller BK, Yamashita T: Myosin IIA is required for neurite outgrowth inhibition produced by repulsive guidance molecule. *Journal of neurochemistry* 2008, 105:113-126.

85. Lin CH, Espreafico EM, Mooseker MS, Forscher P: Myosin drives retrograde F-actin flow in neuronal growth cones. *Neuron* 1996, 16:769-782.

86. Hong K, Nishiyama M, Henley J, Tessier-Lavigne M, Poo M: Calcium signalling in the guidance of nerve growth by netrin-1. *Nature* 2000, 403:93-98.

87. Jin M, Guan CB, Jiang YA, Chen G, Zhao CT, Cui K, Song YQ, Wu CP, Poo MM, Yuan XB: Ca2+-dependent regulation of rho GTPases triggers turning of nerve growth cones. *The Journal of neuroscience : the official journal of the Society for Neuroscience* 2005, 25:2338-2347.

88. Yamamoto H, Fukunaga K, Goto S, Tanaka E, Miyamoto E: Ca2+, calmodulin-dependent regulation of microtubule formation via phosphorylation of microtubule-associated protein 2, tau factor, and

tubulin, and comparison with the cyclic AMP-dependent phosphorylation. *Journal of neurochemistry* 1985, 44:759-768.

89. Duch C, Vonhoff F, Ryglewski S: Dendrite elongation and dendritic branching are affected separately by different forms of intrinsic motoneuron excitability. *Journal of Neurophysiology* 2008, 100:2525-2536.

90. Hartwig CL, Worrell J, Levine RB, Ramaswami M, Sanyal S: Normal dendrite growth in Drosophila motor neurons requires the AP-1 transcription factor. *Developmental Neurobiology* 2008, 68:1225-1242.

91. Tripodi M, Evers JF, Mauss A, Bate M, Landgraf M: Structural homeostasis: compensatory adjustments of dendritic arbor geometry in response to variations of synaptic input. *PLoS biology* 2008, 6:e260.

92. McAllister AK: Cellular and molecular mechanisms of dendrite growth. *Cerebral cortex* 2000, 10:963-973.

93. Kwon H-B, Sabatini BL: Glutamate induces de novo growth of functional spines in developing cortex. *Nature* 2011, 474:100-104.

94. Amthor FR, Oyster CW: Spatial organization of retinal information about the direction of image motion. *Proceedings of the National Academy of Sciences of the United States of America* 1995, 92:4002-4005.

95. Grueber WB, Ye B, Moore AW, Jan LY, Jan YN: Dendrites of distinct classes of Drosophila sensory neurons show different capacities for homotypic repulsion. *Current biology : CB* 2003, 13:618-626.

96. Sagasti A, Guido MR, Raible DW, Schier AF: Repulsive interactions shape the morphologies and functional arrangement of zebrafish peripheral sensory arbors. *Current biology : CB* 2005, 15:804-814.

97. Kramer AP, Kuwada JY: Formation of the receptive fields of leech mechanosensory neurons during embryonic development. *The Journal of neuroscience : the official journal of the Society for Neuroscience* 1983, 3:2474-2486.

98. Garcia-Lopez P, Garcia-Marin V, Martinez-Murillo R, Freire M: Cajals achievements in the field of the development of dendritic arbors. *The International journal of developmental biology* 2010, 54:1405-1417.

99. Hughes M, Bortnick R, Tsubouchi A, Baumer P, Kondo M, Uemura T, Schmucker D: Homophilic Dscam interactions control complex dendrite morphogenesis. *Neuron* 2007, 54:417-427.

100. Matthews B, Kim M, Flanagan J, Hattori D, Clemens J, Zipursky S, Grueber W: Dendrite self-avoidance is controlled by Dscam. *Cell* 2007, 129:593-604.

101. Agarwala K, Nakamura S, Tsutsumi Y, Yamakawa K: Down syndrome cell adhesion molecule DSCAM mediates homophilic intercellular adhesion. *Brain Res Mol Brain Res* 2000, 79:118-126.

102. Schmucker D, Clemens J, Shu H, Worby C, Xiao J, Muda M, Dixon J, Zipursky S: Drosophila Dscam is an axon guidance receptor exhibiting extraordinary molecular diversity. *Cell* 2000, 101:671-684.

103. Hattori D, Demir E, Kim H, Viragh E, Zipursky S, Dickson B: Dscam diversity is essential for neuronal wiring and self-recognition. *Nature* 2007, 449:223-227.

104. Fuerst P, Koizumi A, Masland R, Burgess R: Neurite arborization and mosaic spacing in the mouse retina require DSCAM. *Nature* 2008, 451:470-474.

105. Long H, Ou Y, Rao Y, van Meyel D: Dendrite branching and self-avoidance are controlled by Turtle, a conserved IgSF protein in Drosophila. *Development* 2009, 136:3475-3484.

106. Matsubara D, Horiuchi Sy, Shimono K, Usui T, Uemura T: The seven-pass transmembrane cadherin Flamingo controls dendritic self-avoidance via its binding to a LIM domain protein, Espinas, in Drosophila sensory neurons. *Genes & Development* 2011, 25:1982-1996.

107. Han C, Wang D, Soba P, Zhu S, Lin X, Jan LY, Jan Y-N: Integrins Regulate Repulsion-Mediated Dendritic Patterning of Drosophila Sensory Neurons by Restricting Dendrites in a 2D Space. *Neuron* 2012, 73:64-78.

108. Kim ME, Shrestha BR, Blazeski R, Mason CA, Grueber WB: Integrins Establish Dendrite-Substrate Relationships that Promote Dendritic Self-Avoidance and Patterning in Drosophila Sensory Neurons. *Neuron* 2012, 73:79-91.

109. Zipursky SL, Sanes JR: Chemoaffinity Revisited: Dscams, Protocadherins, and Neural Circuit Assembly. *Cell* 2010, 143:343-353.

110. Emoto K, He Y, Ye B, Grueber WB, Adler PN, Jan LY, Jan Y-N: Control of dendritic branching and tiling by the Tricornered-kinase/Furry signaling pathway in Drosophila sensory neurons. *Cell* 2004, 119:245-256.

111. Emoto K, Parrish J, Jan L, Jan Y-N: The tumour suppressor Hippo acts with the NDR kinases in dendritic tiling and maintenance. *Nature* 2006, 443:210-213.

112. Gao F, Brenman J, Jan L, Jan Y: Genes regulating dendritic outgrowth, branching, and routing in Drosophila. *Genes Dev* 1999, 13:2549-2561.
113. Gao F, Kohwi M, Brenman J, Jan L, Jan Y: Control of dendritic field formation in Drosophila: the roles of flamingo and competition between homologous neurons. *Neuron* 2000, 28:91-101.

114. Kimura H, Usui T, Tsubouchi A, Uemura T: Potential dual molecular interaction of the Drosophila 7-pass transmembrane cadherin Flamingo in dendritic morphogenesis. *Journal of Cell Science* 2006, 119:1118-1129.

115. Li W, Gao FB: Actin filament-stabilizing protein tropomyosin regulates the size of dendritic fields. *The Journal of neuroscience : the official journal of the Society for Neuroscience* 2003, 23:6171-6175.

116. Shima Y, Kawaguchi SY, Kosaka K, Nakayama M, Hoshino M, Nabeshima Y, Hirano T, Uemura T: Opposing roles in neurite growth control by two seven-pass transmembrane cadherins. *Nature Neuroscience* 2007, 10:963-969.

117. Gallegos ME, Bargmann CI: Mechanosensory neurite termination and tiling depend on SAX-2 and the SAX-1 kinase. *Neuron* 2004, 44:239-249.

118. Chalfie M, Sulston J: Developmental genetics of the mechanosensory neurons of Caenorhabditis elegans. *Developmental Biology* 1981, 82:358-370.

119. Sulston J, Horvitz H: Post-embryonic cell lineages of the nematode, Caenorhabditis elegans. *Dev Biol* 1977, 56:110-156.

120. Chalfie M, Thomson JN: Organization of neuronal microtubules in the nematode Caenorhabditis elegans. *The Journal of Cell Biology* 1979, 82:278-289.

121. White JG, Southgate E, Thomson JN, Brenner S: The structure of the nervous system of the nematode Caenorhabditis elegans. *Philosophical transactions of the Royal Society of London Series B, Biological sciences* 1986, 314:1-340.

122. O'Hagan R, Chalfie M, Goodman MB: The MEC-4 DEG/ENaC channel of Caenorhabditis elegans touch receptor neurons transduces mechanical signals. *Nature Neuroscience* 2005, 8:43-50.

123. Way J, Chalfie M: The mec-3 gene of Caenorhabditis elegans requires its own product for maintained expression and is expressed in three neuronal cell types. *Genes Dev* 1989, 3:1823-1833.

124. Chatzigeorgiou M, Yoo S, Watson JD, Lee W-H, Spencer WC, Kindt KS, Hwang SW, Iii DMM, Treinin M, Driscoll M, Schafer WR: Specific roles for DEG/ENaC and TRP channels in touch and thermosensation in C. elegans nociceptors. *Nature Publishing Group* 2010, 13:861-868.

125. Albeg A, Smith CJ, Chatzigeorgiou M, Feitelson DG, Hall DH, Schafer WR, Miller DM, Treinin M: C. elegans multi-dendritic sensory neurons: Morphology and function. *Mol Cell Neurosci* 2010.

126. Yassin L, Gillo B, Kahan T, Halevi S, Eshel M, Treinin M: Characterization of the deg-3/des-2 receptor: a nicotinic acetylcholine receptor that mutates to cause neuronal degeneration. *Mol Cell Neurosci* 2001, 17:589-599.

127. Halevi S, McKay J, Palfreyman M, Yassin L, Eshel M, Jorgensen E, Treinin M: The C. elegans ric-3 gene is required for maturation of nicotinic acetylcholine receptors. *EMBO J* 2002, 21:1012-1020.

128. Husson SJ, Costa WS, Wabnig S, Stirman JN, Watson JD, Spencer WC, Akerboom J, Looger LL, Treinin M, Miller DM, 3rd, et al: Optogenetic analysis of a nociceptor neuron and network reveals ion channels acting downstream of primary sensors. *Current biology : CB* 2012, 22:743-752.

129. Jarman AP: Studies of mechanosensation using the fly. *Human molecular genetics* 2002, 11:1215-1218.

130. Kernan M, Cowan D, Zuker C: Genetic dissection of mechanosensory transduction: mechanoreception-defective mutations of Drosophila. *Neuron* 1994, 12:1195-1206.

131. Lumpkin EA, Marshall KL, Nelson AM: The cell biology of touch. *The Journal of Cell Biology* 2010, 191:237-248.

132. Kernan MJ: Mechanotransduction and auditory transduction in Drosophila. *Pflugers Archiv : European journal of physiology* 2007, 454:703-720.

133. Zhong L, Hwang RY, Tracey WD: Pickpocket is a DEG/ENaC protein required for mechanical nociception in Drosophila larvae. *Current biology : CB* 2010, 20:429-434.

134. Tracey WD, Jr., Wilson RI, Laurent G, Benzer S: painless, a Drosophila gene essential for nociception. *Cell* 2003, 113:261-273.

135. Kim SE, Coste B, Chadha A, Cook B, Patapoutian A: The role of Drosophila Piezo in mechanical nociception. *Nature* 2012, 483:209-212.

136. Fero K, Yokogawa T, Burgess H, al e: The behavioral repertoire of larval zebrafish. *Neuromethods* 2011.

137. Drapeau P, Saint-Amant L, Buss R, al e: Development of the locomotor network in zebrafish. *Progress in …* 2002.

138. Clarke JD, Hayes BP, Hunt SP, Roberts A: Sensory physiology, anatomy and immunohistochemistry of Rohon-Beard neurones in embryos of Xenopus laevis. *The Journal of physiology* 1984, 348:511-525.

139. Kucenas S, Soto F, Cox J, Voigt M: Selective labeling of central and peripheral sensory neurons in the developing zebrafish using P2X(3) receptor subunit transgenes. *Neuroscience* 2006, 138:641-652.

140. Hall DH, Treinin M: How does morphology relate to function in sensory arbors? *Trends in Neurosciences* 2011, 34:443-451.

141. Humphrey T: Primitive neurons in the embryonic human central nervous system. *The Journal of Comparative Neurology* 1944, 81:1-45.

142. Humphrey T: Intramedullary sensory ganglion cells in the roof plate area of the embryonic human spinal cord. *The Journal of Comparative Neurology* 1950, 92:333-399.

143. Lamborghini JE: Disappearance of Rohon-Beard neurons from the spinal cord of larval Xenopus laevis. *The Journal of Comparative Neurology* 1987, 264:47-55.

144. Williams JA, Barrios A, Gatchalian C, Rubin L, Wilson SW, Holder N: Programmed cell death in zebrafish rohon beard neurons is influenced by TrkC1/NT-3 signaling. *Developmental Biology* 2000, 226:220-230.

145. Moorman SJ: Development of sensory systems in zebrafish (Danio rerio). *ILAR journal / National Research Council, Institute of Laboratory Animal Resources* 2001, 42:292-298.

146. Bautista DM, Lumpkin EA: Perspectives on: information and coding in mammalian sensory physiology: probing mammalian touch transduction. *The Journal of general physiology* 2011, 138:291-301.

147. Smith ES, Lewin GR: Nociceptors: a phylogenetic view. *Journal of comparative physiology A, Neuroethology, sensory, neural, and behavioral physiology* 2009, 195:1089-1106.

148. McGlone F, Reilly D: The cutaneous sensory system. *Neurosci Biobehav Rev* 2010, 34:148-159.

149. Blackshaw SE, Nicholls JG, Parnas I: Physiological responses, receptive fields and terminal arborizations of nociceptive cells in the leech. *J Physiol* 1982, 326:251-260.

150. Garel S, Yun K, Grosschedl R, Rubenstein JL: The early topography of thalamocortical projections is shifted in Ebf1 and Dlx1/2 mutant mice. *Development* 2002, 129:5621-5634.

151. Temple S: Division and differentiation of isolated CNS blast cells in microculture. *Nature* 1989, 340:471-473.

152. Bartlett WP, Banker GA: An electron microscopic study of the development of axons and dendrites by hippocampal neurons in culture. I. Cells which develop without intercellular contacts. *J Neurosci* 1984, 4:1944-1953.

153. Scott EK, Luo L: How do dendrites take their shape? *Nature Neuroscience* 2001, 4:359-365.

154. Tobin D, Madsen D, Kahn-Kirby A, Peckol E, Moulder G, Barstead R, Maricq A, Bargmann C: Combinatorial expression of TRPV channel proteins defines their sensory functions and subcellular localization in C. elegans neurons. *Neuron* 2002, 35:307-318.

155. Wittenburg N, Baumeister R: Thermal avoidance in Caenorhabditis elegans: an approach to the study of nociception. *Proc Natl Acad Sci U S A* 1999, 96:10477-10482.

156. Roy PJ, Stuart JM, Lund J, Kim SK: Chromosomal clustering of muscle-expressed genes in Caenorhabditis elegans. *Nature* 2002, 418:975-979.

157. Von Stetina S, Watson J, Fox R, Olszewski K, Spencer W, Roy P, Miller D: Cell-specific microarray profiling experiments reveal a comprehensive picture of gene expression in the C. elegans nervous system. *Genome Biol* 2007, 8:R135.

158. Brenner S: The genetics of Caenorhabditis elegans. *Genetics* 1974, 77:71-94.

159. Gabel CV, Antonie F, Chuang CF, Samuel AD, Chang C: Distinct cellular and molecular mechanisms mediate initial axon development and adult-

stage axon regeneration in C. elegans. *Development* 2008, 135:1129-1136.

160. Inoue T, Wang M, Ririe T, Fernandes J, Sternberg P: Transcriptional network underlying Caenorhabditis elegans vulval development. *Proc Natl Acad Sci U S A* 2005, 102:4972-4977.

161. Von Stetina S, Fox R, Watkins K, Starich T, Shaw J, Miller D: UNC-4 represses CEH-12/HB9 to specify synaptic inputs to VA motor neurons in C. elegans. *Genes Dev* 2007, 21:332-346.

162. Maduro M, Pilgrim D: Identification and cloning of unc-119, a gene expressed in the Caenorhabditis elegans nervous system. *Genetics* 1995, 141:977-988.

163. Watson J, Wang S, Von Stetina S, Spencer W, Levy S, Dexheimer P, Kurn N, Heath J, Miller D: Complementary RNA amplification methods enhance microarray identification of transcripts expressed in the C. elegans nervous system. *BMC Genomics* 2008, 9:84.

164. Fox R, Von Stetina S, Barlow S, Shaffer C, Olszewski K, Moore J, Dupuy D, Vidal M, Miller D: A gene expression fingerprint of C. elegans embryonic motor neurons. *BMC Genomics* 2005, 6:42.

165. Kamath RS, Ahringer J: Genome-wide RNAi screening in Caenorhabditis elegans. *Methods* 2003, 30:313-321.

166. Golden A, O'Connell KF: Silence is golden: combining RNAi and live cell imaging to study cell cycle regulatory genes during Caenorhabditis elegans development. *Methods* 2007, 41:190-197.

167. Yassin L, Samson AO, Halevi S, Eshel M, Treinin M: Mutations in the extracellular domain and in the membrane-spanning domains interfere with nicotinic acetylcholine receptor maturation. *Biochemistry* 2002, 41:12329-12335.

168. Tsalik EL, Hobert O: Functional mapping of neurons that control locomotory behavior in Caenorhabditis elegans. *J Neurobiol* 2003, 56:178-197.

169. Parrish JZ, Emoto K, Kim MD, Jan YN: Mechanisms that regulate establishment, maintenance, and remodeling of dendritic fields. *Annu Rev Neurosci* 2007, 30:399-423.

170. Kaplan JM, Horvitz HR: A dual mechanosensory and chemosensory neuron in Caenorhabditis elegans. *Proc Natl Acad Sci U S A* 1993, 90:2227-2231.

171. Lucanic M, Kiley M, Ashcroft N, L'Etoile N, Cheng HJ: The Caenorhabditis elegans P21-activated kinases are differentially required for UNC-6/netrin-mediated commissural motor axon guidance. *Development* 2006, 133:4549-4559.

172. Kass J, Jacob TC, Kim P, Kaplan JM: The EGL-3 proprotein convertase regulates mechanosensory responses of Caenorhabditis elegans. *J Neurosci* 2001, 21:9265-9272.

173. Wadsworth W, Bhatt H, Hedgecock E: Neuroglia and pioneer neurons express UNC-6 to provide global and local netrin cues for guiding migrations in C. elegans. *Neuron* 1996, 16:35-46.

174. Adler C, Fetter R, Bargmann C: UNC-6/Netrin induces neuronal asymmetry and defines the site of axon formation. *Nature neuroscience* 2006, 9:511-518.

175. Poon V, Klassen M, Shen K: UNC-6/netrin and its receptor UNC-5 locally exclude presynaptic components from dendrites. *Nature* 2008, 455:669-673.

176. Fujisawa K, Wrana JL, Culotti JG: The slit receptor EVA-1 coactivates a SAX-3/Robo mediated guidance signal in C. elegans. *Science* 2007, 317:1934-1938.

177. Eisenmann DM: Wnt signaling. *WormBook : the online review of C elegans biology* 2005:1-17.

178. Wemmie JA, Price MP, Welsh MJ: Acid-sensing ion channels: advances, questions and therapeutic opportunities. *Trends Neurosci* 2006, 29:578-586.

179. Goodman MB, Schwarz EM: Transducing touch in Caenorhabditis elegans. *Annu Rev Physiol* 2003, 65:429-452.

180. Suzuki H, Kerr R, Bianchi L, Frokjaer-Jensen C, Slone D, Xue J, Gerstbrein B, Driscoll M, Schafer WR: In vivo imaging of C. elegans mechanosensory neurons demonstrates a specific role for the MEC-4 channel in the process of gentle touch sensation. *Neuron* 2003, 39:1005-1017.

181. Huang M, Chalfie M: Gene interactions affecting mechanosensory transduction in Caenorhabditis elegans. *Nature* 1994, 367:467-470.

182. Clark SG, Chisholm AD, Horvitz HR: Control of cell fates in the central body region of C. elegans by the homeobox gene lin-39. *Cell* 1993, 74:43-55.

183. Way JC, Chalfie M: mec-3, a homeobox-containing gene that specifies differentiation of the touch receptor neurons in C. elegans. *Cell* 1988, 54:5-16.

184. Clark SG, Chiu C: C. elegans ZAG-1, a Zn-finger-homeodomain protein, regulates axonal development and neuronal differentiation. *Development* 2003, 130:3781-3794.

185. Wacker I, Schwarz V, Hedgecock E, Hutter H: zag-1, a Zn-finger homeodomain transcription factor controlling neuronal differentiation and axon outgrowth in C. elegans. *Development* 2003, 130:3795-3805.

186. Jin Y, Hoskins R, Horvitz HR: Control of type-D GABAergic neuron differentiation by C. elegans UNC-30 homeodomain protein. *Nature* 1994, 372:780-783.

187. Wu J, Duggan A, Chalfie M: Inhibition of touch cell fate by egl-44 and egl-46 in C. elegans. *Genes Dev* 2001, 15:789-802.

188. McGlone F, Spence C: The cutaneous senses: touch, temperature, pain/itch, and pleasure. *Neurosci Biobehav Rev* 2010, 34:145-147.

189. Ferguson K, Long H, Cameron S, Chang WT, Rao Y: The conserved Ig superfamily member Turtle mediates axonal tiling in Drosophila. *J Neurosci* 2009, 29:14151-14159.

190. Sugimura K, Satoh D, Estes P, Crews S, Uemura T: Development of morphological diversity of dendrites in Drosophila by the BTB-zinc finger protein abrupt. *Neuron* 2004, 43:809-822.

191. Baker MW, Macagno ER: In vivo imaging of growth cone and filopodial dynamics: evidence for contact-mediated retraction of filopodia leading to the tiling of sibling processes. *J Comp Neurol* 2007, 500:850-862.

192. Xue D, Tu Y, Chalfie M: Cooperative interactions between the Caenorhabditis elegans homeoproteins UNC-86 and MEC-3. *Science* 1993, 261:1324-1328.

193. Duggan A, Ma C, Chalfie M: Regulation of touch receptor differentiation by the Caenorhabditis elegans mec-3 and unc-86 genes. *Development* 1998, 125:4107-4119.

194. Zhang Y, Ma C, Delohery T, Nasipak B, Foat BC, Bounoutas A, Bussemaker HJ, Kim SK, Chalfie M: Identification of genes expressed in C. elegans touch receptor neurons. *Nature* 2002, 418:331-335.

195. Crews ST, Brenman JE: Spineless provides a little backbone for dendritic morphogenesis. *Genes Dev* 2006, 20:2773-2778.

196. Parrish JZ, Xu P, Kim CC, Jan LY, Jan YN: The microRNA bantam functions in epithelial cells to regulate scaling growth of dendrite arbors in drosophila sensory neurons. *Neuron* 2009, 63:788-802.

197. Komiyama T, Luo L: Intrinsic control of precise dendritic targeting by an ensemble of transcription factors. *Curr Biol* 2007, 17:278-285.

198. Ichikawa H, Mo Z, Xiang M, Sugimoto T: Effect of Brn-3a deficiency on nociceptors and low-threshold mechanoreceptors in the trigeminal ganglion. *Brain Res Mol Brain Res* 2002, 104:240-245.

199. Abrahamsen B, Zhao J, Asante CO, Cendan CM, Marsh S, Martinez-Barbera JP, Nassar MA, Dickenson AH, Wood JN: The cell and molecular basis of mechanical, cold, and inflammatory pain. *Science* 2008, 321:702-705.

200. Zhuo M, Wu G, Wu LJ: Neuronal and microglial mechanisms of neuropathic pain. *Molecular brain* 2011, 4:31.

201. Delmas P, Hao J, Rodat-Despoix L: Molecular mechanisms of mechanotransduction in mammalian sensory neurons. *Nature reviews Neuroscience* 2011, 12:139-153.

202. Tremblay J, Hamet P: Genetics of pain, opioids, and opioid responsiveness. *Metabolism: clinical and experimental* 2010, 59 Suppl 1:S5-8.

203. Flames N, Hobert O: Transcriptional control of the terminal fate of monoaminergic neurons. *Annual review of neuroscience* 2011, 34:153-184.

204. Driscoll M, Chalfie M: The mec-4 gene is a member of a family of Caenorhabditis elegans genes that can mutate to induce neuronal degeneration. *Nature* 1991, 349:588-593.

205. Qin H, Powell-Coffman JA: The Caenorhabditis elegans aryl hydrocarbon receptor, AHR-1, regulates neuronal development. *Developmental Biology* 2004, 270:64-75.

206. Grueber WB, Sagasti A: Self-avoidance and tiling: Mechanisms of dendrite and axon spacing. *Cold Spring Harbor perspectives in biology* 2010, 2:a001750.

207. Topalidou I, Chalfie M: Shared gene expression in distinct neurons expressing common selector genes. *Proceedings of the National Academy of Sciences of the United States of America* 2011, 108:19258-19263.

208. Mitani S, Du H, Hall DH, Driscoll M, Chalfie M: Combinatorial control of touch receptor neuron expression in Caenorhabditis elegans. *Development* 1993, 119:773-783.

209. Treinin M, Gillo B, Liebman L, Chalfie M: Two functionally dependent acetylcholine subunits are encoded in a single Caenorhabditis elegans operon. *Proceedings of the National Academy of Sciences of the United States of America* 1998, 95:15492-15495.

210. Topalidou I, van Oudenaarden A, Chalfie M: Caenorhabditis elegans aristaless/Arx gene alr-1 restricts variable gene expression. *Proceedings of the National Academy of Sciences of the United States of America* 2011, 108:4063-4068.

211. Jan YN, Jan LY: Branching out: mechanisms of dendritic arborization. *Nature reviews Neuroscience* 2010, 11:316-328.

212. Hattori D, Millard S, Wojtowicz W, Zipursky S: Dscam-mediated cell recognition regulates neural circuit formation. *Annu Rev Cell Dev Biol* 2008, 24:597-620.

213. Asakura T, Ogura K, Goshima Y: UNC-6 expression by the vulval precursor cells of Caenorhabditis elegans is required for the complex axon guidance of the HSN neurons. *Dev Biol* 2007, 304:800-810.

214. Killeen M, Tong J, Krizus A, Steven R, Scott I, Pawson T, Culotti J: UNC-5 function requires phosphorylation of cytoplasmic tyrosine 482, but its UNC-40-independent functions also require a region between the ZU-5 and death domains. *Dev Biol* 2002, 251:348-366.

215. Xu Z, Li H, Wadsworth W: The Roles of Multiple UNC-40 (DCC) Receptor-mediated Signals in Determining Neuronal Asymmetry Induced by the UNC-6 (netrin) Ligand. *Genetics* 2009.

216. Oren-Suissa M, Hall DH, Treinin M, Shemer G, Podbilewicz B: The Fusogen EFF-1 Controls Sculpting of Mechanosensory Dendrites. *Science* 2010, 328:1285-1288.

217. Aguirre-Chen C, Bülow HE, Kaprielian Z: C. elegans bicd-1, homolog of the Drosophila dynein accessory factor Bicaudal D, regulates the branching of PVD sensory neuron dendrites. *Development* 2011, 138:507-518.

218. Schwarz V, Pan J, Voltmer-Irsch S, Hutter H: IgCAMs redundantly control axon outgrowth in Caenorhabditis elegans. *Neural development* 2009, 4:13.

219. Yang L, Garbe D, Bashaw G: A frazzled/DCC-dependent transcriptional switch regulates midline axon guidance. *Science* 2009, 324:944-947.

220. Eastman C, Horvitz HR, Jin Y: Coordinated transcriptional regulation of the unc-25 glutamic acid decarboxylase and the unc-47 GABA vesicular transporter by the Caenorhabditis elegans UNC-30 homeodomain protein. *The Journal of neuroscience : the official journal of the Society for Neuroscience* 1999, 19:6225-6234.

221. Bashaw GJ, Goodman CS: Chimeric axon guidance receptors: the cytoplasmic domains of slit and netrin receptors specify attraction versus repulsion. *Cell* 1999, 97:917-926.

222. Hiramoto M, Hiromi Y: ROBO directs axon crossing of segmental boundaries by suppressing responsiveness to relocalized Netrin. *Nature Neuroscience* 2006, 9:58-66.

223. Kuzina I, Song JK, Giniger E: How Notch establishes longitudinal axon connections between successive segments of the Drosophila CNS. *Development* 2011, 138:1839-1849.

224. Alexander M, Chan KK, Byrne AB, Selman G, Lee T, Ono J, Wong E, Puckrin R, Dixon SJ, Roy PJ: An UNC-40 pathway directs postsynaptic membrane extension in Caenorhabditis elegans. *Development* 2009, 136:911-922.

225. MacNeil L, Hardy W, Pawson T, Wrana J, Culotti J: UNC-129 regulates the balance between UNC-40 dependent and independent UNC-5 signaling pathways. *Nature neuroscience* 2009, 12:150-155.

226. Merz DC, Zheng H, Killeen MT, Krizus A, Culotti JG: Multiple signaling mechanisms of the UNC-6/netrin receptors UNC-5 and UNC-40/DCC in vivo. *Genetics* 2001, 158:1071-1080.

227. Yamada KM, Spooner BS, Wessells NK: Ultrastructure and function of growth cones and axons of cultured nerve cells. *The Journal of Cell Biology* 1971, 49:614-635.

228. Ming G, Wong S, Henley J, Yuan X, Song H, Spitzer N, Poo M: Adaptation in the chemotactic guidance of nerve growth cones. *Nature* 2002, 417:411-418.

229. Kapfhammer JP, Raper JA: Interactions between growth cones and neurites growing from different neural tissues in culture. *The Journal of neuroscience : the official journal of the Society for Neuroscience* 1987, 7:1595-1600.

230. Kapfhammer JP, Raper JA: Collapse of growth cone structure on contact with specific neurites in culture. *The Journal of neuroscience : the official journal of the Society for Neuroscience* 1987, 7:201-212.

231. Song HJ, Ming GL, Poo MM: cAMP-induced switching in turning direction of nerve growth cones. *Nature* 1997, 388:275-279.

232. Gertler FB, Doctor JS, Hoffmann FM: Genetic suppression of mutations in the Drosophila abl proto-oncogene homolog. *Science* 1990, 248:857-860.

233. Bashaw G, Kidd T, Murray D, Pawson T, Goodman C: Repulsive axon guidance: Abelson and Enabled play opposing roles downstream of the roundabout receptor. *Cell* 2000, 101:703-715.

234. Gitai Z, Yu T, Lundquist E, Tessier-Lavigne M, Bargmann C: The netrin receptor UNC-40/DCC stimulates axon attraction and outgrowth through enabled and, in parallel, Rac and UNC-115/AbLIM. *Neuron* 2003, 37:53-65.

235. Lebrand C, Dent EW, Strasser GA, Lanier LM, Krause M, Svitkina TM, Borisy GG, Gertler FB: Critical role of Ena/VASP proteins for filopodia formation in neurons and in function downstream of netrin-1. *Neuron* 2004, 42:37-49.

236. Wills Z, Bateman J, Korey CA, Comer A, Van Vactor D: The tyrosine kinase Abl and its substrate enabled collaborate with the receptor phosphatase Dlar to control motor axon guidance. *Neuron* 1999, 22:301-312.

237. Wills Z, Marr L, Zinn K, Goodman CS, Van Vactor D: Profilin and the Abl tyrosine kinase are required for motor axon outgrowth in the Drosophila embryo. *Neuron* 1999, 22:291-299.

238. Kramer A, Goldman J, Stent G: Developmental arborization of sensory neurons in the leech Haementeria ghilianii. I. Origin of natural variations in the branching pattern. *The Journal of neuroscience : the official journal of the Society for Neuroscience* 1985, 5:759-767.

239. Hughes ME, Bortnick R, Tsubouchi A, Baumer P, Kondo M, Uemura T, Schmucker D: Homophilic Dscam interactions control complex dendrite morphogenesis. *Neuron* 2007, 54:417-427.

240. Soba P, Zhu S, Emoto K, Younger S, Yang SJ, Yu HH, Lee T, Jan LY, Jan YN: Drosophila sensory neurons require Dscam for dendritic self-avoidance and proper dendritic field organization. *Neuron* 2007, 54:403-416.

241. Smith CJ, Watson JD, Vanhoven MK, Colon-Ramos DA, Miller DM, 3rd: Netrin (UNC-6) mediates dendritic self-avoidance. *Nature Neuroscience* 2012, 15:731-737.

242. Stavoe AK, Colon-Ramos DA: Netrin instructs synaptic vesicle clustering through Rac GTPase, MIG-10, and the actin cytoskeleton. *The Journal of Cell Biology* 2012, 197:75-88.

243. Klassen MP, Wu YE, Maeder CI, Nakae I, Cueva JG, Lehrman EK, Tada M, Gengyo-Ando K, Wang GJ, Goodman M, et al: An Arf-like Small G Protein, ARL-8, Promotes the Axonal Transport of Presynaptic Cargoes by Suppressing Vesicle Aggregation. *Neuron* 2010, 66:710-723.

244. Piekny AJ: The Caenorhabditis elegans nonmuscle myosin genes nmy-1 and nmy-2 function as redundant components of the let-502/Rho-binding kinase and mel-11/myosin phosphatase pathway during embryonic morphogenesis. *Development* 2003, 130:5695-5704.

245. Li W, Li Y, Gao F: Abelson, enabled, and p120 catenin exert distinct effects on dendritic morphogenesis in Drosophila. *Developmental Dynamics* 2005, 234:512-522.

246. Maniar TA, Kaplan M, Wang GJ, Shen K, Wei L, Shaw JE, Koushika SP, Bargmann CI: UNC-33 (CRMP) and ankyrin organize microtubules and localize kinesin to polarize axon-dendrite sorting. *Nature Neuroscience* 2011:1-11.

247. Andersen EF, Asuri NS, Halloran MC: In vivo imaging of cell behaviors and F-actin reveals LIM-HD transcription factor regulation of peripheral versus central sensory axon development. *Neural Development* 2011, 6:27.

248. Dutta D, Bloor JW, Ruiz-Gomez M, VijayRaghavan K, Kiehart DP: Real-time imaging of morphogenetic movements in Drosophila using Gal4-UAS-driven expression of GFP fused to the actin-binding domain of moesin. *genesis* 2002, 34:146-151.

249. Burkel BM, von Dassow G, Bement WM: Versatile fluorescent probes for actin filaments based on the actin-binding domain of utrophin. *Cell Motility and the Cytoskeleton* 2007, 64:822-832.

250. Steven R, Kubiseski TJ, Zheng H, Kulkarni S, Mancillas J, Ruiz Morales A, Hogue CW, Pawson T, Culotti J: UNC-73 activates the Rac GTPase and is required for cell and growth cone migrations in C. elegans. *Cell* 1998, 92:785-795.

251. Song JK, Kannan R, Merdes G, Singh J, Mlodzik M, Giniger E: Disabled is a bona fide component of the Abl signaling network. *Development* 2010, 137:3719-3727.

252. Vicente-Manzanares M, Ma X, Adelstein RS, Horwitz AR: Non-muscle myosin II takes centre stage in cell adhesion and migration. *Nat Rev Mol Cell Biol* 2009, 10:778-790.

253. Slit and Netrin-1 guide cranial motor axon pathfinding via Rho-kinase, myosin light chain kinase and myosin II. 2010:1-15.

254. Amano M, Chihara K, Nakamura N, Fukata Y, Yano T, Shibata M, Ikebe M, Kaibuchi K: Myosin II activation promotes neurite retraction during the action of Rho and Rho-kinase. *Genes to cells : devoted to molecular & cellular mechanisms* 1998, 3:177-188.

255. Brown J, Bridgman PC: Role of Myosin II in Axon Outgrowth. *Journal of Histochemistry & Cytochemistry* 2003, 51:421-428.

256. Huttelmaier S, Harbeck B, Steffens O, Messerschmidt T, Illenberger S, Jockusch BM: Characterization of the actin binding properties of the vasodilator-stimulated phosphoprotein VASP. *FEBS letters* 1999, 451:68-74.

257. Lambrechts A, Kwiatkowski A, Lanier L, Bear J, Vandekerckhove J, Ampe C, Gertler F: cAMP-dependent protein kinase phosphorylation of EVL, a Mena/VASP relative, regulates its interaction with actin and SH3 domains. *J Biol Chem* 2000, 275:36143-36151.

258. Laurent V, Loisel TP, Harbeck B, Wehman A, Grobe L, Jockusch BM, Wehland J, Gertler FB, Carlier MF: Role of proteins of the Ena/VASP

family in actin-based motility of Listeria monocytogenes. *The Journal of Cell Biology* 1999, 144:1245-1258.

259. Colavita A, Culotti JG: Suppressors of ectopic UNC-5 growth cone steering identify eight genes involved in axon guidance in Caenorhabditis elegans. *Developmental Biology* 1998, 194:72-85.

260. Forrester WC, Garriga G: Genes necessary for C. elegans cell and growth cone migrations. *Development* 1997, 124:1831-1843.

261. Wen Q, Stepanyants A, Elston GN, Grosberg AY, Chklovskii DB: Maximization of the connectivity repertoire as a statistical principle governing the shapes of dendritic arbors. *Proceedings of the National Academy of Sciences of the United States of America* 2009, 106:12536-12541.

262. Sá MJ, Ruela C, Madeira MD: Dendritic right/left asymmetries in the neurons of the human hippocampal formation: a quantitative Golgi study. *Arquivos de neuro-psiquiatria* 2007, 65:1105-1113.

263. Beal JA, Nandi KN, Knight DS: Neurons with asymmetrical dendritic arbors in the substantia gelatinosa of the rat spinal cord. *Experimental brain research Experimentelle Hirnforschung Expérimentation cérébrale* 1990, 83:225-227.

264. Anderson JC, Binzegger T, Kahana O, Martin KA, Segev I: Dendritic asymmetry cannot account for directional responses of neurons in visual cortex. *Nat Neurosci* 1999, 2:820-824.

265. Choi J-H, Law M-Y, Chien C-B, Link BA, Wong RO: In vivo development of dendritic orientation in wild-type and mislocalized retinal ganglion cells. *Neural Development* 2010, 5:29.

266. Kim S, Chiba A: Dendritic guidance. *Trends in Neurosciences* 2004, 27:194-202.

267. Manitt C, Nikolakopoulou A, al e: Netrin participates in the development of retinotectal synaptic connectivity by modulating axon arborization and synapse formation in the developing brain. *The Journal of …* 2009.

268. Adler J: Chemotaxis in bacteria. *Annual review of biochemistry* 1975, 44:341-356.

269. Goodhill GJ, Urbach JS: Theoretical analysis of gradient detection by growth cones. *J Neurobiol* 1999, 41:230-241.

270. Horton AC, Yi JJ, Ehlers MD: Cell type-specific dendritic polarity in the absence of spatially organized external cues. *Brain Cell Biology* 2007, 35:29-38.

271. Basbaum AI, Bautista DM, Scherrer G, Julius D: Cellular and molecular mechanisms of pain. *Cell* 2009, 139:267-284.

272. Zhang S, Banerjee D, Kuhn JR: Isolation and culture of larval cells from C. elegans. *PLoS ONE* 2011, 6:e19505.

273. Gerstein MB, Lu ZJ, Van Nostrand EL, Cheng C, Arshinoff BI, Liu T, Yip KY, Robilotto R, Rechtsteiner A, Ikegami K, et al: Integrative analysis of the Caenorhabditis elegans genome by the modENCODE project. *Science* 2010, 330:1775-1787.

274. Niu W, Lu ZJ, Zhong M, Sarov M, Murray JI, Brdlik CM, Janette J, Chen C, Alves P, Preston E, et al: Diverse transcription factor binding features revealed by genome-wide ChIP-seq in C. elegans. *Genome research* 2011, 21:245-254.

275. Kucik DF, Kuo SC, Elson EL, Sheetz MP: Preferential attachment of membrane glycoproteins to the cytoskeleton at the leading edge of lamella. *The Journal of Cell Biology* 1991, 114:1029-1036.

276. Wang H, Macagno ER: A detached branch stops being recognized as self by other branches of a neuron. *Journal of neurobiology* 1998, 35:53-64.

277. Petersen SC, Watson JD, Richmond JE, Sarov M, Walthall WW, Miller DM, 3rd: A transcriptional program promotes remodeling of GABAergic synapses in Caenorhabditis elegans. *The Journal of neuroscience : the official journal of the Society for Neuroscience* 2011, 31:15362-15375.

278. Park M, Watanabe S, Poon VY, Ou CY, Jorgensen EM, Shen K: CYY-1/cyclin Y and CDK-5 differentially regulate synapse elimination and formation for rewiring neural circuits. *Neuron* 2011, 70:742-757.

Appendix table 1. Plasmids that were used throughout this thesis. Notes indicate how the plasmid was generated

Plasmid Name	Cassette	Date Made	Information	Notes
pCJS01	pF49H12.4::gateway::mcherry	3/12/09	flip in cDNA to be tagged with mcherry. Promoter driven in PVD	modified from Kang Shen constructs
pCJS03	pF49H12.4::intron2::unc-5GFP		temporally express UNC-5 in PVD	
pCJS02	pF49H12.4::gateway::YFP	3/12/09	flip in cDNA to be tagged with YFP. Promoter driven in PVD	modified from Kang Shen constructs
pCJS04	pF49H12.4::mcherry		expresses mcherry in PVD	
pCJS05	pF49H12.4::mcherry:gateway	3/12/09	flip in cDNA to be tagged with YFP. Promoter driven in PVD	modified from Kang Shen constructs
pCJS06	pF49H12.4::mcherry::rab-3	3/12/00	expresses rab-3 (post synaptic marker) in PVD	modified from Kang Shen constructs
pCJS07	pF49H12.4::pat-3::CD4-2::spGFP1-10		expresses half of GFP on the membrane of PVD	modified from Kang Shen constructs
pCJS08	pF49H12.4::unc-5::GFP		expresses unc-5 in PVD tagged with GFP	modified from pU5 from Joe Culotti
pCJS10	pF49H12.4::mig-10::YFP		expresses mig-10 in PVD tagged with YFP	modified from Cori Bargman unc-86::mig-10::YFP
pCJS09	pF49H12.4::pat-3::CD4-2::GFP		membrane bound GFP in PVD	modified from pCJS07
pCJS11	phsp16.2::unc-6::HA		expresses UNC-6 temporally	gift from Cori Bargmann
pCJS12	pItr-1::dys-1::YFP			gift from Kang Shen
pCJS13	pItr-1::F35D2.3::YFP			gift from Kang Shen
pCJS14	pItr-1::unc-9::YFP			gift from Kang Shen
pCJS15	pMig-13::gateway::YFP			gift from Kang Shen
pCJS16	pMig-13::mcherry::gateway			gift from Kang Shen
pCJS17	pUnc-5::mec2intron2::unc-5		expresses unc-5 temporally with intron2	gift from Kang Shen
pCJS18	pVns::UNC-6		expresses UNC-6 tagged with venus	
pCJS19	pegl-17::rde-1::RFP		expresses rde-1 tagged RFP in vuvla precursors	
pCJS20	pUnc-86::GFP::unc-34		expresses unc-34 in HSN	gift from Cori Bargmann
pCJS22	pUnc-86::unc-40::YFP		expresses unc-40 in HSN	gift from Cori Bargmann
pCJS21	pUnc-86::mig-10::YFP		expresses mig-10 in HSN	gift from Cori Bargmann
pCJS23	pMig-13::gateway::mcherry		flip in cDNA to be tagged with mcherry.	gift from Kang Shen
pCJS24	pCR8::rde-1		RDE-1 cDNA in pCR8	amplified from pCJS19
pCJS25	pMig-13::mcherry::rab-3		post synaptic marker	gift from Kang Shen
pCJS26	pF49H12.4::rde-1::mcherry		RDE-1 rescue in PVD	LR rxn from pCJS24 and pCJS01
pCJS27	pCR8::unc-6HA::3' UTR		unc-6 tagged with HA	amplified from pCJS11
pCJS28	pF49H12.4::unc-6HA		UNC-6 tagged with HA in PVD	made from pCJS27 and pCJS04
pCJS29	pUnc-25::gateway::CFP	3/30/09	flip in cDNA to be tagged with CFP Promoter driven in gaba	made from pCJS01
pCJS30	pCR8::unc-34	4/22/09	gateway compatible unc-34	amplified from pCJS20
pCJS31	pF49H12.4::gateway::CFP	4/24/09	flip in cDNA to be tagged with CFP Promoter driven in PVD	modified from pCJS29 and pCJS04
pCJS32	pCR8::unc-40	4/24/09	gateway compatible unc-40	amplified from pCJS22
pCJS33	pCR8::unc-5		gateway compatible unc-5	amplified from pU5
pCJS34	pF49H12.4::unc-5::CFP	5/1/09	UNC-5 expressed in PVD	LR rxn from pCJS31 and pCJS33
pCJS35	pF49H12.4::unc-40::mcherry	5/1/09	UNC-40 expressed in PVD	LR rxn from pCJS32 and pCJS01
pCJS36	pCR8::rig-3::mcherry::GPI	5/7/09	GPI anchor from rig-3	amplified from clay plasmid
pCJS37	pCR8::del-1	5/7/09	promoter used to drive in ventral nerve cord	amplified from steve plasmid
pCJS38	pF49H12.4::unc-6::HA::mcherry::GPI	5/10/09	added GPI anchor to UNC-6	made from pCJS28 and pCJS36
pCJS39	pDel-1::unc-6::HA	5/10/09	drives UNC-6 in ventral nerve cord	made from pCJS28 and pCJS37
pCJS40	pCR8::mec-3	5/13/09	gateway compatible mec-3	amplified from cDNA
pCJS41	pF49H12.4::mec-3::mcherry	5/27/09	mec-3 expressed in PVD	LR rxn from pCJS01 and pCJS40
pCJS42	pUnc-25::flippase::CFP	8/7/09	flippase driven CFP in GABA	used to flp out FRT cassettes. LR rxn with pCJS29 and flippase
pCJS43	pUnc-25::flippase::SL2::CFP	8/7/09	flippase driven CFP in GABA	modifiend from pCJS42
pCJS44	pFlp-18::NLG-1::spGFP11		drives post synaptic marker in AVA	gift from Kang Shen
pCJS45	pCR8::FRT::mcherry::FRT	10/28/09	gateway compatible FRT::mcherry::FRT	amplified from plasmid
pCJS46	pCR8::unc-119 minigene	11/3/09	unc-119 minigene to place in universal cloning constructs	amplified from plasmid
pCJS47	pCR8::unc-119 minigene rev		unc-119 minigene to place in universal cloning constructs reverse	amplified from plasmid
pCJS48	pF49H12.4::FRT::mcherry::FRT::YFP	11/4/09	reporter in combination with flippase	LR rxn from pCJS45 and pCJS02
pCJS49	pCR8::ser2prom3 promoter	11/9/09	promoter used to drive expression in PVD	amplified from pTDO2
pCJS50	pUnc-25::flippase::SL2::CFP::unc-119	11/9/09	bombable construct from unc-25 flippase	modified from PCJS43
pCJS51	pCR8::zag-1		gateway compatible zag-1 cDNA forward direction	amplified from Hutter construct
pCJS52	ser2prom3::unc-40::mcherry		expresses unc-40 in PVD	modified from pCJS01 and pCJS35
pCJS53	pF49H12.4::mcherry::unc-119		bombable PVD mcherry reporter	modified from pCJS04
pCJS54	pCR8::zag-1 reverse		gateway compatible zag-1 cDNA reverse direction	amplified from Hutter construct
pCJS55	pF49H12.4::zag-1::mcherry		expresses zag-1 in PVD	LR rxn from pCJS01 and pCJS51
pCJS56	pCR8::pzag-1		zag-1 promoter in forward direction	amplified from Hutter construct
pCJS57	pCR8::pzag-1 reverse		zag-1 promoter in reverse direction	amplified from Hutter construct
pCJS58	pCR8::phsp16.2 forward	1/7/10	heat shock promoter	amplified from pCJS11
pCJS59	pCR8::phsp16.2 reverse	1/7/10	heat shock promoter reverse direction	amplified from pCJS11
pCJS60	pCR8::pUnc-40 forward		unc-40 promoter forward direction	amplified from genomic DNA
pCJS61	pCR8::pUnc-40 reverse		unc-40 promoter reverse direction	amplified from genomic DNA
pCJS62	pCR8::pUnc-5 forward		unc-5 promoter forward direction	amplified from genomic DNA
pCJS63	pUnc-25::unc-40::mcherry		unc-40 expressed in GABA	LR rxn from pCJS32 and pMLH
pCJS64	ser2prom3::CFP		PVD CFP reporter	LR rxn from pCJS31 and pCJS33 screwed up
pCJS65	unc-5::CFP		UNC-5 CFP reporter	modified from pCJS64 and pCJS62
pCJS66	pUnc-25::CFP		GABA CFP reporter	modified from pCJS64
pCJS67	pF49H12.4::TM::unc-6::mcherry		membrane bound UNC-6 in PVD	made with pCJS01 and DD99

pCJS68	pUnc-25::unc-40::mRFP		unc-40 tagged with mRFP in unc-25	LR rxn with pCJS32 and pMLH48
pCJS69	pSer2prom3::mcherry::unc-119		bombable PVD mcherry reporter	made with pCJS49 and pCJS53
pCJS70	pF49H12.4::flippase::SL2::CFP		flippase driven in PVD	made with pCJS01 and pCJS43
pCJS71	pSur-5::gateway::YFP		flip in cDNA to be tagged with YFP Promoter driven in all cells	
pCJS72	pUnc-25::unc-5::mRFP		UNC-5 expressed in GABA	LR rxn with pCJS33 and pMLH48
pCJS73	pF49H12.4::unc-40::mRFP		UNC-40 expressed in PVD	made with pCJS68 and pCJS01
pCJS74	pF49H12.4::gateway::mRFP		flip in cDNA to be tagged with mRFP Promoter driven inPVD	modifiend from pMLH48 and pCJS01
pCJS75	pSur-5::FRT::mcherry::FRT::YFP		reporter in combination with flippase	
pCJS76	pCR8::unc-30 cDNA for		gateway compatible unc-30 cDNA, missing A in ATG forward	amplified from unc-30 nEx648
pCJS77	pCR8::unc-30 cDNA rev		gateway compatible unc-30 cDNA, missing A in ATG rev	amplified from unc-30 nEx648
pCJS78	pF49H12.4::mcherry:unc-34		unc-34 expressed in PVD	LR rxn from pCJS05 and pCJS30
pCJS79	pCR8::moesin::mcherry		moesin (actin binding protein) mcherry reporter	amplfied from Dave Sherwood plasmid
pCJS80	pCR8::pttr-39 clone 3		promoter used to drive antisense cDNA in universal cloning	amplified from Mallory plasmid
pCJS81	pCR8::UNC-40 truncate extra		extracellular domain of unc-40 is truncated	modified from pCJS32
pCJS82	pF49H12.4::mcherry::moesin	5/28/10	expressed moesin (actin binding protein) in PVD	made from pCJS01 and pCJS79
pCJS83	pCR8::dendra2 for	6/8/10	dendra2, photoconverable fluorophore (GFP>RFP) for	amplified from pDendra2, gift from Blakely lab
pCJS84	pCR8::dendra2 rev	6/8/10	dendra2, photoconverable fluorophore (GFP>RFP) rev	amplified from pDendra2, gift from Blakely lab
pCJS85	pCR8::dat-1::mcherry rev	2/19/10	dat-1::mcherry reporter	dat-1::mcherry to use as a reporter
pCJS86	F49H12.4::mcherry::moesin::unc119	6/14/10	moesin (actin binding protein) mcherry reporter	combined pCJS82 and pCJS46
pCJS87	F49H12.4::GFP::CD4-2::unc119	6/14/10	membrane bound GFP in PVD	combined pCJS09 and pCJS46
pCJS88	F49H12.4::mig-10b::YFP	8/2/10	mig-10 tagged with YFP expressed in PVD	modified from pCJS21
pCJS89	F49H12.4::GFP::unc-34	8/2/10	unc-34 tagged with GFP expressed in PVD	modified with pCJS20
pCJS90	mig-10::pCR8 flanked by NheI	8/31/10	mig-10 flanked by NheI to place in utrophin construct	amplified from pCJS21
pCSJ91	F49H12.4::GFP::utrophin	8/31/10	F-actin binding protein expressed in PVD	modified from DCR utrophin constructs. Promoter flanked by SphI and AscI
pCJS92	unc-6 flanked by XmaI + StuI pCR8	9/15/10		used to make pCJS97 unc-6::unc-40 fusion
pCJS93	F49H12.4::unc-40::GFP	10/4/10	expresses UNC-40::GFP in PVD	modified from DCR construct, SphI and AscI flank promoter
pCJS94	F49H12.4::mig-10c::GFP	10/4/10	expresses MIG-10c::GFP in PVD	modified from DCR construct, SphI and AscI flank promoter
pCJS95	F49H12.4::GFP::CED-10	10/4/10	expresses CED-10 tagged with GFP in PVD	modified from DCR construct, SphI and AscI flank promoter
pCSJ96	F49H12.4::mig-10a::GFP	10/4/10	expresses MIG-10a::GFP in PVD	modified from DCR construct, SphI and AscI flank promoter
pCJS97	F49H12.4::UNC-6::HA::UNC-40::GFP	10/31/10	expresses unc-6 fused with unc-40 in PVD	build from pCJS97 and pCJS92
pCJS98	F49H12.4::UNC-40endo::mcherry	12/14/10	expresses truncated version of UNC-40 lacking ecto domain	modified from DCR construct, SphI and AscI flank promoter
pCJS99	F49H12.4::UNC-40ecto::mcherry	12/14/10	expresses truncated version of UNC-40 lacking endo domain	modified from DCR construct, SphI and AscI flank promoter
pCJS100	pCR8 dab-1 cDNA rev	12/30/10	DAB-1 cDNA in pCR8	flanked with enzymes to insert into pCJS93
pCJS101	F49H12.4::DAB-1::GFP	1/10/11	expresses DAB-1 in PVD	modified from pCJS93 and pCJS100
pCJS102	F49H12.4::unc-5::mRFP	2/21/11	expresses unc-5 tagged with mRFP in PVD	made via gateway with pCJS33 and pCJS74
pCJS103	pCR8 ahr-1 cDNA w/ snp	3/9/11	contains snp. cDNA in rev direction	
pCJS104	pCR8 ahr-1 cDNA w/ snp	3/9/11	contains snp cDNA in for direction	
pCSJ105	pCR8 mec-4 promoter	4/8/11	used to express in touch neurons	mec-4 promoter flanked with SphI and AscI
pCJS106	mec-4::mcherry	4/12/11	expresses mcherry in touch neurons	modified from RLS unc-4::mcherry
pCJS107	mec-4::mcherry::unc119	4/12/11	expresses mcherry in touch neurons	modified from RLS unc-4::mcherry::unc119
pCJS108	mec-4::unc-6::unc-40::GFP	5/10/11	expresses unc-6 fused to unc-40 in touch neurons	modified from pCJS97 with SphI and AscI and pCJS107
pCJS109	rig-3::unc-6::unc-40::GFP	5/10/11	expresses unc-6 fused to unc-40 in AVA	modified from pCJS97 with SphI and AscI and MVC119
pCJS110	mec-4::zag-1::mcherry	5/10/11	expresses zag-1 in touch neurons	modified from pCJS55 and pCJS107
pCJS111	pCR8 ahr-1 cDNA	5/13/11	ahr-1 cDNA flanked with sites to insert into pCJS97	amplified with protaq from cDNA
pCJS112	F49H12.4::zag-1::mcherry::unc119	5/23/11	expresses zag-1 in PVD	modified from pCJS55 and pCJS69
pCJS113	mec-4::zag-1::mcherry::unc119	5/23/11	expresses zag-1 in nouch neurons	modified from pCJS110 and pCJS69
PCJS114	mec-4::ahr-1::mcherry	6/1/11	expresses ahr-1 cDNA in touch neurons	modified from pCJS111 and pCJS106 (made by Lani)
pCJS115	F49H12.4::dab-1::mcherry	6/8/11	out of frame dab-1	
pCJS116	F49H12.4::mig-10c::2XHA	8/9/11	expresses mig-10c tagged with HA in PVD	modified from pCJS94. Flag added with site directed mutagenesis
pCJS117	F49H12.4::dab-1::mcherry not in frame	8/10/11		
pCJS118	F49H12.4:dab-1::GFP not in frame	8/15/11		
pCJS119	mec-3::pCR8	8/24/11	~2 kb of mec-3 promoter flanked with AscI and SphI	flanked with AscI and SphI, amplifeid from genomic DNA
pCJS120	pCR8::cd4	9/5/11	CD4 transmembrane domain flanked by StuI and KpnI/AgeI	flanked with StuI and KpnI/Age, amplified from pCJS07
pCJS121	tph-1::unc-40::CD4::GFP out of frame	9/7/11	CD4 out of frame	
pCJS122	F49H12.4:UNC-6::CD4::GFP out of frame	9/7/11		
pCJS123	tph-1::unc-40::cd4::GFP in frame	10/10/11	used to make UNC-6::CD4	modified from pCJS123 and pCJS120. site directed mutagenesis to put in frame
pCJS124	tph-1::unc-40::cd4::gfp dam- cells	10/11/11	used to make UNC-6::CD4	modified from pCJS123 and pCJS120. site directed mutagenesis to put in frame
pCJS125	pCR8::mec-3 promoter	10/11/11	~2 kb of mec-3 promoter flanked by FseI and AscI	used to expressed cDNA under mec-3 promoter
pCJS126	F49H12.4::UNC-6::CD4::GFP	10/14/11	used to determine short-range signaling of UNC-6	modified from pCJS123 and pCJS97
pCJS127	F49H12.4::dab-1a::mcherry	10/17/11	expresses dab-1 in PVD	site directed mutagenesis to put in frame of pCJS115
pCJS128	F49H12.4::dab-1a::GFP	10/17/11	expresses dab-1 in PVD	site directed mutagenesis to put in frame of pCJS118
pCJS129	F49H12.4::unc-34a::GFP	11/14/11	expresses unc-34a::GfP in PVD	modified from DCR construct, SphI and AscI flank promoter
pCJS130	F49H12.4::unc-34b::GFP	11/14/11	expresses unc-34b in PVD	modified from DCR construct, SphI and AscI flank promoter
pCJS131	F49H12.4::nlg-1::spGFP1-10	11/14/11	expresses GRASP marker in PVD	modified from unc-4::nlg-1::spGFP1-10, SphI and AscI flank promoter